



**HAL**  
open science

# Geometric Aspects in the Hamiltonian Theory of the Fractional Quantum Hall Effect

Kang Yang

► **To cite this version:**

| Kang Yang. Geometric Aspects in the Hamiltonian Theory of the Fractional Quantum Hall Effect. Physics [physics]. Sorbonne Université, 2019. English. NNT : 2019SORUS425 . tel-03144255

**HAL Id: tel-03144255**

**<https://theses.hal.science/tel-03144255>**

Submitted on 17 Feb 2021

**HAL** is a multi-disciplinary open access archive for the deposit and dissemination of scientific research documents, whether they are published or not. The documents may come from teaching and research institutions in France or abroad, or from public or private research centers.

L'archive ouverte pluridisciplinaire **HAL**, est destinée au dépôt et à la diffusion de documents scientifiques de niveau recherche, publiés ou non, émanant des établissements d'enseignement et de recherche français ou étrangers, des laboratoires publics ou privés.

**THÈSE DE DOCTORAT  
DE SORBONNE UNIVERSITÉ**

**Spécialité : Physique**

**École doctorale n°564: Physique en Île-de-France**

**réalisée**

**au Laboratoire de Physique Théorique et Hautes Énergies**

**sous la direction de Benoît Douçot et Mark Goerbig**

**présentée par**

**Kang Yang**

**pour obtenir le grade de :**

**DOCTEUR DE SORBONNE UNIVERSITÉ**

**Sujet de la thèse :**

**Geometric Aspects in the Hamiltonian Theory of the  
Fractional Quantum Hall Effect**

**soutenue le 11<sup>ème</sup> octobre 2019**

**devant le jury composé de :**

<b>Ady Stern</b>	<b>Rapporteur</b>
<b>Zlatko Papic</b>	<b>Rapporteur</b>
<b>Nicolas Dupuis</b>	<b>Examineur</b>
<b>Cristiane Morais Smith</b>	<b>Examinatrice</b>
<b>Benoît Douçot</b>	<b>Directeur de thèse</b>
<b>Mark Goerbig</b>	<b>Directeur de thèse</b>



## Kang Yang

---

CONTACT INFORMATION	LPTHE - CNRS - UPMC Boîte 126, T13-14 4ème étage , 4 place Jussieu, Paris, France, 75005
EDUCATION	<b>Sorbonne Université</b> , Paris, France Ph.D. Physics, 2016-present <b>École Normale Supérieure</b> , Paris, France M.S. Physics, 2014-2016 (120 ECTS completed) Program: Quantum Physics ENS degree, 2014-2016 (36 extra ECTS) <b>Peking University</b> , Beijing, China B.S. Physics, 2010-2014
RESEARCH EXPERIENCE	<ul style="list-style-type: none"><li>• <b>PhD thesis under the supervision of Dr. Benoît Douçot and Dr. Mark Goerbig at Sorbonne Université, 2016.9-present</b> Topic: Geometric effects in the fractional quantum Hall effect.</li><li>• <b>Internship under Dr. Mark Goerbig's supervision at Université Paris-Sud, 2016.1-2016.6</b> Topic: Hamiltonian theory of the fractional quantum Hall effect.</li><li>• <b>Internship under Dr. Benoît Douçot's supervision at Sorbonne Université, 2015.2-2015.6</b> Topic: Periodically driven many-body systems.</li><li>• <b>Bachelor thesis research in Dr. Yifeng Yang's condensed matter theory group at Chinese Academy of Sciences, 2013.9-2014.6</b> Topic: Applications of Ads/CFT in condensed matter theory.</li></ul>
HONORS AND AWARDS	<ul style="list-style-type: none"><li>• Scholarship For Doctoral Students from École Normale Supérieure</li><li>• Scholarship For International Selection Students in École Normale Supérieure</li><li>• Honored Graduate of Weiming Elite Project, Peking University</li><li>• All-around Excellent Student of Peking University</li></ul>
RESEARCH TECHNIQUES	<b>Programming Languages and Programmes</b> C, C++, Fortran; Matlab, Mathematica, L <sup>A</sup> T <sub>E</sub> X, Origin
OTHER SKILLS AND SERVICES	<ul style="list-style-type: none"><li>• Chinese calligraphy and Chinese painting</li><li>• English, Chinese and French (basic)</li></ul>



# List of Publications

1. Mélin R, Caputo J G, **Yang K**, et al. Simple Floquet-Wannier-Stark-Andreev viewpoint and emergence of low-energy scales in a voltage-biased three-terminal Josephson junction[J]. Physical Review B, 2017, 95(8) : 085415.
2. **Yang K**, Goerbig M O, Douçot B. Hamiltonian theory for quantum Hall systems in a tilted magnetic field : Composite-fermion geometry and robustness of activation gaps[J]. Physical Review B, 2018, 98(20) : 205150.
3. Chen S, Ribeiro-Palau R, **Yang K**, et al. Competing fractional quantum hall and electron solid phases in graphene[J]. Physical review letters, 2019, 122(2) : 026802.
4. Mélin R, Danneau R, **Yang K**, et al. Engineering the Floquet spectrum of superconducting multiterminal quantum dots[J]. Physical Review B, 2019, 100(3) : 035450.
5. Doucot B, Danneau R, **Yang K**, et al. Berry phase in superconducting multiterminal quantum dots[J]. arXiv preprint arXiv :1904.03132, 2019.



# Acknowledgements

This thesis is finished in Laboratoire de Physique Théorique et Hautes Énergies (LPTHE) at Sorbonne Université and Laboratoire de Physique des Solides (LPS) at Université Paris-Sud. I really appreciate the three years spent in both laboratories and the academic environments there. I need to thank my master school, École Normale Supérieure, for providing the scholarship as my doctoral funding.

The contents presented in this thesis have been mainly carried out in LPS. I have to thank Mark for his pedagogic introduction leading me to the field of fractional quantum Hall effects. Explaining such an intriguing but rather complicated topic is never an easy task. Mark uses his vivid physical pictures and accurate intuitions to guide me into the core of the quantum Hall physics. As a theorist, Mark always reminds me to connect our results to parameters in realistic settings and how theoretic predictions should be adapted to experimental measurements. Under Mark's organization, we even had a pleasant collaboration with experimentalists in Columbia University. All of those experiences taught me a lot about how to be a condensed-matter physicist. Mark's optimism has also made the pursuit of the doctoral degree much more relaxing.

In LPTHE, I have worked a lot on the issues of periodically driven Josephson junctions, in which I strengthened my understanding in non-equilibrium systems despite these contents will not be presented here due to the pertinence to the topic. In these projects, I benefited from Benoît's serious attitude towards every detail in our research and his broad knowledge in various techniques of condensed-matter physics. Every time when we meet some challenging questions, Benoît is always able to get us out of the difficulties. Apart from the Josephson junction systems, Benoît helped me a lot in working out some very technical issues in quantum Hall systems. He is not only an advisor for physical questions, but also a mentor for my academic career. I thank my two advisors for being so pleasant under their supervision.

I also need to thank other two members in my doctoral monitoring committee, Nicolas and Jean-Bernard, and my collaborators Rebeca, Régis, Shaowen and Yuchi. Without them, this thesis would not be finished. I thank Ady and Zlatko for reviewing this thesis.

During the last five years in Paris, I met many new friends and colleagues. They made the life in this beautiful and elegant city so colorful and brought a lot of happy memories. They are Constantin, Deliang, Enrico, Fan, Fredric, Gregoire, Jiabin, Johannes, Liang, Lingling, Luca, Manali, Manuel, Maxime, Osmin, Pierre, Ruben, Sergueï, Shengquan, Sophie, Thomas, Xin, Yi, Yichang, Yifan, Yoan, Yunlong, Zhihao, Ziwei. In the end, I thank my dearest Lu, who has been accompanying me and spending the best moments together with me in my pursuit of a doctoral degree.





# Table des matières

<b>Introduction</b>	<b>x</b>
<b>I Quantum Hall effects</b>	<b>1</b>
I.1 Integer quantum Hall effects . . . . .	1
I.2 Fractional quantum Hall effects . . . . .	6
I.3 Low-energy effective theory . . . . .	9
<b>II Geometric variational parameter and degrees of freedom</b>	<b>11</b>
II.1 Geometry as a variational parameter in wave functions . . . . .	11
II.2 Spectrum analysis : spin-2 degrees of freedom in low momenta . . . . .	14
II.3 Hall viscosity and static structure factor . . . . .	15
II.3.1 Hall viscosity for FQHE trial states . . . . .	16
II.3.2 Geometry and the static structure factor . . . . .	20
<b>III Composite Fermions and Hamiltonian theory</b>	<b>23</b>
III.1 Composite fermion transformation . . . . .	23
III.2 Hamiltonian description . . . . .	26
III.3 Small-momentum theory of the Hamiltonian theory . . . . .	29
III.3.1 Introducing an auxiliary field . . . . .	30
III.3.2 Separating different energy scales . . . . .	32
<b>IV Composite fermion theory under anisotropy</b>	<b>37</b>
IV.1 Reparametrisation of ladder operators . . . . .	37
IV.2 Effective potential in tilted magnetic field . . . . .	38
IV.3 Calculation of the activation gap . . . . .	42
IV.3.1 Hilbert space and matrix elements . . . . .	42
IV.3.2 Relation between CF LL mixing and generalized pseudopotentials . . . . .	44
IV.3.3 Optimal metrics and the activation gap under a tilted magnetic field . . . . .	48
<b>V Magneto-exciton mode and neutral gap</b>	<b>57</b>
V.1 Conserving method and time-dependent Hartree-Fock approximation . . . . .	58
V.2 Diagrammatic magneto-plasmon calculation . . . . .	62
V.3 Comparison between the electron density computation and preferred density computation . . . . .	66
V.4 Computation in the presence of anisotropy . . . . .	70
V.5 Calculations to all orders in perturbation theory . . . . .	80

<b>VI Charge density wave phases under external anisotropy</b>	<b>87</b>
VI.1 Phase diagrams in higher LLs under isotropic interaction . . . . .	87
VI.1.1 The Hartree-Fock interaction . . . . .	88
VI.1.2 Wigner crystal, bubble phases, and stripe phases . . . . .	89
VI.1.3 Phase transitions in the second LL . . . . .	94
VI.2 Crystal phases in anisotropic interaction . . . . .	95
VI.2.1 Trial density profiles for anisotropic interaction . . . . .	96
VI.2.2 Phase transitions in the presence of anisotropy . . . . .	98
VI.3 Effective elastic theory . . . . .	105
<b>VI Conclusion</b>	<b>111</b>
<b>A Static structure factor in the Hamiltonian theory</b>	<b>115</b>
<b>Bibliographie</b>	<b>119</b>

# Introduction

In condensed-matter physics, there are several topics always capturing physicists' interests. One of them is the emerging behaviours in correlated systems, where physicists find the complicated interacting underlying physics can be described by some simple pictures such as Fermi liquids and quasiparticles. Another very important branch is the order and symmetry in many-body physics. Many remarkable properties are related to symmetry-breaking processes, for instance superfluidity and superconductivity. These phenomena are conveniently described within Landau's theory of phase transitions. However there are several strongly correlated electron systems that are beyond this theoretical framework. One of these systems is the quantum Hall system which exhibits rather fascinating emerging behaviours and orders. The quantum Hall effect [1, 2] is observed in a two-dimensional charged system under a perpendicular magnetic field. The ground state exhibits a robustness and is ordered in a way beyond the traditional Landau symmetry breaking paradigm. It is later realized that such phenomena derive from topological properties [3, 4, 5, 6]. As topology characterizes properties that are invariant under continuous deformation, its manifestation always gives discrete quantization in the physical world, which in quantum Hall effects, is the quantized Hall conductivity. This leads to a stability which is interesting to observe in experiments. After the observation of quantum Hall effects, thorough study has been done towards this direction. The proposal of Chern insulators [7] realizes a similar quantized Hall conductivity albeit in the absence of an external magnetic field. It opens the door to find topological materials without external magnetic field [8, 9]. Along this direction, a lot of efforts are spent to use topology as a tool to look for novel nontrivial states [10, 11, 12, 13, 14]. In the last ten years a lot of progress has been realized for topological materials in crystalline systems [15, 16, 17, 18]. The richness of topological phases provides new candidates and tools for technological innovations.

The topological properties in quantum Hall systems are reflected in several quantities. The Hall conductivity for integer quantum Hall effect (IQHE) is related to the Chern number of the wave function bundle [3]. The ground state degeneracy on a torus comes from the types of Wilson loops winding around the hole of the torus. The appearance of edge states is related to the bulk properties through the bulk-edge correspondence of the same topological field theory in  $2 + 1$  dimensions. Moreover, people have understood that the fractional excitation in the fractional quantum Hall effect (FQHE) is a key ingredient leading to the so-called topological order [19, 20], with which the state exhibits long-range entanglement and cannot be adiabatically connected to a product state without going through a phase transition [21]. On the other hand, the fractional excitations observed in FQHE, recognized as anyons, are attracting great interest from both academia and industry, as some of them are believed to provide a platform to realize fault-tolerant quantum computation [22, 23], which has a

prospective potential in encryption and scientific simulation [24]. The topological aspects in quantum Hall systems provide huge inspiration for modern condensed-matter physics.

In contrast, geometry, which in short characterizes distance between different points, is far from being fully understood in the quantum Hall effect. Although initially it is the geometric Berry curvature that appears in the Hall conductivity, the final result is immediately shown to be independent of geometry through the Gauss-Bonnet theorem. Unlike the discreteness of topology, geometry is a continuous variable in nature compared to topology. Geometric quantities are not always expected to be quantized discretely and robust against perturbation. It is indicated by Wen and Zee [25] that geometric quantities such as the spin connection have to be taken into account to explain the shift of quantum Hall effects on curved spaces, a quantity giving a correction to the relation between the electron number and the magnetic flux number. However their result still only depends on the topology. Later, like the topologically quantized transverse Hall conductivity, a transverse quantity closely connected to geometric moduli space is found as the Hall viscosity in the IQHE [26]. The two geometric quantities, the shift and the Hall viscosity, are even found to be closely related to each other [27]. The higher order term in the Hall conductivity at finite wave vector is also shown to be related to geometric effects [28]. Recently more interests focus on the response of the quantum Hall state under external anisotropy. With the development of experiments, states of the same topological order but different symmetry order are being searched.

In this thesis, I am going to investigate the geometric aspects from the view of composite fermions and test the response of quantum Hall states under anisotropic perturbation. The first chapter I gives an introduction to the integer and the fractional quantum Hall effects. The geometric point of view for quantum Hall systems is introduced in Chapter II. Chapter III explains the composite fermion picture for the FQHE and the Hamiltonian version of it. In Chapter IV we will discuss how to combine a variational metric with the Hamiltonian theory and the test of this combination under external anisotropy. This naturally leads to a investigation of the activation gap. This content was published in [29]. The neutral collective excitations under anisotropy are studied in chapter V. We find that the activation gaps for quasiparticles/quasiholes are robust against anisotropy but the neutral collective gap is rather vulnerable. The last chapter VI is dedicated to charge-density-wave states in quantum Hall systems in an anisotropic effective interaction. We find that the intermediate  $M = 2$  bubble phase is driven out by anisotropy and first-order transitions between different CDW phases in isotropic case are replaced by continuous phase transitions.

Besides the contents introduced in this thesis, I also spent much effort during my PhD in studying Josephson junction systems under periodical driving with my advisor Dr. Benoît Douçot and other collaborators. In a series of work, we studied the quasi-steady state formed by the interplay between dissipation and external energy injecting. There are many novel features emerging in this quasi-steady state, such as its Berry phase and nontrivial monodromy. Those results are published (preprinted) in Ref.[30, 31, 32]. And I had a pleasant collaboration with experimentalists at Colombia University in studying the re-entrant quantum Hall effect in graphene. We studied how the screening effects due to metallic gates can affect the re-entrance observed experimentally. This work is published in Ref. [33].

# I – Quantum Hall effects

Strongly correlated electrons have always captured the interest of physicists. The macroscopic collective behaviors exhibited by electrons and the lattices where they reside are entirely different from their microscopic origins. Especially, there are macroscopic “orders” emerging from the seemingly disordered underlying systems. One example is the relation between symmetry and orders. In the past century Landau’s Fermi liquid theory and symmetry breaking theory helped a lot in understanding how interactions can give rise to various phenomena, such as (anti-)ferromagnetism, superconductivity or charge density orders. They are so successful that people once believed what is left to do is to apply them to every new matter discovered. However the observation of the quantum Hall effect (QHE) gives a glimpse to a new world [1, 2]. The system of two-dimensional electrons moving in a perpendicular magnetic field is found to be in an incompressible fluid state and its bulk excitations are gapped. The properties of this system cannot be characterised by conventional condensed-matter theory. In a seminal paper [3] by Thouless et. al., it is found that integer quantum Hall effects exhibit topological properties associated with the bundle of the ground state wave function. Later fractional charges and statistics are shown to exist in fractional quantum Hall effects [34].

In this chapter, the integer quantum Hall effect is discussed in Section I.1, where Landau quantization and degrees of freedom of different energy scales are introduced. Section I.2 gives a short glimpse at the emergent phenomena in fractional quantum Hall effects. Section I.3 discusses the low-energy effective theory proposed for quantum Hall systems.

## I.1 Integer quantum Hall effects

The quantum Hall system is built from charged particles moving in a two-dimensional space under a perpendicular magnetic field. As shown in Fig. I.1. each particle has a kinetic energy expressed in terms of the mechanical momentum and feels the Coulomb repulsion from others.

To be concrete, we put the electrons in the  $x$ - $y$  plane and apply a constant magnetic field  $B$  in the  $z$ -direction. The Hamiltonian is described by

$$H = \sum_i \frac{\mathbf{\Pi}^{(i)2}}{2m} + V = \sum_i \frac{[\mathbf{p}_i + e\mathbf{A}(\mathbf{r}_i)]^2}{2m} + V, \quad (\text{I.1})$$

where  $\mathbf{\Pi}^{(i)}$  is the gauge-invariant dynamical momentum of the  $i$ -th particle. The vector potential satisfies  $\nabla \times \mathbf{A} = -B\mathbf{e}_z$ . Notice that the convention of the direction of magnetic field can be different in other literature. Here we use the negative  $z$ -direction since the electric

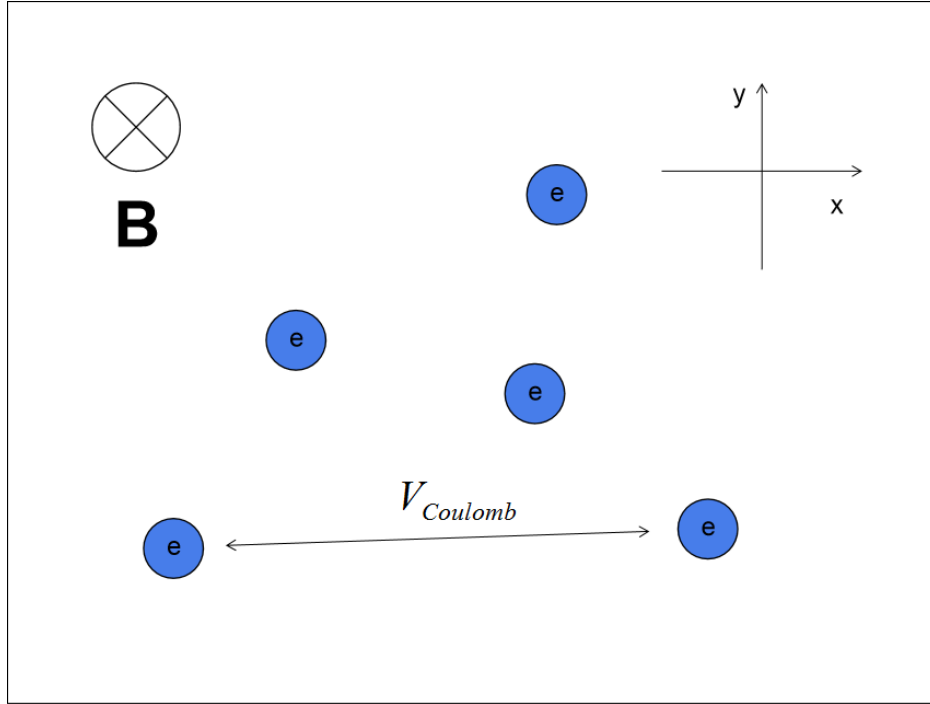


Fig. I.1 The two-dimensional charged particles under a perpendicular magnetic field. The magnetic field is taken to be along the  $z$ -axis. The electrons are moving under the Coulomb repulsion and the Lorentz force.

charge is taken as negative  $e = -|e|$  and is not absorbed into the definition of the magnetic field as what is usually done in most field-theory formalism. Finally  $V$  is the Coulomb interaction between the electrons

$$V = \frac{1}{2} \int \rho d^2\mathbf{r} \int d^2\mathbf{r}' \rho(\mathbf{r}) v(\mathbf{r} - \mathbf{r}') \rho(\mathbf{r}') = \frac{1}{2} \sum_{\mathbf{q}} \rho(\mathbf{q}) v(\mathbf{q}) \rho(-\mathbf{q}), \quad (\text{I.2})$$

where  $\rho(\mathbf{r}) = \sum_i \delta(\mathbf{r} - \mathbf{r}_i)$  is the density of the electrons. Its Fourier transformation in the language of first quantization is  $\rho(\mathbf{q}) = \sum_i \exp(-i\mathbf{q} \cdot \mathbf{r}_i)$ .

Let us first look at how charged particles behave in classical theory. According to the transverse Lorentz force, the perpendicular magnetic field bends the trajectories of charged particles. For electrons of density  $n_e$ , they are following circular motion. If one restricts the electrons into a rectangular space and inject the current in the  $x$ -direction (see Fig. I.2), the electrons are drifting towards the boundaries in the  $y$ -direction under the Lorentz force. The accumulation of electrons creates an electric field  $E_y \hat{e}_y$ . When the electric field reaches  $E_y = Bv_x$ , where the velocity  $v_x$  is related to the current density by  $j_x = -en_e v_x$ , the Lorentz force is balanced by the electric force. As a result there is a transverse Hall conductivity  $j_x = \sigma_{xy} E_y$  :

$$\sigma_{xy} = \frac{en_e}{B}. \quad (\text{I.3})$$

Notice that here  $B$  is taken to be along the negative  $z$ -direction, which compensates the negative sign in charge. In the longitudinal direction, for an ideal perfectly pure sample,

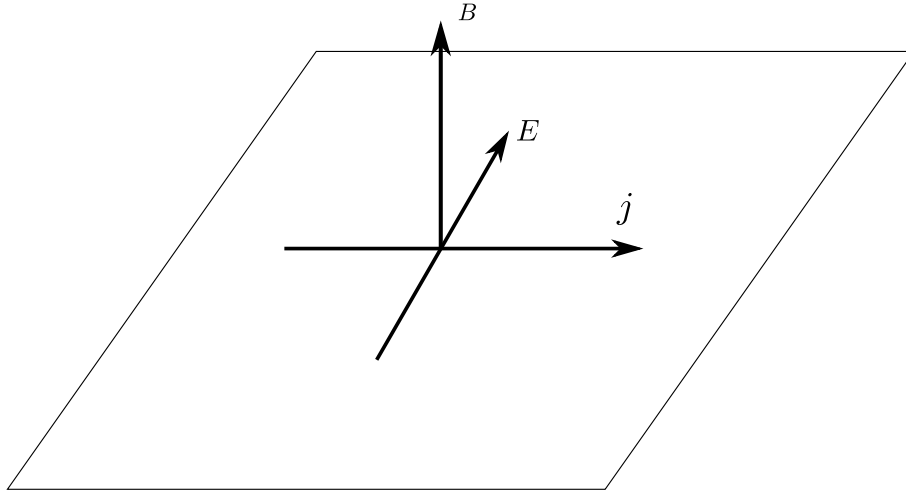


Fig. I.2 Injecting a current  $j$  in  $x$ -direction, an electric potential is induced along  $y$ -direction.

the system is insulating  $\sigma_{xx} = 0$ . By inverting the conductivity, the classical theory thus predicts that there is a Hall resistance growing linearly with the external magnetic field and a vanishing longitudinal resistance

$$\rho = \begin{pmatrix} 0 & -\frac{B}{en_e} \\ \frac{B}{en_e} & 0 \end{pmatrix}. \quad (\text{I.4})$$

In realistic experiments, there is diffusion caused by impurities. When this is taken into account, a Drude model gives a non-vanishing longitudinal resistance. The resistance tensor takes the form [35] :

$$\rho = \begin{pmatrix} \frac{1}{\sigma_0} & -\frac{B}{en_e} \\ \frac{\sigma_0}{B} & \frac{1}{\sigma_0} \end{pmatrix}, \quad (\text{I.5})$$

where  $\sigma_0$  is related to the relaxation time  $\tau$  and electron mass  $m_e$  by  $\sigma_0 = n_e e^2 \tau / m_e$ . In the eighties of the last century, people performed a series of experiments on resistance measurements in quantum Hall systems. In 1980, the integer quantum Hall effect [1] was discovered while in 1982 a similar experimental behaviour was found and named as the fractional quantum Hall effect [2]. Although the experimental results fit the trend of classical theory (Fig. I.3), there is an evident plateau in the Hall resistance at some special magnetic field. And when the Hall resistance transits from one plateau to another, the longitudinal resistance exhibits a spiking behavior. That phenomenon was initially recognized as properties related to specific experimental samples. However later it was realized that the Hall resistance turns out to be quantized to very high accuracy, which indicates a non-trivial phase at special magnetic-field strength.

Now let's go back to the quantum theory. As we will see soon, the integer quantum Hall effect is associated with the kinetic energy quantization whereas the fractional quantum Hall effect happens at the scale of the repulsion interaction. We focus first on the kinetic energy. In high magnetic field experiments, this is reasonable as the Coulomb repulsion is a small energy scale as compared to the typical level spacing due to the quantization of the kinetic



energy. Because of the presence of the magnetic field, we have the following commutation relations between the gauge covariant derivative and the spatial coordinates :

$$[r^a, \Pi_b] = i\hbar\delta_b^a, \quad [\Pi_a, \Pi_b] = i\epsilon_{ab}\hbar eB. \quad (\text{I.6})$$

$\epsilon_{ab} = \epsilon^{ab}$  is the 2D Levi-Civita symbol for the two spatial components  $a, b = x, y$  of a 2D vector. Here we give the coordinates superscripts and momenta subscripts for future convenience. In classical mechanics, the electrons are doing circular motions under the Lorentz force. The radii of the circles are related to the gauge-invariant momenta, namely the kinetic energies, while the centers of the circles can be placed anywhere and are thus constants of motion. To build such an interpretation in the quantum version, we define the cyclotron coordinate as

$$\boldsymbol{\eta} = l^2 \hat{\mathbf{z}} \times \boldsymbol{\Pi}, \quad (\text{I.7})$$

where  $l = \sqrt{\hbar/eB}$  is the magnetic length. We can immediately see from Eq. (I.1) that this coordinate alone determines the kinetic energy. Therefore it indeed corresponds to the radius of the circular motion. Since the position of the electron is the radius plus the center of the circle, we can further define a guiding-center coordinate and decompose the electron coordinate as

$$\mathbf{R} = \mathbf{r} - \boldsymbol{\eta}, \quad \mathbf{r} = \boldsymbol{\eta} + \mathbf{R}, \quad [\mathbf{R}, \boldsymbol{\eta}] = 0 \quad (\text{I.8})$$

This coordinate is another degree of freedom as it commutes with the cyclotron coordinate. Classically the center of the cyclotron motion is a constant of motion. Going to the quantum mechanics, it therefore commutes with the kinetic Hamiltonian  $[\mathbf{R}, H_k] = 0$ . Furthermore it can be used to label the degenerate electron states of the same kinetic energy. The kinetic energy now is expressed by

$$H_k = \frac{\boldsymbol{\eta}^2}{2ml^4}, \quad [\eta^a, \eta^b] = i\epsilon^{ab}l^2, \quad (\text{I.9})$$

which is simply a Hamiltonian of a harmonic oscillator. Its spectrum is equally spaced and consists of the so-called Landau levels (LLs)

$$E_n = \left(n + \frac{1}{2}\right) \hbar\omega_c. \quad (\text{I.10})$$

From now on we take  $\hbar = 1$ . The cyclotron frequency  $\omega_c$  is  $eB/m$ , while the degeneracy of electron states inside each Landau level is related to the guiding center degrees of freedom. As mentioned above, it commutes with the kinetic Hamiltonian. Its available eigenvalues determine the number of states that we can have in a single Landau level and thus its degeneracy. The components of the guiding-center coordinate has the following commutation relations :

$$[R^a, R^b] = -i\epsilon^{ab}l^2. \quad (\text{I.11})$$

From these equations, we can see that the two components of guiding-center coordinates behave like a pair of conjugate coordinates. The uncertainty principle requires in any quantum state the product of  $\Delta R^x$  and  $\Delta R^y$  to have a lower limit about

$$\Delta R^x \cdot \Delta R^y \sim l^2. \quad (\text{I.12})$$

After Bohr-Sommerfeld quantization, it requires an area of  $2\pi l^2$  to accommodate a quantum state. Thus in a two dimensional plane of area  $S$ , the number of allowed positions of the guiding centers, or equivalently the degeneracy of quantum states that we can have in a single Landau level (here we consider spinless electrons) in the thermodynamic limit is given by

$$\simeq N_\phi = S/(2\pi l^2) = SeB/(2\pi) \sim B \cdot S = \phi, \quad (\text{I.13})$$

which is proportional to the magnetic flux through the plane. The expression  $2\pi l^2$  has the unit of area and is regarded as the area per flux quantum. In some specific geometries like the torus, one can show that the number of states per Landau level is precisely given by this formula. The argument for a general geometry is rather complicated, but the above formula still gives the correct number except for a non-extensive correction [36]. The filling factor  $\nu$  is the ratio between the number of electrons and the number of the available quantum states

$$\nu = \frac{N_e}{N_\phi} = \frac{2\pi N_e}{SeB} = \frac{2\pi n_e}{eB}, \quad (\text{I.14})$$

expressed through the average electron density  $n_e$  and the magnetic field  $B$ .

From this derivation, we see that when the magnetic field is tuned to have an integer filling,  $\nu = n$ ,  $n$  Landau levels are completely filled. Every excitation has to move an electron from a lower Landau level to a higher one. Thus the spectrum is gapped. This explains the robustness of the IQHE ground state against external perturbation.

For future usage, we also introduce the wave function for the integer quantum Hall effect. Due to the algebra of cyclotron coordinates and guiding center coordinates, two pairs of ladder operators can be defined :

$$\hat{a} = \frac{\eta^x + i\eta^y}{\sqrt{2}l}, \quad \hat{a}^\dagger = \frac{\eta^x - i\eta^y}{\sqrt{2}l}; \quad \text{and} \quad \hat{b} = \frac{R^x - iR^y}{\sqrt{2}l}, \quad \hat{b}^\dagger = \frac{R^x + iR^y}{\sqrt{2}l}. \quad (\text{I.15})$$

The first set of ladder operators generates the Landau levels while the second set generates the degenerate states inside a LL. Furthermore in the isotropic case, rotational invariance makes the angular momentum a good quantum number. The angular momentum operator is related to the ladder operators as :

$$L_z = \hat{b}^\dagger \hat{b} - \hat{a}^\dagger \hat{a}. \quad (\text{I.16})$$

Notice that the angular momentum depends both on the guiding-center and cyclotron motion. When considering the physics in the same LL, the latter is always neglected by many authors. With these operators, the basis of the Hilbert space is constructed as  $|m, n\rangle = (\hat{b}^\dagger)^m (\hat{a}^\dagger)^n |\Omega\rangle$ , where  $|\Omega\rangle$  is annihilated by  $a$  and  $b$ . The wave function for the  $\nu = 1$  IQHE can be worked out easily by choosing  $n = 0$  and filling electrons from  $|0, 0\rangle$  to  $|N_e - 1, 0\rangle$ . The wave function is a Slater determinant of those single-particle states. In the symmetric gauge, where  $\mathbf{A} = eB(\hat{e}_x y - \hat{e}_y x)/2$ , the annihilation conditions  $a|\Omega\rangle = 0$  and  $b|\Omega\rangle = 0$  require the wave function to be a holomorphic function of electron coordinates  $z = x + iy$ . By rewriting the ladder operators in terms of electron coordinates, the single-body states take the form  $|m, n\rangle = z^m \exp(-z^2/4l^2)$  and the  $\nu = 1$  wave function takes the form :

$$\Psi_{\nu=1} = \prod_{j < i} (z_i - z_j) \exp\left(-\sum_i \frac{|z_i|^2}{4l^2}\right). \quad (\text{I.17})$$

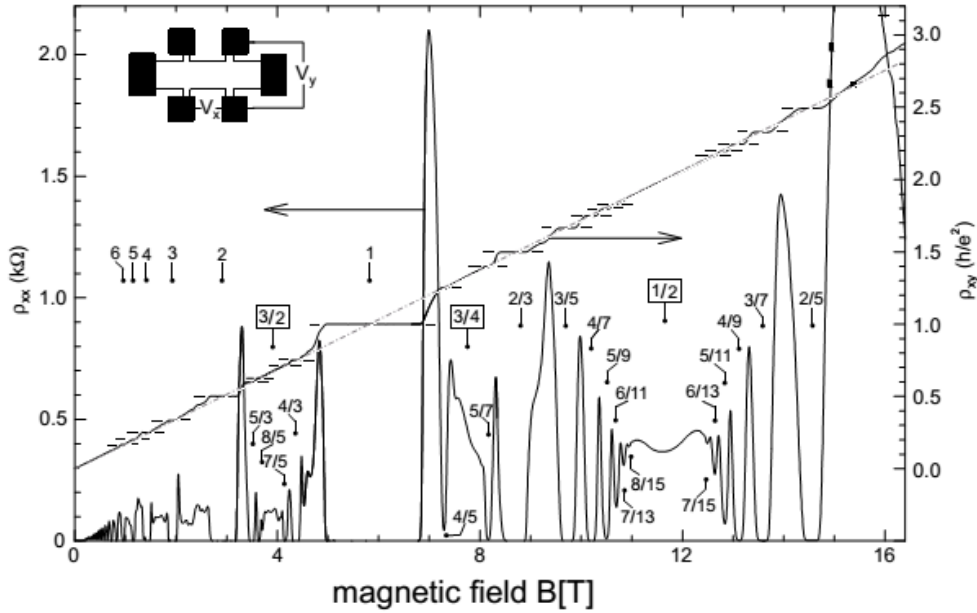


Fig. I.3 The typical experimental observation of quantum Hall effects, measured by J. Smet, MPI-Stuttgart [35]. The Hall resistance follows the trend of the classical prediction but exhibits quantized plateaus at certain magnetic field strength. The plateaus in the Hall resistance are accompanied by zeros in the longitudinal resistance.

We can see that this wave function is indeed odd as for fermions under interchanging a pair electrons  $i \leftrightarrow j$  and it is a Vandermonde matrix determinant. The  $\nu = n$  wave function can be worked out similarly, by rising the Landau level from the above wave function using  $a^\dagger$  operators for each electron.

## I.2 Fractional quantum Hall effects

When the filling factor is a fractional number, the top LL is partially filled. All electrons in this partially filled LL have the same kinetic energy. After taking into account the interaction, the repulsion between electrons is introduced. It influences dynamics within the same LL and introduces inter-LL transitions. In the case of strong magnetic field, the amplitude of the latter is suppressed as  $\sim 1/B$  and thus can be neglected. Those filled LLs and empty LLs are regarded as inert and provide a screening to the Coulomb interaction inside the partially filled LL. Hence in order to understand the fractional quantum Hall effect, it is appropriate to focus on the physics confined to the partially filled LL. Every operator is projected to this partially filled LL. The kinetic energy is therefore frozen. One significant feature of this projection is that the density operators of different momenta do not commute. This brings a huge difference to how electrons occupy their orbitals. Before the discovery of the fractional quantum Hall effect, the Coulomb repulsion led people to believe that the electrons should stay away from each other and form a kind of solid state, the Wigner crystal [37, 38].

However, the solid state does not contribute to the Hall conductivity and is compressible due to the phonon mode, which is not in accordance with the experimental observation of the fractional quantum Hall effect. The strong fluctuations due to the partially filled LL projection destroy the crystal order and turn it into a liquid state when the average distance between the electrons is of the same order as the magnetic length which characterizes the typical quantum fluctuation. Thus the fractional quantum Hall effect is dominated by both the interaction and the algebra of projected operators.

Unlike the IQHE, which can be explained through one-body physics, the FQHE stems from the interaction and is in nature strongly correlated. The FQHE state is the first real system exhibiting topological orders, where the ground state cannot be deformed into a direct product of local states via local unitary evolution [21]. Under local unitary evolution, the ground state is acted on with a time evolution operator made of local Hamiltonians. One way of characterizing the topological order is the underlying fractionalized excitations, the anyons [39, 23]. This kind of excitation behaves quite differently from fermions or bosons in the sense that exchanging two identical anyons does not merely bring a phase  $\pi$  or  $2\pi$ , but a more general unitary transformation. In FQHE, the quasiparticle and quasihole excitations obeys fractional statistics which is significantly different from the underlying electrons and can only emerge from a many-body system. The exotic properties originate from the spatial dimension two and the flux of the external magnetic field. In a two-dimensional plane, each electron creates a defect on the plane, which other electrons following closed trajectories must choose either to wind around or not. For fractional filling, as we will see soon explicitly in the Laughlin wave function, each electron occupies an area of several magnetic flux quanta. When a charged particle bound to magnetic fluxes winds around another one, a nontrivial Berry phase comes from the Aharonov-Bohm effect, leading to a statistic angle different from integer multiples of  $\pi$  [40].

As a starting example, we focus on the situation when the lowest LL (LLL) is partially filled. According to what we have discussed at the beginning of this section, all physical operators should be projected to LLL. Quantities related to the cyclotron coordinates are replaced by their expectation values. The kinetic energy is frozen as it is a constant and does not affect intra-LL physics. The density operator and interaction term (I.2) now are only functions of the guiding-center coordinates, which characterize the positions of the electron cyclotron-motion centers, while the cyclotron coordinate  $\eta$  is averaged over,

$$\rho_e(\mathbf{q}) = \sum_i \langle e^{-i\mathbf{q}\cdot\eta_i} \rangle e^{-i\mathbf{q}\cdot\mathbf{R}_i} = \sum_i e^{-q^2 l^2/4} e^{-i\mathbf{q}\cdot\mathbf{R}_i}, \quad (\text{I.18})$$

$$V = \frac{1}{2} \sum_{\mathbf{q}} \bar{\rho}_e(\mathbf{q}) V_{eff}(\mathbf{q}) \bar{\rho}_e(-\mathbf{q}), \quad (\text{I.19})$$

$$V_{eff}(\mathbf{q}) = v(\mathbf{q}) e^{-q^2 l^2/2}, \quad (\text{I.20})$$

$$\bar{\rho}_e(\mathbf{q}) = \sum_i e^{-i\mathbf{q}\cdot\mathbf{R}_i}. \quad (\text{I.21})$$

The bare interaction  $v(\mathbf{q}) = 2\pi e^2/\varepsilon q$  is the Fourier-transformed Coulomb potential. For convenience, the projected density notation  $\bar{\rho}$  is used, while the Gaussian factor  $\exp(-q^2 l^2/2)$ , which arises as a form factor from the average over the cyclotron motion, is absorbed into the effective interaction potential. After the projection, the  $\bar{\rho}$  operators do not commute, but

satisfy the following Girvin MacDonald Platzman (GMP) algebra [41] :

$$[\bar{\rho}_e(\mathbf{q}), \bar{\rho}_e(\mathbf{q}')] = 2i \sin \left[ \frac{(\mathbf{q} \times \mathbf{q}')l^2}{2} \right] \bar{\rho}_e(\mathbf{q} + \mathbf{q}'). \quad (\text{I.22})$$

The above algebraic structure makes solving the degenerate partially filled LL question almost impossible except for brute force exact diagonalization. The first successful attempt for FQH problems comes from a wave-functional approach [34]. Looking back at the wave function Eq. (I.17) for  $\nu = 1$  IQHE, the power of  $z$  actually counts the number of the magnetic flux quanta in the corresponding orbital. The IQHE wave function simply represents that there is one electron in every orbital. For a fractional filling  $\nu = 1/(2s + 1)$ , a natural generalization is to have one electron in every  $2s + 1$  orbitals :

$$\Psi_{1/(2s+1)} = \prod_{j < i} (z_i - z_j)^{2s+1} \exp \left( - \sum_i \frac{|z_i|^2}{4l^2} \right). \quad (\text{I.23})$$

This is the Laughlin wave function. It comprises an exponential part and a polynomial factor. The latter is usually referred as the Laughlin-Jastrow factor.

The Laughlin wave function is not a rigorous expression of the true ground-state wave function. But it turns out to be lower in its (variational) energy than other ground state candidates, such as the Wigner crystal [34]. The above state has a high overlap with the numerical ground state for small systems [34, 42], exceeding 99% in exact diagonalization calculation [43, 44] for the Coulomb potential. It is incompressible in the sense that it occupies the minimal area for  $\nu = 1/(2s + 1)$ . To see how it manifests the topological order, we present the quasihole wave function as an example to look at the fractional statistics. Since the power of  $z_i$  encodes the magnetic flux quanta encircled, a quasihole is created when the power of every electron is lifted up by 1 :

$$\Psi_{1/(2s+1)}^h = \prod_{i=1}^{N_e} (z_i - w) \Psi_{1/(2s+1)}, \quad (\text{I.24})$$

where  $w$  is the position of the hole. From this expression, every electron (situated at  $z_i$ ) experiences an extra zero at  $w$ . The physical intuition for fractional charge can be imagined as that, if we add  $2s + 1$  quasiholes at the same position

$$\prod_{i=1}^{N_e} (z_i - w)^{2s+1} \Psi_{1/(2s+1)}. \quad (\text{I.25})$$

This wave function is equivalent to adding another electron at  $w$  for the same  $\nu = 1/(2s + 1)$  Laughlin wave function. That is, the charge of three quasiholes is balanced by one electron, and each factor  $\prod_{i=1}^{N_e} (z_i - w)$  can be regarded as a fraction of  $e$ , a quasihole that carries  $-e/(2s + 1)$  charge. Intuitively, the statistical phase of the quasihole should also be one third of an electron. A more rigorous way is to write out the multi-quasihole wave function explicitly and adiabatically braid one quasihole around another. For two quasiholes at  $w_1$  and  $w_2$ , the wave function reads [23]

$$\Psi_{1/(2s+1)}^{2h} = \prod_{i,j=1}^{N_e} (z_i - w_1)(z_j - w_2)(w_1 - w_2)^{1/(2s+1)} \Psi_{1/(2s+1)}, \quad (\text{I.26})$$

where the factor  $(w_1 - w_2)^{1/(2s+1)}$  comes from the normalization. The statistical phase is given by the sum of the monodromy of the wave function and the Berry phase of the adiabatic evolution [23, 45]. For most trial wave functions, the Berry phase merely gives a geometric phase proportional to the area of the braiding process [46]. The statistic angle is read out directly from the wave function as  $\pi/(2s + 1)$

Such a fractional charge  $e/(2s + 1)$  in Laughlin states has been confirmed by experiments later after its proposition [47, 48, 49]. Further, when the Laughlin wave function is put on a torus, with the Laughlin-Jastrow factor replaced by an odd elliptic theta function, the ground state exhibits a  $2s + 1$  fold degeneracy confirmed by numerics [50] as well as by a mathematical proof [51] for an arbitrary Riemann surface, where the degeneracy is related to the genus  $g$  by  $(2s + 1)^g$ . All these properties support that the Laughlin wave function is a very good approximation to the true ground state and that both lie in the same universality class.

### I.3 Low-energy effective theory

The low-energy effective theory describes how the systems respond to external fields. In the case of quantum Hall problem, the most relevant external field is the electromagnetic field. It turns out that the effective theory in the leading order is a topological quantum field theory.

The electron density and the Hall conductance require the following response :

$$J^0 = -en_e = \frac{\nu e^2}{2\pi} \epsilon^{0ij} \partial_i A_j, \quad J^i = \frac{\nu e^2}{2\pi} \epsilon^{i\alpha\beta} \partial_\alpha A_\beta. \quad (\text{I.27})$$

The charge density and current density of charges can be obtained varying the Lagrangian according to Noether's theorem :

$$J^0 = \frac{\delta \mathcal{L}}{\delta A_0}, \quad J^i = \frac{\delta \mathcal{L}}{\delta A_i}. \quad (\text{I.28})$$

Since the charge is conserved,  $\partial_\alpha J^\alpha = 0$ , an auxiliary  $U(1)$  gauge field  $2\pi J^\alpha = \epsilon^{\alpha\beta\gamma} \partial_\beta a_\gamma$  can be introduced to represent charge and current density. Therefore according to Eq. (I.27) and Eq. (I.28) the lowest order effective theory is [52, 23] :

$$\mathcal{L} = -\frac{1}{4\pi\nu} \epsilon^{\alpha\beta\gamma} a_\alpha \partial_\beta a_\gamma + \frac{e}{2\pi} A_\alpha \epsilon^{\alpha\beta\gamma} \partial_\beta a_\gamma. \quad (\text{I.29})$$

If the external electromagnetic field is zero, we obtain the pure Chern-Simons action. The Chern-Simons theory is topological and is invariant under diffeomorphism of the manifold. This can be observed by the fact that metric does not enter the Lagrangian. Further, after performing the Legendre transformation, the Hamiltonian for the above theory vanishes [23], which means that there is no dynamics in this theory. This shows that the Chern-Simons theory is a topological field theory characterizing uniquely the ground state properties.

If solely the electromagnetic response is considered, integrating out  $a_\mu$  (under a gauge choice, for instance  $a_0 = 0$ ) one finds [25] :

$$\mathcal{L} = \frac{\nu e^2}{4\pi} \epsilon^{\alpha\beta\gamma} A_\alpha \partial_\beta A_\gamma. \quad (\text{I.30})$$

This is a Chern-Simons response theory in the external electromagnetic field.

So far we have introduced the wave functional and the Chern-Simons field theory approaches to the FQHE. They give good descriptions of the topological aspects in quantum Hall systems. But there are two points that may capture the reader's interests. First, the Laughlin wave function possesses a rotational symmetry, which should not be necessary for the existence of topological non-triviality. Second, both the wave function and Chern-Simons field theory are not straightforwardly related to the microscopic interaction. In the following two chapters we are going to address these issues.

# II – Geometric variational parameter and degrees of freedom

In this chapter we will focus on the geometric aspects in the fractional quantum Hall effect. The geometry plays an important role in understanding the small momentum excitation in FQHE [53, 54]. It also provides an example for phases sharing the same topological order but different symmetry [55, 56, 57]. We review Haldane’s original idea [58, 59] in Sec. II.1. Then the relation between the geometric degrees of freedom and two pairs of magneto-roton excitation is reviewed in Sec. II.2. Their relation to the Hall viscosity and static structure is included in the Sec. II.3.

## II.1 Geometry as a variational parameter in wave functions

As mentioned before, the Laughlin wave function is a trial wave function. But it does not possess any variational parameters. Indeed, the only variational parameter is the power of the Jastrow factor, which is eventually fixed by the filling factor  $\nu = 1/(2s + 1)$ . However in 2011 Haldane gave a new sight to this picture : he points out [59] that there can be a *hidden* parameter to be varied, the metric of the motion of the electrons. For the Laughlin wave function, we see that all electron orbitals are circular and have a well-defined angular momentum. However this is not a necessary requirement since the electron is free to follow any elliptical orbitals, as long as the enclosed surface remains unchanged because of the incompressibility. As there are two different degrees of freedom for each electron, the cyclotron motion and the guiding center motion, the two coordinates are allowed to follow different shapes of orbitals, as shown in Fig. II.1. Such a deformation of circular orbital is parametrized by a symmetric 2-tensor, which for convenience is called the metric of the corresponding motion. Also here one needs to pay attention to the definition of orbitals. Since the  $x$  components of  $\boldsymbol{\eta}$  and  $\mathbf{R}$  do not commute with their  $y$  counterparts, the orbitals are defined in their respective coherent Hilbert space. The real orbital of an electron is constructed by gluing the two coherent spaces carefully.

The two metrics of  $\boldsymbol{\eta}$  and  $\mathbf{R}$  come from different energy scales. For  $\boldsymbol{\eta}$ , if we impose a mass anisotropy, the ladder operators  $a, a^\dagger$  are no longer defined as in Eq. (I.15), since that definition does not transform the kinetic Hamiltonian into a harmonic oscillator. Assume now we have  $m_x \neq m_y$  (any anisotropic mass tensor can be transformed into this form by taking the principal axes of the tensor) :

$$H_k = \frac{\eta_x^2}{2m\alpha l^4} + \frac{\eta_y^2}{2(m/\alpha)l^4}, \quad (\text{II.1})$$



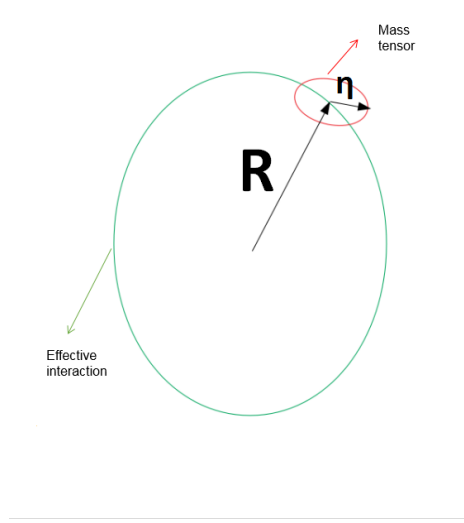


Fig. II.1 The orbitals of the cyclotron coordinate and of the guiding center of an electron. The shape of the cyclotron orbital is determined by the mass tensor while the shape of the guiding center orbital is determined by the effective interaction in the corresponding LL.

where  $\alpha^2 = m_y/m_x$  parametrizes the anisotropic mass ratio (notice from definition of  $\mathbf{\Pi}$  to  $\boldsymbol{\eta}$  the directions  $x$  and  $y$  are interchanged). In order to counterbalance the anisotropy, an easy short-cut is to rescale  $\eta_x$  and  $\eta_y$  via an area-preserving transformation, which does not affect their commutation rule. Therefore one can immediately see that the above Hamiltonian is transformed to a harmonic oscillator if the ladder operators now are defined as :

$$a = \frac{\eta_x}{\sqrt{2\alpha l}} + i \frac{\eta_y \sqrt{\alpha}}{\sqrt{2}l} \quad a^\dagger = \frac{\eta_x}{\sqrt{2\alpha l}} - i \frac{\eta_y \sqrt{\alpha}}{\sqrt{2}l}. \quad (\text{II.2})$$

From this expression, noticing that the ground state is an eigenstate of  $a^\dagger a$ , by computing the expectation value for  $\eta_x^2$  and  $\eta_y^2$  a metric for the cyclotron motion is defined as  $\text{diag}(1/\alpha, \alpha)$ .

For the guiding center  $\mathbf{R}$ , its metric relies on the intra-Landau level physics, i.e. the effective interaction. To see this more concretely, we need another definition of Laughlin states. Although the Laughlin function is not the eigenstate of the Coulomb interaction, it is characterized by another set of hard-core interactions. As noticed before, in the Laughlin state for  $\nu = 1/(2s+1)$ , when two electrons  $i$  and  $j$  come closer, the wave function vanishes at a speed no slower than  $(z_i - z_j)^{2s+1}$ . In this isotropic case, the power is proportional to the angular momentum. This means that every pair of electrons in the Laughlin state carries a relative angular momentum no lower than  $2s+1$ . So for a hard-core repulsion acting on a closer range, the Laughlin wave function gives a zero energy. In fact, the Laughlin state is the unique zero-energy eigenstate of the Haldane pseudopotentials : [60]

$$H_{model} |\Psi_{1/(2s+1)}\rangle = 0, \quad (\text{II.3})$$

$$H_{model} = \sum_{i,j,m}^{m < 2s+1} V_m^H P_m^{ij}, \quad (\text{II.4})$$

$$P_m = \sum_{ij} P_m^{ij} = \frac{1}{N_\phi} \sum_{\mathbf{q}} L_m(q^2 l^2) e^{-(1/2)q^2 l^2} \bar{\rho}(\mathbf{q}) \bar{\rho}(-\mathbf{q}), \quad (\text{II.5})$$

where  $i$  and  $j$  are summed over all pairs of electrons and  $P_m^{ij}$  is a projector to the state of relative angular momentum  $m$  for the electron pair  $(i, j)$ . The expression  $L_m$  is the Laguerre polynomial and  $V_m^H > 0$  are Haldane's pseudopotentials. The first-quantized projector  $P_m$  is a two-body translationally invariant potential. Acting on each pair of electrons, it is nonzero only for the states with relative angular momentum  $m$ .

In the above definition for Haldane's pseudopotentials, the equipotential contour is still circular, as it only depends on  $q^2$ . Meanwhile like the shape of the cyclotron motion this potential is free to deform. A simple way is to extend  $q^2$  to a general quadratic form in  $q_a$  with a symmetric tensor  $q_a \bar{g}^{ab} q_b$  (we use Einstein summation convention), and  $\bar{g}^{ab}$  encodes the stretching and orientation of the circular equipotential contour. This procedure generalizes the relative angular motion between each pair of electrons, deforming the circular orbitals into elliptical ones. Since we only want to change the shapes while keeping the area of the orbital (this can preserve the requirement that each electron must occupy a minimal area of  $2\pi l^2$  Eq. (I.12)), we demand  $\det \bar{g} = 1$ . Then we have the deformed Laughlin wave states according to :

$$P_m(\bar{g})|\Psi_{1/(2s+1)}(\bar{g})\rangle = 0, \quad m < 2s + 1 \quad (\text{II.6})$$

$$P_m(\bar{g}) = \frac{1}{N_\phi} \sum_{\mathbf{q}} L_m(q_a q_b \bar{g}^{ab} l^2) e^{-(1/2)q_a q_b \bar{g}^{ab} l^2} \rho_{\mathbf{q}} \rho_{-\mathbf{q}}. \quad (\text{II.7})$$

The metric  $\bar{g}$  is the guiding-center metric, counterpart of the cyclotron metric.

Now we look at what roles those metrics play in real systems. Let us assume that we have two anisotropies, the mass tensor  $m_{ab}$  and the dielectric tensor  $\epsilon^{ab}$ <sup>1</sup> :

$$H = \sum_i \frac{1}{2m_{ab}} \Pi_{ia} \Pi_{ib} + \frac{1}{2} \sum_{\mathbf{q}} \rho(\mathbf{q}) v_{\bar{g}}(\mathbf{q}) \rho(-\mathbf{q}), \quad (\text{II.8})$$

$$v_{\bar{g}}(\mathbf{q}) = \frac{e^2}{(\epsilon^{ab} q_a q_b)^{-1/2}}. \quad (\text{II.9})$$

First as we know the cyclotron metric is fixed by the mass tensor. This introduces an anisotropic form factor after projection to the LLL. In this case the family of wave functions corresponding to different  $\bar{g}$  can be regarded as a family of trial wave functions with  $\bar{g}$  the variational parameter. In order to find the optimal state, one computes the expectation values of the Hamiltonian for this family of variational wave functions and picks up the one with the lowest energy. The ground state of this more generalized anisotropic FQHE Hamiltonian is therefore found. The motion of the cyclotron coordinates is deformed by  $m_{ab}$  while the guiding-center orbitals are perturbed by both  $m_{ab}$  and  $\epsilon_{ab}$ . In the original case of no deformation, the Hamiltonian (I.1) can be viewed as choose both  $m_{ab}$  and  $\epsilon_{ab}$  to be proportional to  $\delta^{ab}$ . In this case, the Laughlin wave function (of metric  $\delta^{ab}$ ) Eq. (I.23) is known to approximate the true ground state best. The isotropic  $\bar{g}^{ab} = \delta^{ab}$  solution is the optimal one among the family of Laughlin states  $|\Psi_{1/(2s+1)}(\bar{g})\rangle$ . When the mass tensor and the dielectric tensor are anisotropic but equal, one can transform the effective interaction back to an isotropic one via a coordinate transformation. The choice of  $\bar{g} = \epsilon$  will give a Laughlin wave function which is isotropic in an orthogonally transformed coordinate. When  $(m_{ab})^{-1} \neq \epsilon^{ab}$ , there is an intrinsic anisotropy in the effective interaction. The optimal wave

---

1. The dielectric tensor  $\epsilon^{ab}$  should not be confounded with the Levi-Civita symbol used later.

function will take a  $\bar{g}$  between the mass tensor and the dielectric tensor. From here, we can regard the metric as a hidden variational parameter.

In experiments, such a geometrical variational parameter can actually be probed. For half-filled quantum Hall states, it was suggested that a gapless Fermi liquid state under zero effective magnetic field appears [61]. This Fermi liquid state reacts to anisotropy similarly to the above mentioned gapped states. The Fermi surface is distorted under external anisotropy and can be measured with commensurability oscillations in the magnetoresistance (geometric resonance) [62, 63, 64, 65, 66, 67], where the sample is under a periodic unidirectional potential. By adding an additional magnetic field to the Fermi liquid, a minimum in the magnetoresistance appears when the cyclotron radius of the fermions is equal to the periodicity of the unidirectional potential. Therefore the corresponding Fermi vector can be obtained. In those experiments, it is found that the Fermi surface will adapt to the anisotropy introduced to the quantum Hall system, manifesting a variational geometry.

## II.2 Spectrum analysis : spin-2 degrees of freedom in low momenta

After the ground-state properties in FQHE have been studied, the excitation spectrum of FQHE becomes an interesting direction, as this is related to the incompressibility. It is known that FQH states exhibit anyonic excitations, which derive from the intrinsic topological order. But the incompressibility is related to the collective excitation gap. The robustness of this gap is highly relevant to the nematic phase transition [68], which we will further discuss in Sec. V. In a single-mode approximation (SMA), Girvin, MacDonald, and Platzman [69, 41] obtained very good results for small and intermediate momenta. Later the composite fermion picture [70] was used to compute the collective excitation. And more recently, with the help of Jack polynomials [71], model wave functions [54] for excited states have been proposed, which reveal the quadrupole structure near  $\mathbf{q} \sim 0$ .

The SMA is based on the fact that the ground state is a uniform liquid state where single-body excitations are gapped. Therefore the lowest-energy excitations are long-wave-length density oscillations [72], the collective excitations. The presumed excited state is created with the help of the density operator, which in FQHE regime is the projected density :

$$|\Psi_{\mathbf{q}}\rangle = C\bar{\rho}(\mathbf{q})|\Psi_{Laughlin}\rangle, \quad (\text{II.10})$$

where  $C$  is a normalization constant. The excitation energy is given by the expectation of the Hamiltonian under this trial state. So the lowest spectrum is obtained through :

$$E(\mathbf{q}) = \frac{\bar{f}(\mathbf{q})}{\bar{s}(\mathbf{q})} = \frac{\langle\Psi_{Laughlin}|\bar{\rho}(-\mathbf{q})H^p\bar{\rho}(\mathbf{q})|\Psi_{Laughlin}\rangle}{\langle\Psi_{Laughlin}|\bar{\rho}(-\mathbf{q})\bar{\rho}(\mathbf{q})|\Psi_{Laughlin}\rangle}, \quad (\text{II.11})$$

where  $\bar{s}(\mathbf{q})$  is the projected static structure factor to divide out the normalisation constant, and  $\bar{f}(\mathbf{q})$  is the projected oscillator strength. Their normalizations are usually given as :

$$\bar{f}(\mathbf{q}) = \frac{1}{N_e}\langle\bar{\rho}(-\mathbf{q})H^p\bar{\rho}(\mathbf{q})\rangle, \quad \bar{s}(\mathbf{q}) = \frac{1}{N_e}\langle\bar{\rho}(-\mathbf{q})\bar{\rho}(\mathbf{q})\rangle. \quad (\text{II.12})$$

In order to get the low-momentum behaviour of the spectrum, the oscillator strength and static structure factor are studied through expansion in powers of  $\mathbf{q}$ . Kohn's theorem [73] shows that the  $q^2$  power in the oscillator strength is saturated by the inter-LL cyclotron

mode. Therefore the leading order in the projected oscillator strength is  $q^4$ , and so does the static structure  $\bar{s}$  via a similar argument based on sum rules [74, 41, 27]. The leading order expansion of  $\bar{s}$  in the isotropic Laughlin wave function is found to be [41] :

$$\bar{s}(q) = \frac{1-\nu}{8\nu}q^4 + \dots \quad (\text{II.13})$$

It turns out that this coefficient has a very close relationship with geometric properties, which we will review in Sec. II.3.2.

As both the projected oscillator strength  $\bar{f}(\mathbf{q})$  and the projected static structure factor behave as  $k^4$  in the small momentum limit, there is a direct gap at  $\mathbf{q} = 0$ . This gap was also observed experimentally by inelastic light scattering measurements [75]. For  $\nu = 1/3$ , there is a minimum in the spectrum at around  $ql \sim 1.2$ . This is regarded as the lowest magneto-roton mode with frequency  $\Omega_r$ . When  $\mathbf{q}$  becomes further smaller, the spectrum gradually raises to roughly twice of the magneto-roton minimum,  $E(\mathbf{q})|_{\mathbf{q} \rightarrow 0} > 2\Omega_r$ . In this case, if two magneto-rotors at  $\Omega_r$  are excited with momenta in opposite directions with a small total momentum, the total energy is an adjustable variable from  $2\Omega_r$ . This process certainly contributes to the oscillator strength for  $\mathbf{q} \sim 0$ . As a consequence, there is a magneto-roton continuum in the small momentum regime. Since a single magneto-roton has a dipole structure (which is seen explicitly when writing  $\bar{\rho}(\mathbf{q})$  in the Landau gauge in our later computation), this continuum is characterized by a quadrupole structure, which was also confirmed by the inelastic light scattering measurements as the two-photon process is more sensitive to a quadrupolar than a dipolar excitation [75]. It is tempting to compare the quadrupole in FQHE to the gravitational degrees of freedom [53], which is spin-2 in nature and the perturbation brought by a gravitational wave is also quadrupolar. This conjecture is more clearly manifested in the Jack polynomial representation for the lowest excited states in FQHE model wave functions [71]. Such a comparison inspires to identify the low-momentum collective excitation in FQHE as a geometric degree of freedom. Moreover, Ref. [53] suggests that this degree of freedom can be probed by a surface acoustic wave, which induces a strain in the sample and thus modifies its geometry.

Since a spin-2 degree of freedom describes a quadrupolar fluctuation in the space, we need to figure out how such an interpretation can be built locally. In the next section, we will present how a local geometric characteristic naturally emerges from the definition of the Hall viscosity of quantum Hall systems.

## II.3 Hall viscosity and static structure factor

This section is meant to give an interpretation of the metric from a local point of view [59]. Especially its connection to the Hall viscosity and the projected static structure factor.

In quantum Hall systems, the presence of magnetic field leads to the non-commutation between the  $x$ -component and  $y$ -component of the coordinate. In this sense, the two components serve as the generator of translation for each other. This permits a further extension to express the deformation group in terms of the two components of the coordinate. Such a deformation group has a manifest physical observable, the Hall viscosity. To begin with, we start from the elastic theory. The elastic theory focuses on the response under a strain tensor  $u_{ab}$  :

$$x_a \rightarrow x_a + u_a(x, t), \quad u_{ab} = \frac{1}{2} \left( \frac{\partial u_a}{\partial x_b} + \frac{\partial u_b}{\partial x_a} \right). \quad (\text{II.14})$$

Under external strain, the system exhibits a stress tensor  $\sigma_{ab} = \partial E / \partial u_{ab}$  [76]. It can be expanded in terms of the stress tensor as :

$$\sigma_{ab} = - \sum_{cd} \lambda_{abcd} u_{cd} - \sum_{cd} \eta_{abcd} \frac{\partial u_{cd}}{\partial t}. \quad (\text{II.15})$$

The coefficient  $\lambda_{abcd}$  in the first term is the elasticity module tensor. The second part related to the time derivative of the strain tensor involves a viscous tensor. The symmetric part of it describes the dissipation while the anti-symmetric part is non-dissipative. This anti-symmetric viscosity tensor is transverse like the Hall conductivity. So it is always called the Hall viscosity. According to the symmetry of the strain tensor and its definition, the Hall viscosity is anti-symmetric for the two pairs of indices and symmetric for the first two indices and the last two indices. It admits a decomposition into a rank-2 tensor :

$$\eta_H^{abcd} = \frac{1}{2} \left( \varepsilon^{ac} \eta_H^{bd} + \varepsilon^{ad} \eta_H^{bc} + a \leftrightarrow b \right). \quad (\text{II.16})$$

The Hall viscosity can only emerge when both time reversal symmetry and parity are broken. This is because it is odd under time reversal (by definition) and reflection of space (by symmetry, three of its four indices must be the same). Further, the strain tensor has a close relation with the metric of the system, as  $dx_a \rightarrow dx_a + \partial_b u_a dx_b$ . Assuming now we have an isotropic metric  $\delta^{ab}$ , it transforms under strain according to

$$\delta_{ab} dx_a dx_b \rightarrow \delta_{ab} (dx_a + \partial_c u_a dx_c) (dx_b + \partial_d u_b dx_d) = (\delta_{ab} + 2u_{ab}) dx_a dx_b, \quad (\text{II.17})$$

where in the second equality we drop higher order terms in the displacement field so  $\delta g_{ab} = 2u_{ab}$ . Thus we see that the response to the strain tensor has an interpretation in terms of a response to a perturbation of metric. Here we do not distinguish the lower and upper indices since we have an isotropic metric. A more general case can be defined with the help of the vierbein or frame field.

### II.3.1 Hall viscosity for FQHE trial states

In this subsection, we review the Hall viscosity formulae found by Park and Haldane [77]. It describes the Hall viscosity for the family of variational Laughlin wave functions introduced in Eq. (II.6).

The Hall viscosity in quantum Hall systems was first recognized by Avron, Seiler and Zograf [26] in the integer quantum Hall effect. They find that the Hall viscosity takes the following form for  $\nu = N$  IQHE :

$$\eta_H^{ab} = \frac{\hbar \delta^{ab}}{2\pi l^2} \sum_{n=0}^{N-1} s_n, \quad (\text{II.18})$$

where  $s_n = (2n + 1)/2$  is the contribution from LL  $n$  and called as the cyclotron spin by Haldane. This Hall viscosity was found by putting the system on a torus. It can be regarded as an analogue to the Hall conductance. On a torus, the magnetic flux threading through the two cycles gives two flux quanta  $\phi_a, \phi_b$ . The ground state is a wave function with  $\phi_a, \phi_b$  as parameters. The Hall conductance is given as the integral of the Berry curvature with respect to these two flux quanta. On the other hand, the Hall viscosity turns out to be related to the

Berry curvature of the shear ratio, a complex number describing the angle and the relative length of the two periods of a torus, as shown in Ref. [26]. In the case of Hall viscosity, the parameter space of the shear ratio is the fundamental region of the group  $SL(2, \mathbb{Z})$ . The integral of the Berry curvature is done therefore on this open and non-compact space. Hence unlike the Hall conductance the Hall viscosity is *not* quantized in terms of an integer.

Now we turn to the definition of Hall viscosity on a more general geometric setting. In this case, the Hall viscosity should be regarded as the response under a time-dependent displacement perturbation  $u^a(x, t)$ . The stress tensor should be generalized to the canonical energy-momentum tensor [78] :

$$T_b^a = \frac{\delta S}{\delta(\nabla_a u^b)}, \quad (\text{II.19})$$

where  $S$  is the action of the system and  $\nabla$  is the covariant derivative. The Hall viscosity is the odd part of the coefficient in front of the time-derivative term in the expansion of the displacement field :

$$T_b^a = \eta_b^a{}^c{}_d \partial_0 \nabla_c u^d. \quad (\text{II.20})$$

By definition of odd viscosity,  $\eta_b^a{}^c{}_d$  is odd under the interchange  $ab \leftrightarrow cd$ . As the system is assumed to be static and there is no space-time mixing, the time derivative does not need to take the covariant form. Under the elastic field, the metric of the system changes as

$$\delta g_{ab} = g_{ac} \nabla_b u^c + g_{cb} \nabla_a u^c. \quad (\text{II.21})$$

Usually the upper-index canonical energy-momentum tensor  $T^{ab} = T_c^a g^{bc}$  is not symmetric with respect to its two indices, for example in the presence of torsion [79]. But if one assumes that the displacement field does not introduce a rotation of the system, i.e.

$$g^{ac} \nabla_c u^b - g^{bc} \nabla_c u^a = 0, \quad (\text{II.22})$$

only the symmetric part of the energy momentum tensor  $T^{ab}$  needs to be taken into account. Then the above perturbation to the metric translates to the relation :

$$\delta S = \int d^d x \sqrt{-g} T_b^a \delta \nabla_a u^b = \frac{1}{2} \int d^d x \sqrt{-g} T^{ab} \delta g_{ab}, \quad (\text{II.23})$$

where  $\sqrt{-g}$  is the square root of the minus determinant  $-g$  of the space-time metric tensor (with the time component taking a negative length). This is the common definition of the energy-momentum tensor in general gravity (notice  $\delta g^{ab} = -g^{ac} g^{bd} \delta g_{cd}$ ).

The indices of the Hall viscosity with all indices raised can be defined as :

$$\eta_H^{abcd} = \eta_e^a{}^c{}_f \varepsilon^{be} \varepsilon^{df}. \quad (\text{II.24})$$

It can be verified that the indices of  $\eta_H^{abcd}$  have the symmetry as in the introduction of this section for a gapped incompressible system [78].

In quantum Hall systems, as the  $x$ -component of the coordinate does not commute with the  $y$ -component, one can define the area-preserving deformation (APD) operators with the coordinates themselves. Take the guiding center coordinate as an example. The operators  $\Lambda^{ab}$  are generators of the area-preserving deformations

$$\Lambda^{ab} = \frac{1}{4l^2} \sum_i \{R_i^a, R_i^b\} = \frac{1}{4l^2} \sum_i (R_i^a R_i^b + R_i^b R_i^a). \quad (\text{II.25})$$

Those generators satisfy the algebra  $sl(2, \mathbb{R})$  :

$$[\Lambda^{ab}, \Lambda^{cd}] = -\frac{i}{2} \left( \varepsilon^{ac} \Lambda^{bd} + \varepsilon^{ad} \Lambda^{bc} + \varepsilon^{bc} \Lambda^{ad} + \varepsilon^{bd} \Lambda^{cd} \right). \quad (\text{II.26})$$

Similarly, the area-preserving deformation generators for the cyclotron coordinates are defined as  $\tilde{\Lambda}^{ab} = \sum_i \{\eta_i^a, \eta_i^b\} / 4l^2$ . The area-preserving deformation operators are defined by exponentiating the generators :

$$U^R(\alpha) = \exp \left( i \alpha_{ab} \Lambda^{ab} \right), \quad U^\eta(\alpha) = \exp \left( i \alpha_{ab} \tilde{\Lambda}^{ab} \right) \quad (\text{II.27})$$

This is a unitary operator. Since  $\Lambda^{ab}$  is symmetric,  $\alpha$  is also a symmetric tensor. Now we need to see how these operators produce an area-preserving deformation. For this purpose, we need to define a quadratic form in guiding-center/cyclotron coordinates, analogous to how a common metric is used to define distance. For guiding centers, a natural quadratic form is  $g_{ab} R_i^a R_i^b$ . Besides this, a more useful quadratic form of guiding centers is the relative guiding center rotation generator between an electron  $i$  and an electron  $j$  :

$$L_{ij} = \frac{1}{8l^2} g_{ab} \{ R_i^a - R_j^b, R_i^b - R_j^a \}. \quad (\text{II.28})$$

In the isotropic case, where  $g_{ab} = \text{diag}(1, 1)$ , the operator transforms to  $L_{ij} = b^\dagger b + 1/2$ , where  $b, b^\dagger$  are the relative guiding-center-coordinate ladder operator as in Eq. I.15. Compared to Eq. (I.16) the operator  $L_{ij}$  has the interpretation of the relative angular momentum in rotationally invariant system.

Now we apply the APD operators to the quadratic form  $L_{ij}$ . This changes the metric of the relative guiding center rotation generator :

$$L_{ij}(g') = U^\dagger(\alpha) L_{ij}(g) U(\alpha). \quad (\text{II.29})$$

When  $\alpha$  is infinitesimal, the change of the metric is :

$$\delta g_{ab} = g_{ac} \varepsilon^{cd} \alpha_{db} + a \leftrightarrow b. \quad (\text{II.30})$$

We can see that this deformation indeed preserves the area. If we put the deformation around the isotropic metric  $g_{ab} = \delta_{ab}$ , the area element changes according to

$$\delta \det g = 2 \delta_{ac} \varepsilon^{cd} \alpha_{da} = 2 \varepsilon^{ad} \alpha_{db} = 0, \quad (\text{II.31})$$

where we only use the spatial parts of the metric here and in the last equality we use the symmetry  $\alpha_{ab} = \alpha_{ba}$ . Comparing the deformation expression Eq. (II.30) to Eq. (II.21), one can identify the displacement field with the parameter  $\alpha_{ab}$  as

$$\nabla_a u^b = \varepsilon^{bc} \alpha_{ac}. \quad (\text{II.32})$$

With these identification, we can compute the Hall viscosity easily via linear response theory with respect to variation of  $\alpha_{ab}$ .

According to the above discussion, one can calculate the Hall viscosity contribution from the cyclotron coordinate and the guiding-center coordinate respectively. The time-dependent perturbation of the metric in the state  $|\Psi(g(t))\rangle$  can be realized by applying the above defined

APD operators with time-dependent  $\alpha(t)$ . According to the Hellmann–Feynman theorem, there is a generalised force given by [26, 77, 80] :

$$F^{ab} = - \left\langle \Psi(g(t)) \left| \frac{\partial H}{\partial \alpha} \right| \Psi(g(t)) \right\rangle = - \frac{\partial E_G(g)}{\partial \alpha_{ab}} \Big|_{\alpha=0} + \Gamma^{abcd} \dot{\alpha}_{cd}, \quad (\text{II.33})$$

where  $E_G(g)$  is the energy for state  $|\Psi(g)\rangle$ . The second term is a viscosity term and its expression is found through the adiabatic theorem [26, 77] :

$$\Gamma^{abcd} = -i \langle \Psi | [\Lambda^{ab}, \Lambda^{cd}] | \Psi \rangle. \quad (\text{II.34})$$

According to previous discussion on  $\alpha$  and the displacement field, the Hall viscosity is therefore identified as the  $\Gamma^{abcd}$  per area :

$$\eta_H^{abcd} = -\frac{1}{A} \Gamma^{abcd} = \frac{1}{2\pi l_B^2} \frac{i}{N_\Phi} \langle \Psi | [\Lambda^{ab}, \Lambda^{cd}] | \Psi \rangle, \quad (\text{II.35})$$

where  $N_\Phi$  is the flux number. The tensor  $\eta_H^{abcd}$  is anti-symmetric under  $(ab) \leftrightarrow (cd)$  and symmetric under  $a \leftrightarrow b$  and  $c \leftrightarrow d$ . The reduced Hall viscosity tensor is as defined previously and is given as

$$\eta_H^{abcd} = \frac{1}{2} \left( \varepsilon^{ac} \eta_H^{bd} + \varepsilon^{ad} \eta_H^{bc} + a \leftrightarrow b \right), \quad \eta_H^{ab} = \frac{1}{2\pi l_B^2} \frac{1}{N_\Phi} \langle \Psi | \Lambda^{ab} | \Psi \rangle \quad (\text{II.36})$$

For trial wave functions  $\langle \Psi | \Lambda^{ab} | \Psi \rangle$  are available through the help of Jack polynomials. As an example, as to those  $|\Psi_{1/q}(\bar{g})\rangle$  defined in Eq. (II.6), it is possible to show that the state is an eigenstate of the  $L_{ij}(\bar{g})$  generator. The expectation value of the APD generator takes the form

$$\langle \Psi_{1/q}(\bar{g}) | \Lambda^{ab} | \Psi_{1/q}(\bar{g}) \rangle = \frac{1}{2} \bar{g}^{ab} \left( \frac{1}{2} N_e N_\phi + s N_e \right). \quad (\text{II.37})$$

The first super-extensive term  $\sim N_e N_\phi$  is due to the uniform background electron density and should be removed when considering correlated contribution. The second extensive term comes from the internal correlation of the state. It is extensive over the number of electrons, denoted as the regularised contribution :

$$\langle \Psi_{1/q}(\bar{g}) | \delta \Lambda^{ab} | \Psi_{1/q}(\bar{g}) \rangle = \frac{1}{2} \bar{g}^{ab} s N_e. \quad (\text{II.38})$$

For Laughlin states  $\nu = 1/q$ , the number  $s$  is a kind of correlated spin and is given as  $s = (1 - q)/2$ . So the Hall viscosity from the guiding center part is

$$\eta_H^{ab} = \frac{1}{4\pi l^2} s \nu \bar{g}^{ab}. \quad (\text{II.39})$$

Here we see that the guiding center metric defined through the trial wave function manifests itself in the expression for the Hall viscosity.

A similar expression can be found for cyclotron coordinates :

$$\tilde{\eta}_H^{ab} = -\frac{\hbar}{2\pi l^2} \frac{1}{N_\Phi} \langle \Psi | \tilde{\Lambda}^{ab} | \Psi \rangle = -\frac{1}{4\pi l^2} \nu \tilde{s} \tilde{g}^{ab}, \quad (\text{II.40})$$



where  $\tilde{s} = s_n$  is the cyclotron spin in the relevant LL, as shown below Eq. (II.18). In contrast to the guiding center viscosity, the Landau level viscosity does not need regularization as the expectation value of  $\tilde{\Lambda}^{ab}$  is already proportionally to  $N_e$ . The total viscosity is given by the sum  $\eta_H + \tilde{\eta}_H$ . For filling  $\nu = p/q$ , if the two metrics equal  $\bar{g} = \tilde{g} = g$  the result is [77] :

$$|\eta_H + \tilde{\eta}_H| = \frac{1}{4\pi l_B^2} \nu |\tilde{s} - s| g^{ab}, \quad (\text{II.41})$$

which agrees with Read's conformal field theory result [46].

Notice, in the above definition, that the metric  $g_{ab}$  for the guiding center is a constant. However, as it is defined through the APD generator, it can be promoted to a local quantity if one gives APD generator a coordinate dependence. This is natural when the state considered is excited and not uniform in space. This dependence is easily done by noticing that the origin of the guiding-center operator is by default set to  $\mathbf{r} = 0$ . The guiding center in a general coordinate frame is  $\mathbf{R} - \mathbf{r}$ , with  $\mathbf{r}$  the origin of the frame. The APD generator thus gains a coordinate dependence

$$\Lambda^{ab}(\mathbf{r}) = \frac{1}{4l^2} \sum_i \{R_i^a - r^a, R_i^b - r^b\}. \quad (\text{II.42})$$

This APD generator is to deform the guiding center coordinate relative to a spatial point  $\mathbf{r}$ . A local metric is defined with the help of this APD generator as :

$$\frac{1}{2} s \bar{g}(\mathbf{r}) = \frac{1}{N_e} \langle \Psi | \delta \Lambda^{ab}(\mathbf{r}) | \Psi \rangle. \quad (\text{II.43})$$

This metric serves as a measurement of the local quadruple deformation [59, 81]. Its fluctuation is suggested as the geometric degrees of freedom in incompressible FQHE states [59].

Based on the above discussion, how to use the above local metric to describe the dynamics of FQHE is being searched in recent years. An effective bimetric theory [82] is proposed to capture the lowest energy excitation of quantum Hall systems. In this theory there is a metric describing the static anisotropic quantum Hall fluid configuration and a metric describing the dynamical fluctuating geometric degrees of freedom. It gives prediction verified numerically [83] under geometric quench process. Moreover a hydrodynamic effective theory [84] based on Dirac composite fermions [85] is constructed recently with a tensor gauge field characterizing the geometric degrees of freedom. All of these effective theory points out that Haldane's geometric dynamics is unveiled naturally in quantum Hall systems. It will be interesting to investigate how those effective theory may emerge from the microscopic interaction.

### II.3.2 Geometry and the static structure factor

From the algebra of guiding-center coordinates, Haldane [58] finds a bound on the coefficient of  $q^4$  term in the expansion of the projected static structure factor  $\bar{s}(\mathbf{q})$ .

According to Kohn's theorem and a series of sum rules, the  $q^2$  contribution to the static structure factor is saturated by the cyclotron mode, the leading term after projection to the lowest Landau level is  $q^4$  :

$$\langle \delta \bar{\rho}_e(\mathbf{q}) \delta \bar{\rho}_e(-\mathbf{q}) \rangle \sim q^4 l^4, \quad q \rightarrow 0, \quad (\text{II.44})$$

where  $\delta\bar{\rho}_e = \bar{\rho}_e - \langle\bar{\rho}_e(\mathbf{q})\rangle$  is the regularized projected density. The expectation value of the density operator is the uniform one  $\langle\bar{\rho}_e(\mathbf{q})\rangle = \nu\delta(\mathbf{q}l)/2\pi$ . In the first quantization formalism, the projected density is given by  $\bar{\rho}_e(\mathbf{q}) = \sum_i \exp(-i\mathbf{q} \cdot \mathbf{R}_i)$ . Expanding this expression in powers of  $\mathbf{q}$ , the static structure factor has the following expansion in long wavelength :

$$\bar{s}(\mathbf{q}) = \frac{1}{N_e} \langle\delta\bar{\rho}(\mathbf{q})\delta\bar{\rho}(-\mathbf{q})\rangle = C_2^{ab}l^2q_aq_b + C_4^{abcd}l^4q_aq_bq_cq_d + \dots, \quad q \rightarrow 0. \quad (\text{II.45})$$

The coefficients  $C_2^{ab}$  and  $C_4^{abcd}$  are :

$$C_2^{ab} = \frac{1}{N_e l^2} \sum_{ij} \langle R_i^a R_j^b \rangle, \quad C_4^{abcd} = \frac{1}{N_e} \left( \frac{1}{2} \langle \{ \Lambda^{ab}, \Lambda^{cd} \} \rangle - \langle \Lambda^{ab} \rangle \langle \Lambda^{cd} \rangle \right). \quad (\text{II.46})$$

The observation is that  $\sum_i R_i^a$  is a translation generator for the mass center of the system, due to the non-communicative  $x$ - and  $y$ -directions. If the ground state is translation invariant, it is annihilated by the translation generator  $\sum_i R_i^a |\Omega\rangle = 0$ . Therefore the  $q^2$  contribution vanishes in (II.45), which is in accordance with Kohn's theorem. The coefficient  $C_4^{abcd}$  can be combined with an anti-symmetric tensor  $\Gamma_A^{abcd} = -i\langle [\Lambda^{ab}, \Lambda^{cd}] \rangle / (2N_e)$  to form a covariance matrix, which is Hermitian and semi-positive definite :

$$C_4^{abcd} + i\Gamma_A^{abcd} = \frac{1}{N_e} \left( \langle \Lambda^{ab} \Lambda^{cd} \rangle - \langle \Lambda^{ab} \rangle \langle \Lambda^{cd} \rangle \right) \geq 0 \text{ for the pair indices } \{ab\}, \{cd\}. \quad (\text{II.47})$$

According to what we show in the last section, the tensor  $\Gamma_A^{abcd}$  is symmetric with respect to  $ab$  and  $cd$  respectively and anti-symmetric for  $ab \leftrightarrow cd$ . It has the following decomposition for  $\nu = p/q$  :

$$\Gamma_A^{abcd} = -\frac{\pi l^2}{2\nu} \left( \varepsilon^{ac} \eta_H^{bd} + \varepsilon^{ad} \eta_H^{bc} + \varepsilon^{bc} \eta_H^{ad} + \varepsilon^{bd} \eta_H^{ac} \right) = \frac{s}{8\nu} \left( \varepsilon^{ac} g^{bd} + \varepsilon^{ad} g^{bc} + \varepsilon^{bc} g^{ad} + \varepsilon^{bd} g^{ac} \right). \quad (\text{II.48})$$

If the ground state is an eigenstate of  $L(g)$ , the tensor  $C_4^{abcd}$  takes the form [58] :

$$C_4^{abcd} = \frac{1}{4} \kappa \left( g^{ac} g^{bd} + g^{ad} g^{bc} - g^{ab} g^{cd} \right). \quad (\text{II.49})$$

By writing out the explicit form of  $C_4^{abcd}$  and  $\Gamma_A^{abcd}$  (which are  $4 \times 4$  matrices), the semi-positive definite property requires  $|\kappa| \geq |s|/\nu$ . This gives rise to a bound on the coefficient of the  $q^4$  term in the expansion of the static structure factor. As the guiding-center spin  $s$  is related to the Hall viscosity, this bound can be viewed as that the coefficient must be ‘‘larger’’ than the viscosity. The Laughlin states for  $\nu = 1/q$  and More-Read states for  $\nu = 1/2$  saturate this bound [58]. For the Laughlin state  $\nu = 1/q$ , the bound is  $\kappa \geq (q-1)/2$ . However, in the appendix A, we will show that the result of the Hamiltonian theory violates it. This indicates that the Hamiltonian theory does not take into account all degrees of freedom in the projected single LL space.

This bound is also proposed in a paper by Golkar, Nyuyen and Son [86] within a field theory approach. Upon using the Dirac formalism for LLL, it is further proved that the inequality becomes an equality for all model interactions (Laughlin, Moore Read and Parafermions) [87]. From here, we see that geometric quantity, such as the Hall viscosity, also enters correlation functions. It dictates the small- $q$  behaviour of the static structure factor.



# III – Composite Fermions and Hamiltonian theory

Considering only the kinetic energy, inside each LL, there is a large degeneracy for the many-body state when the filling factor is a fractional number. But in FQHE experiments only a unique ground state is observed. Therefore for FQHE one cannot neglect the Coulomb repulsion and the unique ground state is determined by the interaction and the GMP algebra. The similar phenomenology of Hall conductance and longitudinal conductance in FQHE and in IQHE has led some people to link them together. One strategy is to perform the flux attachment, attaching magnetic flux to each electron [88, 89] and form composite particles. The attached magnetic flux is chosen to be opposite to the external magnetic field and thus the composite particle feels a weaker one. At special fillings a mean field theory is obtained as an integer quantum Hall effect for these composite particles. In this chapter we review Shankar and Murthy's Hamiltonian theory of the FQHE [74]. After a brief presentation of the Chern-Simons transformation in Sec. III.1, the composite fermion operator as a composite particle that consists of an electron operator and a vortex operator is discussed in Sec. III.2. Section III.3 is then devoted to a microscopic theory that provides a consistent composite fermion picture in the small wave-vector limit.

## III.1 Composite fermion transformation

The idea of connecting FQHE with IQHE comes from the observation of the wave function. Take the Laughlin wave function at  $\nu = 1/3$  as an example. The wave function can be viewed as a  $\nu = 1$  quantum Hall wave function  $\prod_{i < j} (z_i - z_j) \exp(-\sum_i |z_i|^2/4l^2)$  times a prefactor  $\prod_{i < j} (z_i - z_j)^2$ . Fixing a  $j$ , each factor  $\prod_i (z_i - z_j)$  has a physical interpretation. It is a common zero for all other electrons except  $j$ . In polar coordinate the angle dependence  $\exp(i\theta_{ij})$ , where  $\theta_{ij} = \arg(z_i - z_j)$ , manifests a winding phase  $2\pi$  at  $z_j$ , which is a vortex centered at  $z_j$ . So one sees that the collective configuration of electrons is able to construct a vortex on top of the electrons themselves. On the other hand, the vortex carries magnetic flux opposite to the external one. The flux attached to each electron hence effectively screens the magnetic field seen by the electrons. For the Laughlin state, each vortex carries  $1/3$  external magnetic flux, according to the ratio between the electron density and the magnetic flux density. When 2 vortices are attached to an electron, the effective magnetic field has the relation  $N_\phi^* = N_\phi - 2N_e = N_e$ , which means that exactly one LL is filled, corresponding to the previously mentioned IQHE state. Therefore the Laughlin wave function has the

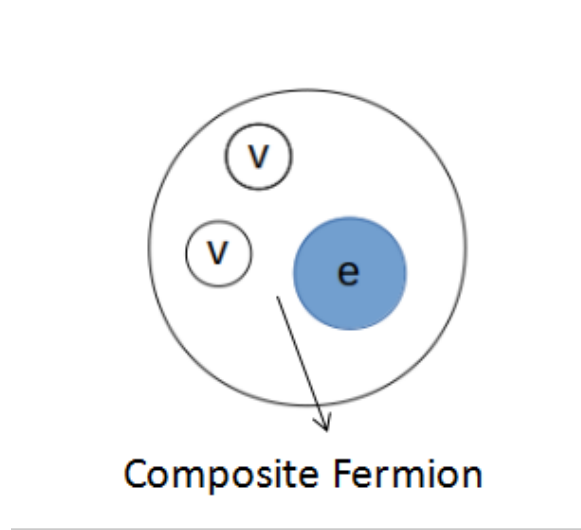


Fig. III.1 The flux attachment makes a composite fermion feel a weaker magnetic field.

following decomposition :

$$\Psi_{1/(2s+1)} = \Phi_{vortex} \Psi_{\nu=1}, \quad (\text{III.1})$$

where  $\Psi_{\nu=1}$  is an IQHE wave function, for the composite particle consisted of an electron and 2 vortices. As it satisfies fermionic statistics, this wave function is known as the composite fermion wave function. The  $\nu = 1$  filling and fermionic statistics tell us that there is a gap to excite the composite fermion from the ground state.

A generalization of Laughlin wave function immediately comes out from this paradigm. It is to let the composite fermion wave function be that of  $\nu = p$  LLs. However, since we are studying a fractional quantum Hall effect, when we restrict ourself to the LLL, the wave function  $\Psi_{\nu=p}$  is not compatible with the LLL condition. In order to remedy this, a projection back to LLL is necessary [89] :

$$\mathcal{P}_{LLL} : \bar{z} \rightarrow 2l^2 \frac{\partial}{\partial z}. \quad (\text{III.2})$$

From this picture, we now work out the corresponding fractional filling  $\nu$ . The magnetic flux quanta carried by each electron vortex is  $N_\phi \nu$ . There are  $2s$  vortices attached to the electron and the result should be a  $p$  filled LL state. If we define the composite-fermion filling factor  $\nu^*$  with respect to the effective magnetic field, the filling factor of electrons is found to be

$$\nu^* = \frac{N_e}{N_{\phi^*}} = \frac{N_e}{N_\phi - 2sN_e} = p \Rightarrow \nu = \frac{N_e}{N_\phi} = \frac{p}{2ps + 1}. \quad (\text{III.3})$$

This is the series found by Jain [88, 89] and it enlarges the family obtained by Laughlin, especially providing the wave function for the well observed  $\nu = 2/5$  state. The general composite-fermion state now is written as :

$$\Psi_{p/(2ps+1)} = \Phi_{vortex} \Psi_{\nu=p}. \quad (\text{III.4})$$

Now we proceed to seeing how the above picture can be captured by the flux attachment procedure in the kinetic energy. This method is first used instead in the composite-boson

theory [90], for establishing a Ginzburg-Landau Chern-Simons theory for the FQHE. But the method was immediately generalized to the composite fermion situation [91]. For the FQHE of filling factor  $\nu = p/(2ps + 1)$ , the Chern-Simons transformation is defined as

$$\Psi_e = \prod_{i < j} \frac{(z_i - z_j)^{2s}}{|z_i - z_j|^{2s}} \Psi_{CF} = \exp \left( i2s \sum_{i < j} \theta_{ij} \right) \Psi_{CF}, \quad (\text{III.5})$$

where  $\theta_{ij}$  is the phase between particles  $i$  and  $j$ , as defined in the last paragraph and  $\Psi_{CF}$  is the composite-fermion wave function. This is a unitary transformation carrying the same amount of flux as the vortex decomposition Eq. (III.1). The prefactor to  $\Psi_{CF}$  is equivalent to adding an Aharonov-Bohm flux generated by the electrons. It is proportional to electron density and produces a Berry phase. That phase creates an effective magnetic field, the Chern-Simons field, described by a vector  $\mathbf{a}_{cs}$ ,

$$\mathbf{a}_{cs}^{(i)} = 2s \nabla \sum_{j \neq i} \theta_{ij}, \quad \nabla \times \mathbf{a}_{cs} = 4s\pi \sum_i \delta(\mathbf{r} - \mathbf{r}_i) = 4s\pi n_e. \quad (\text{III.6})$$

This vector field is determined by the density of electrons and is thus not an independent degree of freedom. The kinetic Hamiltonian, by commuting the momentum operator and the Chern-Simons prefactor, transforms to

$$H_{CF} = \sum_i \frac{(\mathbf{p}_i + e\mathbf{A}(\mathbf{r}_i) + \mathbf{a}_{cs}(\mathbf{r}_i))^2}{2m} + V. \quad (\text{III.7})$$

As we can see now, the composite fermions have the same density as the electrons as they are still labelled by  $i$ . Furthermore they satisfy fermion statistics since the powers of  $z_i - z_j$  in Eq. (III.5) are even. Finally the ‘‘magnetic field’’ felt by the fermions is weakened due to the emergence of a Chern-Simons field. Separating the Chern-Simons field into its average value and fluctuation  $\mathbf{a}_{cs} = \langle \mathbf{a}_{cs} \rangle + : \mathbf{a}_{cs} :$ , the Hamiltonian can be rewritten as

$$\begin{aligned} H_{CS} &= \sum_i \frac{(\mathbf{p}_i + e\mathbf{A}(\mathbf{r}_i) + \langle \mathbf{a}_{cs}(\mathbf{r}_i) \rangle + : \mathbf{a}_{cs}(\mathbf{r}_i) :)^2}{2m} + V \\ &= \sum_i \frac{(\mathbf{\Pi}^{(i)*} + : \mathbf{a}_{cs}(\mathbf{r}_i) :)^2}{2m} + V, \end{aligned} \quad (\text{III.8})$$

$$\mathbf{\Pi}^* = \mathbf{p} + e\mathbf{A} + \langle \mathbf{a}_{cs} \rangle = \mathbf{p} + e\mathbf{A}^*. \quad (\text{III.9})$$

Now for the effective reduced vector potential  $\mathbf{A}^*$ , the composite fermions have a filling factor of  $p$ ,

$$\nabla \times e\mathbf{A}^* = -eB + 4s\pi n_e = -2\pi n_e(2ps + 1)/p + 4s\pi n_e = -2\pi n_e/p, \quad (\text{III.10})$$

because  $\nabla \times \langle \mathbf{a}_{cs} \rangle = 4\pi s \langle \rho_{CF} \rangle = 4\pi s n_e$ , with  $n_e$  the density of electrons. If we neglect the fluctuation of the Chern-Simons field, the composite fermions will completely fill  $p$  Landau levels in the ‘‘magnetic field’’  $\mathbf{B}^* = -\nabla \times \mathbf{A}^*$ . Therefore we can use this as the unperturbed ground state to do mean-field calculations. For  $p = 1$ , the composite-fermion ground state is the same as Eq. (III.1).

At the mean-field level, the result of the above transformation is not exactly the same as Jain’s wave-functional approach in the number of zeroes in the wave function, because

the Chern-Simons transformation is unitary. Kane *et al.* [92] show that the correct zeroes can be restored at long wave-length when the fluctuation of  $\mathbf{a}_{cs}$  is included while Lopez and Fradkin [93] prove the equivalence at the response-theory level. Now the FQHE question is transformed to an IQHE question. The robustness and gaps of the FQHE ground state come from the incompressibility of the IQHE of composite fermions. The complicated interacting system behaves like a free charged-particle system in an infrared limit.

## III.2 Hamiltonian description

Jain's composite fermion enables a good picture to understand many properties of FQHE and look for new FQHE states at different fillings [94], for example generalization from Laughlin's series to Jain's series. It also provides a good tool to compute numerically many physical properties of the FQH state, such as the activation gap [95, 96] and dispersion of the spectrum [70]. However, in the establishment of the composite-fermion theory, in the framework of flux attachment, it is not quite straightforward to see what role the interaction plays. The composite fermions form an IQHE, whose nature is a single-body effect and the CF dynamics is controlled by a kinetic energy, while the electron only feels the many-body Coulomb interaction after the projection to an LL. The success of the CF picture indicates that a free composite fermion should emerge from the interacting system. How to provide a microscopic explanation remains at large in this wave-function approach.

A Hamiltonian theory of composite fermions is proposed by Murthy and Shankar [74] to provide a description emerging from the two-body interaction. This theory is proved to be successful in providing a microscopic explanation of the composite fermion and calculating the activation gap of a pair of well-separated quasiparticle/quasihole. The Hamiltonian theory can be derived in the small-momentum limit via the Chern-Simons transformation that we have introduced. There the Chern-Simons field  $\mathbf{a}_{cs}$  is removed by an auxiliary field and a physical constraint appears from the auxiliary field, which is interpreted as the degree of freedom for the vortex dynamics. Before introducing this small-momentum limit in Sec. III.3, we first present the physical picture of the Hamiltonian and its conclusions on the FQHE.

When the system is projected into the partially filled LL, the kinetic energy is frozen and the remaining degrees of freedom are associated with the guiding-center coordinates  $\mathbf{R}_e = (R_{ex}, R_{ey})$  of electrons. Physically, this coordinate represents the classical center of cyclotron motion, which is a constant of motion for a homogeneous magnetic field, and its components obey the commutation relation  $[R_{ex}, R_{ey}] = -il^2$ , where  $l = \sqrt{1/eB}$  is the magnetic length. The projected Hamiltonian merely contains the interaction part, with the density operator replaced by the projected one :

$$H^p = \frac{1}{2} \sum_{\mathbf{q}} V_{\text{eff}}(\mathbf{q}) \bar{\rho}_e(\mathbf{q}) \bar{\rho}_e(-\mathbf{q}), \quad (\text{III.11})$$

where  $\bar{\rho}_e(\mathbf{q}) = \sum_i \exp(-i\mathbf{q} \cdot \mathbf{R}_i)$  is the projected density operator, as we have already mentioned in Sec. I.2. It is constructed by keeping only the guiding-center coordinate in the density operator while averaging the cyclotron motion over the LL wave function. The latter averaging results in a form factor that is then absorbed into the effective interaction  $V_{\text{eff}}(\mathbf{q})$ . The effective interaction also encodes other effects such as the finite width of the sample and the anisotropy induced by the tilted magnetic field, as we will discuss in later.

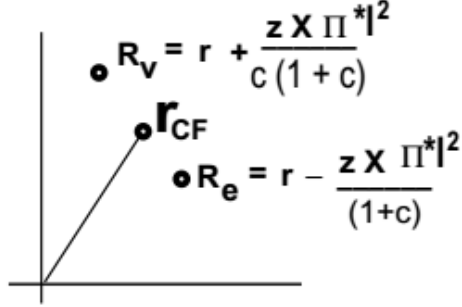


Fig. III.2 The construction of composite fermions [74].

In order to perform the procedure of flux attachment, we need another coordinate to describe vortices. The guiding-center coordinates  $\mathbf{R}_v$  of these vortices are introduced, which satisfy the commutation relation  $[R_{vx}, R_{vy}] = il^2/c^2$  with  $c^2 = 2ps/(2ps + 1)$  characterizing the flux carried by the attached vortices. This value  $c$  can be found in the small momentum expansion in the Sec. III.3. Intuitively each vortex quantum carries  $p/(2ps + 1)$  magnetic flux quanta and we are attaching  $2s$  vortex quanta to an electron. Because of the definition of the covariant derivative, the charge and magnetic field are always combined into  $eB$ , especially in the form of the magnetic length  $l = \sqrt{1/eB}$ . The screening of the external magnetic field is therefore equivalent to screening the charge. Here and after, we also use the term effective charge. The composite fermion can be deemed as well feeling the original external magnetic field with a reduced charge  $e^* = e(1 - c^2)$ . The parameter  $c$  can also be viewed as the charge carried by the attached vortices. A canonical transformation involving the guiding-center coordinates  $\mathbf{R}_e$  and  $\mathbf{R}_v$  allows us then to introduce the CF cyclotron  $\boldsymbol{\eta}$  and guiding-center coordinates  $\mathbf{R}$ ,

$$\boldsymbol{\eta} = \frac{c}{1 - c^2}(\mathbf{R}_v - \mathbf{R}_e), \quad \mathbf{R} = \frac{\mathbf{R}_e - c^2\mathbf{R}_v}{1 - c^2}, \quad (\text{III.12})$$

which satisfy the commutation relations  $[\eta_x, \eta_y] = il^{*2}$  and  $[R_x, R_y] = -il^{*2}$ , while  $\boldsymbol{\eta}$  and  $\mathbf{R}$  commute  $[\eta_{x/y}, R_{x/y}] = 0$ . The magnetic length is switched to that of an effective CF magnetic length  $l^* = \sqrt{2ps + 1}l$ .

On the other hand, vortices are collective configuration of electrons, and the newly introduced vortex operators in fact doubly count the physical degrees of freedom. To heal this double counting, we need to restrict the dynamical variables to the physical sub-Hilbert space, which is subject to a constraint  $\chi(\mathbf{q})|\text{phys}\rangle = 0$ , where  $\chi(\mathbf{q}) = \sum_i \exp(-i\mathbf{q} \cdot \mathbf{R}_v)$  is the vortex density operator [74]. This constraint has the interpretation that the vortex operator is redundant (thus we also call them pseudovortices). The leading order expansion of this constraint can be derived in the small-momentum limit (see Sec III.3). Reversing Eq. (III.12), the electron density operator can be expressed as  $\bar{\rho}_e(\mathbf{q}) = \sum_i \exp[-i\mathbf{q} \cdot (\mathbf{R}_i + c\boldsymbol{\eta}_i)]$ .

In the lowest LL, the Hamiltonian is simply given by the two-body interaction Eq. (III.11). According to Eq. (III.12), the magnetic field felt by the CFs is reduced to  $B/(2ps + 1)$ . Since the CF density is equal to the density of electrons, the CFs now fill completely  $p$  CF LLs. Therefore the huge degeneracy for fractional fillings is lifted and our calculation can be based



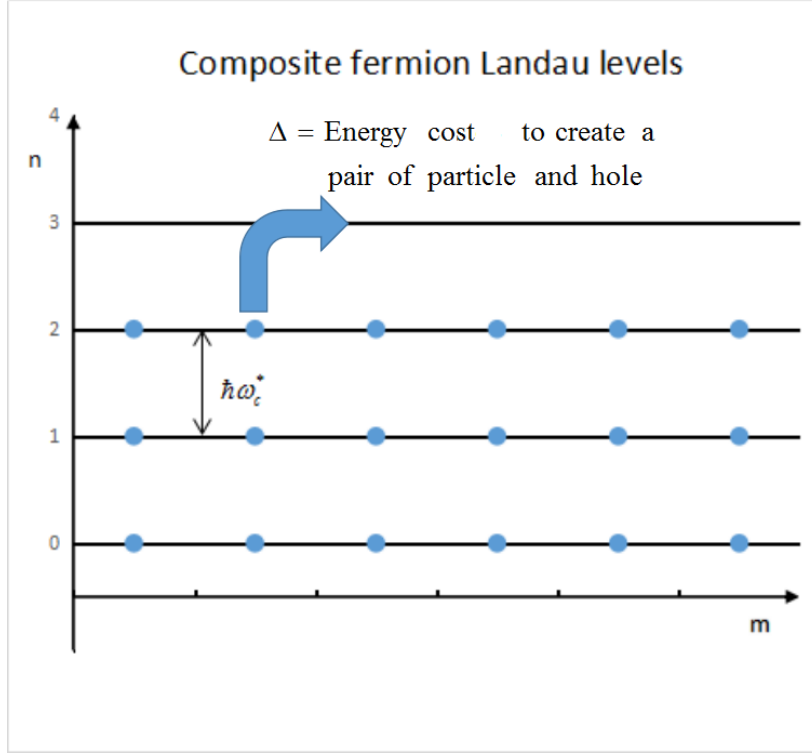


Fig. III.3 Calculation of the activation gap : the energy of creating a CF hole plus the energy of creating a CF.

on a state with these  $p$  filled CF LLs. It serves as the reference state for further diagrammatic approaches, such as the Hartree-Fock approximation, which we use to calculate the activation gap given by Fig. III.3

$$\Delta = \langle \mathbf{p} + PH | H^p | \mathbf{p} + PH \rangle - \langle \mathbf{p} | H^p | \mathbf{p} \rangle, \quad (\text{III.13})$$

where  $|\mathbf{p}\rangle$  stands for the ground state with  $p$  filled CF LLs and  $PH$  symbolizes a widely separated quasiparticle-quasihole pair. In practice, the quasiparticle and quasihole are so far away that they have no correlations and both of their gaps (called charge gaps) are computed individually in the single-particle/hole excitation Hilbert space. The activation gap is then the sum of the two charge gaps,

$$\Delta = \Delta_P + \Delta_H, \quad (\text{III.14})$$

where their explicit expressions are given by creating a particle in the  $p$ -th CF LL by applying  $d_p^\dagger |\mathbf{p}\rangle$  or a hole in the  $(p-1)$ -th CF LL via  $d_{p-1} |\mathbf{p}\rangle$ ,

$$\Delta_P = \langle \mathbf{p} + P | H^p | \mathbf{p} + P \rangle = \langle \mathbf{p} | d_p H^p d_p^\dagger | \mathbf{p} \rangle, \quad (\text{III.15})$$

$$\Delta_H = \langle \mathbf{p} + H | H^p | \mathbf{p} + H \rangle = \langle \mathbf{p} | d_{p-1}^\dagger H^p d_{p-1} | \mathbf{p} \rangle. \quad (\text{III.16})$$

$d_p^\dagger$  is the creation operator creating a quasiparticle in the CF LL  $p$  and  $d_p$  is the corresponding annihilation operator. The above picture naturally follows from the CF transformation. However the Hartree-Fock ground state  $|\mathbf{p}\rangle$  does not obey the physical constraint  $\chi(\mathbf{q})|\mathbf{p}\rangle = 0$ .

If we plug in the projected Hamiltonian Eq. (III.11) and the electron density  $\rho_e$ , this naive procedure therefore suffers from strong corrections. A practical solution is to employ the preferred density  $\rho^p = \rho_e - c^2\chi$  instead of  $\rho_e$  in the Hamiltonian. Because  $\chi|\text{phys}\rangle = 0$ , the preferred density gives the same result as the original electron density for physical quantities. Moreover, if one expands the preferred density, it gives

$$\rho^p(\mathbf{q}) = \sum_j e^{-i\mathbf{q}\cdot\mathbf{r}_j} \left( \frac{1}{2ps+1} - il^2\mathbf{q} \times \mathbf{\Pi}^{(j)} + O(q^3) \right). \quad (\text{III.17})$$

where  $\mathbf{\Pi}$  now is the gauge covariant momentum for composite fermions. When  $\nu \rightarrow 1/2$ ,  $p \rightarrow \infty$ , one can see that the preferred density has a dipole structure. This is in accordance with the result found by Pasquier, Haldane [97] and Read [98]. Also in the above expression, the charge carried by the composite fermion is in accordance with the quasiparticle in the corresponding state. And this density operator has no matrix elements between different composite fermion LL in the order of  $q$ , which will make the theory consistent with Kohn's theorem in the composite fermion Hilbert space [74]. With those merits, Shankar and Murthy find that it is then possible to perform the activation gap computation within the full composite fermion Hilbert space while neglecting the physical constraint, simply by employing the preferred density in the projected Hamiltonian :

$$H^p = \frac{1}{2} \sum_{\mathbf{q}} \rho^p(\mathbf{q}) V_{\text{eff}}(\mathbf{q}) \rho^p(-\mathbf{q}) \quad (\text{III.18})$$

This provides a short-cut in practical calculation. As mentioned above the preferred density has a good physical interpretation in  $q \rightarrow 0$  limit. This tells us that this short-cut method works best for an interaction potential involving only within small momenta, i.e. with a large-momentum cut-off. One of such potentials is the Zhang-Das Sarma potential [99] :

$$v_{ZDS} = \frac{2\pi e^2 e^{-q\lambda}}{q}. \quad (\text{III.19})$$

The  $\lambda$  parameter here even has the physical meaning of the sample thickness in reality, which we will discuss later. Their result is in good agreement with the activation gap computed by Park, Meskini and Jain [96].

From here and on, Eq. (III.18) will serve as the starting point in our Hamiltonian theory calculations for activation gaps presented in the following sections. The details of how to evaluate Eq. (III.15) and Eq. (III.16) will be given in Sec. IV.3.1. There we show that the computation by Murthy and Shankar can be generalized with elliptical orbitals of CF cyclotron coordinates and guiding center coordinates.

### III.3 Small-momentum theory of the Hamiltonian theory

As we mentioned above, the Hamiltonian description of composite fermion can be actually derived in the small-momentum limit. In this section we review the small- $q$  limit of the Hamiltonian theory, based on Ref. [100, 101]. Furthermore, we perform the derivation for an anisotropic kinetic energy, which is characterized by a metric. We show that the small-momentum derivation is also valid in the presence of this anisotropy.

### III.3.1 Introducing an auxiliary field

In this part, we start from the kinetic energy term of the electron and perform the flux attachment procedure. A metric  $g$  is introduced for a general discussion in the kinetic term of the Hamiltonian. The metric is symmetric and have determinant  $\det g = 1$  to preserve the area. We perform the transformation in [100, 101] to see what the outcome will be. After doing the Chern-Simons transformation, the kinetic part of the Hamiltonian is

$$H_k = \frac{1}{2m} \sum_{i,a,b} (p + eA + \langle a_{cs} \rangle + : a_{cs} :)_a^{(i)} g^{ab} (p + eA + \langle a_{cs} \rangle + : a_{cs} :)_b^{(i)}, \quad (\text{III.20})$$

where the index  $i$  is to sum over all electrons. To eliminate the fluctuations of the Chern-Simons transformation, we introduce an auxiliary field  $\mathbf{a}$  in the quadratic form and impose the constraint that its action on a physical state is zero

$$H_k = \sum_{i,a,b} (p + eA^* + : a_{cs} : + a)_a^{(i)} g^{ab} (p + eA^* + : a_{cs} : + a)_b^{(i)}, \quad (\text{III.21})$$

$$\mathbf{a}|\text{physical state}\rangle = 0 \quad (\text{III.22})$$

So this Hamiltonian has the same action as the original Hamiltonian on physical states. The field  $\mathbf{a}$  is a transverse vector field. It has only one dynamical component. We define it and its conjugate variable by a pair of scalar operators as

$$a^a(\mathbf{q}) = i\epsilon^{ab} \frac{q_b}{|\mathbf{q}|} a(\mathbf{q}), \quad P_a(\mathbf{q}) = \frac{q_a}{|\mathbf{q}|} P(\mathbf{q}); \quad (\text{III.23})$$

$$[a(\mathbf{q}), P(-\mathbf{q}')] = i\delta(\mathbf{q} - \mathbf{q}'), \quad |\mathbf{q}| = q = \sqrt{q_a q_b g^{ab}}. \quad (\text{III.24})$$

Now let us make a unitary transformation shifting  $\mathbf{a}$  to eliminate  $: \mathbf{a}_{cs} :$

$$U = \exp \left[ \sum_{\mathbf{q}} P(\mathbf{q}) \frac{4\pi i s}{q} \rho(-\mathbf{q}) \right] = \exp \left[ \sum_{\mathbf{q}} P(\mathbf{q}) \frac{4\pi i s}{q} \sum_i e^{i\mathbf{q} \cdot \mathbf{r}_i} \right]. \quad (\text{III.25})$$

The Hamiltonian and the constraint become then

$$H_k = \sum_{i,a,b} (\Pi^* + a + 4\pi s P)_a^{(i)} g^{ab} (\Pi^* + a + 4\pi s P)_b^{(i)}, \quad (\text{III.26})$$

$$(qa(\mathbf{q}) - 4\pi s \rho(\mathbf{q}))|\text{physical state}\rangle = 0, \quad (\text{III.27})$$

where  $\Pi^* = \mathbf{p} + eA^*$  is the covariant momentum in the reduced field. The  $P(\mathbf{q})$  terms in the Hamiltonian arise from commuting the derivative in  $\Pi^*$  and the  $\mathbf{r}_i$  operators in  $U$ . Expanding the quadratic form, we obtain three terms describing different dynamics of the system. The first part represents a composite particle moving in the effective field  $\mathbf{A}^*$ . The second part is the energy of a bosonic field, in the form of harmonic oscillators, described by the pair of conjugate variables  $a$  and  $P$ . The third part is the coupling between these two kinds of dynamical variables

$$\begin{aligned} H_k = & \sum_{i,a,b} \frac{\Pi_a^{*(i)} g^{ab} \Pi_b^{*(i)}}{2m} + \sum_{i,a,b} \frac{1}{2m} [a + 4\pi s P]_a^{(i)} g^{ab} [a + 4\pi s P]_b^{(i)} \\ & + \sum_{i,a,b} \frac{1}{2m} g^{ab} [\Pi_a^{*(i)} (a + 4\pi s P)_b^{(i)} + (a + 4\pi s P)_a^{(i)} \Pi_b^{*(i)}]. \end{aligned} \quad (\text{III.28})$$

Now we are going to treat the three terms individually. As the metric  $g$  is symmetric and of determinant one, it has two free components so we can parameterize it as

$$g^{ab} = v^a \bar{v}^b + \bar{v}^a v^b, \quad (\text{III.29})$$

where  $\bar{v}^a$  means the complex conjugate of  $v^a$  and the components of the complex vector  $v^a$  are required to satisfy

$$v^a \bar{v}^b - \bar{v}^a v^b = -i\epsilon^{ab}. \quad (\text{III.30})$$

The index of the complex vector  $v^a$  can be lowered by the metric  $g$ , and there are some useful formulae concerning the metric and the complex vector

$$g_{ab} = (g^{ab})^{-1}, \quad v_a = g_{ab} v^b \quad (\text{III.31})$$

$$g_{ab} = v_a \bar{v}_b + \bar{v}_a v_b. \quad (\text{III.32})$$

They mean that we can just plug in  $v$  regardless of upper or lower indices and treat it as an ordinary vector. For the first term in Eq. (III.28) we define a pair of ladder operators as

$$\Pi_-^* = \sqrt{2} \bar{v}^a \Pi_a^*, \quad \Pi_+^* = \sqrt{2} v^a \Pi_a^*, \quad (\text{III.33})$$

that satisfy the commutation relation

$$[\Pi_-^*, \Pi_+^*] = -2eB/(2ps + 1) = -2eB^*. \quad (\text{III.34})$$

The energy of the auxiliary field can be rewritten as

$$\begin{aligned} & \sum_{i,a,b} \frac{1}{2m} [a + 4\pi s P]_a^{(i)} g^{ab} [a + 4\pi s P]_b^{(i)} \\ &= \frac{g^{ab}}{2m} \int d^2 r \rho(\mathbf{r}) [a(\mathbf{r}) + 4\pi s P(\mathbf{r})]_b [a(\mathbf{r}) + 4\pi s P(\mathbf{r})]_a \\ &\simeq \frac{n_e g^{ab}}{2m} \int d^2 r [a(\mathbf{r}) + 4\pi s P(\mathbf{r})]_b [a(\mathbf{r}) + 4\pi s P(\mathbf{r})]_a + O(\rho) \\ &\simeq \frac{n_e}{2m} \sum_{\mathbf{q}} [ |a(\mathbf{q})|^2 + |4\pi s P(\mathbf{q})|^2 ]. \end{aligned} \quad (\text{III.35})$$

In the first step, we replace the sum over particle indices by an integral with weight  $\rho$ . Furthermore, we have made the mean-field approximation  $\rho(\mathbf{r}) \sim n_e$  in the third step. This approximation may be justified by the fact that the FQHE state has a uniform density, and the density fluctuations are quenched by the state's incompressibility. In the last step, we plug in the vector definition of  $\mathbf{a}$  and  $P$  in Eq. (III.24). If we define  $A$  and  $A^\dagger$  as

$$A(\mathbf{q}) = \frac{[a(\mathbf{q}) + 4i\pi s P(\mathbf{q})]}{\sqrt{8\pi s}}, \quad A^\dagger(\mathbf{q}) = \frac{[a(\mathbf{q}) - 4i\pi s P(\mathbf{q})]}{\sqrt{8\pi s}}, \quad (\text{III.36})$$

their commutator reads as

$$[A(\mathbf{q}), A^\dagger(\mathbf{q}')] = (2\pi)^2 \delta^2(\mathbf{q} - \mathbf{q}'). \quad (\text{III.37})$$

According to Eq. (III.35) the bosonic field  $A(q)$  just forms a harmonic oscillator, with a frequency  $\omega_c(2ps)/(2ps + 1)$ .

### III.3.2 Separating different energy scales

At this point, one thing worth noticing is that if we neglect the coupling term in Eq. (III.28), the first term will give a lower Landau level spacing  $\omega_c/(2ps+1)$  and the second term will be a harmonic oscillator of frequency  $\omega_c(2ps)/(2ps+1)$ . Comparing this to the original Hamiltonian, it can be interpreted as a part of the Landau level energy that is transferred from the electronic degrees of freedom to the oscillator. If this process can be carried on, the cyclotron energy can be transformed entirely into the harmonic oscillator, which is decoupled from the low-energy part of our system. Thus we will realize the separation of the high-energy (cyclotron energy) from the low-energy (Coulomb interaction) physics in FQHE. As shown later, this is exactly what happens after considering and eliminating the coupling term in Eq. (III.28).

First we rephrase the coupling term into a form more familiar in second quantization language. We define the following ladder operators for the density

$$c(\mathbf{q}) = \hat{q}_- \sum_i \Pi_+^{*(i)} e^{-i\mathbf{q}\cdot\mathbf{r}_i}, \quad c^\dagger(\mathbf{q}) = \hat{q}_+ \sum_i \Pi_-^{*(i)} e^{i\mathbf{q}\cdot\mathbf{r}_i}; \quad (\text{III.38})$$

$$q_- = \sqrt{2}\bar{v}_a q^a/q, \quad q_+ = \sqrt{2}v_a q^a/q. \quad (\text{III.39})$$

The commutator of  $c, c^\dagger$  is

$$\begin{aligned} [c(\mathbf{q}), c^\dagger(\mathbf{q}')] &= \hat{q}'_- \hat{q}_+ \sum_i [\Pi_+^{*(i)}, \Pi_-^{*(i)}] e^{-i(\mathbf{q}-\mathbf{q}')\cdot\mathbf{r}_i} + O(\mathbf{q}) \\ &\simeq 2eB^* n_e (2\pi)^2 \delta^2(\mathbf{q} - \mathbf{q}'). \end{aligned} \quad (\text{III.40})$$

In the second line, we have made the random phase approximation

$$\sum_i e^{-i(\mathbf{q}-\mathbf{q}')\cdot\mathbf{r}_i} \simeq n_e (2\pi)^2 \delta^2(\mathbf{q} - \mathbf{q}'), \quad (\text{III.41})$$

i.e. we leave omitted the operator character of the coordinate  $\mathbf{r}_i$  here. This makes sense, as stated before, because the FQH state is a uniform liquid. Other commutators between  $c, c^\dagger$  are of the order of  $\mathbf{q}$  and thus vanish in the small- $q$  theory. With these operators, we focus on the coupling term in Eq. (III.28). In the small- $q$  limit,  $\Pi^*$  and  $a + 4\pi sP$  commute to the order  $\mathbf{q}$ . After plugging in  $A, A^\dagger$  we have

$$\begin{aligned} &\sum_{i,a,b} \frac{1}{m} g^{ab} \Pi_a^{*(i)} (a + 4\pi sP)_b^{(i)} \\ &= \sum_{i,a,b} \frac{i\sqrt{2\pi s}}{m} g^{ab} \Pi_a^{*(i)} \sum_{\mathbf{q},c} \left[ \varepsilon_{bc} \frac{q^c}{q} (A(\mathbf{q}) + A^\dagger(\mathbf{q})) + \frac{q_b}{q} \frac{A(\mathbf{q}) - A^\dagger(\mathbf{q})}{i} \right] e^{i\mathbf{r}_i\cdot\mathbf{q}} \\ &= \sum_{i,a,b,\mathbf{q},c} \frac{i\sqrt{2\pi s}}{m} g^{ab} \Pi_a^{*(i)} \frac{A^\dagger(\mathbf{q})}{q} (\varepsilon_{bc} q^c + i q_b) e^{i\mathbf{r}_i\cdot\mathbf{q}} + \text{h.c.} \end{aligned} \quad (\text{III.42})$$

Notice that  $\varepsilon$  is a tensor and because of  $\det g = 1$ , we can transform the above equation to

$$\begin{aligned}
 & \sum_{i,a,b} \frac{1}{m} g^{ab} \Pi_a^{*(i)} (a + 4\pi s P)_b^{(i)} \\
 = & \sum_{i,a,b,\mathbf{q}} \frac{\sqrt{2\pi s} A^\dagger(\mathbf{q})}{mq} \Pi_a^{*(i)} (-g^{ab} + i\epsilon^{ab}) q_b e^{i\mathbf{r}_i \cdot \mathbf{q}} + \text{h.c.} \\
 = & \sum_{i,a,b,\mathbf{q}} \frac{\sqrt{2\pi s} A^\dagger(\mathbf{q})}{mq} \Pi_a^{*(i)} [-v^a \bar{v}^b - v^b \bar{v}^a - v^a \bar{v}^b + v^b \bar{v}^a] q_b e^{i\mathbf{r}_i \cdot \mathbf{q}} + \text{h.c.} \\
 = & \sum_{i,a,b,\mathbf{q}} \frac{\sqrt{2\pi s} A^\dagger(\mathbf{q})}{mq} \Pi_+^{*(i)} q_- e^{i\mathbf{r}_i \cdot \mathbf{q}} + \text{h.c.} = \frac{\sqrt{2\pi s}}{m} \sum_{\mathbf{q}} (A^\dagger(\mathbf{q}) c(\mathbf{q}) + \text{h.c.}) \quad (\text{III.43})
 \end{aligned}$$

In the second step, we plug in Eq. (III.29), Eq. (III.30) and utilize the relation Eq. (III.32). Eventually, the Hamiltonian Eq. (III.28) is turned into the standard coupling system form in second quantization language

$$H_k = \sum_{i,a,b} \frac{g^{ab} \Pi_a^{*(i)} \Pi_b^{*(i)}}{2m} + \sum_{\mathbf{q}} \frac{4\pi n s}{m} A^\dagger(\mathbf{q}) A(\mathbf{q}) + \frac{\sqrt{2\pi s}}{m} \sum_{\mathbf{q}} (A^\dagger(\mathbf{q}) c(\mathbf{q}) + \text{h.c.}). \quad (\text{III.44})$$

To completely decouple  $\Pi^*$  and  $A$ , a transformation flow is needed

$$U(\lambda) = \mathcal{T}_\lambda e^{i \int_0^\lambda S(\lambda) d\lambda}, \quad (\text{III.45})$$

where the symbol  $T_\lambda$  means that we put the exponential in the order of decreasing  $\lambda$ . The exponent  $S(\lambda)$  is given by

$$S(\lambda) = \theta \sum_{\mathbf{q}} \left( c^\dagger(\mathbf{q}, \lambda) A(\mathbf{q}, \lambda) - A^\dagger(\mathbf{q}, \lambda) c(\mathbf{q}, \lambda) \right), \quad \theta = \frac{\sqrt{2\pi s}}{4\pi n} \quad (\text{III.46})$$

The value of  $\lambda$  will be determined by the decoupling criterion as we will show. Notice that this decoupling transformation is the same as in Ref. [100, 101] since it does not explicitly depend on the metric, which is absorbed in the definition of the  $c(\mathbf{q})$  operator [Eq. (III.38)]. The  $c(\mathbf{q}, \lambda)$ ,  $A(\mathbf{q}, \lambda)$  are operators obtained after doing  $U(\lambda)$  transformation

$$O(\lambda) = U^\dagger O U. \quad (\text{III.47})$$

How all the operators in Eq. (III.44) evolve under  $U(\lambda)$  can be obtained from the differential equation

$$\frac{d}{d\lambda} O(\lambda) = i [O(\lambda), S(\lambda)]. \quad (\text{III.48})$$

Here we list the results of the three terms in Eq. (III.44). The kinetic (cyclotron) energy transforms to

$$\begin{aligned}
 H_c(\lambda) = & H_c(0) + \frac{eB^* \theta}{m} \sum_{\mathbf{q}} \left[ \frac{\sin(2\lambda\mu)}{2\mu} \left( c^\dagger(\mathbf{q}) A(\mathbf{q}) + A^\dagger(\mathbf{q}) c(\mathbf{q}) \right) \right. \\
 & \left. + \frac{1 - \cos(2\lambda\mu)}{2\mu} \left( \frac{\mu}{\theta} A^\dagger(\mathbf{q}) A(\mathbf{q}) - \frac{\theta}{\mu} c^\dagger(\mathbf{q}) c(\mathbf{q}) \right) \right], \quad (\text{III.49})
 \end{aligned}$$

where  $\mu^2 = 2eB^*n_e\theta^2$ . The coupling between the cyclotron motion and harmonic oscillator becomes

$$H_{\text{coupling}}(\lambda) = \frac{\sqrt{2\pi s}}{m} \sum_{\mathbf{q}} \left[ \cos(2\mu\lambda) \left( c^\dagger(\mathbf{q})A(\mathbf{q}) + A^\dagger(\mathbf{q})c(\mathbf{q}) \right) + \sin(2\mu\lambda) \left( \frac{\mu}{\theta} A^\dagger(\mathbf{q})A(\mathbf{q}) - \frac{\theta}{\mu} c^\dagger(\mathbf{q})c(\mathbf{q}) \right) \right]. \quad (\text{III.50})$$

The oscillator after the evolution is given by

$$H_{\text{osc}}(\lambda) = \frac{4\pi n}{m} \sum_{\mathbf{q}} \left[ \cos^2(2\mu\lambda) A^\dagger(\mathbf{q})A(\mathbf{q}) - \frac{\theta}{2\mu} \sin(2\mu\lambda) \left( c^\dagger(\mathbf{q})A(\mathbf{q}) + A^\dagger(\mathbf{q})c(\mathbf{q}) \right) + \frac{\theta^2}{\mu^2} \sin^2(\mu\lambda) c^\dagger(\mathbf{q})c(\mathbf{q}) \right]. \quad (\text{III.51})$$

All the three terms are intertwined with each other. In particular for the crossing term  $c^\dagger A$ , we find if we set  $\lambda = \lambda_0$  with

$$\tan(\lambda_0\mu) = \frac{\mu}{s} = \frac{1}{\sqrt{2ps}}, \quad (\text{III.52})$$

its coefficient will vanish. On the other hand, this choice gives rise to the Hamiltonian

$$H_k = \sum_i \frac{\Pi_-^{*(i)} \Pi_+^{*(i)}}{2m} - \frac{1}{2mn_e} \sum_{i,j,\mathbf{q}} \Pi_-^{*(i)} \Pi_+^{*(j)} e^{-i\mathbf{q}\cdot(\mathbf{r}_i - \mathbf{r}_j)} + \sum_{\mathbf{q}} \omega_c A^\dagger(\mathbf{q})A(\mathbf{q}). \quad (\text{III.53})$$

From this expression, we observe that the frequency of the harmonic oscillator is exactly at  $\omega_c$ , the Landau level spacing of the starting Hamiltonian (I.1). Notice that this is also required by Kohn's theorem, which stipulate that the collective  $\mathbf{q} = 0$  excitations, which potentially couple to the external electromagnetic field, must have an energy  $\omega_c$  if the dispersion is parabolic such as in the present case. If we further impose  $\sum_{\mathbf{q}} = N_e$ , i.e. the number of oscillators equal to the number of electrons, the diagonal parts of the kinetic term in Eq. (III.53) will be zero. For the non-diagonal parts, it is shown to be convertible to a short range term [100] and can be dropped. Therefore, by now the harmonic oscillator obtains the correct coefficient and the cyclotron energy is totally decoupled. In this sense, we “freeze” the Landau level, such that we can concentrate on the interactions solely.

Another important result of the above calculation is that it recovers the operators constructed in the Hamiltonian theory in Sec. III.2 in the  $ql \rightarrow 0$  limit. The constraint obtained here is

$$\sum_i e^{-i\mathbf{q}\cdot\mathbf{r}_i} \left( 1 + il^2 \frac{q_a \epsilon^{ab} \Pi_b^{*(i)}}{c(1+c)} \right) |\text{physical state}\rangle = 0, \quad (\text{III.54})$$

This is the original physical constraint found by Shankar and Murthy. By exponentiating the  $q$ -part in the parentheses, this gives precisely the compact form  $\chi(\mathbf{q}) = \sum_i \exp(-i\mathbf{q}\cdot\mathbf{R}_v) |\text{phys}\rangle = 0$  to linear order in  $q$ . The density operator evolves into

$$\rho(\mathbf{q}, \lambda_0) = \sum_i e^{-i\mathbf{q}\cdot\mathbf{r}_i} \left( 1 - il^2 \frac{q_a \epsilon^{ab} \Pi_b^{*(i)}}{1+c} + \frac{q\sqrt{s}}{\sqrt{8\pi}} [A(\mathbf{q}) + A^\dagger(\mathbf{q})] \right). \quad (\text{III.55})$$

Like what is done for the physical constraint, neglecting the harmonic oscillator contribution due to the fact that this high energy degree of freedom is frozen, one can immediately obtain the expression  $\rho_e(\mathbf{q}) = \sum_i \exp[-i\mathbf{q} \cdot (\mathbf{R}_i + c\boldsymbol{\eta}_i)]$  by exponentiating the  $q$ -dependent part in the parentheses of the above density.

The decoupling transformation in the small- $q$  limit discussed in the present section therefore allows one to understand the density operators introduced in Sec. III.2 in a more pedagogical manner. Indeed, one finds that the constraint Eq. (III.54), expanded to the lowest order of  $\mathbf{q}$ , is interpreted as the (pseudo)vortex density. This reflects again the fact that the (pseudo)vortex is an auxiliary degree of freedom eventually constructed from the electronic degrees of freedom. The latter is precisely given by Eq. (III.55). Moreover, we show here that the small-momentum derivation is also valid for an anisotropic kinetic energy. The projection to the intra-LL physics is the same as before by dropping the higher-energy harmonic oscillator  $A(\mathbf{q}), A^\dagger(\mathbf{q})$ .





# IV – Composite fermion theory under anisotropy

In this chapter, we study how composite fermions react to the presence of anisotropy in the interaction from the Hamiltonian theory. In experiments, anisotropy serves as a tool to probe and perturb the existing topologically ordered liquid states. Besides the liquid phases, there are plenty of other compressible and incompressible candidates for quantum Hall systems. The stability of these liquid states under different perturbations can help us to better understand the competition between different phases. Two of such realizations are to add an anisotropic mass tensor or tilt the magnetic field. How a FQH liquid reacts to anisotropic perturbation remains interesting both in theory [102, 103, 104] and in experiments [105, 106]. The stripe phase [107, 108] and the nematic phase [109] with broken rotation symmetry are relevant and possible candidates of competition in such cases. The former is common in higher ( $n \geq 2$ ) Landau levels, which we will discuss in detail in chapter VI, while the latter is suggested being the rotation-symmetry broken phase after the collective excitation mode is softened. Two gaps in quantum Hall states can be related to the issue of stability, the activation gap and the collective excitation gap. In this chapter, we discuss how the activation gap of a well separated quasiparticle/quasihole pair reacts to the anisotropic effective interaction. We show how tilted magnetic field produces an effective anisotropic interaction and its influence on CF LLs. A variational metric for CFs is defined. In chapter V, we present how the neutral collective gap behaves under such kind of anisotropy.

The structure of this chapter is as follows. In Sec. IV.1 we introduce a reparametrization of ladder operators via a metric. How anisotropy is turned on by tilting the magnetic field is presented in Sec. IV.2. In Sec. IV.3 we compute the activation gap when the magnetic field is tilted.

## IV.1 Reparametrisation of ladder operators

As we have shown in the previous chapters, Haldane [59] points out that the quantum Hall liquid state has an internal geometrical degree of freedom. It can respond to the external anisotropy and its static value is viewed as the shape of the Hall liquid. In order to introduce the metric variable into the Hamiltonian theory formalism, we start from defining the single-particle Hilbert space. As mentioned in the previous chapter, the Hamiltonian theory is based on the fact that CFs fill  $p$  LLs. For a charged particle under magnetic field, the CF cyclotron and guiding-center coordinates satisfy the following commutation relations :

$$[\eta^a, \eta^b] = i l^{*2} \epsilon^{ab}, \quad [R^a, R^b] = -i l^{*2} \epsilon^{ab}. \quad (\text{IV.1})$$

They can be combined with a complex vector to form ladder operators which define the CF LLs and their angular momenta,

$$\hat{a} = \frac{v_a \eta^a}{l^*}, \hat{a}^\dagger = \frac{\bar{v}_a \eta^a}{l^*}, \hat{b} = \frac{\bar{v}'_b R^b}{l^*}, \hat{b}^\dagger = \frac{v'_b R^b}{l^*}, \quad (\text{IV.2})$$

where the complex vector  $v, v'$  satisfies  $v_a \bar{v}_b - \bar{v}_a v_b = -i\epsilon_{ab}$ . One can verify that the commutation relations for the ladder operators remain unchanged,  $[\hat{a}, \hat{a}^\dagger] = [\hat{b}, \hat{b}^\dagger] = 1$ . Here we use Einstein's convention according to which we sum over repeated indices of co- and contra-variant vectors. A complete basis of the one-body Hilbert space is defined as  $|m, n\rangle \propto (\hat{a}^\dagger)^n (\hat{b}^\dagger)^m |0\rangle$ . By changing the form of this vector, the eigenstates of ladder operators exhibit different orbital shapes of  $\boldsymbol{\eta}$  and  $\mathbf{R}$ . In general, the complex vector multiplied with the cyclotron coordinate and that with the guiding-center coordinate can be different, as is shown in the original idea by Haladane of anisotropic Laughlin states. However, in the Hamiltonian theory case, both of the two CF coordinates arise from the guiding-center coordinates of electrons, because the pseudovortex is only an auxiliary variable composed of electronic degrees of freedom. Remembering in the original electronic picture, only the guiding center of electrons serves as a variational parameter. Intuitively, for the composite fermions, we expect that for the CF cyclotron motion and guiding-center motion only one metric can appear as a variational parameter. This will be shown to be true in Sec. IV.3. A metric  $g$  conserving the area  $\det(g) = 1$  is associated with such a complex vector,

$$g_{ab} = v_a \bar{v}_b + \bar{v}_a v_b. \quad (\text{IV.3})$$

When  $v = (1, i)/\sqrt{2}$ , the metric is isotropic  $\text{diag}(1, 1)$  and the corresponding ladder operators are those defined by Shankar and Murthy [74]. As one varies the vector  $v$ , the metric associated with it is a direct reflection of the internal geometry.

## IV.2 Effective potential in tilted magnetic field

Let us step back and discuss where an anisotropic interaction may come from and consider the following one-body problem. For an ideally 2D system, adding an inplane magnetic field has no effects, except for an enhancement of the global Zeeman effect, since it only causes movements in the restricted perpendicular direction. However, in realistic systems, usually the sample has a finite thickness. While the motion of the electrons remains restricted in the  $z$ -direction, they can respond to the parallel component of the magnetic field. Indeed, the electron tends to perform its cyclotron motion in a plane perpendicular to the total magnetic field such that the plane of motion is tilted, as sketched in Fig. IV.1(a). The projection of the associated wave function is therefore an ellipse, as shown in Fig. IV.1(b). One thus notices already a possible origin of anisotropy in the effective interaction potential. For a more quantitative analysis, we model the restriction in the  $z$ -direction by a parabolic confining potential  $m\Omega z^2/2$ , which, together with the kinetic energy in the perpendicular direction, needs to be added to the one-particle Hamiltonian,

$$H_z = \frac{\Pi_z^2}{2m} + \frac{m\Omega^2 z^2}{2}. \quad (\text{IV.4})$$

The total Hamiltonian is therefore that of a pair of coupled harmonic oscillators and can be solved exactly.

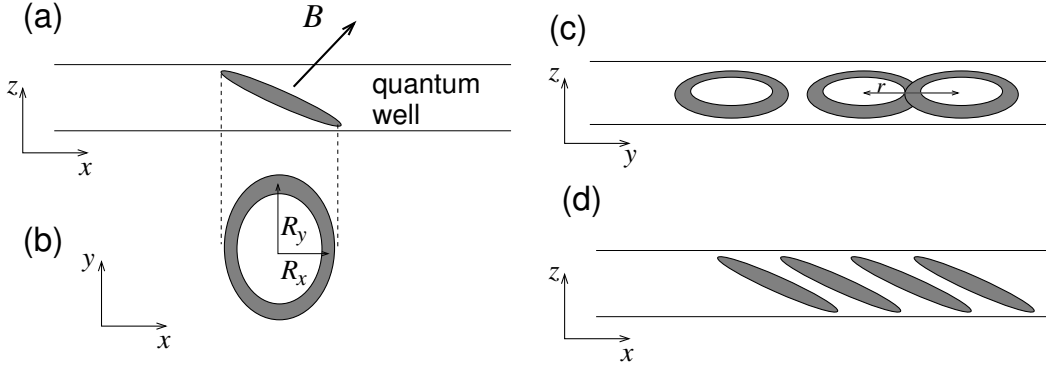


Fig. IV.1 Effect of a tilted magnetic field in a wide quantum well. (a) The wave functions tend to be in a plane roughly perpendicular to the total magnetic field. In contrast to a perfect 2D system, the wide quantum well allows for the tilt of the plane of cyclotron motion. (b) Resulting cyclotron motion projected to the  $xy$  plane. (c) Adjacent wave functions of electrons in the  $y$ -direction. (d) Adjacent wave functions of electrons in the  $x$ -direction – their wave-function overlap is largely reduced as compared to that in the  $y$ -direction [panel (c)].

Now we start to diagonalize this Hamiltonian. We choose the Landau gauge and the gauge potential is given as  $(0, zB \tan \theta - xB, 0)$ , where  $\theta$  is the tilting angle between the direction of the magnetic field and the perpendicular  $z$ -direction. The symbol  $B$  here is the component of the magnetic field in the  $z$ -direction, not the total one. Neglecting the Coulomb interaction, the total Hamiltonian including the inplane part is :

$$\begin{aligned}
 H_{tlm} = & \frac{1}{2m} (p_x^2 + p_y^2 + p_z^2) - \frac{eB}{m} p_y x + \frac{eB}{m} p_y z \tan \theta + \frac{1}{2} \left( \frac{e^2 B^2}{m} \tan^2 \theta + m\Omega^2 \right) z^2 \\
 & + \frac{e^2 B^2}{2m} x^2 - \frac{e^2 B^2}{m} xz \tan \theta.
 \end{aligned} \tag{IV.5}$$

The Hamiltonian is both quadratic in momenta and positions. It will be later transformed into a canonical form by a coordinate transformation. First the above notation can be further simplified with the help of the cyclotron frequency and magnetic length. The cyclotron frequency  $\omega_c$  and the magnetic length  $l$  are defined with respect to the magnetic field  $B$  in the  $z$ -direction :

$$\omega_c = \frac{eB}{m}, \quad l = \sqrt{\frac{1}{eB}}, \tag{IV.6}$$

where we set  $\hbar = 1$  as before. The above Hamiltonian is invariant under translation in the  $y$ -direction. The eigenstate can thus be chosen to be plane wave in the  $y$ -direction, taking the form :

$$\Psi = \frac{1}{\sqrt{2\pi}} e^{-i\frac{x_0 y}{l^2}} \Phi(x, z), \tag{IV.7}$$

where  $x_0 = l^2 p_y$  is proportional to the momentum in the  $y$ -direction, and plays the role of the guiding center in the Landau gauge. If we use the magnetic length as the unit of length, i.e.  $l = 1$ ,  $x_0$  is just the momentum in the  $y$ -direction. The Hamiltonian written in units of

the cyclotron frequency is

$$\frac{H_{tlm}}{\omega_c} = \frac{p_x^2 + p_z^2}{2} + \frac{(x - x_0)^2}{2} + \left( \tan^2 \theta + \frac{\Omega^2}{\omega_c^2} \right) \frac{z^2}{2} - (x - x_0)z \tan \theta. \quad (\text{IV.8})$$

The dependence on  $x$  only relies on the combination  $x - x_0$ . For convenience, one can put  $x_0 = 0$  and the above Hamiltonian is quadratic in  $p_x, p_z, x, z$  with only a mixing between the  $x$ - and  $z$ -coordinates :

$$\frac{H_{tlm}}{\omega_c} = \frac{p_x^2 + x^2}{2} + \frac{p_z^2 + \left( \tan^2 \theta + \frac{\Omega^2}{\omega_c^2} \right) z^2}{2} - xz \tan \theta. \quad (\text{IV.9})$$

The momentum parts  $p_x$  and  $p_z$  are already diagonal and in order to decouple the two harmonic oscillators, we only need to diagonalize the coordinate part  $-xz \tan \theta$ . This is easily done by a rotation in the  $x - z$  plane. The degrees of freedom are separated by doing an orthogonal transformation :

$$\begin{pmatrix} \xi \\ \zeta \end{pmatrix} = \begin{pmatrix} \cos \tilde{\theta} & -\sin \tilde{\theta} \\ \sin \tilde{\theta} & \cos \tilde{\theta} \end{pmatrix} \begin{pmatrix} x \\ z \end{pmatrix}. \quad (\text{IV.10})$$

Inserting the above transformation into the Hamiltonian and requiring no mixing term, one can find that  $\tilde{\theta}$  is a function of the tilted angle  $\theta$ , vanishing when there is no tilt :

$$\tan 2\tilde{\theta} = \frac{2 \tan \theta}{1 - \tan^2 \theta - \frac{\Omega^2}{\omega_c^2}}. \quad (\text{IV.11})$$

One may also observe that in the large confinement limit  $\Omega \rightarrow \infty$ , the anisotropic parameter  $\tilde{\theta} \rightarrow 0$ . The Hamiltonian after transformation is given as

$$H_{tlm} = \frac{p_\xi^2}{2m} + \frac{m\omega_-^2 \xi^2}{2} + \frac{p_\zeta^2}{2m} + \frac{m\omega_+^2 \zeta^2}{2}. \quad (\text{IV.12})$$

Now the Hamiltonian is in its canonical form and describes two decoupled harmonic oscillators, one for the confined motion in the  $z$ -direction and another one for the cyclotron motion in the external magnetic field. Their corresponding frequencies are given by

$$\frac{\omega_\pm^2}{\omega_c^2} = \frac{1}{2} \left[ \lambda^2 + 1 \pm \sqrt{(\lambda^2 - 1)^2 + 4 \tan^2 \theta} \right], \quad (\text{IV.13})$$

where  $\lambda^2 = (\tan^2 \theta + \Omega^2/\omega_c^2)$ . The two harmonic oscillators naturally define two length scales  $l_\pm^2 = (\omega_c/\omega_\pm)l^2$ . From the above definition,  $\omega_+$  is always larger than  $\omega_-$ . Hence  $\omega_+$  is always treated as the confining frequency while  $\omega_-$  is treated as the effective LL cyclotron frequency. The eigenstate is a product of the two harmonic oscillator eigenstates :

$$\Phi(x, z) = \Phi_N^{\omega_+}(\zeta) \Phi_n^{\omega_-}(\xi), \quad (\text{IV.14})$$

where the subscripts  $N, n$  denote the level in the harmonic oscillator and the Landau level. The explicit form of the wave function is easily expressed through the Hermite polynomials :

$$\Phi_n^\omega(x) = \frac{1}{\sqrt{\sqrt{\pi} 2^n n! l_\omega}} H_n \left( \frac{x}{l_\omega} \right), \quad (\text{IV.15})$$

where  $l_\omega = l_\pm$  is the magnetic length corresponding to  $\omega = \omega_\pm$  respectively.

So with such a decoupled Hamiltonian, the eigenstates of  $H_{tlm}$  are denoted as  $|N, n, m\rangle$ , where the first index corresponding to the higher frequency represents the level (band) in the confining potential and  $n$  represents the cyclotron level, while the quantum number  $m$  denotes the LL degeneracy associated with the guiding-center coordinate. In the Landau gauge, this is the  $y$ -direction momentum  $x_0$ . The lowest LL is naturally generated by  $|0, 0, m\rangle$  states. To focus on the physics inside the lowest LL, the density operator is projected into this state :

$$\rho_e(q_x, q_y, q_z) = \sum_{m, m'} \langle 0, 0, m | e^{-iq \cdot \mathbf{r}} | 0, 0, m' \rangle d_m^\dagger d_{m'}. \quad (\text{IV.16})$$

The indices of higher levels depend on the exact strength of the confining potential : when  $\Omega \rightarrow \infty$ , the level  $|0, n, m\rangle$  becomes the usual  $n$ -th LL for 2D electrons. In this case, the matrix element is found to be

$$\langle 0, n, x_0 | e^{-iq \cdot \mathbf{r}} | 0, n, x'_0 \rangle = \delta_{x_0 - x'_0, q_y l^2} e^{-\frac{i}{2} q_x (x_0 + x'_0)} e^{-\frac{l \gamma_+ l^2}{2}} e^{-\frac{l \gamma_- l^2}{2}} L_n(|\gamma_-|^2), \quad (\text{IV.17})$$

with  $\gamma_\pm$  given by

$$\gamma_+ = \frac{1}{\sqrt{2}} \left( \frac{q_y \sin \tilde{\theta}}{l_+} - i l_+ q_\zeta \right), \quad \gamma_- = \frac{1}{\sqrt{2}} \left( \frac{q_y \cos \tilde{\theta}}{l_-} - i l_- q_\xi \right). \quad (\text{IV.18})$$

$q_\xi$  and  $q_\zeta$  are related to  $q_x, q_z$  by the same matrix of Eq. (IV.10).

The effective 2D Hamiltonian is obtained by projecting the interaction to the required level of these two harmonic oscillators. The projection is done with the help of the above density operators and changes the interaction between electrons in a similar way of projecting the physics to the LLL. Inserting the equations above into the interaction part of the Hamiltonian, after integrating out the  $z$ -coordinate, we obtain the effective two-dimensional interaction for the  $n$ -th LL [102, 110] :

$$\begin{aligned} V_{eff}(\mathbf{q}) = & \int \frac{dq_z}{2\pi} \frac{4\pi e^2}{q^2} e^{-\frac{1}{2} \left[ \frac{q_y^2 \sin^2 \tilde{\theta}}{l_+^2/l^4} + l_+^2 (q_x \sin \tilde{\theta} - q_z \cos \tilde{\theta})^2 \right]} \\ & \times e^{-\frac{1}{2} \left[ \frac{q_y^2 \cos^2 \tilde{\theta}}{l_-^2/l^4} + l_-^2 (q_x \cos \tilde{\theta} + q_z \sin \tilde{\theta})^2 \right]} \\ & \times L_n^2 \left[ \frac{1}{2} \left( \frac{q_y^2 \cos^2 \tilde{\theta}}{l_-^2/l^4} + l_-^2 (q_x \cos \tilde{\theta} + q_z \sin \tilde{\theta})^2 \right) \right]. \end{aligned} \quad (\text{IV.19})$$

In the absence of the inplane magnetic field, the effective two-dimensional interaction can be calculated explicitly

$$V_{||}(q) = \frac{2\pi e^2}{q} e^{(qlb)^2} \text{Erfc}(qlb), \quad (\text{IV.20})$$

where  $b = \omega_c/2\Omega$ ,  $\omega_c = eB/m$  is the cyclotron frequency and  $\text{Erfc}(x)$  is the complimentary error function. Notice that the typical length  $bl$  of this potential provides a natural cutoff at short distance such that we expect the Hamiltonian theory to be a valid approach for the description of the FQHE in this case. One can easily verify that the effective interaction is invariant under spatial inversion  $q_x \rightarrow -q_x, q_y \rightarrow -q_y$ . We also comment here that although the effective interaction is obtained from Landau gauge, it is immediately eligible for symmetric gauge because the projection procedure is gauge-invariant.

### IV.3 Calculation of the activation gap

In this part, we are performing the computation of the activation gap under tilted magnetic field. Most saliently we find that the activation gaps are extremely robust against the anisotropy of the interaction induced by the in-plane component of the magnetic field. This robustness is due to the adjustment of the underlying guiding-center metric and thus the hidden deformation of the incompressible liquid. In the Hamiltonian theory, the calculation of the activation gap amounts to calculating the expectation value of the Hamiltonian when exciting a well-separated quasiparticle/quasi-hole pair. This is made possible by the fact that there is no CF LL mixing and CF LLs are orthogonal. This can be proven as we will show in Eq. (IV.31) when rotation symmetry is assumed. By contrast, in the anisotropic situation, the CF LLs are no longer orthogonal to each other. In principle they do not serve to construct a good Hartree-Fock ground state as they are not well defined. However, in most cases, the non-orthogonality of the CF LLs is small and it is reasonable to use perturbation theory. In this part, we compute the CF LL mixing and use perturbation theory to compute the activation gap.

#### IV.3.1 Hilbert space and matrix elements

To start the calculation, we need to define the basis of the Hilbert space and the matrix elements in the corresponding many-body Fock space. As before we start from the cyclotron and guiding-centre coordinates. The ladder operators are as defined in Sec. IV.1 with two parameters  $g_{ab}^\eta$  and  $g_{ab}^R$ . As we will show in our calculation, the latter actually does not enter into the activation gap, it can be regarded as a redundant parameter and only  $g^\eta$  inherits the geometric information of the underlying electrons.

From the basis of single-CF states,

$$|mn\rangle = \frac{(\hat{b}^\dagger)^m (\hat{a}^\dagger)^n}{\sqrt{m!} \sqrt{n!}} |00\rangle, \quad (\text{IV.21})$$

one can construct coherent states that are eigenstates of the ladder operators. Taking e.g. the operators  $\hat{a}$ , the coherent states are defined as :

$$|z\rangle = e^{a^\dagger z} |0\rangle = \sum_{n=0}^{\infty} \frac{|n\rangle}{\sqrt{n!}} z^n, \quad \langle \bar{z} | z \rangle = e^{z\bar{z}}. \quad (\text{IV.22})$$

Here the normalization is not fixed to one in order to compare the coefficients with the matrix elements later and  $z = (x + iy)/l^*$  plays the role of a position (associated with the CF cyclotron variable). In the definition of coherent states, the cyclotron coordinates naturally appear in the exponent. Thus the expectation value of the density operator for coherent states can be expressed as :

$$\langle \bar{z} | e^{-i\mathbf{q}\cdot\boldsymbol{\eta}} | z \rangle = \sum_{n_1=0}^{\infty} \sum_{n_2=0}^{\infty} \frac{\bar{z}^{n_2}}{\sqrt{n_2!}} \frac{z^{n_1}}{\sqrt{n_1!}} \langle n_2 | e^{-i\mathbf{q}\cdot\boldsymbol{\eta}} | n_1 \rangle. \quad (\text{IV.23})$$

On the other hand, the above expectation can be obtained from expanding the density operator in terms of ladder operators :

$$q_a \eta^a = q_a \delta_b^a \eta^b = q_a (v^a \bar{v}_b + \bar{v}^a v_b) \eta^b = q_a v^a \hat{a}^\dagger + q_a \bar{v}^a \hat{a}, \quad (\text{IV.24})$$

where the contra-variant vector  $v^a = g^{ab}v_b$  is defined with the help of the inverse of the metric,  $g^{ab} = (g_{ab}^{-1})$ . In the second equality we use the property  $g^{ac}g_{cb} = \delta_b^a \rightarrow v^a\bar{v}_b + \bar{v}^a v_b = \delta_b^a$ . So the expectation value can be written as :

$$\begin{aligned} \langle \bar{z} | e^{-i\mathbf{q}\cdot\boldsymbol{\eta}} | z \rangle &= \langle \bar{z} | \exp \left[ -il^*(q_+a^\dagger + q_-a) \right] | z \rangle \\ &= \langle \bar{z} - il^*q_+ | z - il^*q_- \rangle e^{q^2l^{*2}/4} \\ &= \exp \left[ \bar{z}z - il^*(q_+z + q_-\bar{z}) \right] e^{-q^2l^{*2}/4}, \end{aligned} \quad (\text{IV.25})$$

where  $q_+ = q_a v^a, q_- = q_a \bar{v}^a$ . Comparing the the above equation with Eq. (IV.23), one obtains :

$$\langle n_2 | e^{-i\mathbf{q}\cdot\boldsymbol{\eta}} | n_1 \rangle = \sqrt{\frac{n_2!}{n_1!}} e^{-x/2} (-iq_+l^*)^{n_1-n_2} L_{n_2}^{n_1-n_2}(x), \quad (\text{IV.26})$$

where  $x = q_a q_b g^{ab} l^{*2}/2$  and  $L_n^\alpha$  are associated Laguerre polynomials. The result is valid for  $n_1 \geq n_2$ . For  $n_1 \leq n_2$ , the matrix elements are obtained from the complex conjugation  $\langle n_2 | e^{-i\mathbf{q}\cdot\boldsymbol{\eta}} | n_1 \rangle = \langle n_1 | e^{i\mathbf{q}\cdot\boldsymbol{\eta}} | n_2 \rangle$ .

Now we proceed to the evaluation of the activation gap. The ingredient is the matrix element of the Hamiltonian in states excited from the reference state of  $p$  filled CF LLs. The Hamiltonian (III.18) is written in second quantization as

$$H = \frac{1}{2} \sum_{1,2,3,4} V_{eff}(\mathbf{q}) \rho_{12}^p(\mathbf{q}) \rho_{34}^p(-\mathbf{q}) d_1^\dagger d_2 d_3^\dagger d_4. \quad (\text{IV.27})$$

The subscripts  $i = 1, 2, 3, 4$  are abbreviations of  $(m_i, n_i)$  corresponding to the CF states defined before.  $d_i$  and  $d_i^\dagger$  are annihilation and creation operators of CFs in this basis with  $\{d_i, d_i^\dagger\} = \delta_{ij}$ , and  $\rho_{ij}^p(\mathbf{q})$  is the matrix element of the preferred density operator :

$$\rho^p(\mathbf{q})_{m,n;m',n'} = \langle m, n | \rho_e(\mathbf{q}) - c^2 \chi(\mathbf{q}) | m', n' \rangle. \quad (\text{IV.28})$$

The above matrix has a product structure for the indices of angular momenta and Landau levels,  $\rho^p(\mathbf{q})_{m,n;m',n'} = \rho^{p(m)}(\mathbf{q})_{m,m'} \otimes \rho^{p(n)}(\mathbf{q})_{n,n'}$ . With the Hartree-Fock assumption, the activation gap can be calculated using Wick's theorem. Notice that if one contracts indices 12 or 34, it will give a  $\delta(\mathbf{q})$ . This contribution vanishes because the interaction is assumed to be screened by the positive charge background  $V_{eff}(0) = 0$ . The matrix element of the Hamiltonian between two one-particle excitation states is :

$$\begin{aligned} \langle \mathbf{p} | d_f H d_i^\dagger | \mathbf{p} \rangle &= \frac{1}{2} \int \frac{d^2q}{4\pi^2} V_{eff}(\mathbf{q}) \rho_{12}^p(\mathbf{q}) \rho_{34}^p(-\mathbf{q}) \times \sum_{1,2,3,4} [\delta_{f1}(1-n_1)\delta_{23}(1-n_2)\delta_{4i}(1-n_4) \\ &\quad - \delta_{f3}(1-n_3)\delta_{14}n_4\delta_{2i}(1-n_2)], \end{aligned} \quad (\text{IV.29})$$

and a similar expression for hole excitations. Because of the product structure of  $\rho^p$ , it can be shown that the interaction preserves the CF angular momentum (more precisely the momentum of guiding centers). Using the identity  $\exp(-i\mathbf{q}\cdot\mathbf{R}) \times \exp(i\mathbf{q}\cdot\mathbf{R}) = \mathbf{1}$ , the above expression is thus proportional to  $\delta_{m_f, m_i}$ . It only mixes different Landau levels of the



composite fermion. By summing up all guiding-center parts, one obtains :

$$\begin{aligned} \langle \mathbf{p} | d_f H d_i^\dagger | \mathbf{p} \rangle = & \frac{1}{2} \int \frac{d^2 q}{4\pi^2} V_{eff}(\mathbf{q}) \Theta(n_f - p) \Theta(n_i - p) \times \left[ \sum_{n_2=p}^{\infty} \rho_{n_f, n_2}^p(\mathbf{q}) \rho_{n_2, n_i}^p(-\mathbf{q}) \right. \\ & \left. - \sum_{n_1=0}^{p-1} \rho_{n_1, n_i}^p(\mathbf{q}) \rho_{n_f, n_1}^p(-\mathbf{q}) \right] \delta_{m_f, m_i}, \end{aligned} \quad (\text{IV.30})$$

and a similar formula for hole excitations. Here  $\Theta$  is the step function with  $\Theta(x < 0) = 0$  and  $\Theta(x \geq 0) = 1$ . We use the symbol  $\rho_{n_1, n_2}^p$  to represent the matrix elements of the preferred density operator between CF LL  $n_1$  and CF LL  $n_2$ . As the guiding-center counter part of the density operator always does not enter the calculation, in our future expressions the matrix elements  $\rho_{n_1, n_2}^p$  always refers to that between two CF LLs. In order to study the role of anisotropy in  $V_{eff}$ , we need to insert the explicit expressions for the matrix elements of the density operator  $\rho_{n_1, n_2}^p$  obtained before with the help of coherent states.

With these expressions for  $\rho^p(\mathbf{q})$  at hand, we are able to evaluate the Hamiltonian in one-particle/hole excitation space. The interaction preserves particle numbers. Therefore for the excitation of a CF, both the initial state and the final state should have the quasiparticle on an empty CF LL, such that there is no mixing between hole excitations and particle excitations in the one-particle/hole excitation space. Now if we choose the metric  $g_{ab}$  to be isotropic, i.e.  $v = (1, i)/\sqrt{2}$ , the reduced matrix elements behaves like  $\rho_{n_1, n_2}^p(\mathbf{q}) \sim \exp[-i(n_1 - n_2)\phi]$ , where  $\phi$  is the angle between  $\mathbf{q}$  and the  $x$ -axis. Hence according to Eq. (IV.30) we observe that

$$\langle \mathbf{p} | d_f H d_i^\dagger | \mathbf{p} \rangle \propto \int d\phi V_{eff}(\mathbf{q}) e^{-i(n_f - n_i)\phi}. \quad (\text{IV.31})$$

This actually gives an angular decomposition of the effective potential, which means that, if  $V_{eff}$  is isotropic, there is no mixing between different single-particle excitation states, as mentioned at the beginning of this section. The Hartree-Fock assumption is self-consistent and stable. However, if  $V_{eff}$  is anisotropic, it will induce transitions from one CF LL to another. When these transitions are small, the anisotropy is simply a perturbation to the picture of  $p$  filled CF LLs. However, when the transitions are sufficiently prominent, the spacing between LLs may even close due to the mixing, in which case the liquid state is no longer stable. Most saliently, as mentioned above, the metric  $g_{ab}$  in the CF is a parameter that one can vary to account for the anisotropy of the underlying interaction potential. In this way the angular decomposition changes its shape (from circular orbitals to elliptical orbitals) so that the mixing Eq. (IV.31) takes a minimal value. As a result an optimal metric is obtained. This angular decomposition is better seen in the language of generalized pseudopotentials, which we will briefly discuss in the next section.

### IV.3.2 Relation between CF LL mixing and generalized pseudopotentials

In particular, we can also interpret CF LL mixing in the language of generalized pseudopotentials. As we have already mentioned in Sec. II.1, in an isotropic translationally invariant quantum Hall system, any two-body interaction  $\hat{V}$ , when specified to a particular pair of electrons, can be expanded in terms of the relative-angular-momentum basis,  $\hat{V} = \sum_m V_m |m\rangle \langle m|$ , where  $|m\rangle$  is the two-body state with relative angular momentum  $m$  [60]. For fermions only odd values of  $m$  are relevant to insure the antisymmetry of the wave

function. The Laughlin state for filling  $\nu = 1/q$  is characterized as the unique zero-energy eigenstate of a certain class of Haldane's pseudopotential [60],  $H_M = \sum_{m=1}^{q-2} V_m P_m$ , where  $P_m$  is a projection operator  $|m\rangle\langle m|$  to the space with relative angular momentum  $m$  [see Eq. (II.5) for explicit forms], and the pseudopotentials  $V_m$  are positive coefficients that specify the energy of two electrons in the relative angular momentum state  $|m\rangle$ . In an anisotropic but translationally invariant system, the interaction is no longer diagonal in the angular-momentum basis, and Haldane's original projectors  $P_m$  no longer form a complete basis in the two-body interaction space. A generalization of Haldane's pseudopotentials has recently been proposed to incorporate those off-diagonal parts  $|m+n\rangle\langle m|$  ( $n \neq 0$ ) [111] :

$$H = \frac{1}{2} \sum_{m,n,\sigma,\mathbf{q}} V_{m,n}^\sigma P_{m,n}^\sigma(\mathbf{q}) \bar{\rho}_e(\mathbf{q}) \bar{\rho}_e(-\mathbf{q}). \quad (\text{IV.32})$$

where for each pair of electrons,  $\sigma = \pm$  is for symmetric and anti-symmetric combinations of  $|m+n\rangle\langle m|$  and  $|m\rangle\langle m+n|$  in order to make the interaction Hermitian. The above form makes use of the density operator  $\bar{\rho}_e(\mathbf{q})$  to sum over all pairs of electrons. The  $P_{m,n}^\sigma(\mathbf{q})$ , the explicit forms of which will be discussed later on in Eqs. (IV.34) and (IV.35), are now a complete basis of orthogonal polynomials for any two-body translationally invariant interaction  $V_{eff}(\mathbf{q})$  projected into the LLL and the expansion coefficients  $V_{m,n}^\sigma$  are the generalized pseudopotentials :

$$V_{eff}(\mathbf{q}) = \sum_{m,n,\sigma} V_{m,n}^\sigma P_{m,n}^\sigma(\mathbf{q}),$$

$$V_{m,n}^\sigma = \int d^2q V_{eff}(\mathbf{q}) P_{m,n}^\sigma(\mathbf{q}). \quad (\text{IV.33})$$

In this expansion, the diagonal components  $V_{m,0}^+ = V_m$  are Haldane's original pseudopotentials and the other components are referred to as off-diagonal pseudopotentials. In their presence, no model wave function is known as the zero-energy ground state. In comparison with the diagonal parts which define the Laughlin state, the off-diagonal parts thus serve as perturbations to the liquid state. Their relative magnitude with respect to the diagonal pseudopotentials provides a good criterion for stability issues [110, 112].

The explicit expressions of the associated projectors are as follows [111] :

$$P_{m,n}^+(\mathbf{q}, g) = \lambda_n \mathcal{N}_{m,n} \left( L_m^n (|q|^2 l^2) e^{-\frac{1}{2}|q|^2 l^2} (q_+ l)^n + \text{c.c.} \right), \quad (\text{IV.34})$$

$$P_{m,n}^-(\mathbf{q}, g) = -i \mathcal{N}_{m,n} \left( L_m^n (|q|^2 l^2) e^{-\frac{1}{2}|q|^2 l^2} (q_+ l)^n - \text{c.c.} \right), \quad (\text{IV.35})$$

where  $\lambda_n = 1/\sqrt{2}$  when  $n = 0$  and  $\lambda_n = 1$  for  $n \neq 0$ . There is a variational metric  $g$  and it enters the definition by  $|q|^2 = q_a q_b g^{ab}$  and  $q_+$  (as defined before). By varying this metric, the amplitudes of different generalized pseudopotential components vary in the expansion of an interaction. Furthermore, as this potential here is for electrons, the original magnetic length  $l$  is used and  $\mathcal{N}_{m,n}$  is the normalization for the expansion of the two-body interaction. The projectors are chosen to be real and the components  $P_{m,n}^-$  with negative superscripts are only non-vanishing for  $n \neq 0$  and therefore do not exist in an isotropic case.

For the isotropic metric, the matrix of the preferred density can be denoted as ( $n_1 \geq n_2$ ) :

$$\rho_{n_2, n_1}^p(\mathbf{q}) = (\exp i\phi)^{n_1 - n_2} \rho_{n_2, n_1}^p(q), \quad (\text{IV.36})$$

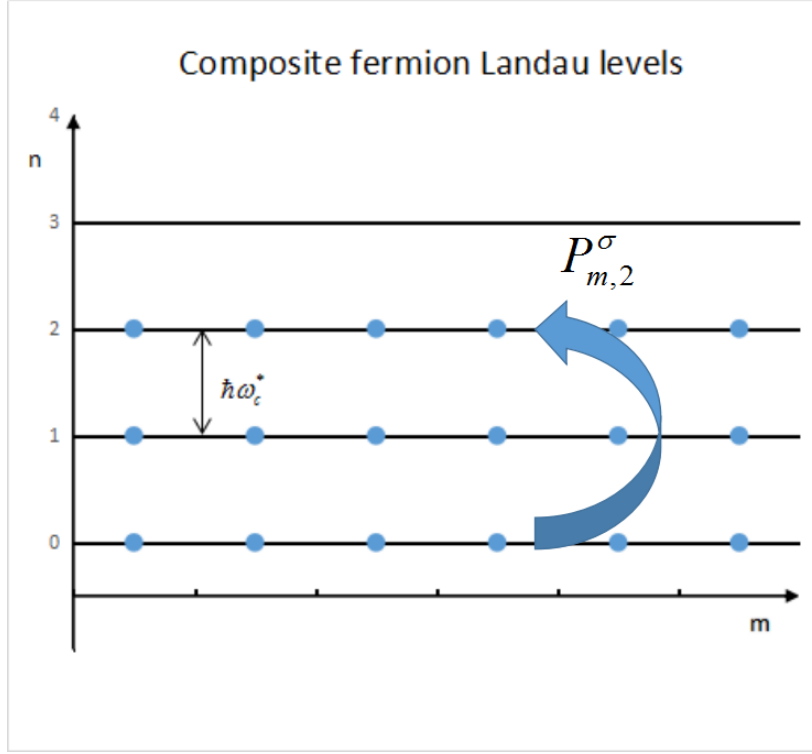


Fig. IV.2 The anisotropic components of the generalised pseudopotentials introduce CF LL mixing.

where we use the parametrization  $q_x + iq_y = q \exp(i\phi)$  and  $\rho_{n_2, n_1}^p(q)$  is a function only relying on the norm of  $\mathbf{q}$  :

$$\rho_{n_2, n_1}^p(q) = \sqrt{\frac{n_2!}{n_1!}} \left( \frac{-iq l^* c}{\sqrt{2}} \right)^{n_1 - n_2} \left[ e^{-q^2 l^{*2} c^2 / 4} L_{n_2}^{n_1 - n_2} \left( \frac{q^2 l^{*2} c^2}{2} \right) - c^{2+2n_2-2n_1} f e^{-q^2 l^{*2} / 4c^2} L_{n_2}^{n_1 - n_2} \left( \frac{q^2 l^{*2}}{2c^2} \right) \right], \quad (\text{IV.37})$$

with  $L_m^n$  the associated Laguerre polynomial. Here,  $f = \exp(-q^2 l^2 / 4c^2) / \exp(-q^2 l^2 / 4)$  is a factor to account for the difference in the LLL projection between electrons and pseudovortices [113].

The mixing between CF LLs can be calculated straightforwardly using the above expressions. As mentioned in the beginning of the section, the mixing for quasiparticle excitation is given by :

$$M_{n_f, n_i} = \frac{1}{2} \int \frac{d^2 q}{4\pi^2} V_{eff}(\mathbf{q}) \left[ \langle n_f | \rho^p(\mathbf{q}) \rho^p(-\mathbf{q}) | n_i \rangle - 2 \sum_{n_1=0}^{p-1} \rho_{n_1, n_i}^p \rho_{n_f, n_1}^p \right] \delta_{m_f, m_i}. \quad (\text{IV.38})$$

Assuming the initial and final states are different with  $n_i > n_f$ , plugging Eq. (IV.36), we

find that the above equation gives :

$$M_{n_f, n_i} = \int \frac{d^2q}{8\pi^2} V_{eff}(\mathbf{q}) e^{i\phi(n_i - n_f)} \left[ -c^2 f \left( \frac{c^2 - 1}{c} \right)^{n_i - n_f} \rho_{n_f, n_i}^p \left( q \frac{c^2 - 1}{c} \right) - 2 \sum_{n_1=0}^p q^{2(n_f - n_1)} \rho_{n_1, n_i}^p(q) \right]. \quad (\text{IV.39})$$

According to the angular part integral, where  $\phi$  is the angle between  $\mathbf{q}$  and the  $x$ -axis, the above equation is only non-vanishing when  $V_{eff}(\mathbf{q})$  has the component  $\exp[i(n_f - n_i)\phi]$  in its angular decomposition. These are exactly the generalized pseudopotentials  $V_{m,n}^\pm$  with  $n = n_i - n_f$ . For a generalized pseudopotential  $V_{m, n_i - n_f}^+ P_{m, n_i - n_f}^+$ , it contributes to the mixing between CF LL  $n_i$  and  $n_f$  as :

$$M_{n_f, n_i}^m = V_{m, n_i - n_f}^+ \int \frac{qdq}{4\pi} \lambda_{n_i - n_f} \mathcal{N}_{m, n_i - n_f} L_m^{n_i - n_f}(q^2) e^{-\frac{1}{2}q^2} \left[ -2 \sum_{n_1=0}^p q^{2(n_f - n_1)} \rho_{n_1, n_i}^p(q) \right. \\ \left. \rho_{n_1, n_f}^p(q) - c^2 f \left( \frac{c^2 - 1}{c} \right)^{n_i - n_f} \rho_{n_f, n_i}^p \left( q \frac{c^2 - 1}{c} \right) \right]. \quad (\text{IV.40})$$

The contribution from  $V_{m,n}^- P_{m,n}^-$  can be worked out similarly. When several generalized pseudopotentials with the same second indices are present,  $\sum_{m,\sigma} V_{m,n}^\sigma P_{m,n}^\sigma$ , all of them influence the amplitude  $M_{n_i - n, n_i}$  with different weights, as calculated above. A special situation arises when only one pseudopotential is dominant, say  $V_{m_0, n}^\sigma \gg V_{m, n}^\sigma$  with  $m \neq m_0$ . Then the mixing amplitude is merely proportional to this pseudopotential such that Eq. (IV.40) becomes simply

$$M_{n_f, n_i} \propto V_{m_0, n_i - n_f}^\sigma, \quad (\text{IV.41})$$

In this case, minimizing the mixing amplitude is equivalent to minimizing the coefficient of this pseudopotential. As a result, all fillings exhibit the same optimal metric. Our following calculation shows that this is almost the case for the anisotropy induced by parallel magnetic field.

So we conclude that choosing the isotropic metric  $g = \mathbf{1}$ ,  $q_+ = |q|e^{i\phi}/\sqrt{2}$ , one can immediately observe that  $P_{m,n}^\pm$  introduces transition from a CF LL  $n'$  to  $n' \pm n$ . Notice, however, that since the CF does not have the same magnetic length as an electron, the  $P_{m,n}^\pm$  associated with the off-diagonal pseudopotentials  $V_{m,n}^\pm$  are not in one-to-one correspondence with the different CF LL transitions, but they rather mix all the CF LLs separated by a multiple of  $n$ . The mixing due to an off-diagonal component of the generalized pseudopotential is a superposition of

$$M_{n_f, n_i}^m = \langle \mathbf{p} | d_f H d_i^\dagger | \mathbf{p} \rangle \propto V_{m, |n_i - n_f|}^+. \quad (\text{IV.42})$$

Above we neglect the contribution from  $V^-$  because these generalized pseudopotentials are odd under spatial inversion and therefore do not exist in the tilted magnetic field situation. In Ref. [110], the optimal  $g$  is chosen such as to minimize the off-diagonal components  $n \neq 0$ , because they are perturbations to Haldane's pseudopotentials which define the liquid state. The Hamiltonian theory provides us with a complementary picture : the off-diagonal pseudopotentials cause transitions between CF LLs and thus destroy the Hartree-Fock nature of the ground state. However, the variation of the metric  $g$  allows us to minimize CF LL

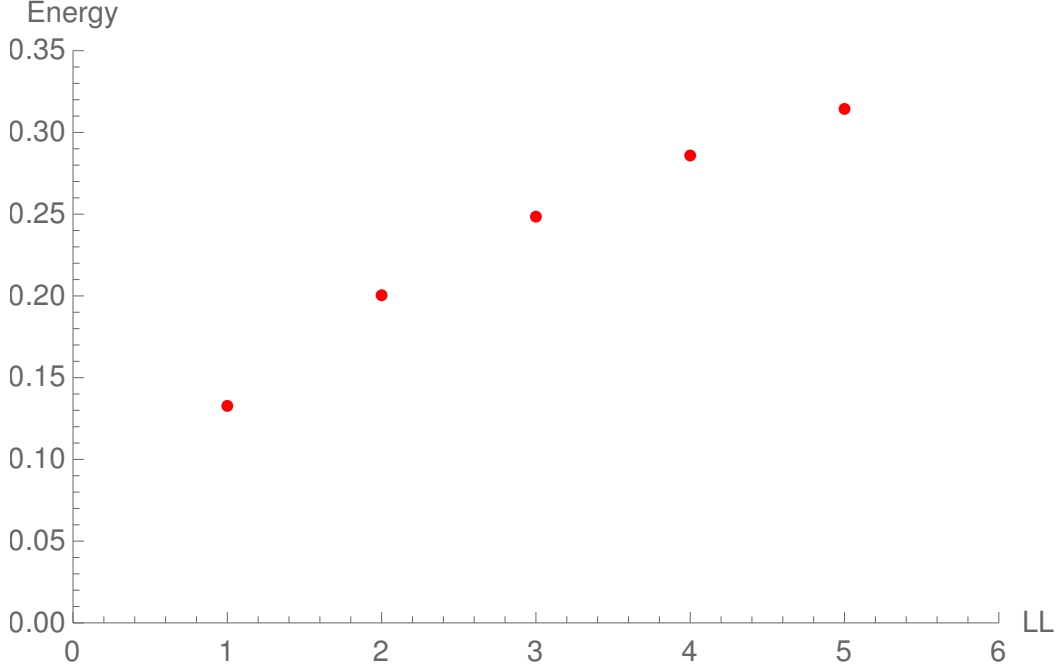


Fig. IV.3 The energy of creating a composite fermion with respect to the CF LL index for  $\nu = 1/3$ ,  $\tan \theta = 0$ ,  $\Omega/\omega_c = 2$ , in the unit of  $e^2/\varepsilon l$  with  $\varepsilon$  the dielectric constant.

mixing and thus to save the picture of  $p$  filled CF LLs. The optimal metric is defined to have the minimal CF LL mixing  $M_{n_f, n_i}$  ( $n_f \neq n_i$ ). Since this transition amplitude is proportional to the off-diagonal pseudopotentials [see Eq. (IV.42)], the optimal metric obtained in this way agrees with that of Ref. [110], as we also check numerically in the following section.

Notice that the generalized pseudopotential has a certain parity symmetry. So for the situation of tilting the magnetic field, where the effective potential is invariant under  $q_x \rightarrow -q_x$ ,  $q_y \rightarrow -q_y$  its generalized pseudopotential decomposition thus has no components of  $P_{r,s}^\pm$  with  $s$  odd since the latter do not have an inversion symmetry. According to the discussion above, this anisotropic interaction only mixes CF LLs which differ by an even index.

### IV.3.3 Optimal metrics and the activation gap under a tilted magnetic field

Making use of the operator expression of  $\rho^p(\mathbf{q})\rho^p(-\mathbf{q})$ , Eq. (IV.30) is further simplified to

$$\begin{aligned} \langle \mathbf{p} | d_f H d_i^\dagger | \mathbf{p} \rangle = & \frac{1}{2} \int \frac{d^2 q}{4\pi^2} V_{\text{eff}}(\mathbf{q}) \left\{ (1 + c^4 f^2) \delta_{n_f, n_i} - 2c^2 f \cos \left[ \mathbf{q} \cdot \boldsymbol{\eta} \left( c - \frac{1}{c} \right) \right] \right\}_{n_f n_i} \\ & - 2 \sum_{n_1=0}^{p-1} \rho_{n_1, n_i}^p(\mathbf{q}) \rho_{n_f, n_1}^p(-\mathbf{q}) \left\} \delta_{m_f, m_i}, \end{aligned} \quad (\text{IV.43})$$

which allows us to calculate the matrix elements of  $H$ . The Hilbert space is infinite and we have an infinite number of CF LLs, which makes it impossible to diagonalize the single-particle excitations. In order to obtain a quantitative result, we truncate the number of

CF LLs. As pointed out in Ref. [114], even if the preferred density is assumed to take into account non-perturbative corrections, the physical constraint is still not imposed faithfully, and higher CF LLs are actually nonphysical. A reasonable approximation is to examine up to which CF LL the following relation holds :

$$\langle \mathbf{p} + m | H | \mathbf{p} + m \rangle - \langle \mathbf{p} | H | \mathbf{p} \rangle \approx |m - p| \hbar \omega_* + \text{cst.}, \quad (\text{IV.44})$$

where  $|\mathbf{p} + m\rangle$  means the state obtained by creating a quasiparticle ( $m \geq p$ ) or a quasi-hole ( $m < p$ ) of LL  $m$  on top of the  $p$ -filled ground state  $|\mathbf{p}\rangle$ . The above formula derives from the fact that the CF experiences a reduced magnetic field. For high indices of the CF LL, this relation is no longer valid (see Fig. IV.3). A reasonable criterion is to take into account only  $2p + 1$  CF Landau levels for a filling  $\nu = p/(2ps + 1)$  [114]. For Landau levels higher than  $2p + 1$ , their energies become closer and closer and approach a continuum limit, as the composite fermion is no longer a well-defined quasiparticle.

We first calculate the activation gaps and optimal metrics for filling  $\nu = 1/3$  in the LLL. As mentioned in the last section, the anisotropy introduces transitions between different Landau levels. Recall that the single-particle excitation matrix is defined as the expectation value of  $H$  when creating a hole in a filled CF Landau level or a particle in an empty level

$$M_{m,n} = \langle \mathbf{p} + m | H | \mathbf{p} + n \rangle. \quad (\text{IV.45})$$

The spectrum of exciting a single particle/hole is obtained by diagonalizing this matrix. First, we calculate the matrix elements in the case of an isotropic metric. For  $\nu = 1/3$ , the ground state consists of a completely filled  $n = 0$  CF LL. Holes are created in the  $n = 0$  CF LL while particles are created in  $n > 0$  CF LLs. The hole excitation has no mixing with the particle excitation because of particle number conservation. So the perturbation to the activation gap comes from the transition from  $n = 1$  to higher CF LLs. According to the previous arguments, the first three states are deemed to be physical. As the system has an inversion symmetry, the lowest LL that perturbs the activation gap is the  $n = 3$  level, at the brim of physical states. Therefore, to obtain the leading perturbation, it is reasonable to take only the transition from  $n = 1$  to  $n = 3$  into account. The relevant LL mixing amplitude is  $M_{1,3} = M_{3,1}^*$ . It is the direct reflection of the anisotropic effects.

Let us now add the variational metric to the Hamiltonian theory. The optimal metric is now the one which minimizes the inter-LL transition amplitude  $M_{1,3}$ . As the inplane magnetic field picks a preferred direction and the interaction is inversion invariant, the system has two principal axes. Due to this symmetry, the ansatz of the metric takes the form :

$$g_{ab} = \begin{pmatrix} \alpha^2 & 0 \\ 0 & 1/\alpha^2 \end{pmatrix}. \quad (\text{IV.46})$$

The corresponding complex vector of this metric can be parameterized by  $v_a = (\alpha, i/\alpha)/\sqrt{2}$ . The results of  $\alpha$  are shown in Fig. IV.4. The optimal metric starts to deviate from one at around  $\tan \theta = 0.5$  ( $\theta = 27^\circ$ ) for all thicknesses. As the anisotropic effects come from the movements in  $z$ -direction, we expect that the metric is more anisotropic for large thickness. This is indeed the behavior in our results. The thicker the sample is, the more rapidly the optimal metric parameter  $\alpha$ , which is approximately linear in  $\tan \theta$ , grows with respect to the tilting angle. Notice, however, that the deformation is always a small one. To connect

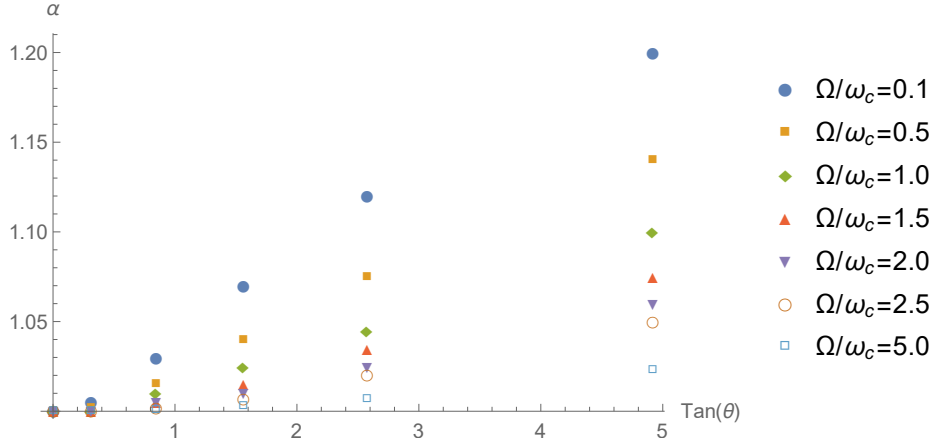


Fig. IV.4 Values of  $\alpha$  of optimal metrics as a function of the tilt angle  $\theta$ , for  $\nu = 1/3$ , in the LLL, at different confining potentials.

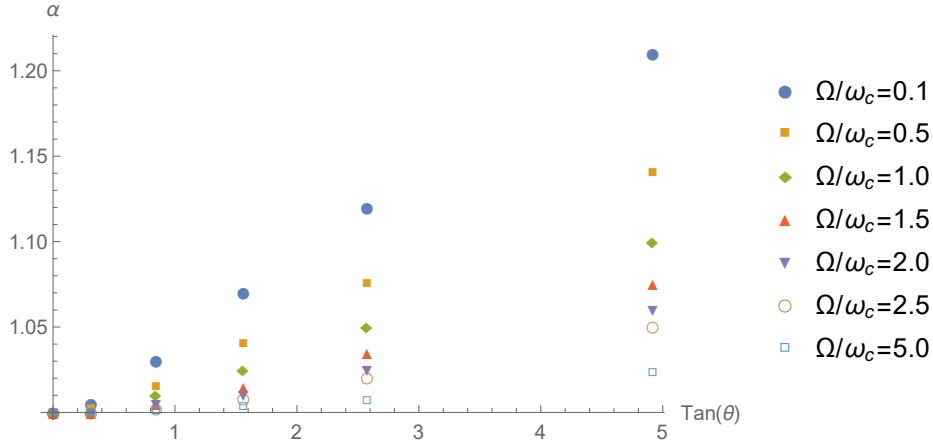


Fig. IV.5 Values of  $\alpha$  of optimal metrics as a function of the tilt angle  $\theta$ , for  $\nu = 2/5$  in the LLL, for the same set of confining potentials.

our calculation to tilted magnetic field experiments, for a wide quantum well of width 50 nm [106], the ratio between the confining frequency and the cyclotron frequency is estimated to be  $\Omega/\omega_c = 2/B[\text{T}]$ . At the filling  $\nu = 1/3$  and  $2/5$ , the confining frequency can be much smaller than the cyclotron frequency for such wide quantum wells,  $\Omega/\omega_c \simeq 0.1 \sim 0.2$ . So we set  $\Omega/\omega_c = 0.1$  as our lowest value in calculation. We see that even in the extreme case, with  $\Omega/\omega_c = 0.1$  and  $\tan \theta = 5$ , the optimal metric deviates from the isotropic one by only 20%. Therefore, the deformation remains small. This agrees with the results from the analysis in terms of generalized pseudopotentials [110].

Figures IV.6 to IV.7 show our results for the activation gap, for two different values of the confinement potential, as a function of the tilt angle. The yellow squares indicate those calculated for the optimal metric evaluated for each value of the tilt angle, in comparison with the activation gaps obtained from a purely isotropic metric (blue circles). We note that for moderate parameters, the inter-Landau level transition  $M_{1,3}$  is always much smaller than the Landau level spacing  $M_{1,1} + M_{0,0}$ . For  $\Omega/\omega_c = 2$  and  $\theta = 35^\circ$ ,  $M_{1,3} = 0.002$  while

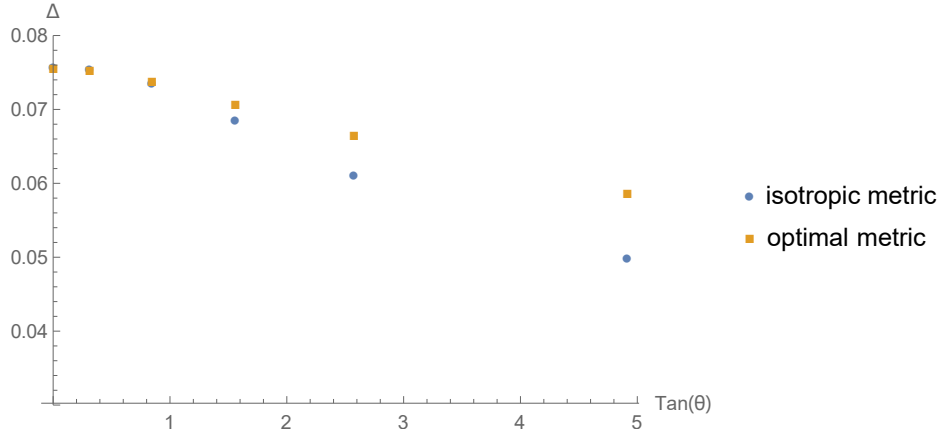


Fig. IV.6 The activation gap as a function of  $\tan \theta$  for  $\nu = 1/3$  of a weak confining potential  $\Omega/\omega_c = 0.1$ .

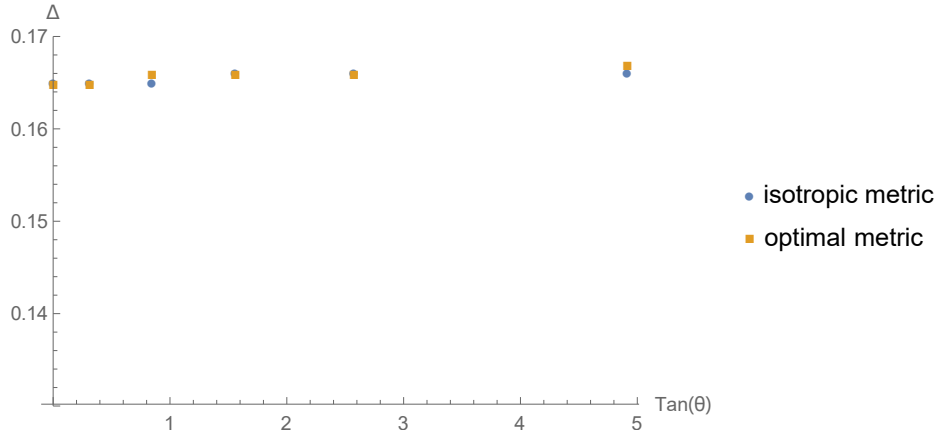


Fig. IV.7 The activation gap as a function of  $\tan \theta$  for  $\nu = 1/3$  of a strong confining potential  $\Omega/\omega_c = 5$ .

$M_{1,1} + M_{0,0} = 0.147$ , the former is only one percent of the latter. Notice that even in the extreme case of a wide quantum well  $\Omega/\omega_c = 0.1$  with  $\tan \theta = 5$ , i.e. an inplane component of the magnetic field that is five times larger than its perpendicular component, the ratio between  $M_{1,1} + M_{0,0} = 0.050$  and  $M_{1,3} = 0.017$  is roughly  $1/3$  only, such that our variational metric can still cope with this situation. Hence the activation gap is robust against the parallel magnetic field – when the CFs pick the optimal metric, the activation gap decreases much more slowly than that obtained from a isotropic metric even for a weak confining potential and large tilting angles.

We also perform the same calculation for the  $\nu = 2/5$  filling [see Figs. IV.8 and IV.9]. Among the physically relevant CF LLs, the lowest one perturbing the activation gap is the  $n = 4$  level. The optimal metric, which we have calculated for  $\Omega/\omega_c$  between 0.1 and 5, is almost the same as that in  $\nu = 1/3$  [see Fig. IV.5]. This is in accordance with our discussion in Sec. IV.3.2. Indeed, all we are minimizing is the  $\delta n = 2$  transition, which is proportional to the  $V_{m,2}^\pm$  pseudopotential components. If one of them is dominant, say  $V_{1,2}^+$ , as the strategy



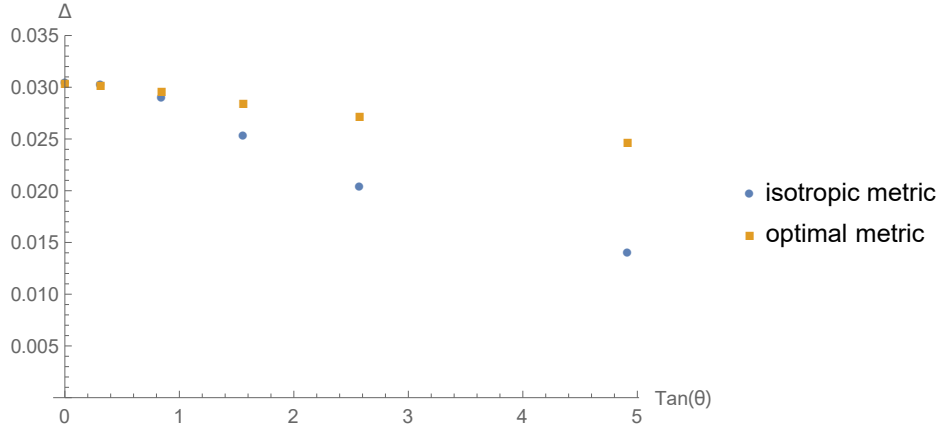


Fig. IV.8 The activation gap as a function of  $\tan \theta$  for  $\nu = 2/5$  of a weak confining potential  $\Omega/\omega_c = 0.1$ .

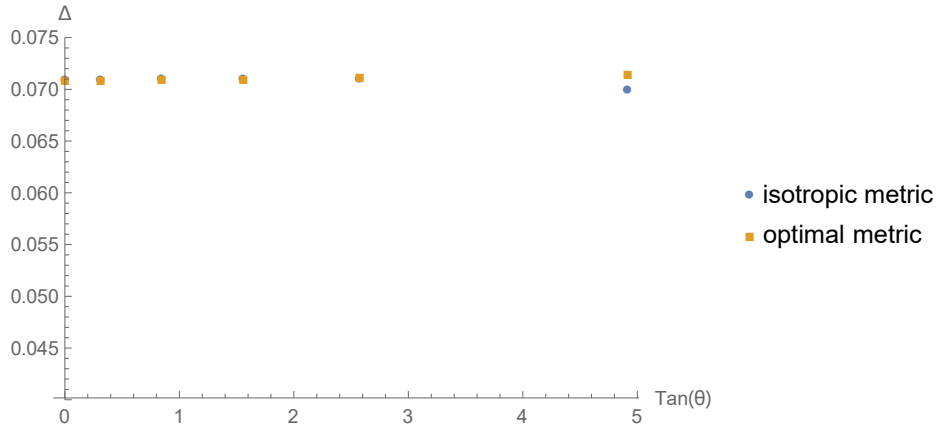


Fig. IV.9 The activation gap as a function of  $\tan \theta$  for  $\nu = 2/5$  of a strong confining potential  $\Omega/\omega_c = 5$ .

adapted in Ref. [110], then  $M_{m,m+2}$  is simply controlled by this pseudopotential  $V_{1,2}^+$  (also see Sec. IV.3.2). In such case, when the metric is chosen to minimize this coefficient, the transition amplitude is also minimal, so that the optimal metrics for  $\nu = 1/3$  and  $\nu = 2/5$  are very close. On the other hand, as the activation gap itself for  $\nu = 2/5$  is smaller, the perturbation due to the parallel magnetic field is stronger. One can see that for large tilting the LL mixing amplitude  $M_{2,4}$  is of the same magnitude as the Landau level spacing  $M_{2,2} + M_{1,1}$ . This means that the Hartree-Fock ansatz receives strong correction. However, the activation gaps under the optimal metrics are still very robust.

As an additional support to the truncation that we use, we also verify the perturbations from higher CF LLs. Take  $\nu = 2/5$  for example, the mixing between the second and the sixth CF LLs  $M_{2,6}$  is always one magnitude smaller than the mixing between the second and the fourth LLs  $M_{2,4}$ . In table IV.1, the extreme case of large tilting and thickness is listed. The matrix elements  $M_{2,4}$  and  $M_{4,6}$  are comparable to the activation gap, but the higher transition  $M_{2,6}$  is merely one tenth of them. So it is valid to neglect the mixing from higher LLs and restrict the perturbative approach to the first five LLs in order to illustrate the

Table IV.1 Matrix elements of  $M$ , the expectation value of  $H$  in the single-particle/hole excitation space, for filling  $\nu = 2/5$  at  $\tan \theta = 5$ ,  $\Omega/\omega_c = 0.1$ , the most extreme case in our calculation.

$M_{2,2}$	$M_{4,4}$	$M_{6,6}$	$M_{2,4}$	$M_{2,6}$	$M_{4,6}$
0.039	0.060	0.075	-0.018	-0.002	-0.021

result qualitatively.

We finally remark that the above computation is only valid in the perturbative sense. The Hartree-Fock ground state of  $p$  filled LLs should be calculated in a self-consistent way in order to give the accurate activation gap. However there is no simple self-consistent approach in FQH problems. All of this is based on the special form of trial wave functions. Nonetheless, our calculation is valid when the inter-CF LL transitions are small, as reflected in our work. It provides a qualitative criterion for the robustness of activation gaps. In particular, in the computation of the optimal metric, we observe that when tuning the metric, the transition amplitude goes from positive to negative values. So at some point we can turn off the transition from, for example,  $n = 1$  to  $n = 3$  Landau levels. This means for the optimal metric, the Hartree-Fock ansatz is self-consistent in the first few LLs.

We finish this section with a brief discussion of some CF states in the first excited LL, where the CF liquid state is more vulnerable to other clustered phases, such as non-Abelian phases [115] or solid phases [116, 117, 118]. We construct the optimal metrics for fillings  $\nu = 7/3$  and  $\nu = 11/5$  and corroborate the robustness of the activation gaps to a parallel component of the magnetic field.

The optimal metrics are shown in Fig. IV.10 and Fig. IV.11. In the first LL, there is a transition of the principal axis of the optimal metric. At small tilting angle, the  $y$ -axis is slightly favoured and  $\alpha < 1$ . When the tilting angle increases,  $\alpha$  gradually returns to 1 and then increases such that the  $x$ -direction becomes the principal axis of  $g_{ab}$  as in the LLL. The transition takes place at higher values of parallel magnetic field for stronger confining potential in  $z$ -direction. Its value is close to the transition points of  $V_{1,2}^+$  in Ref. [110]. Such a phenomenon further convinces us that only one pseudopotential component is dominant, i.e. the  $V_{1,2}^+$  component.

The activation gaps for  $\nu = 7/3$ ,  $\nu = 11/5$ , and  $\nu = 20/9$  are also computed, as shown in Fig. IV.12. We have chosen these fractions since there is experimental [119, 120] and theoretical [117, 118] evidence that the CF family with  $s = 2$  flux pairs attached is generically more robust to CDW type instability than that with a single flux pair ( $s = 1$ ). While the  $\nu = 7/3$  quantum Hall state is clearly visible, the  $\nu = 12/5$  is absent – calculations within the CF wave-function approach have found an instability of collective excitations at finite wave vector [121]. The neutral gap for  $\nu = 11/5$  is shown to be higher than that of  $\nu = 7/3$  via single mode approximation [122], however in this calculation it turns out that the charge gap of the latter is higher. This may be a long-wave-vector behaviour of the dispersion, as the activation gap of  $\nu = 7/3$  for pure 2D Coulomb potential is also slightly higher than that of  $\nu = 11/5$ [118]. On the other hand, for the wide quantum well that we are using here, the confining potential has a lower energy scale than the Landau level. The actual first excited level should correspond to that with index 1 in the confining level, instead of the Landau level. This can cause a difference in the behaviour of the gaps.

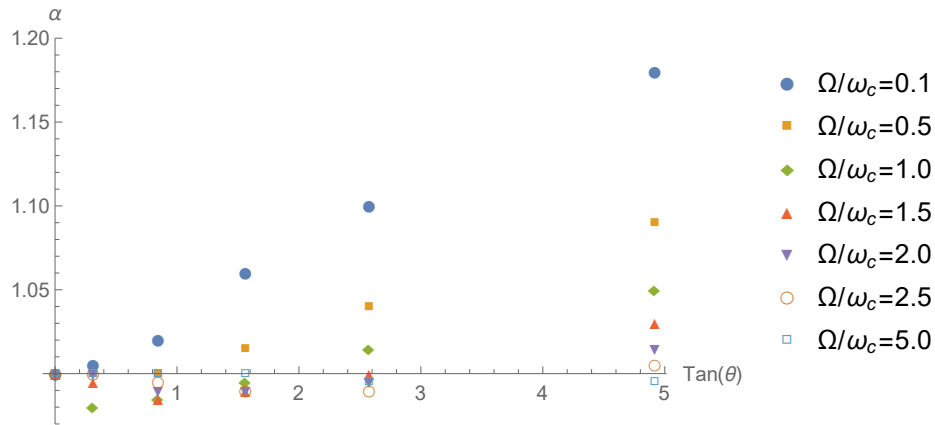


Fig. IV.10 Values of  $\alpha$  of optimal metrics for  $\nu = 7/3$  as a function of  $\tan \theta$ , at different confining potentials.

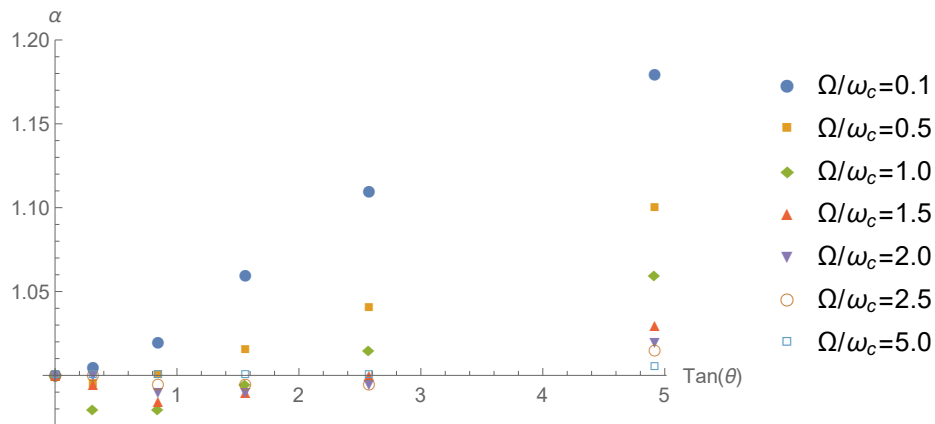


Fig. IV.11 Values of  $\alpha$  of optimal metrics for  $\nu = 11/5$  as a function of  $\tan \theta$ .

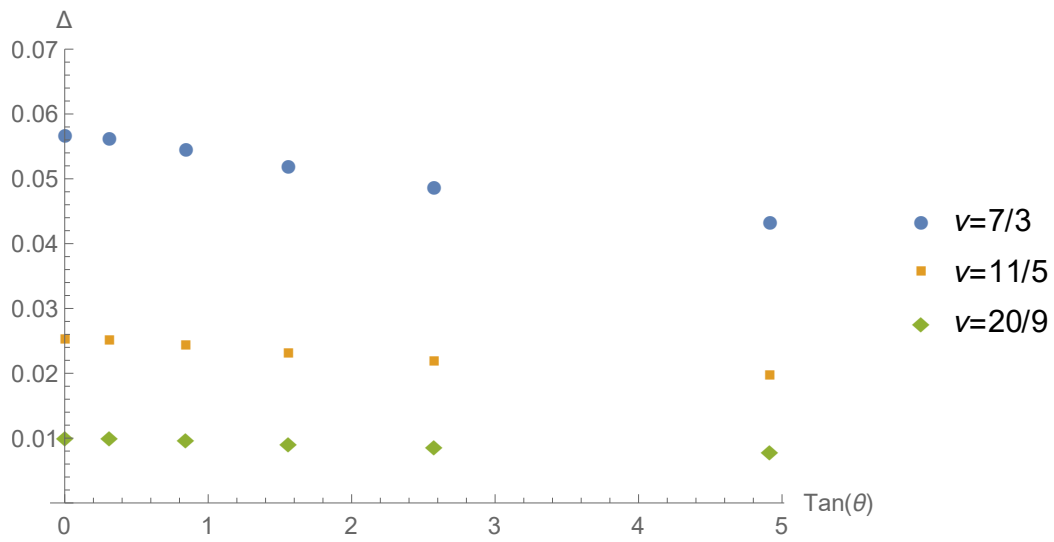


Fig. IV.12 The activation gaps for first LL at  $\nu = 7/3$ ,  $11/5$  and  $\nu = 20/9$  as a function of  $\tan \theta$ , using the optimal metrics.



# V – Magneto-exciton mode and neutral gap

In quantum Hall systems, besides the excitation of a single quasiparticle or a single quasihole, collective excitations also exist. One example is the density modulation in this incompressible state, which inspires the single mode approximation. In the composite fermion theory, one way to study the collective spectrum comes from the analogy with IQHE. In integer quantum Hall effects there is a collective magneto-plasmon mode, studied by Kallin and Halperin [123]. This can be imagined easily from the LL picture. Apart from the excitation of a hole in the filled LL or the excitation of an electron in an empty LL, there exists a particle-hole excitation where the particle and the hole are interacting with the Coulomb repulsion. This excitation is neutral and carries a specific momentum. If the particle-hole excitation is associated with a particular inter-LL transition, this is precisely the magneto-exciton while the magneto-plasmon can be viewed as a superposition of such magneto-excitons. In the composite fermion formalism, the FQHE of electrons is translated into the IQHE of CFs. It is interesting to investigate if the magneto-excitons of the composite fermion can capture essential information of the neutral collective excitations in FQHE. Park and Jain showed that this is feasible from the wave-function side in the spherical geometry [70]. In this chapter, we will discuss how the magneto-exciton mode is established in the Hamiltonian description of composite fermions and investigate the effects of anisotropy on the neutral gap. Sec. V.1 introduces the time-dependent Hartree Fock approximation formalism used by Murthy to find the dispersion relation in the Hamiltonian theory. In Sec. V.2, we introduce the diagrammatic method as complementary, from which we can see more explicitly what is considered and what is neglected in the time-dependent Hartree-Fock approximation. A discussion on the large-momentum limit of the collective mode is given in Sec. V.3. The perturbative calculation for the anisotropic case is presented in Sec. V.4. In the end of this part, Sec. V.5, we present how the results can be calculated beyond the perturbative sense, to all orders of the external anisotropy, despite we do not have enough time and computational source to carry out the whole numerical calculation.

We clarify the notation in this chapter. Since in this part, we will switch from the preferred density to the projected electron density and compare the calculations based on  $\bar{\rho}_e$  and  $\rho^p$ , we use  $\rho$  to represent either of them and use  $\rho_{n_1, n_2}$  or  $\rho_{m_1, m_2}$  to represent the matrix elements of the density operator between two CF LLs  $n_1, n_2$  or  $m_1, m_2$  (not confused with the notation in the activation gap, the  $m$ -indices here always refer to CF LL instead of guiding-center degrees of freedom).

## V.1 Conserving method and time-dependent Hartree-Fock approximation

In the Hamiltonian theory, there is a physical constraint that the action of the pseudovortex operator on physical states should vanish. The naive reference state of  $p$  filled CF LLs does not turn out to satisfy this constraint. In the previous calculation a preferred density  $\rho^p$  is employed to replace  $\bar{\rho}_e$  in order to circumvent the constraint. Despite the difficulty, it is still possible to incorporate this constraint in the calculation of the spectrum and keep using the electron density  $\bar{\rho}_e$ . This can be done with the conserving approximation, also called time-dependent Hartree-Fock approximation (TDHF) [124, 125]. The correlation function is computed and the pseudovortex operator corresponds to an unphysical mode, which actually decouples from the physical ones. In this section, we review the method used in Ref. [114, 126]. Their calculation shows that when the electron density instead of the preferred density is employed, the dispersion takes the correct shape.

The time-dependent Hartree-Fock approximation is to solve the evolution equation of the correlation function by applying the Hartree-Fock approximation to reduce the many-body problem to a set of self-consistent equations. As shown in Girvin, MacDonald and Platzman's computation, the  $\mathbf{q} \rightarrow 0$  spectrum is saturated by the single mode approximation. A relevant way of finding the spectrum is to compute the time-ordered density correlation function :

$$i\chi(t, \mathbf{r}) = \langle \mathcal{T} \rho(t, \mathbf{r}) \rho(0, 0) \rangle. \quad (\text{V.1})$$

We add a dependence  $(t, r)$  so as not to confuse the density correlation function with the pseudovortex density operator. The equation of motion of it is written as :

$$-i \frac{d}{dt} \langle \mathcal{T} \rho(t, \mathbf{r}) \rho(0, 0) \rangle = \langle \mathcal{T} [H(t), \rho(t, \mathbf{r})] \rho(0, 0) \rangle - i\delta(t) \langle [\rho(0, \mathbf{r}), \rho(0, 0)] \rangle. \quad (\text{V.2})$$

The Dirac  $\delta$ -function comes from the time derivative with respect to the time-ordering operator  $\mathcal{T}$ . We give a time dependence to  $H$  in order to remind that  $H(t)$  takes the same time as  $\rho(t)$  in the commutator (although  $H$  itself is conserved, but this notation facilitates the ladder-operator calculations). As we are studying the dispersion of the spectrum with respect to the momentum  $\mathbf{q}$ , it is more convenient to work in the Landau gauge. The density operator takes a product form for intra- and inter-CF LL physics and satisfies a decomposition into exciton operators :

$$\rho(\mathbf{q}) = \sum_{n_1, n_2} \rho_{n_1 n_2}(\mathbf{q}) O_{n_1 n_2}(\mathbf{q}); \quad (\text{V.3})$$

$$O_{n_1 n_2}(\mathbf{q}) = \sum_X e^{-iq_x X} d_{n_1, X - q_y l^* 2/2}^\dagger d_{n_2, X + q_y l^* 2/2}, \quad (\text{V.4})$$

where the subscript  $X \pm q_y l^* 2/2$  labels the  $x$ -position of the state in the Landau gauge (or  $y$ -momentum). The expression  $\rho_{n_1 n_2}(\mathbf{q})$  is the matrix elements of the density operator between CF LL  $n_1$  and CF LL  $n_2$ . For electron density this is  $\langle n_1 | e^{-ic\mathbf{q}\cdot\boldsymbol{\eta}} | n_2 \rangle$ , which can be calculated through Eq. (IV.26). So in order to study the density correlation function, it is enough to study the correlation function of excitons  $\langle \mathcal{T} O_{m_1 m_2}(t, \mathbf{q}) O_{n_1 n_2}(0, -\mathbf{q}) \rangle$ . For the  $p$  filled reference state, the equal time commutator of the exciton operators takes an orthogonal form :

$$\langle [O_{m_1, m_2}(\mathbf{q}), O_{n_2, n_1}(-\mathbf{q})] \rangle = N_{\phi^*} \delta_{m_1, n_1} \delta_{m_2, n_2} [N_F(m_1) - N_F(m_2)], \quad (\text{V.5})$$

where  $N_{\phi^*}$  is the number of magnetic flux quanta felt by the CF and  $N_F$  is Fermi distribution function. For the  $p$  filled reference state, it is given by  $N_F(n) = \Theta(p - 1 - n)$ .

From this form, we see that the exciton operators  $O_{n_1, n_2}$  can be classified into three types, depending on how they act on the  $p$  filled reference state :

1.  $n_1 \geq p, n_2 < p$  or  $n_1 < p, n_2 \geq p$ , these  $O_{n_1, n_2}$  create excitations across the Fermi-level, the  $p$ -th CF LL. Their action on the reference state of  $p$  filled CF LL  $|\mathbf{p}\rangle, \langle \mathbf{p}|$  is non-zero.
2.  $n_1 \geq p, n_2 \geq p$  and  $n_1 < p, n_2 < p$ , these operators annihilate  $|\mathbf{p}\rangle$  and  $\langle \mathbf{p}|$ . If the reference state is the true ground state, those operators do not enter the density correlation function.
3.  $n_1 = n_2$ , these  $O_{n_1, n_2}$  create and annihilate the CFs in the same LL. Its average energy is zero. Their action on the reference state is also vanishing for  $\mathbf{q} \neq 0$ .

In the remaining part of this section, we do not write out the explicit dependence on  $q$  of exciton and simply use  $O_{n_1, n_2}$ .

Before going to the calculation in detail, we take a look at how the physical constraint on pseudovortex density is imposed, if we use the electron density  $\bar{\rho}_e$  in the Hamiltonian and above calculation. By construction, the Hamiltonian commutes with the pseudovortex density  $[H, \chi] = 0$ . From this equation and the information that  $[\bar{\rho}_e(\mathbf{q}), \chi(\mathbf{q}')] = 0$ , we find that the correlation function between the electron density and the pseudovortex density vanishes :

$$\langle \mathcal{T} \chi(t, \mathbf{q}) \rho(0, \mathbf{q}') \rangle = 0. \quad (\text{V.6})$$

So there is always a zero mode solution to the exciton correlation function :

$$-i \frac{d}{dt} \sum_{m_1, m_2} \chi_{m_1, m_2} \langle \mathcal{T} O_{m_1, m_2}(t) O_{n_1, n_2}(0) \rangle = 0, \quad (\text{V.7})$$

where  $\chi_{m_1, m_2} = \langle m_1 | \exp -i\mathbf{q} \cdot \mathbf{R}_v | m_2 \rangle$  is the matrix element of the pseudovortex operator between CF LL  $m_1$  and CF LL  $m_2$ . This is an evidence that the pseudovortex operator “vanishes” as required by the physical constraint. After finding the equation of motion, we will further show that this unphysical zero-mode does not enter the density correlation function and the physical constraint is reimposed self-consistently.

Now we continue studying the equation of motion of the correlation function. The Hamiltonian only contains the interaction, which is a two-body operator of the form  $d_1^\dagger d_3^\dagger d_2 d_4$  (plus a chemical potential term for normal ordering), where the subscripts are as before simplification of the CF LL indices and intra-CF LL indices. So in order to compute the commutator between the Hamiltonian and the exciton, we need the following relation :

$$[d_1^\dagger d_3^\dagger d_4 d_2, d_1^\dagger d_2] = \delta_{1'2} d_1^\dagger d_3^\dagger d_4 d_2' - \delta_{2'1} d_1^\dagger d_3^\dagger d_4 d_2 - \delta_{1'4} d_1^\dagger d_3^\dagger d_2 d_2' + \delta_{2'3} d_1^\dagger d_1^\dagger d_4 d_2. \quad (\text{V.8})$$

Notice that here we do not write out the explicit dependence on  $t$ . All ladder operators above should be  $d^\dagger(t), d(t)$ . Since the two-body interaction operator appears in the form  $\sum_{\mathbf{q}} (1/2) V_{eff}(\mathbf{q}) \rho(\mathbf{q})_{12} \rho(-\mathbf{q})_{34} d_1^\dagger d_3^\dagger d_4 d_2$ , the Hamiltonian is invariant under the interchange (12)  $\leftrightarrow$  (34). The last two terms on the right hand side of Eq. (V.8) are equal to the first two terms. We can omit them and suppress the factor 1/2 in front of  $V_{eff}(\mathbf{q})$ . The commutator



is formed by monomials of two creation operators and two annihilation operators. The time-dependent Hartree-Fock approximation is to replace one  $d^\dagger(t)d(t)$  by their expectation value  $\langle d^\dagger(t)d(t) \rangle$  :

$$d_1^\dagger d_3^\dagger d_4 d_2 \rightarrow \langle d_1^\dagger d_2 \rangle d_3^\dagger d_4 + \langle d_3^\dagger d_4 \rangle d_1^\dagger d_2 - \langle d_1^\dagger d_4 \rangle d_3^\dagger d_2 - \langle d_3^\dagger d_2 \rangle d_1^\dagger d_4. \quad (\text{V.9})$$

If there is no CF LL mixing at the HF level, the occupation is conserved  $\langle d^\dagger(t)d(t) \rangle = \langle d^\dagger(0)d(0) \rangle$  and proportional to a Dirac  $\delta$ -function times the Fermi distribution function. Then we have the following result :

$$\begin{aligned} [d_1^\dagger d_3^\dagger d_4 d_2, d_1^\dagger d_2] \rightarrow & N_F(1') \delta_{2'1} (\delta_{1'4} d_3^\dagger d_2 - \delta_{1'2} d_3^\dagger d_4) + N_F(2') \delta_{1'2} (\delta_{12'} d_3^\dagger d_4 - \delta_{32'} d_1^\dagger d_4) \\ & + N_F(2) \delta_{2'1} \delta_{32} d_1^\dagger d_4 - N_F(1) \delta_{1'2} \delta_{14} d_3^\dagger d_2'. \end{aligned} \quad (\text{V.10})$$

We need to recombine the above operators with the interaction and the corresponding matrices of the density operator. For convenience we treat the first and the second line on the right-hand side separately. The first line translates to

$$\begin{aligned} \sum_{X'_1, X'_2, X, n_1, n_2} \int \frac{d^2 \mathbf{k}}{(2\pi)^2} V_{eff}(\mathbf{k}) [N_F(m_2) - N_F(m_1)] d_{n_1, X'_2 + k_y l^{*2}/2}^\dagger d_{n_2, X'_2 - k_y l^{*2}/2} e^{-ik_x(X'_1 - X'_2)} \\ \delta \left( X'_1 + \frac{k_y l^{*2}}{2} - X + \frac{q_y l^{*2}}{2} \right) \left[ \rho_{m_2 m_1}(\mathbf{k}) \rho_{n_1 n_2}(-\mathbf{k}) \delta \left( X'_1 - \frac{k_y l^{*2}}{2} - X - \frac{q_y l^{*2}}{2} \right) \right. \\ \left. - \rho_{n_1 m_1}(\mathbf{k}) \rho_{m_2 n_2}(-\mathbf{k}) \delta \left( X'_2 + \frac{k_y l^{*2}}{2} - X - \frac{q_y l^{*2}}{2} \right) \right] e^{-iq_x X} \end{aligned} \quad (\text{V.11})$$

Above we replace indices  $1', 2'$  by their full expressions  $(m_1, X - q_x l^{*2}/2), (m_2, X + q_x l^{*2}/2)$ . The summation over dummy indices is also written out through  $n_1, n_2, X'_1, X'_2$ . By carefully evaluating the  $\delta$ -function in Eq. (V.11), the ladder operators  $d^\dagger, d$  can be recombined into magneto-exciton operators  $O_{n_1, n_2}$ . Meanwhile the two terms in the bracket of the second line of Eq. (V.11) transform to  $V(\mathbf{q})\rho(\mathbf{q})_{12}\rho(-\mathbf{q})_{34}$  and its Fourier transformation respectively. So this parts gives a scattering from an exciton  $O_{n_1, n_2}$  to an exciton  $O_{m_1, m_2}$ . In constrast, the second line of Eq. (V.10) gives a very different contribution. It only modifies one of the two indices  $(m_1, m_2)$  in  $O_{m_1, m_2}$  :

$$\sum_n \int \frac{d^2 k}{4\pi^2} V_{eff}(\mathbf{k}) \sum_{l=0} N_F(l) [\rho_{ln}(\mathbf{k}) \rho_{m_2 l}(-\mathbf{k}) O_{m_1, n} - \rho_{l m_1}(\mathbf{k}) \rho_{nl}(-\mathbf{k}) O_{n, m_2}]. \quad (\text{V.12})$$

In the absence of anisotropy, the angular integral in the above equation gives a  $\delta$ -function on  $n$ , transforming it to the HF energy difference between CF LL  $m_1$  and CF LL  $m_2$  :

$$(\epsilon_{m_1} - \epsilon_{m_2}) O_{m_1, m_2}. \quad (\text{V.13})$$

Combining all of our calculation and transforming from time space to frequency space, we find the equation of motion of the exciton correlation function :

$$\begin{aligned} \omega \langle O_{m_1 m_2} O_{l_2 l_1} \rangle = & (\epsilon_{m_1} - \epsilon_{m_2}) \langle O_{m_1 m_2} O_{l_2 l_1} \rangle + [N_F(m_2) - N_F(m_1)] \sum_{n_1, n_2} \left[ \frac{V_{eff}(\mathbf{q})}{2\pi l^{*2}} \right. \\ & \times \rho_{n_1 n_2}(\mathbf{q}) \rho_{m_2 m_1}(-\mathbf{q}) - \int \frac{d^2 \mathbf{k}}{(2\pi)^2} V_{eff}(\mathbf{k}) \rho_{n_1 m_1}(\mathbf{k}) \rho_{m_2 n_2}(-\mathbf{k}) e^{i\mathbf{k} \times \mathbf{q} l^{*2}} \left. \right] \\ & \times \langle O_{n_1 n_2} O_{l_2 l_1} \rangle - i N_{\phi^*} \delta_{m_1, l_1} \delta_{m_2, l_2} [N_F(m_1) - N_F(m_2)]. \end{aligned} \quad (\text{V.14})$$

This is an inhomogeneous matrix equation with the equal-time commutator as the source. A vector is labelled by the double indices  $(m_1 m_2)$ . For future convenience we introduce the following notations corresponding to the last two terms in the above equation :

$$V_{n_1, n_2, n_3, n_4}^{(1)}(q_x, q_y) = \frac{1}{2\pi} \int \frac{dk_x dk_y}{2\pi} V_{eff}(\mathbf{k}) \rho_{n_2 n_3}(\mathbf{k}) \rho_{n_1 n_4}(-\mathbf{k}) e^{i\mathbf{k} \times \mathbf{q} l^{*2}}, \quad (\text{V.15})$$

$$V_{n_1, n_2, n_3, n_4}^{(2)}(q_x, q_y) = \frac{1}{2\pi l^{*2}} V_{eff}(\mathbf{q}) \rho_{n_2 n_3}(\mathbf{q}) \rho_{n_1 n_4}(-\mathbf{q}). \quad (\text{V.16})$$

Because of the factor  $[N_F(m_2) - N_F(m_1)]$ , we need to treat different types of excitons separately. According to our previous classification [below Eq. (V.5)], type 3 and type 2 excitons act differently on the reference state from type 1 excitons. We group all our matrices and vectors into a block form of two, one for type 1 excitons and another for type 3 and type 2 excitons. Eq. (V.14) takes the block form :

$$\begin{pmatrix} \omega - A & -B \\ 0 & \omega - D \end{pmatrix} \begin{pmatrix} a & b \\ c & d \end{pmatrix} = \begin{pmatrix} \tilde{I} & 0 \\ 0 & 0 \end{pmatrix}, \quad (\text{V.17})$$

where  $\tilde{I}$  is the source matrix with elements  $-iN_{\phi^*} \delta_{m_1, l_1} \delta_{m_2, l_2} [N_F(m_1) - N_F(m_2)]$ . Furthermore  $\omega$  in matrices is the simplification of the frequency times an identity matrix  $\omega I$ . By performing the block multiplication directly, we can see that  $c$  has to vanish as long as  $\omega$  is not an eigenvalue of  $D$ . The elements  $b$  and  $d$  vanish identically because the type 3 and type 2 excitons annihilate the  $p$  filled CF LLs. So the exciton correlation function is only non-zero for those belonging to  $a$  and  $a = (\omega - A)^{-1} \tilde{I}$ . Therefore the poles of the exciton correlation function are the eigenvalues of the matrix  $A$ , i.e. the matrix

$$A_{m_1 m_2, n_1 n_2} = (\epsilon_{m_1} - \epsilon_{m_2}) \delta_{m_1 n_1} \delta_{n_2 m_2} + [N_F(m_2) - N_F(m_1)] \left[ \frac{V_{eff}(\mathbf{q})}{2\pi l^{*2}} \rho_{n_1 n_2}(\mathbf{q}) \rho_{m_2 m_1}(-\mathbf{q}) - \int \frac{d^2 \mathbf{k}}{(2\pi)^2} V_{eff}(\mathbf{k}) \rho_{n_1 m_1}(\mathbf{k}) \rho_{m_2 n_2}(-\mathbf{k}) e^{i\mathbf{k} \times \mathbf{q} l^{*2}} \right] \quad (\text{V.18})$$

with the double indices  $(m_1, m_2)$  and  $(n_1, n_2)$  restricted in the type 1 subspace where  $[N_F(m_2) - N_F(m_1)] \neq 0$  and  $[N_F(n_2) - N_F(n_1)] \neq 0$ . The density correlation function is a linear combination of the exciton correlation function. Assume the matrix  $\omega - A$  is diagonalized by a matrix  $P$  made of its right eigenvectors :

$$\omega - A = P \Sigma(\omega) P^{-1}, \quad (\text{V.19})$$

where  $\Sigma(\omega)$  is diagonal with eigenvalues of  $\omega - A$  as its diagonal entries.  $P^{-1}$  is comprised by the rows of  $A$ 's left eigenstates. The density correlation function can be written as :

$$\langle \mathcal{T} \rho(\mathbf{q}) \rho(-\mathbf{q}) \rangle = \rho^{(n)} P \Sigma(\omega)^{-1} P^{-1} \tilde{I} \rho^{(n)*}, \quad (\text{V.20})$$

where  $\rho^{(n)} = \rho(\mathbf{q})_{n_1, n_2}$  is the vector formed by the matrix elements of the density. Therefore the poles of the density correlation function are given by the eigenvalues of the matrix  $A$ , Eq. (V.18).

One can then verify by straightforward calculation that  $\chi_{m_1, m_2}$  is indeed a left zero-eigenstate of the matrix Eq. (V.18). Moreover  $\chi_{m_1, m_2}$  is also an eigenstate of the matrix  $A$ , the subspace of type 1 excitons. This is seen by observing

$$(\chi_1, \chi_2) \begin{pmatrix} A & B \\ 0 & D \end{pmatrix} = 0 \Rightarrow \chi_1 A = 0, \quad (\text{V.21})$$

where the vector  $\chi_{m_1, m_2}$  is also decomposed into the block  $(\chi_1, \chi_2)$  according to our classification of excitons. Now we study how this mode decouples from Eq. (V.20). With  $\chi_1$  being a zero eigenvector of  $A$ , noticing that  $P^{-1}$  is made of the left-row eigenvectors of  $A$ , the vector  $\chi_1$  appears in it. Due to the commutation  $\langle [\bar{\rho}_e(\mathbf{q}), \chi(\mathbf{q}')] \rangle = 0$ , we see that the zero mode is orthogonal to the density matrix via  $\chi_1 \tilde{I} \rho^{(m)*} = 0$ . So in Eq. (V.20), the unphysical mode  $\chi_1$  in  $P^{-1}$  does not enter the decomposition Eq. (V.20), which manifests that the pseudovortex mode does not interfere with those physical modes.

With the above discussions, we conclude that we can find the neutral collective excitation and the unphysical pseudovortex mode by diagonalizing the matrix  $A$  in the subspace of type 1 excitons. We compute  $\nu = 1/3$  for a Zhang-Das Sarma potential with  $\lambda = 2$  and  $\nu = 2/5$  for a pure Coulomb potential. The results are summarized in Fig. V.1 and Fig. V.2. We use 20 CF LLs for calculation. As we will show in Sec. V.3, the larger  $q$  is, the more LLs we need to keep the unphysical mode much smaller than the physical one. For  $\nu = 1/3$ , it turns out that 20 LLs are enough to compute the spectrum until  $ql = 2$ . The magneto-exciton minimum can be clearly seen. For  $\nu = 2/5$ , the numerical complexity increases rapidly. More LLs are needed to keep the unphysical mode correct for  $ql > 1.2$ . We will discuss further the effects of finite CF-LL truncation in Sec. V.3. Nevertheless, we still observe a two-minimum structure, first recognized in Ref. [70].

## V.2 Diagrammatic magneto-plasmon calculation

In the original work by Kallin and Halperin [123], the magneto-plasmon approximation consists of using directly diagrammatic tools to compute the time-ordered density correlation function for the IQHE of electrons. This method can be borrowed immediately to composite fermions since the CF also satisfies an IQHE. Such computation is equivalent to the TDHF method that we presented in the last section but the decoupling of the unphysical pseudovortex mode is not as obvious as in the TDHF approximation. In comparison, the diagrammatic tool enables us to see more clearly what contribution, such as a frequency-dependence in the self-energy, is neglected in the TDHF approximation. So from a heuristic view, we provide an introduction to how the conserving method is carried out through diagram expansion.

As before, we consider the composite fermion theory for filling  $\nu = p/(2ps + 1)$ , where the CFs fill  $p$  LLs. In the diagrammatic conserving approximation, only ladder and bubble diagrams are considered. The element needed to perform the calculation is the propagator,

$$G_{\alpha, \beta}(\omega) = \frac{1}{i} \int dt \langle \mathcal{T} d_{\alpha}(t) d_{\beta}^{\dagger}(0) \rangle e^{i\omega t} = \text{---}, \quad (\text{V.22})$$

where we use a thick line to represent it diagrammatically. The subscript  $\alpha(\beta)$  denotes both the CF LL index and intra-CF LL index. In the picture of  $p$  filled CF LLs, it is easy to verify that the propagator is proportional to  $\delta_{\alpha\beta}$  and does not depend on the intra-CF LL index. In this case, we denote it as  $G_n(\omega)$ , where  $n$  is the CF LL index of  $\alpha$ . In the FQH problem, we have only the interaction as the Hamiltonian, under the conserving-method approximation

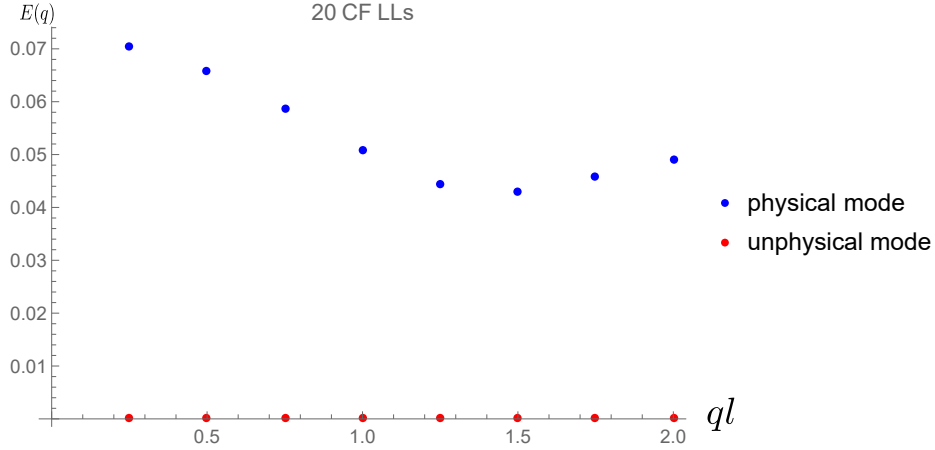


Fig. V.1 The magneto-exciton spectrum as a function of the wave vector  $q$  for  $\nu = 1/3$  using the TDHF approximation with 20 LLs considered. The zero unphysical mode and the lowest physical mode are labelled with red and blue dots. The magneto-roton minimum is around  $ql = 1.4$ .

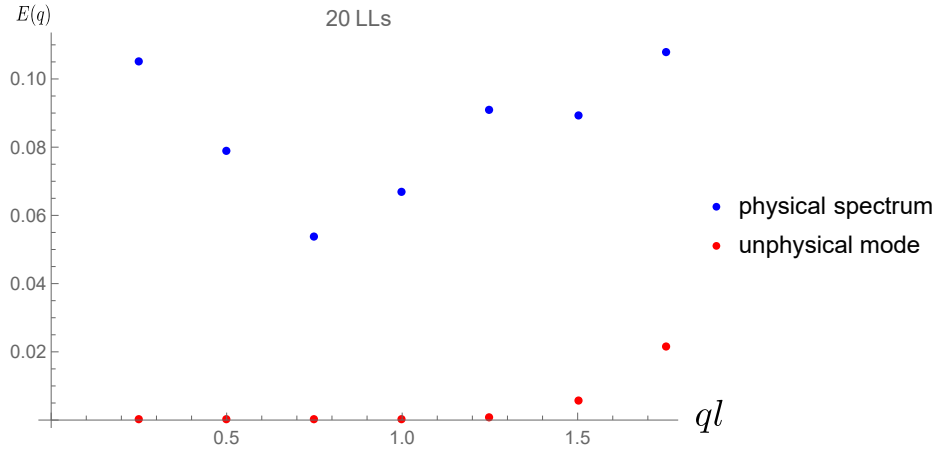


Fig. V.2 The magneto-exciton spectrum as a function of the wave vector  $q$  for  $\nu = 2/5$  using the TDHF approximation with 20 LLs considered. The zero unphysical mode and the lowest physical mode are labelled with red and blue dots. In this case, 20 LLs are not enough to have the unphysical mode much smaller than the physical mode for  $ql > 1.2$ . The numerical difficulty rises rapidly.

the propagator satisfies the following equation :

$$\text{---} = \text{---} + \text{---} \text{---} + \text{---} \text{---} \text{---}, \quad (\text{V.23})$$

where the hollow dot represents a density vertex  $\rho_{n_1, n_2}$  and the thin line is the propagator without interaction. On the right hand side of the above equation, the first term is  $1/\omega$  since the Hamiltonian only comprises the interaction. The second term is the tadpole, whose contribution is zero if momentum is conserved and the interaction is screened by the positive charge, i.e.  $V(\mathbf{q})|_{\mathbf{q}=0} = 0$ . The third term contributes the self-energy  $\Sigma_n$ . In this approximation, vertex corrections are neglected in the propagator.

If there is no CF LL mixing, as shown in our previous calculation when the interaction is isotropic, the above equation admits an exact solution and one obtains a free-fermion propagator  $(\omega - E)^{-1}$  with the energy replaced by the self-energy  $\Sigma_n$  [127] :

$$G_n(\omega) = \frac{1 - N_F(n)}{\omega - \Sigma_n + i0^+} + \frac{N_F(n)}{\omega - \Sigma_n - i0^-}, \quad (\text{V.24})$$

where  $N_F(n) = \Theta(p - n - 1)$  is the Fermi distribution function for CF. Here  $\Sigma_n$  is actually equivalent to the CF LL energy  $\epsilon_n$  in the last section. The symbol  $0^+$  is an infinitesimal real positive number, and the poles of  $G$  for filled CF LL and poles for empty CF LL lie on the different sides of the real axis. The magneto-exciton mode is identified as the poles of the time-ordered density correlation function  $\chi(\omega, \mathbf{q})$  :

$$\chi(\omega, \mathbf{q}) = -i \int dt d\mathbf{q}' e^{i\omega t - i\mathbf{q}\cdot\mathbf{r}} \langle \mathcal{T} \rho(t, \mathbf{r}) \rho(0, 0) \rangle. \quad (\text{V.25})$$

To evaluate the above expression, one inserts the time-evolution operators  $U(\infty, 0)$  and  $U(0, -\infty)$  and then expands  $\exp(i \int dt H)$  to all orders [127]. As a first step, one can compute the static Hartree-Fock contribution to the density correlation function, where we only consider the contribution from the Green's function and the two-body part of the interaction is dropped. This is a ring diagram connecting two density vertices with the propagator :

$$\chi^0(\omega, \mathbf{q}) = \text{---} \text{---} = \sum_{n_1, n_2, k'_1, k'_2} \int \frac{d\mathbf{k}}{(2\pi)^2} \rho(\mathbf{q})_{n_1 k'_1, n_2 k'_2} \int \frac{d\omega'}{2\pi} iD(\omega)_{n_1, n_2} \rho(-\mathbf{k})_{n_2 k'_2, n_1 k'_1}, \quad (\text{V.26})$$

where  $D_{n_1, n_2}$  is the double-particle propagator :

$$D_{n_1, n_2} = \int \frac{d\omega'}{2\pi} iG_{n_2}(\omega + \omega') G_{n_1}(\omega') = \left[ \frac{N_F(n_1)(1 - N_F(n_1))}{\omega - (\Sigma_{n_1} - \Sigma_{n_2}) - i\gamma} - \frac{N_F(n_1)(1 - N_F(n_1))}{\omega - (\Sigma_{n_1} - \Sigma_{n_2}) + i\gamma} \right]. \quad (\text{V.27})$$

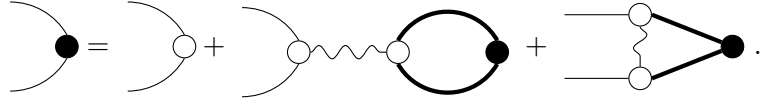
From this expression, we can immediately see that in the static HF approximation, the poles of the density correlator are given as the energy difference between two different CF LLs.

In the composite fermion case, the energy scale of CF LL is of the same order as the interaction, so the above HF approximation is strongly perturbed by the two-body interaction.

With this in mind, now let's add back the two-body interaction. In the bubble diagram plus ladder diagram approximation, one of the density operator in Eq. (V.26) has to be modified to incorporate the interaction :

$$\chi(\omega, \mathbf{q}) = \sum_{n_1, n_2, k'_1, k'_2} \int \frac{d\mathbf{k}}{(2\pi)^2} \rho(\mathbf{q})_{n_1 k'_1, n_2 k'_2} \int \frac{d\omega'}{2\pi} G_{n_2}(\omega + \omega') G_{n_1}(\omega') \Gamma(\mathbf{k})_{n_1 k'_1, n_2 k'_2}. \quad (\text{V.28})$$

The vertex operator  $\Gamma$  (solid dot) satisfies a self-consistent equation given by the bubble diagram and the ladder diagram :



$$\Gamma = \rho + \rho \text{---} \Gamma + \rho \text{---} \rho \text{---} \Gamma + \rho \text{---} \rho \text{---} \rho \text{---} \Gamma. \quad (\text{V.29})$$

In the above representation, the thin line merely labels the legs of vertices and does not represent a propagator. The first term on the right-hand side is the density vertex  $\rho_{n_1, n_2}$ . The second/third term is to contract the two legs from the same/different density vertex(es) in the interaction with the dressed vertex operators. Comparing to the Hartree-Fock approximation, we call them direct and exchange interaction and denote them as  $V^{(2)}$  and  $V^{(1)}$ . By doing the following replacement :

$$M_{An_1 n_2}(\mathbf{q}) \delta(p - q_x) \delta(\Delta k + q_y) = \int dk e^{ipkl^*2} \rho(\mathbf{q})_{n_1 k_1, n_2 k_2}, \quad (\text{V.30})$$

$$\Gamma'_{n_1, n_2}(\omega, \mathbf{q}) \delta(p - q_x) \delta(\Delta k + q_y) = \int dk e^{ipkl^*2} \Gamma(\mathbf{q})_{n_1 k_1, n_2 k_2}, \quad (\text{V.31})$$

where  $k = (k_1 + k_2)/2$ ,  $\Delta k = k_1 - k_2$ , the density correlation function can be rewritten as :

$$\chi(\omega, \mathbf{q}) = \sum_{n_1, n_2} M_{An_1 n_2}(\mathbf{q}) \Pi_{n_1, n_2}(\omega, \mathbf{q}). \quad (\text{V.32})$$

Now  $\Pi_{n_1, n_2}(\omega, \mathbf{q}) = D_{n_1, n_2} \Gamma'_{n_1, n_2}(\omega, \mathbf{q})$  is a dressed operator to transfer a CF in LL  $n_2$  to another CF in LL  $n_1$ . It can be shown [123] to satisfy the following matrix equation (for  $n_1 \geq p > n_2$ ) :

$$\left\{ \delta_{n_1, \lambda} \delta_{n_2, \mu} [D(\omega)]_{n_1, n_2}^{-1} - V_{n_1, \mu, n_2, \lambda}^{(1)} + V_{n_1, \mu, \lambda, n_2}^{(2)} \right\} \Pi_{\lambda, \mu}(\omega, \mathbf{q}) = M_{An_1 n_2}^*(\mathbf{q}). \quad (\text{V.33})$$

This is a vertex equation for the density correlation function. The direct interaction  $V^{(2)}$  and exchange interaction  $V^{(1)}$  are given by :

$$V_{n_1, n_2, n_3, n_4}^{(1)}(q_x, q_y) = \frac{1}{2\pi} \int \frac{dk_x dk_y}{2\pi} V_{eff}(\mathbf{k}) \rho_{n_2 n_3}(\mathbf{k}) \rho_{n_1 n_4}(-\mathbf{q}) e^{i\mathbf{k} \times \mathbf{q} l^*2}, \quad (\text{V.34})$$

$$V_{n_1, n_2, n_3, n_4}^{(2)}(q_x, q_y) = \frac{1}{2\pi l^*2} V_{eff}(\mathbf{q}) \rho_{n_2 n_3}(\mathbf{q}) \rho_{n_1 n_4}(-\mathbf{q}). \quad (\text{V.35})$$

The pole of the above matrix equation gives the excitation spectrum. The expression  $[D]_{n_1 n_2}^{-1}$  is simply the inverse value of  $[D]_{n_1 n_2}$  not the matrix inverse. In order to find the pole, it is equivalent to solve the eigenvalues of the equation below :

$$\left\{ \delta_{n_1, \lambda} \delta_{n_2, \mu} [D(\omega)]_{n_1, n_2}^{-1} - V_{n_1, \mu, n_2, \lambda}^{(1)} + V_{n_1, \mu, \lambda, n_2}^{(2)} \right\} B_{\lambda, \mu} = 0. \quad (\text{V.36})$$

Such an equation admits an effective Hamiltonian for the magneto-exciton indices  $\{n_1, n_2\}$ , written as :

$$\mathcal{H}_{n_1, n_2; \lambda, \mu} = \begin{cases} \delta_{n_1, \lambda} \delta_{n_2, \mu} (\Sigma_{n_1} - \Sigma_{n_2}) - V_{n_1, \mu, n_2, \lambda}^{(1)} + V_{n_1, \mu, \lambda, n_2}^{(2)}, & \text{for } n_1 \geq n_2; \\ \delta_{n_1, \lambda} \delta_{n_2, \mu} (\Sigma_{n_1} - \Sigma_{n_2}) + V_{n_1, \mu, n_2, \lambda}^{(1)} - V_{n_1, \mu, \lambda, n_2}^{(2)}, & \text{for } n_1 < n_2. \end{cases} \quad (\text{V.37})$$

The above equation is identical with the TDHF result Eq. (V.14) apart from a complex conjugate. So the eigenvalues of the two computations are equal. The equation of motion in the TDHF approximation becomes a vertex equation for the density correlation function in this diagrammatic approach. From the diagrammatic evaluation, we can easily find what types of diagrams are neglected in the conserving method. For example, there is a possible vertex correction for the propagator and the following diagram is neglected in the contribution to the propagator :


(V.38)

This diagram gives a frequency-dependence to the self-energy [127] but still preserves the CF LL indices with no CF LL mixing. There are more examples when we consider the vertex diagram. Some of the diagrams ignored in the conserving method can be found in [123].

On the other hand, when CF LL mixing is explicit in the HF calculation, it is not very easy to find a vertex equation as Eq. (V.33) permitting the unphysical pseudovortex mode at a perturbative level. The diagrams directly lead to the non-perturbative equations in Sec. V.5. So in order to perturbatively compute the correction in the presence of anisotropy, we will turn back to the TDHF formalism.

### V.3 Comparison between the electron density computation and preferred density computation

In the Hamiltonian theory, two kinds of density operators have been involved. One is the electron density  $\bar{\rho}_e$ , which has the charge of an electron and derives from the original Hamiltonian. Another is the preferred density  $\rho^p = \bar{\rho}_e - c^2 \chi$ . This preferred density acting on a physical states gives the same effect as the electron density. It carries the charge of a composite fermion and is used to compute the activation gap. In the formulation using preferred density, the constraint on the Hilbert space is neglected. Both densities are allowed to be used as the basis in the conserving approximation [114, 126]. The preferred density to the leading order of  $q$  was used by Murthy to obtain the magneto-exciton spectrum but turns out to be very different in dispersion from the GMP mode, whereas the results using electron density looks consistent with the GMP dispersion. As the preferred density gives the correct estimation of the activation gap, it is interesting to see whether the magneto-exciton dispersion obtained by the electron density can be consistently extended to the activation gap obtained through the preferred density. In this section, we compare the two kinds of computations and examine some general properties of the use of the two densities.

The first issue we study is the convergence to the activation gap. The activation gap is the energy to create a pair of well-separated quasiparticle and quasihole. In quantum Hall

systems, since the momentum in the  $x$ -direction is proportional to the distance in the  $y$ -direction (like shown in the Landau gauge), the distance between the quasiparticle and the quasihole is proportional to the momentum  $q$  they carry (this is also reflected in the form of the exciton operator). Their energy  $E(\mathbf{q})$  should converge to the activation gap  $\Delta$  in the  $\mathbf{q} \rightarrow \infty$  limit. Below we show that in the Hamiltonian theory, the calculation based on the electron density and preferred density exhibit entirely different behaviours in the  $\mathbf{q} \rightarrow \infty$  limit. The former needs an infinite number of CF LLs to maintain its validity while the latter converges to the activation gap rapidly.

The basic elements in the conserving method is the exciton operator  $O(\mathbf{q})_{n_1, n_2}$ , creating a hole in LL  $n_2$  and a CF in LL  $n_1$ . A relevant energy associated with the exciton is the HF energy difference between CF LL  $n_2$  and CF LL  $n_1$  :

$$\epsilon_{n_1} - \epsilon_{n_2} = \Sigma_{n_1} - \Sigma_{n_2}, \quad (\text{V.39})$$

where the HF energy is exactly given by the commonly used self-energy in many-body theory. The above term appears in the vertex equation [Eq. (V.14) or Eq. (V.33)] as the diagonal matrix element. Different exciton operators are coupled through the direct and exchange interactions  $V^{(2)}$  and  $V^{(1)}$ . Now we focus on a finite number of CF LLs and study the asymptotic behaviours of  $V^{(2)}$  and  $V^{(1)}$  for large momentum.

The direction interaction  $V^{(2)}(\mathbf{q})$  is easily seen to decay exponentially when  $\mathbf{q} \rightarrow \infty$ . It does not couple different excitons at large momentum. Let's now focus on the behaviour of  $V^{(1)}(\mathbf{q})$ . For the isotropic Coulomb potential, after performing the angular integral the integrand is a combination of Bessel function and the decaying Gaussian factor :

$$\begin{aligned} V^{(1)}(\mathbf{q}) &= \int d\theta dk \sum_{m,n} c_{m,n} k^m e^{in\theta} e^{-\frac{k^2}{2}} e^{-iqk \sin(\theta-\bar{\theta})} \\ &= \int_0^\infty dk \sum_{m,n} c_{m,n} 2\pi J_n(qk) e^{-\frac{k^2}{2}} k^m e^{in\bar{\theta}} \end{aligned} \quad (\text{V.40})$$

where  $J_n$  is the Bessel function,  $q = |\mathbf{q}|$ ,  $\bar{\theta} = \arg \mathbf{q}$ . In the above expansion  $m$  and  $n$  must have the same parity, because  $k \rightarrow -k$  is equivalent to  $\theta \rightarrow \theta + \pi$ . For convenience here the magnetic length  $l^*$  is set to 1 here and  $q$  is rescaled to have the exponents normalized as above. Such an integral can be worked out exactly as a confluent hypergeometric function :

$$V^{(1)}(\mathbf{q}) = \sum_{m,n} c_{m,n} e^{in\bar{\theta}} 2^{(1+m-n)/2} \pi q^n \frac{\Gamma[(1+m+n)/2]}{\Gamma(1+n)} {}_1F_1 \left[ \frac{1}{2}(1+m+n), 1+n, -\frac{q^2}{2} \right]. \quad (\text{V.41})$$

Usually the confluent hypergeometric function is capable of being written in terms of the sum of modified Bessel functions  $I_n$  times some powers of  $q$ . This can be seen if we perform



the radial integral first and then the angular integral :

$$\begin{aligned}
V^{(1)}(\mathbf{q}) &= \int d\theta dk \sum_{m,n} c_{m,n} k^m e^{in\theta} e^{-\frac{k^2}{2}} e^{-iqk \sin(\theta-\bar{\theta})} \\
&= \int_0^{2\pi} d\theta \int_{-\infty+iq \sin(\theta-\bar{\theta})}^{+\infty+iq \sin(\theta-\bar{\theta})} \frac{dk}{2} \sum_{m,n} c_{m,n} [k - iq \sin(\theta - \bar{\theta})]^m e^{in\theta} e^{-\frac{k^2}{2}} e^{-\frac{q^2}{2} \sin^2(\theta-\bar{\theta})} \\
&= \int_0^{2\pi} d\theta \sum_{m,n} \sum_{l=0}^{[m/2]} c_{m,n} \binom{m}{2l} (-iq \sin \theta)^{m-2l} e^{\frac{q^2}{4} \cos 2\theta} e^{in\bar{\theta}} \Gamma\left(\frac{2l+1}{2}\right) 2^{\frac{2l-1}{2}} e^{-\frac{q^2}{4}}.
\end{aligned} \tag{V.42}$$

In the second step, we shift the Gaussian integral from the real axis to the complex plane. This is valid because the  $k$  integral from 0 to  $\infty$  can be extended to that from  $-\infty$  to  $\infty$  by combining the integrand  $f(\theta)$  and  $f(\theta + \pi)$  and then dividing it by two, using the condition that  $m$  and  $n$  have the same parity. In the third step, the integral of  $k$  is dragged back to the real axis. All odd powers of  $k$  are eliminated by symmetry. After expanding  $2i \sin(\theta) = \exp(i\theta) - \exp(-i\theta)$  in the polynomial factor, each monomial becomes a modified Bessel function times some power of  $q$ .

To show the large- $\mathbf{q}$  limit, it is more convenient to use Eq. (V.41). In this case the asymptotic form of the confluent hypergeometric function is :

$${}_1F_1 \left[ \frac{1}{2}(1+m+n), 1+n, -\frac{q^2}{2} \right] \sim \Gamma(1+n) \left( \frac{e^{-\frac{q^2}{2}} \left(\frac{-q^2}{2}\right)^{(m-n-1)/2}}{\Gamma\left[\frac{1+m+n}{2}\right]} + \frac{\left(\frac{q^2}{2}\right)^{-(1+m+n)/2}}{\Gamma\left[\frac{1+n-m}{2}\right]} \right). \tag{V.43}$$

Going back to the summation in Eq. (V.41), the leading term decays  $1/q$  for large  $\mathbf{q} \rightarrow \infty$ . This shows the exchange interaction  $V^{(1)}$  also goes to zero as the separation of the quasiparticle/quasihole pair becomes larger and larger. So for a finite truncation on the number of CF LLs, the different exciton operators in Eq. (V.14) or Eq. (V.33) become decoupled for large  $\mathbf{q}$ . The eigenvalues of the vertex equation Eq. (V.36) soon converge to the energy difference of two CF LLs,  $\epsilon_{n_1} - \epsilon_{n_2}$ .

However, the above convergence is only meaningful when this finite truncation on the number of LLs is valid in the  $q \rightarrow \infty$  limit. This is not the case when using  $\bar{\rho}_e$ , where the validity of the calculation relies on the fact that the physical constraint  $\chi(\mathbf{q})$  is faithfully implemented. For the conserving method with  $\bar{\rho}_e$ , there is an unphysical zero mode :

$$\chi_{n_1, n_2}(\mathbf{q}) = \sqrt{\frac{n_2!}{n_1!}} e^{-q^2 l^{*2}/(2c^2)} \left(-i \frac{q+l^*}{c}\right)^{n_1-n_2} L_{n_2}^{n_1-n_2} \left(\frac{q^2 l^{*2}}{2c^2}\right). \tag{V.44}$$

From this expression, we can see that when  $q$  is large, the component  $\chi_{n_1, n_2}$  is controlled by a power term  $q^{n_1+n_2}$  times an exponentially decaying factor  $\exp[-q^2 l^{*2}/(2c^2)]$ . So we see that the weight of this vector are shifted towards higher and higher CF LLs as  $q$  increases. In a practical numeric calculation, when a finite number CF LLs are kept from  $n = 0$  to  $n = n_{max}$ , this mode, treated as a vector, is going to have all its components going to zero in the  $q \rightarrow \infty$  limit while the true nontrivial components are far above  $n_{max}$  and truncated. From a computational point of view, when we diagonalize a finite truncation of the vertex equation (V.36) for large  $q$ , the lower CF-LL components of  $\chi_{n_1, n_2}$  soon become an identical

zero vector  $\chi_{n_1, n_2} \sim 0$  and is not reflected as an eigenvector. This means the finite truncation soon loses its unphysical zero mode as  $q$  becomes larger. In other words, if one keeps only a finite number of CF LLs, in the large- $q$  limit the unphysical zero mode  $\chi_{n_1, n_2}$  disappears from the eigenvector series. In Fig. V.2 we show both the lowest and second lowest eigenvalues of the vertex equation truncated for 20 LLs. We find that the lowest eigenvalues deviate from 0 rapidly after  $ql = 1.25$ . In order to keep the unphysical mode at zero energy, one has to keep an rapidly increasing number of LLs for larger  $q$  so that at least one of the components  $\chi_{n_1, n_2}$  (Eq. (V.44)) is significantly different from zero. In this situation, we can hardly draw any conclusion on the convergence of the dispersion curve in  $q \rightarrow \infty$  limit, except for reading from the trend of the curve. Moreover the composite fermion picture is a variation of the Fermi liquid theory, one could not expect that arbitrarily higher CF LL should always be physical, which actually nearly forms a continuum instead of discrete levels [114]. So we need to be careful on the large-momentum limit of the dispersion computed from  $\bar{\rho}_e$ .

From the above derivation, we can see the following points :

1. When we keep a finite number of CF LLs, both direct interaction  $V^{(2)}(\mathbf{q})$  and exchange interaction  $V^{(1)}(\mathbf{q})$  converge to zero when  $\mathbf{q} \rightarrow \infty$ , for whatever  $\rho$  used in  $\hat{V}$  ;
2. If one uses the preferred density  $\rho^p$ , the magneto-plasmon mode converges to the correct activation gap. But the spectrum near  $\mathbf{q} \rightarrow 0$  is not correct as we will show below ;
3. If one uses the electron density  $\bar{\rho}_e$ , the spectrum gives a good result at small momentum but it does not necessarily converge to the correct activation gap for  $\mathbf{q} \rightarrow \infty$ , where more and more CF LLs need to be taken into account.

We now present a numerical comparison between the calculations based on two densities in Fig. V.3. We choose the interaction with large- $q$  cut-off so as the Hamiltonian theory gives a good estimate for the true activation gap :

$$V_{eff}(q) = 2\pi \frac{e^{-q^2 l^2 / 2}}{q} e^{-\lambda^2 q^2 l^2 / 2}. \quad (\text{V.45})$$

The second exponential comes from the LLL projection and in our calculation we take  $\lambda = 1$ . The activation gap is computed from the preferred density. The numbers of CF LLs used in the computation are chosen such as to obtain a stable dispersion upon adding further levels. In Fig. V.3, the dispersion computed from the preferred density correctly converges to the activation gap. But its behaviour at small momentum is terribly inconsistent with the single-mode approximation. It keeps lowering down when the momentum goes zero. This is also the behaviour found by Murthy [114] using the leading order expansion of  $\rho^p$ . On the side of  $\bar{\rho}_e$ , the dispersion is similar to the single mode approximation, especially the lowest point is almost at the same position. But the exact value of energy does not match the single mode approximation. This numerical discrepancy may not be so serious a problem since even the Laughlin state used in the single-mode approximation is an estimation for the true ground state. In Fig. V.3, the dispersion of  $\rho^e$  seems to converge to the activation gap for large momentum. It remains interesting to see if this convergence applies to other fillings and potentials.

The physical intuition for the difference between the two densities may be understood through the following picture of composite fermions. At large distance, the interaction between the quasiparticle and the quasihole is weak. They behave like a free CF and a free

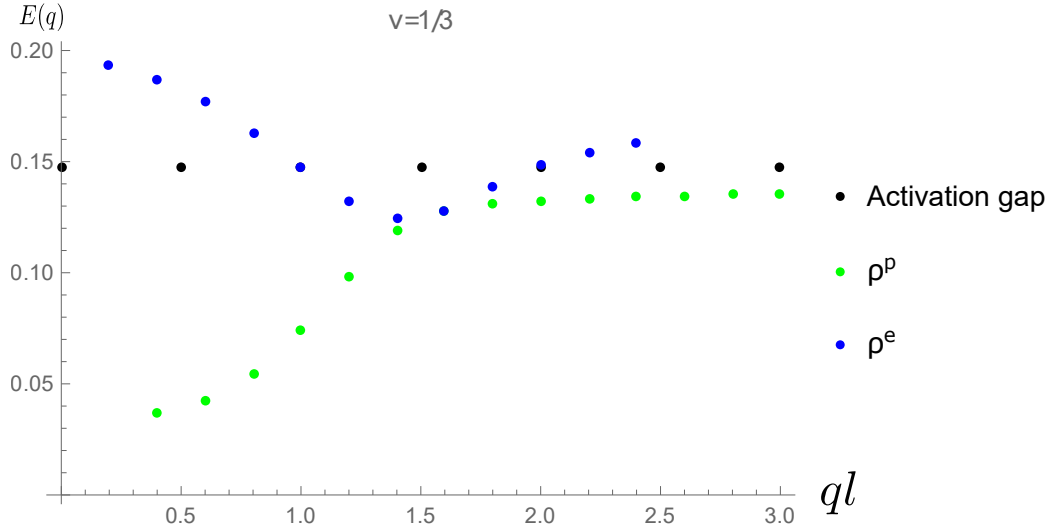


Fig. V.3 The comparison between the dispersion computed from the electron density and preferred density. The Green line is computed from  $\rho^p$  and the blue line is computed from  $\rho^e$ . The number of CF LLs for  $\bar{\rho}_e$  is 20, while 7 for  $\rho^p$ . The activation gap is computed using  $\rho^p$ .

CF hole. The activation gap is captured by the composite fermion interaction, through  $\rho^p$ . At small distance, the quasiparticle/quasihole pair is strongly interacting. They cannot be approximated by a free quasiparticle plus a free free quasihole that are independent from each other. Only electron interaction can be seen at short distance. So it is necessary to go back to the electron density  $\bar{\rho}_e$  so as to compute the dispersion for small momentum.

## V.4 Computation in the presence of anisotropy

According to the classification of topological phases in Ref. [21], the phases with topological orders are characterized by their long-range entanglement and can be enriched by their symmetries. Phases with the same topological order but different symmetry orders are allowed to exist. There is a long search for the so-called nematic phases in quantum Hall systems [128]. The quantum Hall nematic phase is assumed to have a broken rotational symmetry but preserves the topological order [57]. Such a phase is suggested in anisotropically perturbed experiments by detecting quantized Hall resistance and anisotropic longitudinal resistance [129, 105]. The phase transition from a quantum Hall liquid to a quantum nematic phase can be induced by softening the GMP mode, the neutral collective excitation [109, 56]. We have already shown in Sec. IV.3.3 that the activation gap is robust against external anisotropy. As the activation gap is related to the stability of quasiparticle/hole excitations, their persistence preserves the topological order associated with the FQHE. In order to specify the existence of the quantum Hall nematics in tilted magnetic field experiments, it would be useful to investigate how the neutral collective mode reacts.

Now we solve the magneto-exciton spectrum in the presence of anisotropy. Looking back at the vertex equation Eq. (V.14) or Eq. (V.33), it is tempting to insert directly the aniso-

tropic interaction. However, one can verify easily that this naive insertion is incorrect in the sense that the vertex equation Eq. (V.14) or Eq. (V.33) no longer admits the existence of a non-physical zero eigenvalue.

So we proceed in two steps. First we treat the anisotropy in a perturbative sense and obtain an equation of motion admitting a non-physical zero eigenvalue. In a second step, we study the non-perturbative equation in the presence of anisotropy. The solution of this equation needs highly numerical calculations. It also gives a non-perturbative answer to the calculation of activation gap in the previous Sec. IV.3. This section focuses on the first step, while the second step is left to Sec. V.5.

Before doing the calculation, we first need to define what the perturbative parameter is and how the perturbation theory is established. We consider a generic anisotropic interaction with inversion symmetry ( $\mathbf{q} \rightarrow -\mathbf{q}$ ) and a reflection plane ( $q_x \rightarrow -q_x$ ). According to Fourier series expansion, the angular part of the interaction is a periodic function of the angle  $\phi = \arctan(q_y/q_x)$  and thus can be expanded according to

$$V(\mathbf{q}) = \sum_n V_n(q) \cos(2n\phi), \quad (\text{V.46})$$

where  $V(q)$  is a function only of the norm of  $\mathbf{q}$  and  $\phi$  the angle of the polar coordinate in  $xy$ -plane. This is a simplified version of the generalized pseudopotential expansion, where the radial part is also expanded according to the associated Laguerre polynomials. In the generalized pseudopotential expansion, the radial expansion corresponds to different electronic angular momentum states. But for our question, the angular expansion is enough as we are studying composite fermions that have a different magnetic length than electrons and we are mainly interested in their inter-LL physics. For isotropic interaction, one has only the  $n = 0$  component. From the perturbation point of view, we now start from an interaction with only  $V_0$  component and switch on small  $V_n$  ( $n \neq 0$ ) components. Those  $V_n$  ( $n \neq 0$ ) components perturb the CF picture since they introduce CF LL mixing. This naturally leads us to treating the CF LL mixing as the perturbation. The amplitudes of the components  $V_n$  ( $n \neq 0$ ) serve as the perturbation parameter.

We have already encountered how to compute the CF LL mixing amplitude in the calculation of the activation gap. To simplify the notations later, we first work out how the anisotropic components affect the Hartree-Fock Hamiltonian of composite fermions. The Hartree-Fock Hamiltonian of composite fermions is obtained through the following replacement of the interaction operator [see also Eq. (V.9)] :

$$d_1^\dagger d_2^\dagger d_3 d_4 \rightarrow \langle d_1^\dagger d_4 \rangle d_2^\dagger d_3 + \langle d_2^\dagger d_3 \rangle d_1^\dagger d_4 - \langle d_1^\dagger d_3 \rangle d_2^\dagger d_4 - \langle d_2^\dagger d_4 \rangle d_1^\dagger d_3, \quad (\text{V.47})$$

where  $d_1^\dagger d_2^\dagger d_3 d_4$  are the operators multiplied by the interaction  $V_{eff}(\mathbf{q})$  and matrix elements of density operators. After the above replacement, the interaction becomes a one-body operator. Here we do not give a time-dependence to  $d^\dagger, d$ , whose importance will be discussed in the later TDHF calculation. The ladder operators take their static values  $d^\dagger(0), d(0)$ , which for the  $p$  filled CF LL picture satisfy  $\langle d_{n_1, m_1}^\dagger d_{n_2, m_2} \rangle = \delta_{m_1 m_2} \delta_{n_1 n_2} N_F(n_1)$ , where  $n$  labels the CF LL and  $m$  labels the intra-LL physics. This occupation pattern is independent of the intra-LL physics. This leads to the result that the intra-LL index does not enter the HF Hamiltonian. In the isotropic case, one can find that the Hartree-Fock Hamiltonian of composite fermions is diagonal in CF LL indices, similar to the orthogonality relation Eq.

(IV.31). In the anisotropic case, a CF LL mixing term enters and we find in general the Hartree-Fock Hamiltonian :

$$\frac{1}{2} \sum_{1234} \int \frac{d^2q}{(2\pi)^2} V(\mathbf{q}) \rho(\mathbf{q})_{12} \rho(-\mathbf{q})_{34} d_1^\dagger d_2^\dagger d_3 d_4 \rightarrow \sum_n \epsilon_n d_n^\dagger d_n + \sum_{m \neq n} \left( M_{m,n} d_m^\dagger d_n + \text{c.c.} \right), \quad (\text{V.48})$$

where the indices  $m, n$  now only label the CF LL and those implicit intra-LL indices in the right-hand side of the above formula are diagonal. The Hartree-Fock energy  $\epsilon_n$  and the mixing amplitude  $M_{m,n}$  are given by

$$\begin{aligned} M_{m,n} &= \frac{1}{2} \int \frac{d^2q}{4\pi^2} V(\mathbf{q}) \left[ \delta_{m,n} - 2 \sum_{l=0} N_F(l) \rho_{ln}(\mathbf{q}) \rho_{ml}(-\mathbf{q}) \right] \\ &= \frac{1}{2} \int \frac{qdq}{2\pi} \left[ V_0(q) \delta_{m,n} - \sum_{l=0} N_F(l) (1 + \delta_{m,n}) \rho_{ln}(q) \rho_{ml}(-q) V_{|m-n|}(q) \right], \end{aligned} \quad (\text{V.49})$$

$$\epsilon_n = M_{n,n}, \quad (\text{V.50})$$

where  $\rho(q)$  is the radial dependent part of  $\rho(\mathbf{q})$ . For  $n_2 \geq n_1$ , it is given by :

$$\rho_{n_1, n_2}(q) = \sqrt{\frac{n_1!}{n_2!}} e^{-q^2 l^{*2}/4} \left( \frac{iq l^*}{\sqrt{2}} \right)^{n_2 - n_1} L_{n_1}^{n_2 - n_1} \left( \frac{q^2 l^{*2}}{2} \right) \quad (\text{V.51})$$

From its expression, we can see that the matrix  $M_{m,n}$  is Hermitian,  $M_{m,n} = M_{n,m}^*$ .

Now we proceed as before and work out the equation of motion for the magneto-excitons. Here we still evaluate the density correlation function with  $p$  filled CF LLs as the reference state. This time the reference state is not a good candidate for the true ground state because of the CF LL mixing terms. To see the usefulness of the time-ordered correlation function, we need to decompose it into the eigenstates of the Hamiltonian :

$$\chi(\omega, \mathbf{q}) = \sum_{m,n} \frac{\langle \mathbf{p} | m \rangle \langle m | \rho(\mathbf{q}) | n \rangle \langle n | \rho(-\mathbf{q}) | \mathbf{p} \rangle}{\omega - (E_m - E_n) + i0^+} - \frac{\langle \mathbf{p} | \rho(-\mathbf{q}) | n \rangle \langle n | \rho(\mathbf{q}) | m \rangle \langle m | \mathbf{p} \rangle}{\omega - (E_m - E_n) - i0^+}, \quad (\text{V.52})$$

where  $|m\rangle, |n\rangle$  represent the  $m$ -th and the  $n$ -th eigenstate of the system. From this decomposition, we observe that the poles of this density correlation function can still give information about the neutral excitation.

The evaluation of the equation of motion is done as before, by computing the commutator between the Hamiltonian and the magneto-exciton operator and approximating a pair of creation and annihilation operators with their expectation value. However, this time the expectation value is not conserved self-consistently due to the CF LL mixing  $\langle d^\dagger(t) d(t) \rangle \neq \langle d^\dagger(0) d(0) \rangle$ . Empty CF LLs will be populated and filled CF LLs will be losing CFs during the time evolution. From a perturbative point of view, if we treat the CF LLs as a true free-particle structure but not an emerging one, this perturbation should be oscillating in time with a small amplitude [130]. So as a first step towards the anisotropic perturbation, we still put the time-dependent occupation expectation to be its value at  $t = 0$

$$\langle d_{n_1, m_1}^\dagger(t) d_{n_2, m_2}(t) \rangle \simeq \delta_{m_1 m_2} \delta_{n_1 n_2} N_F(n_1). \quad (\text{V.53})$$

Then the calculation for the equation of motion is almost identical to the isotropic situation, except that the mixing matrix  $M_{m,n}$  appears in addition to the original CF LL energy

$\epsilon_{m_1} - \epsilon_{m_2}$  difference, scattering one leg of  $O_{m_1, m_2}$ . One finds that now the equation takes the form :

$$\begin{aligned} \omega \langle O_{m_1 m_2} O_{l_2 l_1} \rangle &= \sum_{n_1, n_2} (M_{n_1, m_1} \delta_{m_2, n_2} - M_{m_2, n_2} \delta_{m_1, n_1}) \langle O_{n_1 n_2} O_{l_2 l_1} \rangle + [N_F(m_2) - N_F(m_1)] \\ &\quad \left[ \frac{V(\mathbf{q})}{2\pi l^{*2}} \rho_{n_1 n_2}(\mathbf{q}) \rho_{m_2 m_1}(-\mathbf{q}) - \int \frac{d^2 \mathbf{k}}{(2\pi)^2} V(\mathbf{k}) \rho_{n_1 m_1}(\mathbf{k}) \rho_{m_2 n_2}(-\mathbf{k}) e^{i\mathbf{k} \times \mathbf{q} l^{*2}} \right] \\ &\quad \langle O_{n_1 n_2} O_{l_2, l_1} \rangle - i N_{\phi^*} \delta_{m_1, l_1} \delta_{m_2, l_2} [N_F(m_1) - N_F(m_2)]. \end{aligned} \quad (\text{V.54})$$

With inclusion of the  $M_{m, n}$  matrix, one can easily verify that the above matrix equation admits a left zero-energy eigenvector, given by  $\chi_{m_1, m_2}(\mathbf{q})$ .

As before we group the above matrix equation into a block form according to the types of excitons classified in Sec. V.1. Due to the matrix  $M_{m, n}$ , there is a mixing between type 1 excitons and type 2, type 3 excitons. The block matrix equation is expressed as :

$$\begin{pmatrix} \omega - A & -B \\ -C & \omega - D \end{pmatrix} \begin{pmatrix} a & b \\ c & d \end{pmatrix} = \begin{pmatrix} \tilde{I} & 0 \\ 0 & 0 \end{pmatrix}, \quad (\text{V.55})$$

The vectors  $b$  and  $d$  satisfy two homogeneous matrix equations,  $(\omega - A)b - Bd = 0$  and  $Cb - (\omega - D)d = 0$ . In general they have to be zero as there are no common solutions to both equations. For the same reasons that we used before, this is also easily understood because the type 2 and type 3 exciton operators annihilate the reference state. The block  $c$  is not an independent variable and is given by  $c = -D^{-1}Ca$ . Therefore the above matrix equation transforms to

$$\left[ (\omega - A) - B(\omega - D)^{-1}C \right] a = \tilde{I}. \quad (\text{V.56})$$

Compared to the isotropic case, we have an  $\omega$ -dependent perturbation. This equation no longer takes the form of an eigenvalue question. The poles of the correlation function are given by the condition  $\det[(\omega - A) - B(\omega - D)^{-1}C] = 0$ . But from a perturbative point of view, when we need to find the perturbation to  $\omega^{(0)}$ , the eigenvalue of the isotropic  $A^{(0)}$ , we can simply replace the  $\omega$  in  $(\omega - D)^{-1}$  by  $\omega^{(0)}$  in Eq. (V.56) and the question again takes an eigenvalue form, which we denote as  $(\omega - \mathcal{H})a = \tilde{I}$ .

With these equations we perform the standard perturbation expansion. The anisotropic components of the interaction are treated as the perturbation. They introduce the mixing matrix  $M_{m, n}$  ( $m \neq n$ ). Notice here the matrix  $\mathcal{H}_{\mu, \nu}$  is not Hermitian. We have to distinguish left and right eigenvectors. According to the non-degenerate perturbation theory, the correction to the eigenvalue to leading order can in this case be given by the expectation value of the perturbation. In this question, we need the eigenstates of the first positive non-zero eigenvalue, denoted as  $|\Psi_1^R\rangle$  and  $\langle \Psi_1^L|$ . The matrix  $\mathcal{H}$  is decomposed into  $\mathcal{H} = A^{(0)} + \mathcal{H}'$ , with  $\mathcal{H}'$  the difference between  $A^{(0)}$  and  $\mathcal{H}$ . Perturbation theory for a non-degenerate eigenstate tells us that the correction to the energy is given by :

$$\delta E(\mathbf{p}) = \frac{\langle \Psi_1^L | \mathcal{H}' | \Psi_1^R \rangle}{\langle \Psi_1^L | \Psi_1^R \rangle}. \quad (\text{V.57})$$

In the magneto-exciton approximation, the  $V^{(2)}$  term [Eq. (V.35)] in the vertex equation is given by the interaction times the matrix elements of the density operator. The  $V^{(1)}$  term

[Eq. (V.15)] is an exchange energy and needs to perform a Fourier transformation. In the anisotropic situation, it can be expressed as :

$$V^{(1)}(\mathbf{q}) = \int \frac{kdk}{2\pi} \rho_{n_1 m_1}(k) \rho_{m_2 n_2}(-k) \sum_n \frac{V_n(k)}{2} e^{i(n_1+m_2-m_1-n_2)\bar{\phi}} \left[ J_{n_1+m_2-m_1-n_2+2n}(kq) e^{i2n\bar{\phi}} + J_{n_1+m_2-m_1-n_2-2n}(kq) e^{-i2n\bar{\phi}} \right], \quad (\text{V.58})$$

where  $\bar{\phi}$  is the angle between  $\mathbf{q}$  and the  $x$ -axis, and  $\rho_{n_1, n_2}(q)$  is as before the radial part of  $\rho_{n_1, n_2}(\mathbf{q})$ .

With these formulae in mind, we compute the collective modes in the small tilting angle limit and thin sample limit of a quantum Hall system under tilted magnetic field. It is shown in the work of Yang, Lee et al. [110] that in these cases the effective two-dimensional interaction is perturbed by a polynomial of  $\exp(i\phi)$ . The exchange interaction can be computed easily with the help of Bessel functions as we have shown.

The effective 2D interactions in limiting situations are listed below :

1. Thin sample limit : in this case,  $\Omega \gg \omega_c$ , the effective interaction in the LLL takes the form :

$$V_{eff} \simeq 2\pi \frac{e^{-q^2 l^2 / 2}}{q} \left( 1 - \sqrt{\frac{2\omega_c}{\pi\Omega}} ql + \frac{q^2 - 2q_x^2 \tan^2 \theta}{2(\Omega/\omega_c)} l^2 \right), \quad (\text{V.59})$$

where  $\theta = B_x/B_z$  is the tilting angle. The effective interaction is obtained by the projection to the 0-th LL and 0-th level of the confining potential.

2. Small tilting limit : in this case,  $B_x \ll B_z$ , the effective interaction in the LLL reads

$$V_{eff} \simeq 2\pi \frac{e^{-q^2 l^2 / 2}}{q} \left\{ A[z] + \left[ \sqrt{\frac{2\omega_c}{\pi\Omega}} ql - A[z] \left( 1 + \frac{q^2 l^2 \omega_c}{\Omega} \right) \right] \frac{q_x^2 l^2 \tan^2 \theta}{(\Omega/\omega_c)} \right\}, \quad (\text{V.60})$$

with  $z = ql/\sqrt{2(\Omega/\omega_c)}$  and  $A[z] = \exp(z^2)(1 - \text{Erf}[z])$ .

Comparing the interaction with the expansion Eq. (V.46), we find in these two limits, only  $V_0$  and  $V_2$  defined in Eq. (V.46) are non-vanishing. For the thin sample limit, the expansion is

$$V_0(q) = 2\pi e^{-q^2 l^2 / 2} \left( 1 - \sqrt{\frac{2\omega_c}{\pi\Omega}} ql + \frac{q^2 l^2 (1 - \tan^2 \theta)}{2(\Omega/\omega_c)} \right), \quad (\text{V.61})$$

$$V_2(q) = -2\pi e^{-q^2 l^2 / 2} \frac{q^2 l^2 \tan^2 \theta}{2(\Omega/\omega_c)}, \quad (\text{V.62})$$

where for the small tilting limit :

$$V_0(q) = 2\pi e^{-q^2 l^2 / 2} \left\{ A[z] + \left[ \sqrt{\frac{2\omega_c}{\pi\Omega}} ql - A[z] \left( 1 + \frac{q^2 l^2 \omega_c}{\Omega} \right) \right] \frac{q^2 l^2 \tan^2 \theta}{2(\Omega/\omega_c)} \right\}, \quad (\text{V.63})$$

$$V_2(q) = 2\pi e^{-q^2 l^2 / 2} \left[ \sqrt{\frac{2\omega_c}{\pi\Omega}} ql - A[z] \left( 1 + \frac{q^2 l^2 \omega_c}{\Omega} \right) \right] \frac{q^2 l^2 \tan^2 \theta}{2(\Omega/\omega_c)}. \quad (\text{V.64})$$

Using the above expressions, we compute the collective modes for a series of tilting angles and sample thickness. Notice that introducing the tilting angle not only introduces

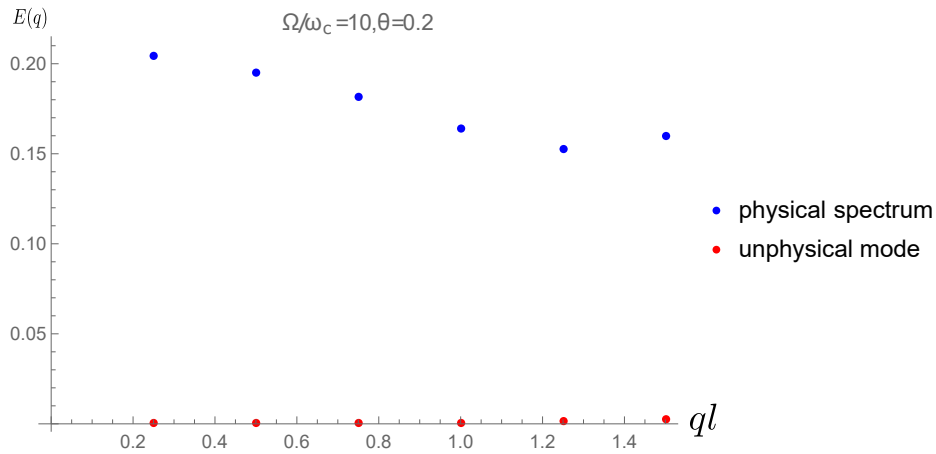


Fig. V.4 The isotropic contribution to the neutral collective mode  $\nu = 1/3$  as a function of  $ql$ . The potential is taken in the thin sample limit. The confining potential is chosen as  $\Omega/\omega_c = 10$ . The tilting angle is  $\theta = 0.2$ .

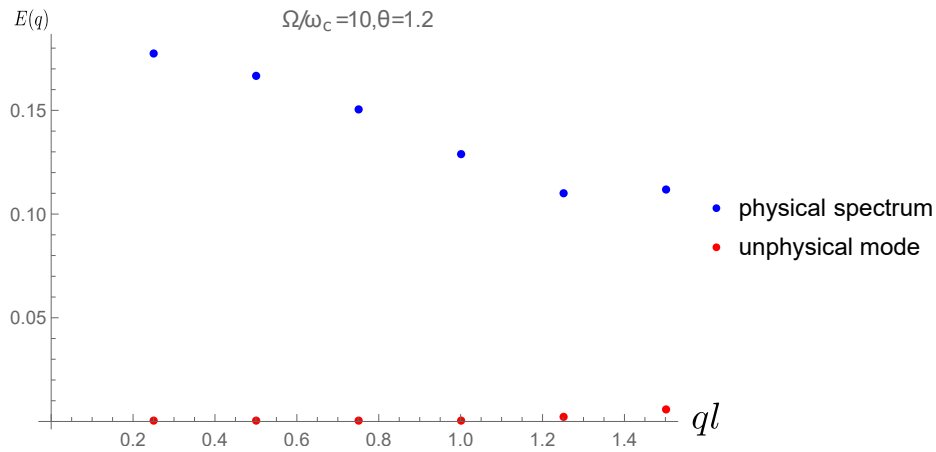


Fig. V.5 The isotropic contribution to the neutral collective mode  $\nu = 1/3$  as a function of  $ql$ . The potential is taken in the thin sample limit. The confining potential is chosen as  $\Omega/\omega_c = 10$ . The tilting angle is  $\theta = 1.2$ .



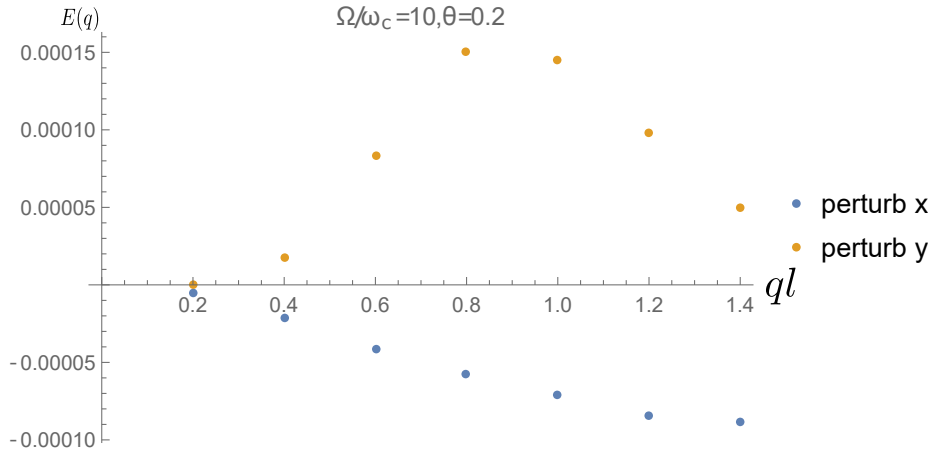


Fig. V.6 The perturbation to the neutral collective mode as a function of  $q_x$  or  $q_y$  for  $\nu = 1/3$ . The potential is taken in the thin sample limit. The confining potential is chosen as  $\Omega/\omega_c = 10$ . The tilting angle is  $\theta = 0.2$ .

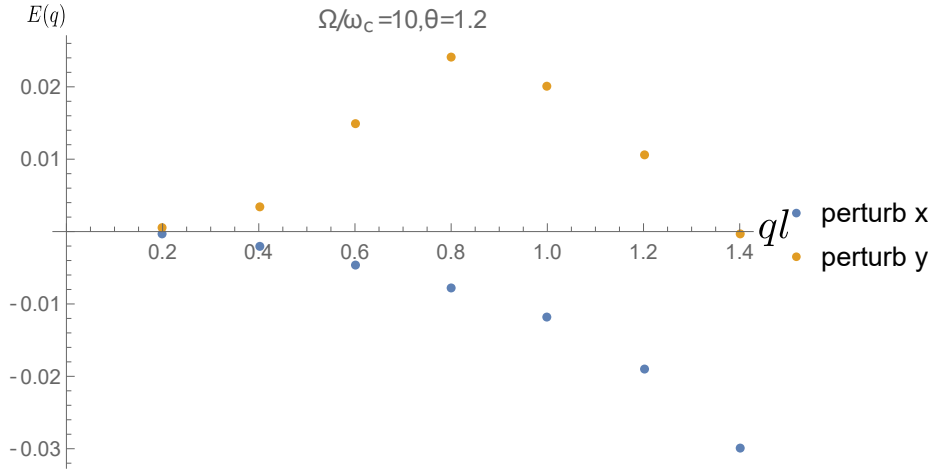


Fig. V.7 The perturbation to the neutral collective mode as a function of  $q_x$  or  $q_y$  for  $\nu = 1/3$ . The potential is taken in the thin sample limit. The confining potential is chosen as  $\Omega/\omega_c = 10$ . The tilting angle is  $\theta = 1.2$ .

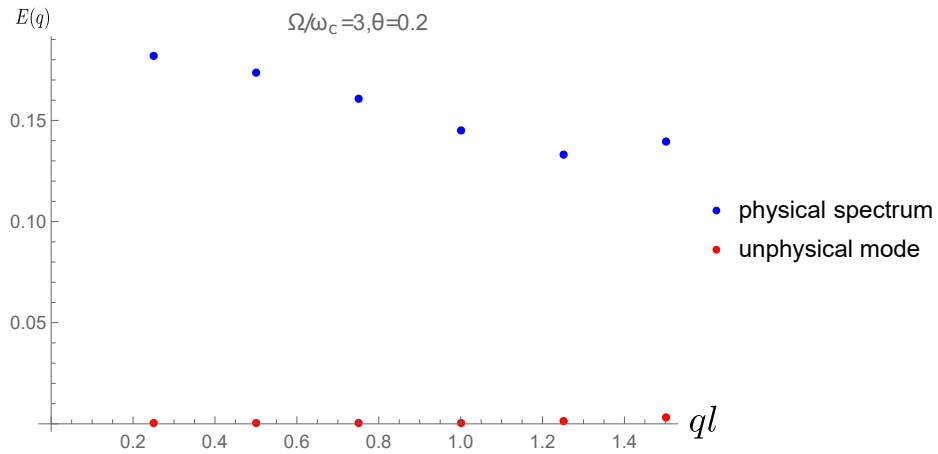


Fig. V.8 The isotropic contribution to the neutral collective mode  $\nu = 1/3$  as a function of  $ql$ . The potential is taken in the small tilt limit. The confining potential is chosen as  $\Omega/\omega_c = 3$ . The tilting angle is  $\theta = 0.2$ .

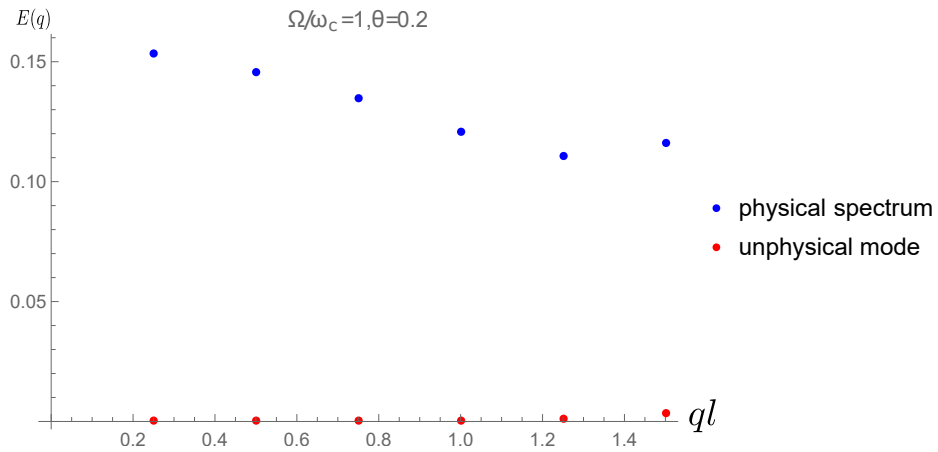


Fig. V.9 The isotropic contribution to the neutral collective mode  $\nu = 1/3$  as a function of  $ql$ . The potential is taken in the small tilt limit. The confining potential is chosen as  $\Omega/\omega_c = 1$ . The tilting angle is  $\theta = 0.2$ .

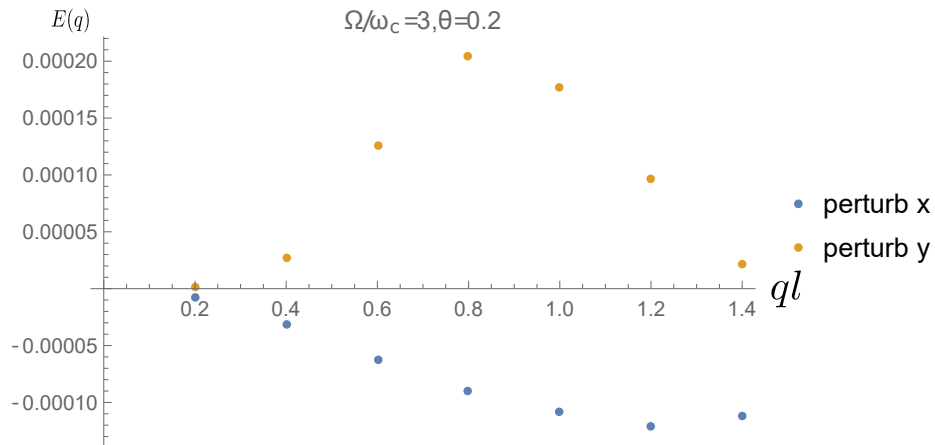


Fig. V.10 The perturbation to the neutral collective mode as a function of  $q_x$  or  $q_y$  for  $\nu = 1/3$ . The potential is taken in the small tilt limit. The confining potential is chosen as  $\Omega/\omega_c = 3$ . The tilting angle is  $\theta = 0.2$ .

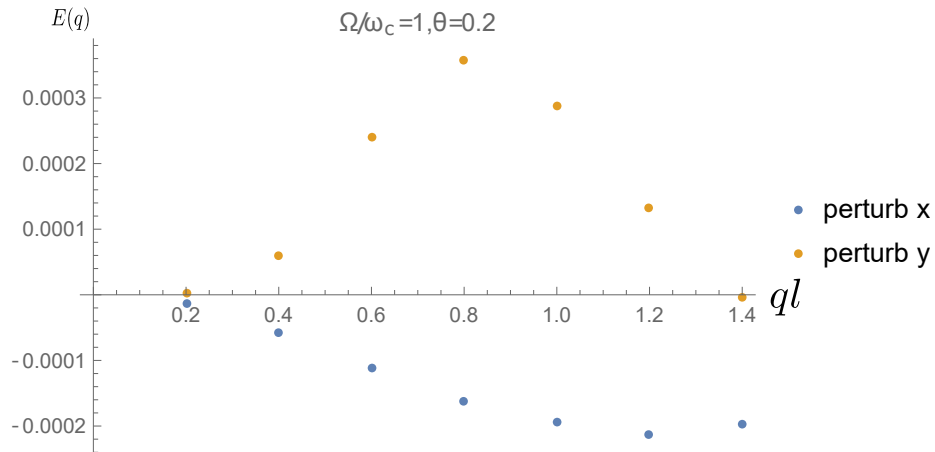


Fig. V.11 The perturbation to the neutral collective mode as a function of  $q_x$  or  $q_y$  for  $\nu = 1/3$ . The potential is taken in the small tilt limit. The confining potential is chosen as  $\Omega/\omega_c = 1$ . The tilting angle is  $\theta = 0.2$ .

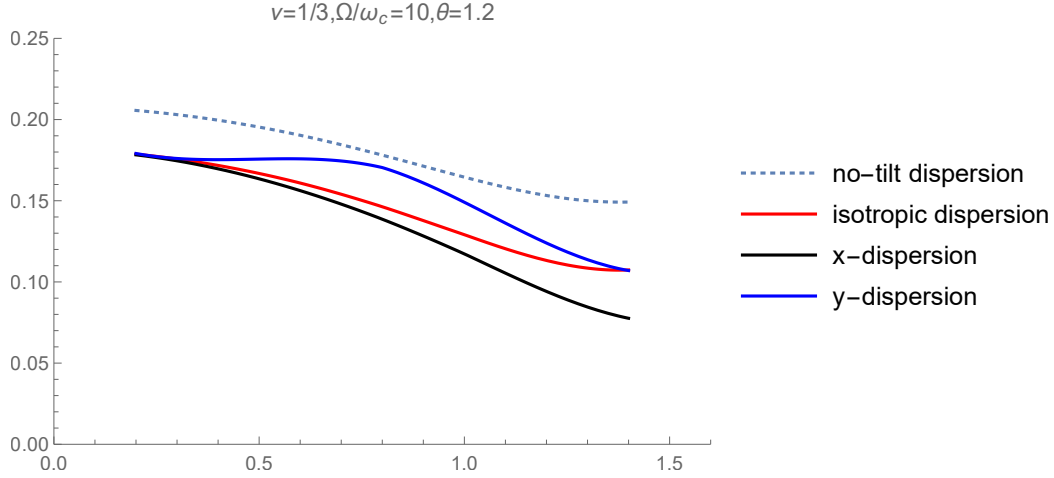


Fig. V.12 Comparison between the collective mode dispersion at  $\theta = 0$  and the dispersion at  $\theta = 1.2$  at  $\nu = 1/3$ . The dashed line is for  $\theta = 0$ . For  $\theta = 1.2$ , we draw its isotropic contribution due to  $V_0$  and the dispersion along  $x$ - and  $y$ -directions.

an anisotropic perturbation  $V_2$ , but it also modifies the isotropic part  $V_0$ . The perturbation theory we perform is hence not an expansion on the tilting angle  $\theta$ , but merely on  $V_2$ . The isotropic contribution  $V_0$  is treated as the unperturbed contribution. For  $\nu = 1/3$ , the anisotropic correction can be usually much smaller than the neutral collective mode itself. So we present the anisotropic correction independently from the isotropic contribution. Fig. V.4 and Fig. V.5 present the neutral mode computed with only the isotropic interaction  $V_0$ . Here we truncate the number of CF LLs to 10. The potential used is the one in the thin sample limit for tilting angle  $\theta = 0.2$  (Fig. V.4) and  $\theta = 1.2$  (Fig. V.5). We take  $\Omega/\omega_c = 10$ . Although this is not so thin as to make the thin sample limit potential accurate enough, we believe that it predicts schematically the physical evolution under anisotropy. We can see in Fig. V.5 that tilting the magnetic field can soften the magneto-roton gap. This is an isotropic influence when the magnetic field is tilted. Fig. V.6 and Fig. V.7 show the corrections due to  $V_2(q)$  for  $\mathbf{q}$  along  $x$ - and  $y$ -directions. The directional dependence is clearly reflected. We notice that through a large regime of  $|q|$ , the mode is softened in the  $x$ -direction (the direction of the in-plane magnetic field) but strengthened in the  $y$ -direction. This suggests the possibility that the magneto-roton gap can close in one direction but still remains open in the other direction. Comparing Fig. V.4 to Fig. V.7, we observe that there is such a trend if the isotropic contribution is further softened by the tilting angle  $\theta$ . The parameters here are not quite adequate for the thin sample limit, as we only take  $\Omega/\omega_c = 10$  and in large angle the term  $\tan^2 \theta / (\Omega/\omega_c)$  can be non-perturbative. It has to be confirmed with further numerical calculations. Fig. V.8 and Fig. V.9 show the neutral mode dispersion for the small tilting limit and Fig. V.10, Fig. V.11 show the corresponding anisotropic correction. In this case, the anisotropic correction is almost linear to  $1/\Omega$ . This is because the anisotropic interaction is proportional to  $1/\Omega$  and we are doing perturbation expansion to the leading order proportional to it. We can see that the influence of the sample thickness is not as strong as the tilting angle. Increasing the sample thickness lowers the overall scale of the neutral mode. So the incompressibility is reduced when we have a wider quantum well. A

summarization for  $\theta = 1.2, \Omega/\omega_c = 10$  is given in Fig. V.12.

We also compute the perturbation to the  $\nu = 2/5$  state. As this filling belongs to  $p = 2$  Jain's series, the numerical complexity is twice that of  $\nu = 1/3$ . Fig. V.13 and Fig. V.14 show the isotropic part contribution for  $\theta = 0.2$  and  $\theta = 0.7$  using 15 CF LLs. The gap of the  $\nu = 2/5$  mode is smaller than  $\nu = 1/3$  and the unphysical mode soon becomes uncontrolled for a finite truncation on the number of CF LLs. The neutral gap in this case is more vulnerable. We can observe that from  $\theta = 0.7$ , the anisotropic perturbation has almost the same amplitude as the isotropic contribution. At this point, the perturbation theory breaks down. A gap closing is likely to be induced in the  $x$ -direction (in-plane magnetic field direction) if the tilting angle is increased further. We also plot a comparison between the anisotropic collective modes with its unperturbed isotropic counterpart in Fig. V.17. There the dispersion with no tilt, the contribution from  $V_0$  at  $\theta = 0.7$  and the final anisotropic dispersion at this angle are presented together.

## V.5 Calculations to all orders in perturbation theory

In previous sections, we have computed the activation gap and the neutral mode in the perturbative sense, where the reference state is still taken as the  $p$  filled CF LLs. In this section, we provide how to obtain a self-consistent solution beyond that. The key formula is to work out the expectation of density iteratively. The solution to these equations requires relatively large numerical work. Due to the time limit, we only outline the analytic part and the numerical part has not been realized when this thesis is being written.

As we have seen, anisotropy introduces CF LL mixing. As the CF LL structure itself emerges from the strongly correlated interaction, the CF LL mixing cannot be eliminated simply within the one-body Hilbert space, say by changing the basis of the one-body states. We have to go back to the many-body Hilbert space and include the strongly correlated interaction. This is reminiscent of the Fermi liquid theory [52], where the energy of the electron near the Fermi sea depends on how electrons fill the energy levels under the Fermi sea. A self-consistent way to solve this problem is to apply the TDHF approximation first to the single-body Green's function, the propagator. This formula is similar to the TDHF calculation for charge density wave states [131]. And as we will explain later, the equation will turn out to emerge naturally from the diagrammatic language, which was used by Read [98] to address the gapless Fermi liquid at half filling in quantum Hall systems.

The equation of motion for the propagator is :

$$\frac{d}{dt}G_{\alpha\beta}(t) = -i\frac{d}{dt}\langle\mathcal{T}d_{\alpha}(t)d_{\beta}^{\dagger}(0)\rangle = \langle\mathcal{T}[H, d_{\alpha}(t)]d_{\beta}^{\dagger}(0)\rangle - i\delta(t)\delta_{\alpha\beta}, \quad (\text{V.65})$$

where the indices  $\alpha, \beta$  encode both the LL degrees of freedom and intra-LL degrees of freedom. In the above equation every expectation value is to be evaluated in the self-consistent HF ground state of the system  $|0\rangle$ , which will need to be worked out self-consistently, not the  $p$  filled reference state  $|\mathbf{p}\rangle$ . The density of the composite fermions is fixed to that of  $\nu = p$  IQHE. For this HF state  $|0\rangle$ , the expectation value of any operator is conserved. The equal-time expectation value is to take the  $t \rightarrow 0^-$  limit of the propagator :

$$\langle d_{\alpha}^{\dagger}d_{\beta}\rangle = -iG_{\alpha\beta}(t)|_{t\rightarrow 0^-}. \quad (\text{V.66})$$

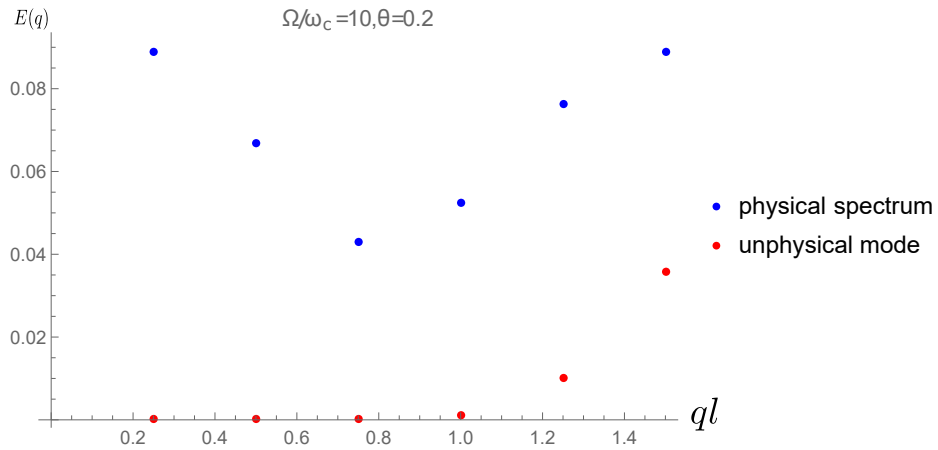


Fig. V.13 The isotropic contribution to the neutral collective mode  $\nu = 2/5$  as a function of  $ql$ . The potential is taken in the thin sample limit. The confining potential is chosen as  $\Omega/\omega_c = 10$ . The tilting angle is  $\theta = 0.2$ .

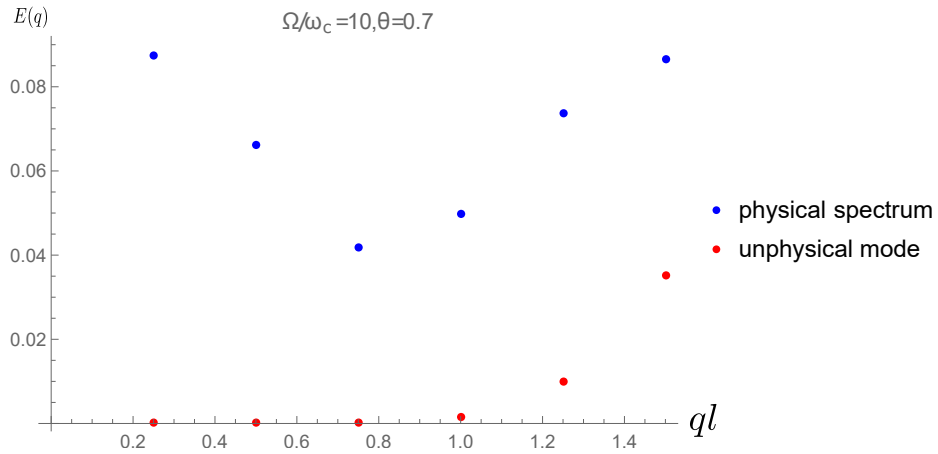


Fig. V.14 The isotropic contribution to the neutral collective mode  $\nu = 2/5$  as a function of  $ql$ . The potential is taken in the thin sample limit. The confining potential is chosen as  $\Omega/\omega_c = 10$ . The tilting angle is  $\theta = 0.7$ .

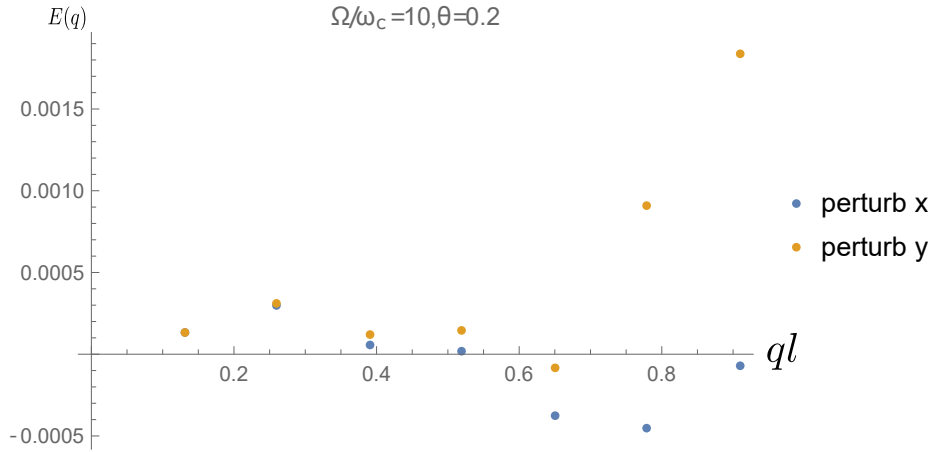


Fig. V.15 The perturbation to the neutral collective mode as a function of  $q_x$  or  $q_y$  for  $\nu = 2/5$ . The potential is taken in the thin sample limit. The confining potential is chosen as  $\Omega/\omega_c = 10$ . The tilting angle is  $\theta = 0.2$ .

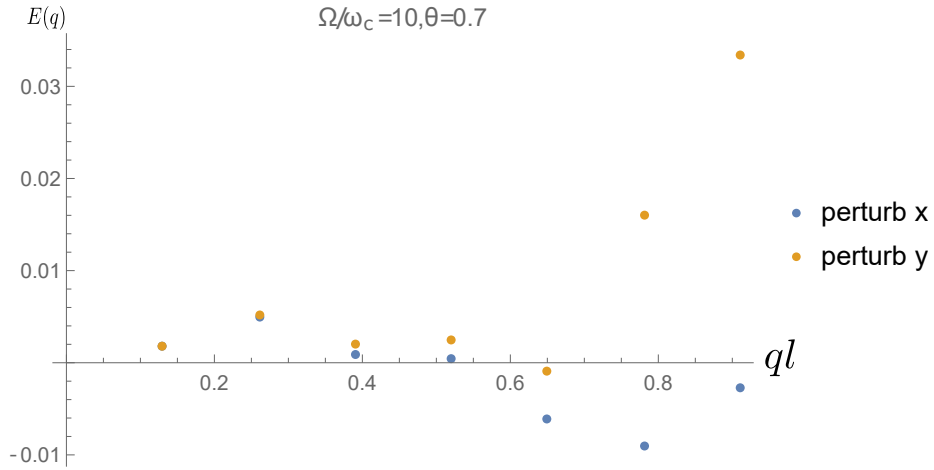


Fig. V.16 The perturbation to the neutral collective mode as a function of  $q_x$  or  $q_y$  for  $\nu = 2/5$ . The potential is taken in the thin sample limit. The confining potential is chosen as  $\Omega/\omega_c = 10$ . The tilting angle is  $\theta = 0.7$ .

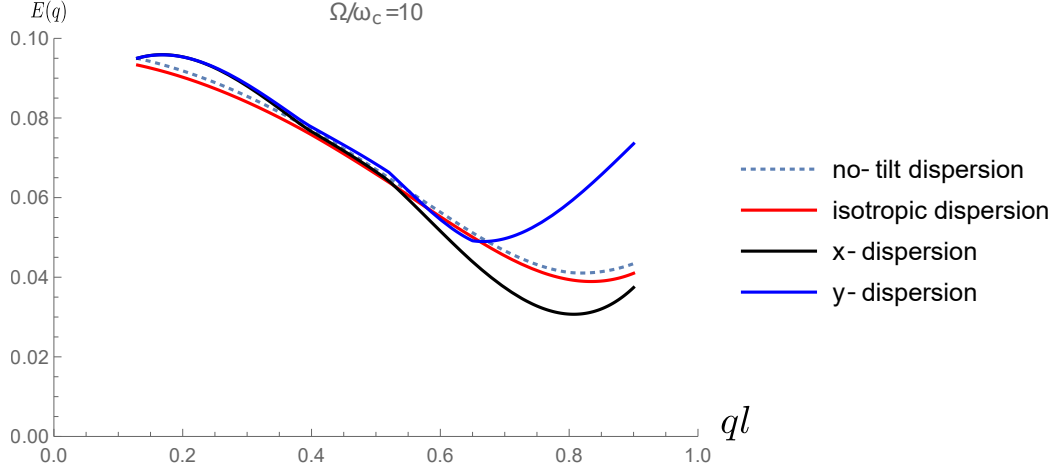


Fig. V.17 Comparison between the collective mode dispersion at  $\theta = 0$  and the dispersion at  $\theta = 0.7$  at  $\nu = 2/5$ . The dashed line is for  $\theta = 0$ . For  $\theta = 0.7$ , we draw its isotropic contribution due to  $V_0$  and the dispersion along  $x$ - and  $y$ -directions.

In order to maintain the CF density, a chemical potential has to be added to the Hamiltonian so that  $\sum_{\alpha} \langle d_{\alpha}^{\dagger} d_{\alpha} \rangle = pN_{\phi^*}$ . As the number of states inside each CF LL is extensively large, it would be more convenient to put everything in terms of the exciton operator and its correlation function counterpart, because the system has a translational symmetry. In this case we use the momentum  $\mathbf{q}$  to encode the intra-LL degrees of freedom :

$$G_{n_1 n_2}(t, \mathbf{q}) = \sum_X e^{-iq_x X l^{*2}} \left\langle \mathcal{T} d_{n_1, X+q_y l^{*2}/2}(t) d_{n_2, X-q_y l^{*2}/2}^{\dagger}(0) \right\rangle. \quad (\text{V.67})$$

$$\langle O_{n_1, n_2}(\mathbf{q}) \rangle = -G_{n_2, n_1}(t, \mathbf{q})|_{t \rightarrow 0^-} \quad (\text{V.68})$$

$G_{12}(t)$  can be obtained from  $G_{n_1 n_2}(\mathbf{q})$  by reversing the above equation :

$$G_{n_1 X, n_2 X'}(t) = \sum_{q_x} \frac{1}{N_{\phi^*}} e^{i(X+X')l^{*2}q_x/2} G_{n_1 n_2}[t, q_x, (X-X')/l^{*2}]. \quad (\text{V.69})$$

With those notations, we proceed to the equation of motion for  $G_{n_1, n_2}(t, \mathbf{q})$ . Using the commutation relation and momentum conservation, we find

$$-i \frac{d}{dt} G_{n_1, n_2}(t, \mathbf{q}) = - \sum_{m, \mathbf{q}'} \mathcal{H}_{n_1 m}^G(\mathbf{q} - \mathbf{q}') e^{i\frac{1}{2}\mathbf{q} \times \mathbf{q}'} G_{m, n_2}(\mathbf{q}') - i\delta(t) \delta_{n_1 n_2} \delta(\mathbf{q}), \quad (\text{V.70})$$

where we use the matrix  $\mathcal{H}^G$  to denote the commutator between  $H$  and the annihilation operator in  $G_{n_1 n_2}(t, \mathbf{q})$ . Its choice of parametrization will become clear soon. To evaluate the first term on the right-hand side, we need the following commutation rule :

$$[d_1^{\dagger} d_3^{\dagger} d_4 d_2, d_{1'}] = \delta_{1'3} d_1^{\dagger} d_4 d_2 - \delta_{1'1} d_3^{\dagger} d_4 d_2. \quad (\text{V.71})$$

As before, after applying the Hartree-Fock approximation, the above commutator becomes

$$\begin{aligned} \langle [d_1^{\dagger} d_3^{\dagger} d_4 d_2, d_{1'}](t) d_{2'}^{\dagger}(0) \rangle &= \delta_{1'3} \left( \langle d_1^{\dagger}(t) d_4(t) \rangle \langle d_2(t) d_{2'}^{\dagger}(0) \rangle - \langle d_1^{\dagger}(t) d_2(t) \rangle \langle d_4(t) d_{2'}^{\dagger}(0) \rangle \right) - \\ &\quad \delta_{1'1} \left( \langle d_3^{\dagger}(t) d_4(t) \rangle \langle d_2(t) d_{2'}^{\dagger}(0) \rangle - \langle d^{\dagger}(t)_3 d_2(t) \rangle \langle d_4(t) d_{2'}^{\dagger}(0) \rangle \right). \end{aligned} \quad (\text{V.72})$$



In the above formula we can drop the time-dependence in all equal-time correlation functions as now they are evaluated in the self-consistent HF ground state. As we have already encountered, because of the symmetry (12)  $\leftrightarrow$  (34), the first line and the second line give the same contribution and we simply suppress the 1/2 factor in the front of  $V_{eff}(\mathbf{q})$ . Recombining the matrices of density operators  $\rho_{n_1 n_2}$  and compare it with Eq. (V.70), the matrix  $\mathcal{H}^G$  again takes the form of a direct interaction minus an exchange interaction :

$$\mathcal{H}_{n,m}^G(\mathbf{q}) = \tilde{u}_d(\mathbf{q}) - \tilde{u}_{exc}(\mathbf{q}), \quad (\text{V.73})$$

where the direct and exchange interactions are given by

$$\tilde{u}_d(\mathbf{q}) = \sum_{l_1 l_2} V_{eff}(\mathbf{q}) \rho_{l_1 l_2}(\mathbf{q}) \rho_{n,m}(-\mathbf{q}) \langle O_{l_1 l_2}(\mathbf{q}) \rangle, \quad (\text{V.74})$$

$$\tilde{u}_{exc}(\mathbf{q}) = \sum_{\mathbf{k}, l_1, l_2} V_{eff}(\mathbf{k}) \rho_{l_1 m}(\mathbf{k}) \rho_{n l_2}(-\mathbf{k}) \langle O_{l_1 l_2}(\mathbf{q}) \rangle e^{i\mathbf{k} \times \mathbf{q} l^{*2}}. \quad (\text{V.75})$$

These equations are also found in Ref. [131]. Going to the frequency space, the equation of motion becomes a matrix equation for  $G_{n_1, n_2}(\omega, \mathbf{q})$  :

$$\sum_{m, \mathbf{q}'} \left[ \omega \delta_{n_1, m} \delta(\mathbf{q} - \mathbf{q}') - \mathcal{H}_{n_1, m}^G(\mathbf{q} - \mathbf{q}') \right] G_{m, n_2}(\mathbf{q}') = \delta_{n_1, n_2} \delta(\mathbf{q}). \quad (\text{V.76})$$

Now  $G_{n_1, n_2}(\omega, \mathbf{q})$  can be worked out by reversing the above equation. Since  $\mathcal{H}^G$  itself depends on the exciton operator expectation,  $\langle O_{n,m}(\mathbf{q}) \rangle$ , the above equation is a set of self-consistent equations. In the absence of anisotropy, a solution to it is the state of  $p$  filled composite fermion LLs, where

$$\langle O_{nm}(\mathbf{q}) \rangle = N_F(m) \delta_{n,m} \delta(\mathbf{q}) \quad (\text{V.77})$$

$$G_{n,m}(\omega, \mathbf{q}) = \frac{[1 - N_F(n)] \delta_{n,m} \delta(\mathbf{q})}{\omega - \epsilon_n + i0^+} + \frac{N_F(n) \delta_{n,m} \delta(\mathbf{q})}{\omega - \epsilon_n - i0^+}. \quad (\text{V.78})$$

In the presence of anisotropy, a practical way to solve Eq. (V.76) is to solve it iteratively from the above isotropic solution. First insert the above  $\langle O_{nm}(\mathbf{q}) \rangle$  into Eq. (V.76) and find  $G_{n,m}(\omega, \mathbf{q})$ . Then use Eq. (V.68) to find the new  $\langle O_{nm}(\mathbf{q}) \rangle$  and insert it back into Eq. (V.76) again. After enough iterations, when  $G_{n,m}(\omega, \mathbf{q})$  and  $\langle O_{nm}(\mathbf{q}) \rangle$  become steady, they can be taken as the solution to Eq. V.76.

Now we give an estimate for the difficulty of carrying out the above approach numerically. If the CFs do not have a charge density wave type instability and stay in an translation-invariant state, then we expect that  $G_{n,m}(\omega, \mathbf{q})$  and  $\langle O_{nm}(\mathbf{q}) \rangle$  are only non-vanishing for  $\mathbf{q} = 0$ . In this situation, the above procedure is simplified to find a set of self-consistent solutions only labelled by the CF LL indices. In practice, we need to keep  $n_{max}$  CF LLs. The TDHF equations are equivalent to solving a vector of dimensions  $\sim n_{max}^2$  iteratively. The main numerical difficulty comes from the convergence of the iteration. However, if the CFs are susceptible to a charge density wave instability, then one cannot neglect those  $\mathbf{q} \neq 0$  contributions. In this case the relevant solution space becomes much larger and the CF picture may not be a good way of characterizing the FQH problem. In this case, the charge density wave instability should also be reflected through closing the neutral gap at some finite momentum.

The above TDHF calculation can also be immediately derived using the diagrammatic expansion. For the propagator, we still need the two types diagrams in Sec. V.2. These diagrams can be written more systematically if we use the Dyson equation and one-particle irreducible diagrams :

$$\text{---} = \text{---} - \text{---} \text{---} \text{irr} \text{---}, \quad (\text{V.79})$$

$$\text{irr} = \text{---} \text{---} \text{---} + \text{---} \text{---} \text{---} \text{---} \text{---}. \quad (\text{V.80})$$

The above diagrams correspond to the following equations for the propagator  $G_{\alpha\beta}(\omega)$

$$G_{\alpha\beta}(\omega) = G_{\alpha\beta}^0(\omega) - G_{\alpha\gamma}^0(\omega)\Sigma_{\gamma\lambda}G_{\lambda\beta}(\omega) \quad (\text{V.81})$$

$$\Sigma_{\alpha\beta} = \sum_{\mathbf{q}} V_{eff} [(\mathbf{q})\rho_{\beta\alpha}(\mathbf{q})\rho_{\gamma\lambda}(-\mathbf{q})G_{\lambda\gamma}(\omega) - \rho_{\beta\gamma}(\mathbf{q})\rho_{\lambda\alpha}(-\mathbf{q})G_{\lambda\alpha}(\omega)], \quad (\text{V.82})$$

where the density matrices  $\rho_{\alpha,\beta}$  are the complete one, the CF-LL part times the intra-CF LL part.

With those self-consistent CF occupation patterns, the density correlation function is then again given by summing over bubble diagrams and ladder diagrams or the TDHF equation of motion. The only change is that we need to insert the  $\langle O_{nm}(\mathbf{q}) \rangle$  found iteratively into the contraction in the evaluation. The neutral excitations are still given by the poles of the density correlation function. The activation gap can be worked by inserting  $\langle O_{nm}(\mathbf{q}) \rangle$  to find the Hartree-Fock Hamiltonian and then looking at the excitation across the CF Fermi-level. Due to the time limit, such self-consistent calculation has not been performed until this thesis is finished. It remains to see whether this computation can provide new insight into anisotropic FQHE states.



# VI – Charge density wave phases under external anisotropy

The Laughlin wave function and the composite fermion picture have proved successful in the description of correlated electron phases in the LLL. In higher Landau levels, the effective interaction  $V_{eff}(\mathbf{q})$  can have nodes due to the Laguerre polynomial in the form factor. The scenarios are quite different from the LLL. These nodes lead to a possibility that the electrons can further cluster. In this chapter, we focus on those charge density wave states in the  $n = 2$  LL. The quantum Hall system goes through a series of charge density wave states as the filling factor is increasing from  $\tilde{\nu} = 0$  to  $\tilde{\nu} = 1/2$ . We study how this process will behave in the presence of anisotropy. After a brief review of charge density wave phases in higher LLs for an isotropic interaction in Sec. VI.1, I discuss their fates once the interaction becomes anisotropic (Sec. VI.2). Section VI.3 is devoted to an introduction of an elastic theory of the charge density wave phases that may provide further insight into the stability of these phases. This project is carried out in collaboration with Yuchi He at Carnegie Mellon University.

## VI.1 Phase diagrams in higher LLs under isotropic interaction

As we mentioned in the introductory chapter, before the discovery of FQHE and the proposition of the Laughlin liquid state in the LLL, charge density wave states (CDW) were considered as promising candidates for the two-dimensional electron gas under strong magnetic field [37]. They are natural ground states within Hartree-Fock approximation [38, 132]. However these CDW states have gapless phonon excitations and do not produce the incompressible states observed experimentally except for very dilute fillings [133]. Therefore the Hartree-Fock approximation is not valid in general in LLL. From what is clear now, in the LLL, the fractional quantum Hall effects are prominent at many fillings. Almost all of them can be described in terms of Laughlin states and their daughter hierarchy states (or CF states). In contrast the CDW states have gapless edge states in the bulk, due to the rim of bubbles or the edge of stripes. In the LLL the fluctuations of those edge states are large and thus destroy the CDW states. In higher LLs, because of the different profiles of the effective interaction, more possibilities are opened. In the  $n = 1$  LL, non-Abelian quantum Hall states [134, 135] remain promising candidates. The anyons there exhibit non-Abelian statistics and can provide a possible tool for performing fault-tolerant quantum computation in the future. The existence of non-Abelian state at  $\nu = 5/2$  is further strengthened by recent thermal Hall conductance measurements [136]. For  $n \geq 2$ , experimentally no FQHE has been

observed [45] except for the possible  $\tilde{\nu} = 1/5$  and  $\tilde{\nu} = 4/5$  states [137] in the  $n = 2$  LL at intermediate temperatures. The initially considered charge density wave instability leads to Wigner crystals, bubble phases and stripe phases [138, 107, 139].

### VI.1.1 The Hartree-Fock interaction

First, we take a look at the effective interaction in the  $n = 2$  LL. The contour of the effective interaction scales as the cyclotron radius  $\sqrt{2n+1}l$  for the LL index  $n$  [139]. Intuitively the CDW periodicity is scaling in the same way so that it becomes larger and larger compared to the scale of edge fluctuations  $l$ . So the Hartree-Fock result becomes more accurate when  $n$  becomes larger. Moessner and Chalker [108] showed that Hartree-Fock approximation is valid in higher LLs with the perturbation theory. And later in intermediate LLs, Hartree-Fock approximation [117, 118] also successfully confirms the solid phases observed experimentally [119, 120, 140]. So in  $n = 2$  LL, it is legitimate to use Hartree-Fock approximation as a powerful tool to investigate the phase diagram. The key ingredient is to work out the Hartree-Fock interaction and compute the cohesive energy defined per particle. The Hamiltonian consists as before only of the interaction term. Within the Hartree-Fock approximation, the fermionic operators are contracted in pairs :

$$E_{HF} = \frac{1}{2A} \sum_{\mathbf{q}} V_{eff}(\mathbf{q}) \rho_{12}(\mathbf{q}) \rho_{34}(-\mathbf{q}) \left( \langle d_1^\dagger d_2 \rangle \langle d_3^\dagger d_4 \rangle - \langle d_1^\dagger d_4 \rangle \langle d_3^\dagger d_2 \rangle \right), \quad (\text{VI.1})$$

where in this chapter  $\rho$  always denotes the projected electron density  $\bar{\rho}_e$ . Here  $A$  is the area of the system. In this chapter, for the calculation of CDW phases, we will jump between the discrete sum  $\sum_{\mathbf{q}}$  and the continuous integral  $\int d\mathbf{q}$  whenever convenient. The two sets of notations can be converted to each other by replacing the area  $A$  in the discrete momentum formalism with  $(2\pi)^2$  in the continuous momentum formalism. By writing out the matrix elements of the density explicitly in the Landau gauge, like in Sec. V.1, the above operators can be recombined with the matrix elements of the density to form the expectation value of the density operator. The interaction is replaced by the Hartree-Fock interaction :

$$E_{HF} = \frac{1}{2A} \sum_{\mathbf{q}} u_{HF}(\mathbf{q}) \langle \rho(\mathbf{q}) \rangle \langle \rho(-\mathbf{q}) \rangle, \quad (\text{VI.2})$$

where the Hartree Fock potential is given by the effective potential minus its Fourier transformation

$$u_{HF}(\mathbf{q}) = V_{eff}(\mathbf{q}) - \sum_{\mathbf{p}} \frac{1}{N_\phi} V_{eff}(\mathbf{p}) \exp(-i\mathbf{p} \times \mathbf{q}l^2), \quad (\text{VI.3})$$

where  $N_\phi$  is the number of magnetic flux quanta. We denote the two terms like before as a direct interaction potential and an exchange interaction potential. The density operator  $\rho(\mathbf{q})$  is normalised to  $\rho(0) = N_e$  and the cohesive energy is defined as the energy per particle,  $E_{coh} = E_{HF}/N_e$ .

Let us look at the profile of the HF interaction  $u_{HF}$ , as shown in Fig VI.1. The direct potential  $V_{eff}$  is in general repulsive. It consists of the Coulomb potential (or a variant taking account of the sample width, screening etc.) multiplied with the LL form factor, while the exchange potential is attractive. Due to the Laguerre polynomial in the form factor, the direct potential has a series of zeroes. At its first zero the exchange potential is

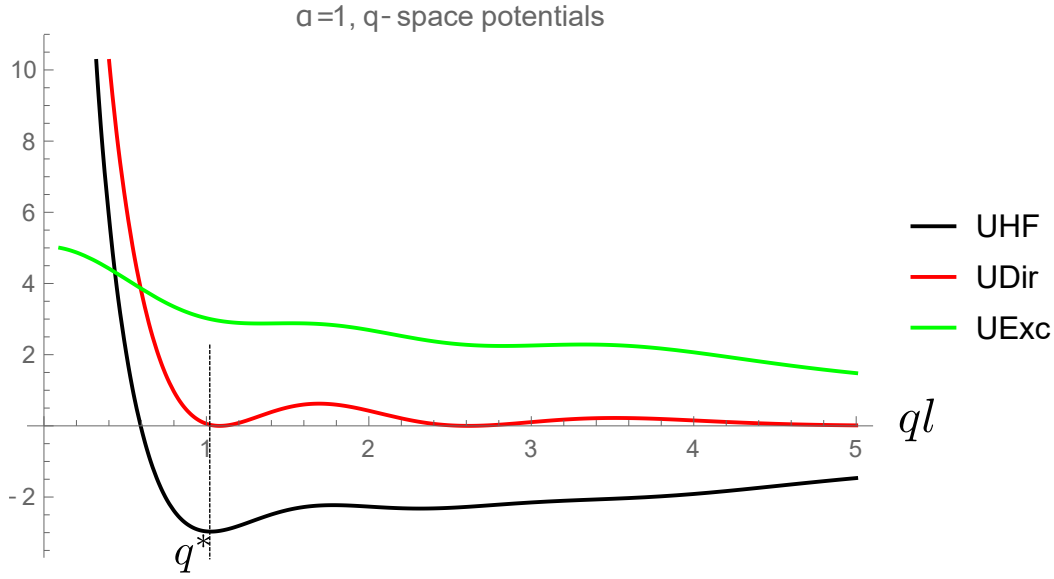


Fig. VI.1 The direct potential, exchange potential and Hartree-Fock potential in the  $n = 2$  LL, remembering that the exchange potential takes a minus sign in its contribution to  $u_{HF}$ . One notices a minimum at  $q^*l \simeq 1$ , which actually scales as  $q^* \sim 1/(\sqrt{2n+1}l)$  for higher LLs.

still large and dominating, giving rise to an attraction. So around the first zero of the direct potential, the total Hartree-Fock potential has a minimum, which we label as  $q^*$ . It scales as  $1/(\sqrt{2n+1}l)$  for higher LL  $n$ . Any state with a spatial order around  $q^*$  can benefit from this minimum. This is the reason leading to the CDW instability with a characteristic periodicity  $1/q^* \sim R_c = l\sqrt{2n+1}$  (cyclotron radius).

### VI.1.2 Wigner crystal, bubble phases, and stripe phases

Depending on the periodic structure, there are several kinds of CDW phases. Fig. VI.2 and Fig. VI.3 show schematically two kinds of charge density wave configurations. The grey areas have a high density of electrons while the white areas are exhausted. When the filling factor is very low  $\tilde{\nu} \rightarrow 0$ , the electrons have enough space to stay away from each other due to the Coulomb repulsion. They are likely to form a sparse crystal phase, which is the Wigner crystal and can be viewed as a CDW phase on a two-dimensional lattice. At each lattice site, there is one electron. When the filling factor increases, looking at the effective potential Fig. VI.6 in real space, there is an intermediate region where the repulsion is weaker than the pure Coulomb potential. So at intermediate filling factors, some electrons have the tendency to cluster into this weaker repulsive area while stay far away from other clusters. A bubble phase with  $M$  electrons at each lattice site is formed, still lying on a two-dimensional lattice. The Wigner crystal can be regarded as the  $M = 1$  bubble phase. At larger densities, the system still sits on a 2D lattice but there are more than one electron clustered on each lattice site. With the filling factor further approaching one half  $\tilde{\nu} \rightarrow 1/2$ , a particle-hole symmetry emerges. In this case, a stripe phase is the natural candidate near  $\tilde{\nu} \sim 1/2$ . The stripe phase is uniform in one direction but periodic in the perpendicular one (see Fig. VI.3) with width

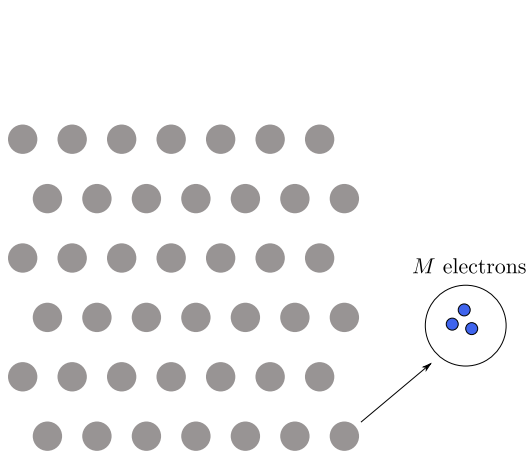


Fig. VI.2 A schematic drawing of bubble phases. The bubbles are lying on a lattice. At each lattice site, a bubble comprises  $M$  electrons.

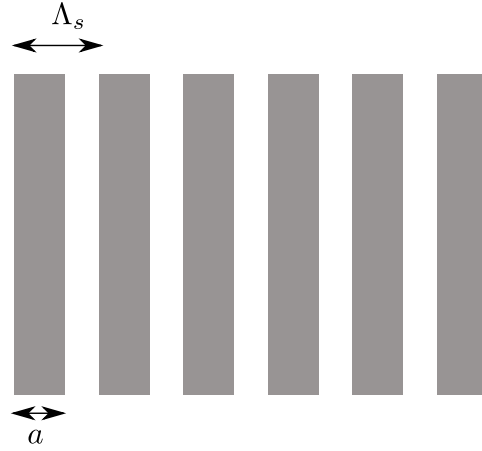


Fig. VI.3 A schematic drawing of the stripe phase. This unidirectional stripe phase is uniform in one direction and periodic in another direction. The density is alternating as shown in the form of stripes.

$\Lambda_s$ . This periodicity is again dictated by the Hartree-Fock interaction and thus scales as  $\Lambda_s \sim l\sqrt{2n+1}$ . Near half filling, the width of the exhausted area  $\Lambda_s - a$  and the width of the stripe  $a$  becomes equal, so that a particle-hole symmetry manifests, which is compatible with the half filling particle-hole symmetry and makes it an appealing candidate for ground state.

The competitions between different CDW phases are based on their energy. To determine which CDW phase the system is in, we need to know the density profile  $\langle \rho(\mathbf{q}) \rangle$ . For simple configurations of CDW phases, the density profiles are presumed as we will show. In this static Hartree-Fock method, different CDW phases can be treated as trial states and the true ground state takes the state with the minimal energy among them. An improved method would be using the time-dependent Hartree-Fock approximation [131], in which the dynamics of the interaction is considered and the trial energy can be further lowered down. Since in the anisotropic case, even the HF interaction itself needs to be computed numerically, the TDHF requires large computational source and we stick to the static HF approximation.

Experimentally, the bubble phases are pinned by disorders in the sample. Therefore they are insulating phases and do not contribute to the Hall conductivity. When such a phase forms, the Hall resistance jumps to the value of the nearest IQHE (see Fig. VI.4), resulting in the re-entrant integer quantum Hall effect [139, 119]. Such an effect was also predicted [141] and is observed in graphene in our recent work [33] in collaboration with Cory Dean's group in Columbia University, where we predicted and verified the re-entrant IQHE in the  $n = 2$  LL of graphene. In that situation, the only modification needed is to replace the 2D electron gas effective interaction by the graphene effective interaction [142]. We also found that the scaling rule of the melting temperature can be modified by screening effects due to the metallic gates in which the sample is sandwiched. For the stripe phase, the system strongly breaks the rotational symmetry. The signature is a large anisotropy in the transport measurement, namely longitudinal resistance.

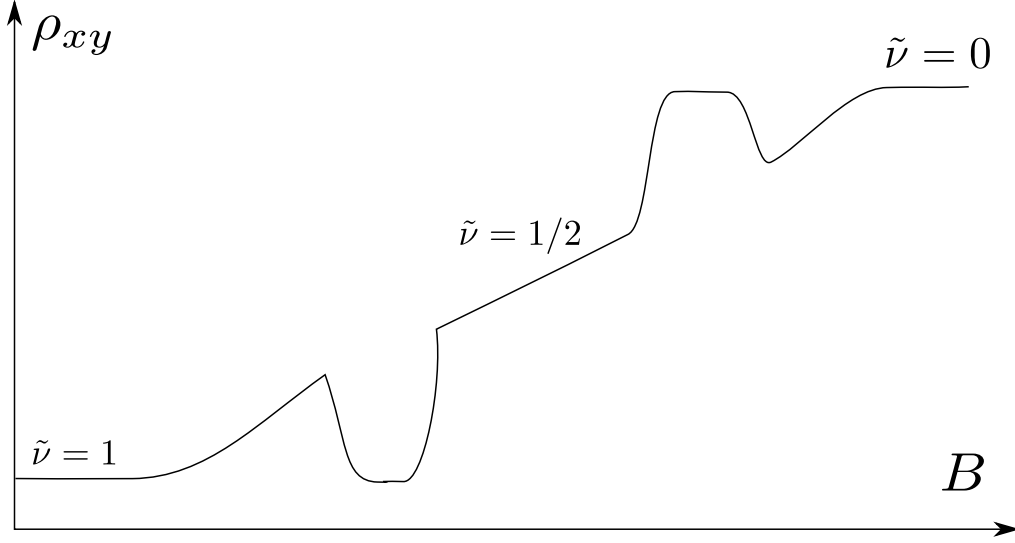


Fig. VI.4 A schematic drawing for the re-entrant integer quantum Hall effect. When this effect happens, the Hall resistance jumps or drops to the value of its nearest integer quantum Hall effect.

Now we work out how the cohesive energy of different CDW phases are computed. The cohesive energy is defined as the energy per particle  $\langle H \rangle / N_e$  with respect to the energy of a structureless homogeneous liquid. For a crystal like CDW phase, there is a periodicity compatible with the lattice structure. The expectation value of the density takes a decomposition :

$$\langle \rho(\mathbf{q}) \rangle = \rho_b(\mathbf{q}) \sum_j e^{-i\mathbf{q} \cdot \mathbf{R}_j}, \quad (\text{VI.4})$$

in which  $\mathbf{R}_j$  lies on a lattice labeled by  $j$ . The function  $\rho_b$  represents the density profile at each lattice site. In this section, we use  $\mathbf{R}_i$  to label the lattice site and use  $\mathbf{R}^g$  to represent the guiding-center coordinate. In quantum Hall systems, the non-commutativity of the  $x$ - and  $y$ -coordinates requires that each electron must occupy a smearing region around area  $l^2$ . So at each lattice site, the density distribution cannot be point-like (also see Fig. VI.5). This is exactly parametrized by  $\rho_b$ . On each site there are  $M$  electrons and so are there in a unit cell. The normalization therefore requires  $\rho_b(0) = M$ . The area  $A_u$  of the unit cell and the highest partially filled LL filling  $\tilde{\nu}$  satisfy  $2\pi l^2 M = \tilde{\nu} A_u$ . Then using the identity

$$\sum_j \exp(-i\mathbf{q} \cdot \mathbf{R}_j) = \frac{A}{A_u} \sum_{\mathbf{Q}} \delta_{\mathbf{q}, \mathbf{Q}}, \quad (\text{VI.5})$$

where  $\mathbf{Q}$  is a reciprocal lattice vector, one can find that the cohesive energy is given by :

$$E_{coh} \equiv \frac{E_{HF}}{N_e} = \sum_{\mathbf{Q} \neq 0} \frac{n_B \tilde{\nu}}{2M^2} u_{HF}(\mathbf{Q}) |\rho_b(\mathbf{Q})|^2, \quad (\text{VI.6})$$

where  $n_B = 1/(2\pi l^2)$  is the flux density. In the above summation the  $Q = 0$  point is excluded due to the screening and self-energy subtraction. For a triangular lattice, the reciprocal lattice



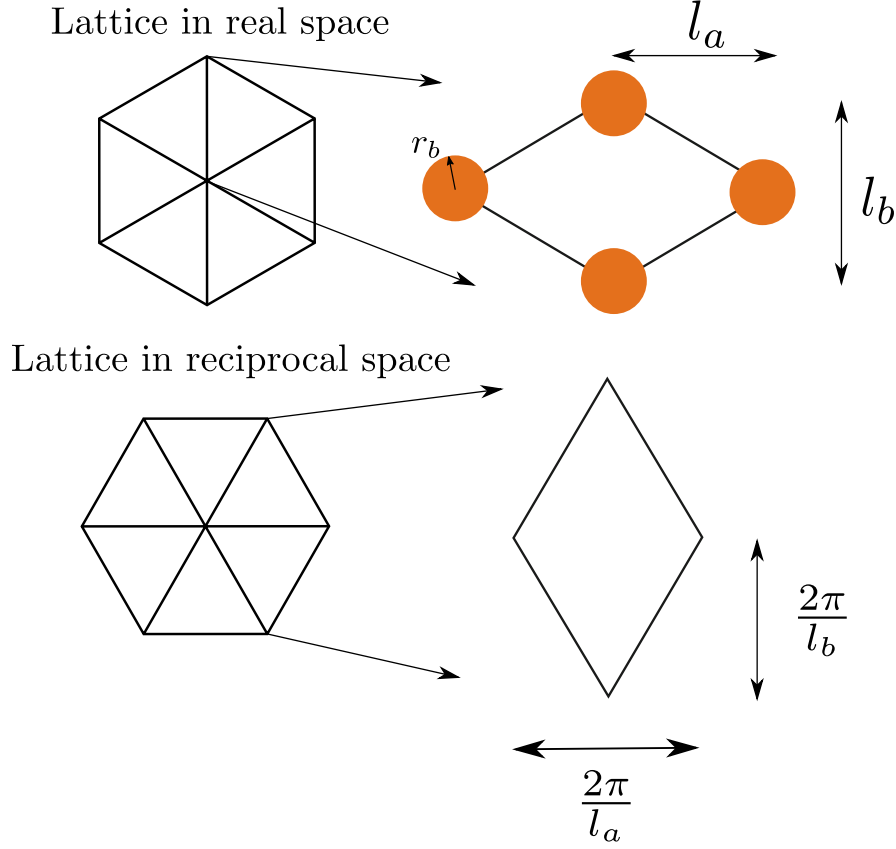


Fig. VI.5 The unit cell of the bubble phase. For later purposes of describing the deformation in the presence of anisotropy, the lattice is parametrized by its diagonals. The reciprocal lattice is also a triangular lattice. The bubble at each lattice site has a smearing region, due to the fact that each guiding center orbital occupies a finite area  $2\pi l^2 = 1/eB$ .

is triangular as well with parameters in Fig. VI.5. For practical calculation, the summation in Eq. VI.6 is usually taken over a dozen of shells in the reciprocal space for sufficient convergence of the energy.

There are several assumptions for the density profile  $\rho_b(\mathbf{q})$  at each lattice site. Most of them are based on the fact that the electrons in the highest partially filled LL form some local  $\tilde{\nu} = 1$  states. Here we introduce two such assumptions. The first assumption is a uniform distribution of  $\tilde{\nu} = 1$  inside a disc [107, 118]. In real space this can be represented as :

$$\rho_b(r) = \frac{1}{2\pi l^2} \Theta(r_b - r), \quad (\text{VI.7})$$

with  $r_b$  the radius of the disc (see Fig.VI.5), which will be determined later. Transforming it to momentum space, we find

$$\rho_b(q) = \frac{r_b}{l^2 q} J_1(qr_b), \quad (\text{VI.8})$$

where  $J_1$  is a Bessel function. The normalization requirement  $\rho_b(0) = M$  leads to  $r_b = \sqrt{2M}l$ .

So for the disc density profile, the cohesive energy is

$$E_{coh} = \sum_{\mathbf{Q} \neq 0} \frac{n_B \tilde{\nu}}{M} u_{HF}(\mathbf{Q}) \frac{J_1^2(\sqrt{2M}|\mathbf{Q}|l)}{|\mathbf{Q}|^2}. \quad (\text{VI.9})$$

The uniform disc distribution is in a sense a classical distribution. Since in quantum Hall systems, quantum fluctuation are important in low LLS, a more accurate density profile is to take  $\rho_b$  as that of a  $M$ -particle  $\tilde{\nu} = 1$  wave function [116], for example Eq. (I.17). In this state, the electrons inside a bubble fill all the states from the one with the lowest angular momentum to the one with the highest angular momentum. The density profile is then given by

$$\rho_b(\mathbf{q}) = \sum_{n=0}^{n=M} \langle n | \exp(-i\mathbf{q} \cdot \mathbf{R}^g) | n \rangle = L_{M-1}^1 \left( \frac{q^2 l^2}{2} \right) e^{-q^2 l^2 / 4}. \quad (\text{VI.10})$$

where  $L_M^1$  is the associated Laguerre polynomial. The normalization  $\rho_b(0) = M$  is automatically satisfied. The cohesive energy for this IQH wave function density profile is given by

$$E_{coh} = \sum_{\mathbf{Q} \neq 0} \frac{n_B \tilde{\nu}}{2M^2} u_{HF}(\mathbf{Q}) L_{M-1}^1 \left( \frac{|\mathbf{Q}|^2 l^2}{2} \right)^2 e^{-|\mathbf{Q}|^2 l^2 / 2}. \quad (\text{VI.11})$$

For the stripe phase, the periodicity structure is only along one direction. A classical density profile is to have alternating uniform  $\tilde{\nu} = 1$  and  $\tilde{\nu} = 0$  unidirectional strips along the periodic direction [118]. The distribution is written as

$$\langle \rho(\mathbf{r}) \rangle = \sum_j \frac{1}{2\pi l^2} \Theta \left( \frac{a}{2} - |\mathbf{r} \cdot \hat{\mathbf{e}} - j\Lambda_s| \right), \quad (\text{VI.12})$$

where  $\hat{\mathbf{e}}$  is the direction of the CDW, perpendicular to the extensive direction of the stripe.  $\Lambda_s$  is the stripe period. The width of the stripe  $a$  has to satisfy the filling factor  $\tilde{\nu} = a/\Lambda_s$ . Its cohesive energy is given by :

$$E_{coh} = \frac{n_B}{2\pi^2 \tilde{\nu}} \sum_{l \neq 0} u_{HF} \left( \frac{2\pi \hat{\mathbf{e}}}{\Lambda_s} l \right) \frac{\sin^2(\pi \tilde{\nu} l)}{l^2}. \quad (\text{VI.13})$$

The stripe periodicity is a variational parameter. Its value is fixed by minimizing the stripe cohesive energy. As the stripe periodicity is the only periodic structure in the stripe phase, we can immediately link it to the minimum of the HF potential. It is found that this periodicity is almost overlapping with the inverse of the HF potential minimum [138, 107, 118] :

$$\Lambda_s \sim 2\pi/q^*. \quad (\text{VI.14})$$

Unlike the bubble phases, there is no very simple expression for the quantum version of the density profile of the stripe phase. The quantum fluctuations in this situation comes from the chiral edge modes moving along the stripe borders [143]. In our later calculations, in order to compare the cohesive energy between the bubble phases and the stripe phase on an equal footing, we take both of them to be the classical distributions.

### VI.1.3 Phase transitions in the second LL

We review some previous studies by other authors for the phase transitions in the  $n = 2$  LL before presenting our original work on the evolution of the phases in the presence of anisotropic interaction.

The first question we need to clarify is whether the quantum Hall liquid phase intervenes in the problem. As mentioned before, experimentally the liquid phase is only observed at  $\tilde{\nu} = 1/5$  and  $\tilde{\nu} = 4/5$  at intermediate temperature in the  $n = 2$  LL. For those CDW phases, the stripe-like phase is observed at  $\tilde{\nu} = 1/2$  [144, 145] and the formation of bubble phases appears around  $\tilde{\nu} = 1/4$  and  $\tilde{\nu} = 3/4$ . In Ref. [118], it is found that the  $\tilde{\nu} = 1/5$  phase is in a close competition with a mixed phase in which a Wigner crystal and  $M = 2$  bubble phase coexist, whereas the Wigner crystal is stable between  $0.15 < \tilde{\nu} < 0.19$ . Numerically, the translation symmetry is shown to break spontaneously with  $\tilde{\nu} = 1/4$  and  $\tilde{\nu} = 1/3$  interpreted as the  $M = 2$  bubble phase while  $\tilde{\nu} = 2/5$  is interpreted as a stripe phase [146]. So in the  $n = 2$  LL, the CDW phases play a dominant role and it is reasonable to focus on the competition among themselves while neglecting the FQH liquid phase as a first step towards understanding how the system reacts to external anisotropy.

From these results, we discuss the CDW phases that the system should go through when the filling factor is increasing from  $\tilde{\nu} = 0$  towards  $\tilde{\nu} \sim 1/2$ . Under the isotropic effective interaction, first the system stays in a Wigner crystal in the dilute limit. The lattice takes a triangular form, which has a maximal rotational symmetry and minimizes the repulsion energy [147]. As the filling factor  $\tilde{\nu}$  goes larger, there is a phase transition between the Wigner crystal and the  $M = 2$  bubble phase. Meanwhile a mixed phase that consists of a Wigner coexisting with the  $M = 2$  bubble phase can form near the transition, depending on whether the coexistence is stable against the long-range Coulomb energy penalty. The  $M = 2$  bubble phase still lies on a triangular lattice but has a different number of electrons in each unit cell. Therefore the dependence of the lattice constants on the filling factor  $\tilde{\nu}$  is different from that of a Wigner crystal. This leads to a discontinuity in the derivative of  $E_{coh}(\tilde{\nu})$ . The phase transition is first-order and discontinuous. When the filling is increased further, the  $M = 2$  phase transforms to the stripe phase. The two phases have different order parameters. The cohesive energy  $E_{coh}(\nu)$  is again discontinuous in its derivative. The system goes through this first-order phase transition and stays in the stripe phase until  $\tilde{\nu} = 1/2$ .

In addition to the above picture, it is found that away from  $\nu = 1/2$ , the uniform stripe phase is not stable against fluctuation along its extensive direction [143, 148]. These fluctuations lead to a modulation along the extensive direction within each stripe, where the resulting phase has every stripe broken into a one-dimensional crystal with only one electron per unit cell. Due to the Coulomb repulsion, the lowest energy static configuration is to make all neighbouring 1D crystals have a phase difference  $\pi$ . On the other hand, there is also a dynamical process allowing those 1D crystals to move in their parallel direction. Whether this array of one-dimensional crystals behaves like a unidirectional stripe phase depends on whether the neighbouring stripes are free to slide, that is whether the relative phase difference between two neighbouring 1D crystals is locked or unlocked. The energy cost by sliding is reflected in the shear elastic modulus [149, 150]. When the shear elastic modulus is small, the neighbouring stripes can move independently in the parallel direction and the average density in the stripe's extensive direction is still uniform. When the shear elastic modulus is large enough, the neighbouring stripes can only move simultaneously and this phase behaves

like an anisotropic crystal. The former phase is usually called the smectic phase and the latter is called the stripe crystal phase. Another way of interpreting the smectic phase and the stripe crystal phase is to view a sliding across one period as a soliton. The transition from a stripe crystal phase to a smectic phase comes from the unbinding of soliton/anti-soliton pairs [151], similar to the usual Berezinskii–Kosterlitz–Thouless phase transition in superfluids. Both criteria predict that when the filling  $\tilde{\nu}$  deviates sufficiently enough from  $\tilde{\nu} = 1/2$ , the uniform smectic phase transits into a stripe crystal, which itself, is a highly anisotropic Wigner crystal. This indicates that before going to particle-hole symmetric limit at  $\tilde{\nu} = 1/2$ , there is in addition a continuous phase transition from a highly anisotropic stripe (Wigner) crystal to a smooth smectic phase. Moreover, it is believed that away from  $\tilde{\nu} = 1/2$  the (highly anisotropic) stripe crystal corresponds to the true configuration for the stripe phase obtained by the static HF calculation [139].

In conclusion, under an isotropic Coulomb interaction, when the filling factor  $\tilde{\nu}$  is increased from 0 to  $1/2$ , the quantum Hall system in the  $n = 2$  LL is likely to go from a Wigner crystal, via a  $M = 2$  bubble phase, a stripe crystal phase and to the smectic stripe phase successively. The phase transition between Wigner crystal and the  $M = 2$  bubble phase is first order and so is the transition between the  $M = 2$  bubble phase and the stripe crystal, while the stripe crystal and the smectic phase are connected by a continuous phase transition.

## VI.2 Crystal phases in anisotropic interaction

The anisotropic effective interaction that we study is created with the help of the mass anisotropy. This can be realized in a two-dimensional electron gas in an AlAs quantum well [152]. From the physical intuition, the external anisotropy breaks the rotational symmetry and gives two preferred axes. This symmetry does not favour a triangular lattice but is in accordance with the symmetry of a stripe phase or an anisotropic rhombus phase. Therefore we anticipate that with larger mass anisotropy, a stripe-like (smectic and stripe crystal) phase is more dominant. Here and below, we are going to show that this is the case in  $n = 2$  LL.

To include the mass anisotropy, we take the following kinetic Hamiltonian :

$$H_k = \sum_i \frac{\Pi_x^2}{2m/\alpha} + \frac{\Pi_y^2}{2m\alpha}. \quad (\text{VI.15})$$

where mass ratio is characterized by  $m_y/m_x = \alpha^2$ . The cyclotron coordinate is defined as  $\eta_i = -\sum_j l^2 \epsilon_{ij} \Pi_j$ . The ladder operators are related to  $\eta_x$  and  $\eta_y$  through Eq. (II.2). Reversing it, the cyclotron coordinates are given in terms of the ladder operators as

$$\eta_x = (a + a^\dagger)\sqrt{2\alpha}l^2, \quad \eta_y = -i(a - a^\dagger)\sqrt{\frac{2}{\alpha}}l^2. \quad (\text{VI.16})$$

The projection to a specific LL  $n$  is done by computing the expectation value  $\langle n | \exp(-i\mathbf{q} \cdot \boldsymbol{\eta}) | n \rangle$ . When  $\alpha = 1$ , namely in the absence of mass anisotropy, this projection gives rise to the following effective interaction in the LL  $n$  :

$$V_{eff}(n, \mathbf{q}) = F_n^2(q_x^2, q_y^2) \frac{2\pi e^2}{\sqrt{q_x^2 + q_y^2}}, \quad (\text{VI.17})$$

where  $F_n$  is the form factor from projection to the  $n$ -th Landau level :

$$F_n(q_x^2, q_y^2) = L_n \left( \frac{q_x^2 + q_y^2}{2} l^2 \right) e^{-(q_x^2 l^2 + q_y^2 l^2)/4}, \quad (\text{VI.18})$$

with  $L_n$  the Laguerre polynomial. When  $\alpha \neq 1$ , the only difference is to scale  $\eta_x, \eta_y$  to  $\eta'_x \sqrt{\alpha}, \eta'_y / \sqrt{\alpha}$ . So in this case the form factor is obtained from replacing  $q_x, q_y$  with  $q_x \sqrt{\alpha}$  and  $q_y / \sqrt{\alpha}$ . From this simple rescaling calculation, the effective interaction in the  $\nu = n$  LL becomes :

$$V_{eff}(n, \mathbf{q}) = F_n^2(\alpha q_x^2, q_y^2 / \alpha) \frac{2\pi e^2}{\sqrt{q_x^2 + q_y^2}}. \quad (\text{VI.19})$$

The bare Coulomb interaction is still isotropic. The mass anisotropy affects the effective interaction through the form factor. Intuitively, the effective interaction is the average repulsion between two electrons following cyclotron motions. At large distance, the repulsion still behaves as Coulomb interaction while at short distance, the overlap of the cyclotron motion brings significant modification. The profiles of the effective interaction in coordinate space for different mass ratios are presented in Fig. VI.6-Fig. VI.8. We can clearly see a weakly repulsive region at intermediate distances, in a darker color between the first and the second brighter annulus around the white core. This region is the key reason leading to the clustering of bubble phases mentioned in Sec. VI.1.2. When mass anisotropy is switched on, the equipotential contour near the weakly repulsive region is deformed into an elliptic shape, indicating that the bubble phases are likely to be strongly influenced.

On the other hand, looking at Eq. (VI.19), we can deduce that the zeros of the direct potential are scaling as  $1/\sqrt{\alpha}$  in the  $q_x$ -direction and  $\sqrt{\alpha}$  in the  $q_y$ -direction. The minimum point  $q^*$  scales in the same way. This suggests that for stripes arrayed in  $x$ -direction, the periodicity  $\Lambda_s$  behaves as  $\sqrt{\alpha}$  and that for stripes arrayed in the  $y$ -direction, the periodicity  $\Lambda_s$  behaves as  $1/\sqrt{\alpha}$ . As the rotation symmetry is broken completely, we expect that one of them is lower in energy than the other, and the true stripe periodicity scales monotonically with  $\alpha$ .

### VI.2.1 Trial density profiles for anisotropic interaction

In the presence of anisotropy, the triangular lattice is definitely not the optimal periodical structure. It is natural to anticipate a deformed lattice. In our calculation, we parameterize the lattice as shown in Fig. VI.5. The unit cell takes the shape of a rhombus. Its diagonals are along the  $x$ - and  $y$ -directions, the principal axes of the anisotropy. The lengths  $l_a$  and  $l_b$  satisfy

$$l_a l_b = \frac{2\pi l^2 M}{\tilde{\nu}}, \quad (\text{VI.20})$$

such that a unit cell contains  $M$  electrons. Therefore  $l_a$  is not fixed and is used as the variational parameter. At each  $\tilde{\nu}$ , we work out the  $l_a$  with the lowest energy.

In addition to the deformation of the lattice, we also need to consider the deformation of  $\rho_b(\mathbf{q})$ . As we have already explained, the profile  $\rho_b(\mathbf{q})$  describes the smearing region of the guiding centers around each lattice site. In the isotropic case, this smearing region is either assumed to be a disc or an isotropic incompressible IQH droplet. In the anisotropic case, the anisotropy does not only affect the lattice shape, but also should affect the shape

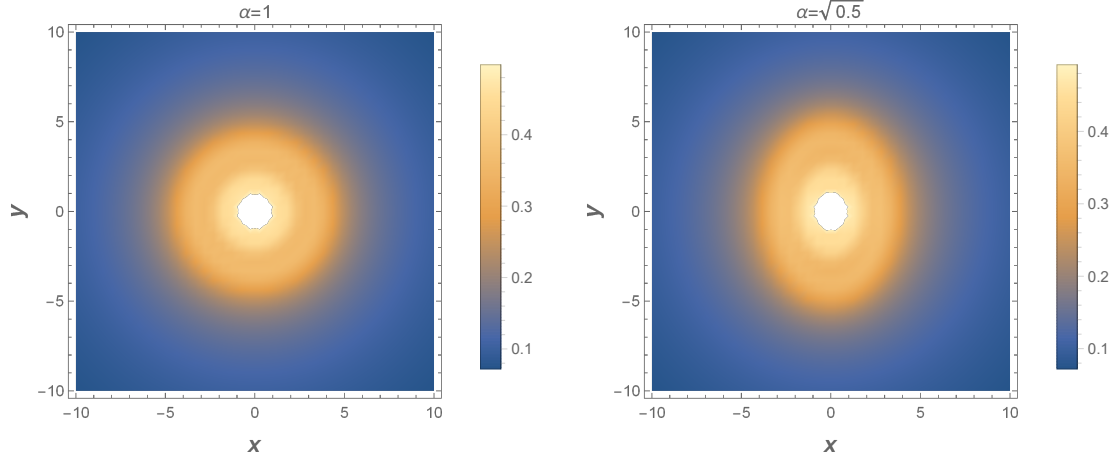


Fig. VI.6 The effective interaction for  $n = 2$  LL in coordinate space at  $m_y/m_x = 1$ . Fig. VI.7 The effective interaction for  $n = 2$  LL in coordinate space at  $m_y/m_x = 0.5$ .

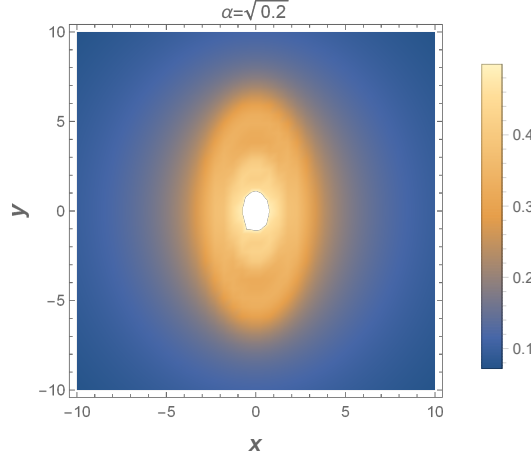


Fig. VI.8 The effective interaction for  $n = 2$  LL in coordinate space at  $m_y/m_x = 0.2$ .

of this smearing region at each lattice site. Since the static HF computation is to search for the lowest-energy state variationally, it is not very efficient when both the deformation of the lattice and that of the smearing region are included so that the searching dimensions become 2. The optimal smearing region is more accessible through numerical methods, such as the TDHF calculation [131, 148]. In order to get a good estimate of this deformation, we adapt two kinds of trial density profiles. The first is still assuming the profile  $\rho_b(\mathbf{q})$  to be a round shape. The second is to deform  $\rho_b(\mathbf{q})$  according to how the cyclotron orbital is deformed, namely the ratio  $\sqrt{\alpha}$ . We expect the true underlying deformation of  $\rho_b(\mathbf{q})$  is between these two configurations. This is reminiscent of how the guiding-center metric varies in the presence of mass anisotropy for quantum Hall liquids. There the guiding-center metric is between the mass tensor and the dielectric tensor. In the case of bubble phase, since  $\rho_b(\mathbf{q})$  describes how the guiding center is smeared, the shape of it is a variation of the liquid guiding-center metric. This is more manifest if we take  $\rho_b(\mathbf{q})$  to be an IQH droplet, where

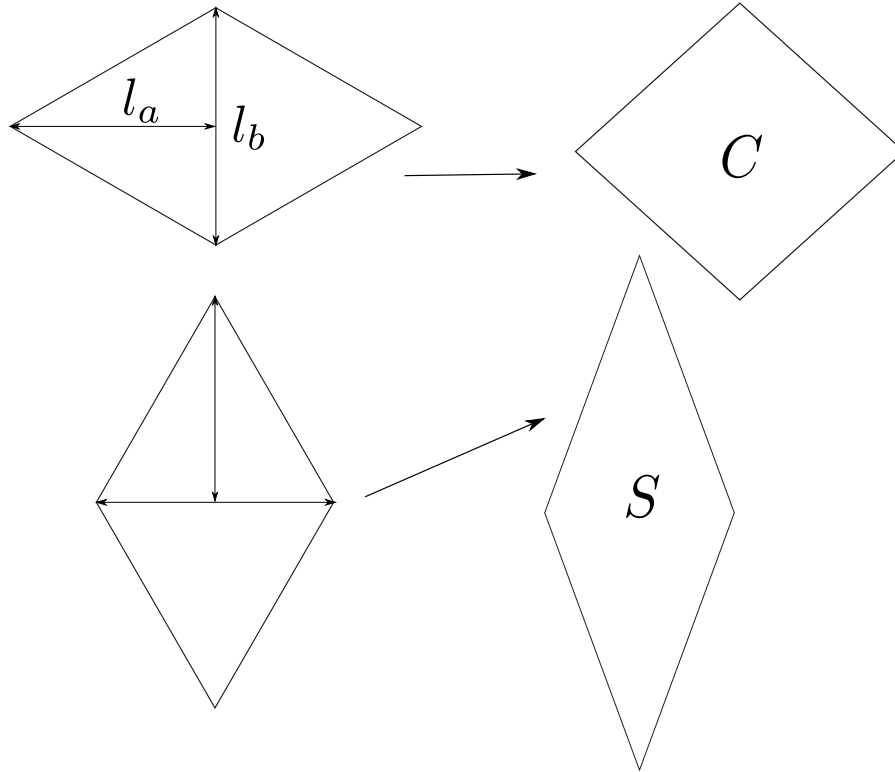


Fig. VI.9 How triangular lattices deform under external anisotropy. The two triangular lattices on the left hand side are degenerate for isotropic interaction. When the interaction becomes anisotropic, both of them will be stretched in one direction and compressed in another direction, leading to two different lattices, one becoming thinner (denoted  $S$  lattice) and another becoming more square (denoted as  $C$  lattice).

the shape parameter is a metric for guiding centers in the IQH wave function. In fact, in the result that we will present, we find that the energy difference between the two configuration is not very large. So these two  $\rho_b(\mathbf{q})$  are still good trial profiles.

### VI.2.2 Phase transitions in the presence of anisotropy

In this part, we summarize our results for different mass ratios. Here we consider  $\alpha = 1$ ,  $\alpha = \sqrt{0.5}$  and  $\alpha = \sqrt{0.2}$ .

Before going to the cohesive energy, we first focus on the geometrical parameters of the CDW phases. A feature worth noticing is that due to the anisotropy, there are two kinds of deformed lattices favoured in the crystal phase. In order to see this, we start from the isotropic triangular lattice. A unit cell in the triangular lattice can be chosen to be a rhombus. When we add anisotropy with  $D_2$  symmetry, the diagonals of the rhombus are reoriented to the two principal axes of the  $D_2$  anisotropy, with one diagonal stretched and another compressed due to the anisotropic interaction. In our case, the  $x$ -direction length should be compressed and  $y$ -direction length should be stretched. As a result, we can expect two local

optimal configurations, as shown in Fig. VI.9. The two triangular lattices on the left side are degenerate when the interaction is isotropic. As anisotropy is switched on, one rhombus is becoming thinner and thinner, while the other becomes closer to a square. They are denoted as  $S$  lattice and  $C$  lattice respectively. In our calculation, we find that for  $1 \geq \alpha \geq \sqrt{0.2}$  both lattices remain close in their energy through the regime where the corresponding bubble phases are stable. It would be interesting to see whether these two lattices can be observed experimentally.

On the side of the stripe phase, the direction of the stripes naturally goes along either  $x$ - or  $y$ -direction, the two principal directions of the anisotropy. In our calculation, because of the fact that the HF potential in the  $y$ -direction is lower than that in the  $x$ -direction (for example, as reflected in Fig. VI.15), we find that the stripe arrayed in  $y$ -direction is much lower in energy compared to the stripe arrayed in  $x$ -direction. The former has a periodicity in the  $y$ -direction close to the  $2\pi/q^*$  in this direction.

Now we take a look at the cohesive energy competition. The significant feature is that, with the increasing of mass ratio, the stripe phase is more and more favoured. From  $\alpha = 1$  to  $\alpha = \sqrt{0.2}$ , the  $M = 2$  bubble phase gives way to the stripe phase, shown in Fig. VI.10-Fig. VI.12. We list out the optimal energy for the stripe phase, bubble phases with a round shape at each lattice site and bubble phases with an elliptical shape at each lattice site. The  $S$  lattice is taken. The other lattice exhibits similar behaviours for the mass ratios chosen. In our plots, the number  $M$  of electrons in a unit cell of bubble phases is chosen with reference to the  $\alpha = 1$  situation, where the  $M = 1$  bubble phase (Wigner crystal) is formed in  $0 < \tilde{\nu} \leq 0.20$ , the  $M = 2$  phase dominating in  $0 < \tilde{\nu} \leq 0.35$ , and the  $M = 3$  bubble phase gets lower for  $\tilde{\nu} > 0.35$ . We compare the lowest bubble phase with the energy of the stripe phase. For  $\alpha = 1$ , the result is the same as in Ref. [118]. The stripe phase is only a bit lower in energy than the  $M = 3$  bubble phase. At  $\alpha = \sqrt{0.5}$ , the stripe phase now is definitely preferred compared to the  $M = 3$  bubble phase. And its energy is comparable to the  $M = 2$  bubble phase at  $\tilde{\nu} \simeq 0.3$ . When the mass ratio further goes down to  $\alpha = \sqrt{0.2}$ , we can see that the  $M = 2$  phase is completely erased by the stripe phase. Only Wigner crystal and stripe phase appear in the phase diagram. According to our previous introduction, the stripe phase computed here at low filling actually corresponds to a highly anisotropic Wigner crystal with one electron per unit cell. So we expect that at such mass ratio, the system goes directly from Wigner crystals at small  $\tilde{\nu}$  to a smectic stripe phase around  $\tilde{\nu} = 1/2$ .

As we have mentioned before, the stripe crystal itself is a Wigner crystal and its transition to the smectic phase is continuous, after the disappearance of the  $M = 2$  bubble phase, it is tempting to conclude that under large anisotropy all first-order phase transitions disappear and the system goes from a Wigner crystal phase to the stripe phase continuously. However, the situation is a bit more complicated than that. In the isotropic  $\alpha = 1$  case, if one focuses on the triangular Wigner crystal and studies which lattice minimizes the cohesive energy, the TDHF study [149] shows that there is actually a spontaneous deformation of the triangular lattice around  $\tilde{\nu} \simeq 0.22$ . There the authors find that the ratio  $l_a/l_b$  suddenly jumps from  $l_a/l_b = \sqrt{3}/2$  (triangular lattice) to around  $l_a/l_b \simeq \sqrt{3}$  at  $\tilde{\nu} \simeq 0.22$ . This leads to a discontinuity of the cohesive energy  $E(\nu)$  at this point, and as a result a first-order phase transition. Such a sudden jump in lattice structure may not be seen in real experiments, because at  $\nu = 0.22$ , the  $M = 2$  bubble phase is lower in energy than the Wigner crystal. This spontaneous deformation of the Wigner crystal is thus hidden. But as our calculation reveals, large mass anisotropy will suppress the  $M = 2$  bubble phase. What are left are only



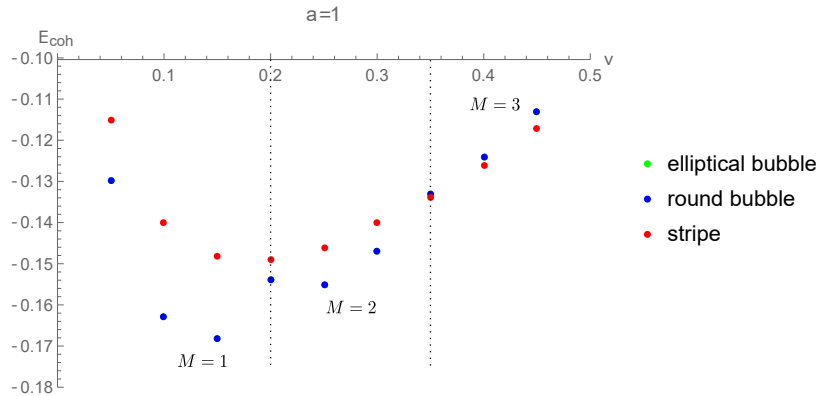


Fig. VI.10 The competition between bubble phases and stripe phases for  $\alpha = 1$  as a function of the partial filling factor of the last LL. The  $S$  lattice is chosen here.

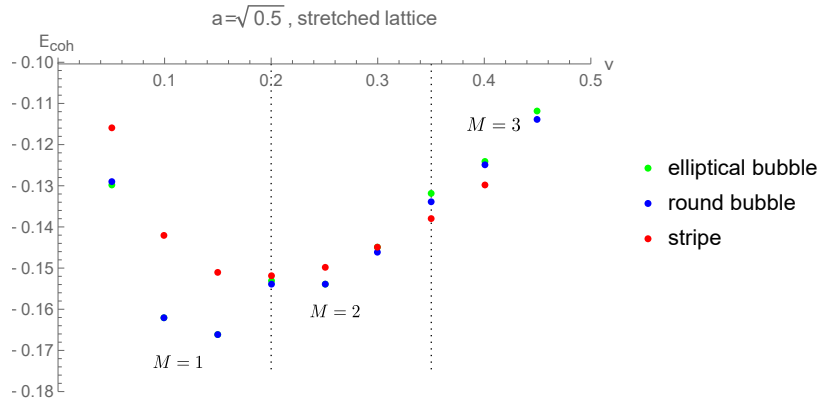


Fig. VI.11 The competition between bubble phases and stripe phases for  $\alpha = \sqrt{0.5}$  as a function of the partial filling factor of the last LL, for the  $S$  lattice.

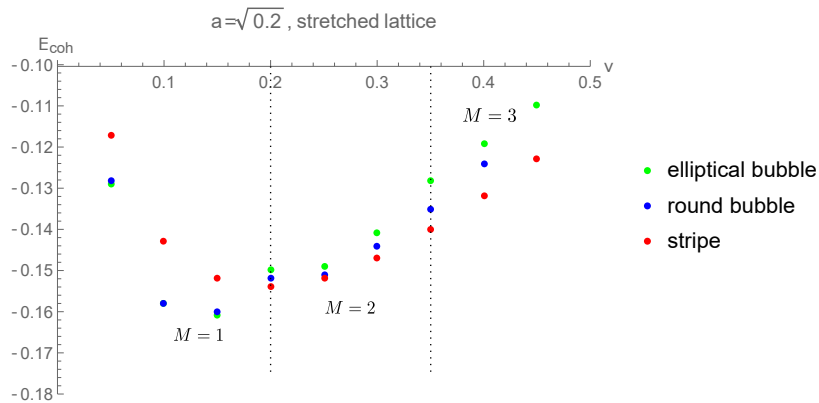


Fig. VI.12 The competition between bubble phases and stripe phases for  $\alpha = \sqrt{0.2}$  as a function of the partial filling factor of the last LL, for the  $S$  lattice.

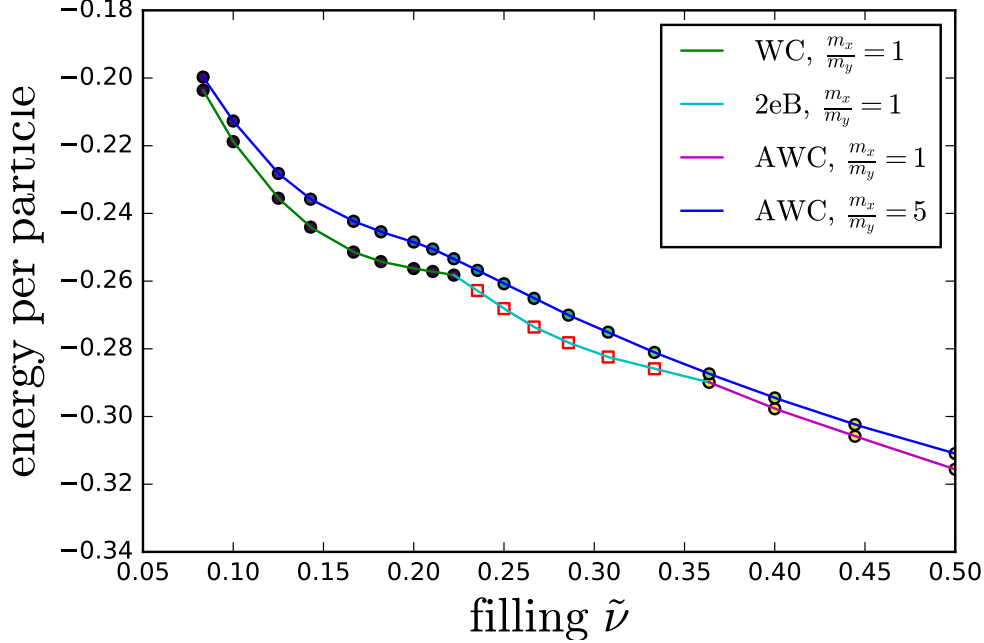


Fig. VI.13 The DMRG result for  $E_{coh}(\tilde{\nu})$ , carried out by Yuchi He in Carnegie Mellon University. The calculation is performed on infinite cylinder geometry with a finite circumference. The Landau gauge is used to construct the matrix product state wave function. The CDW states are found by varying the finite circumference carefully. The cohesive energy here is different from the HF results by a difference in the subtraction of the exchange energy, which is equivalent to a chemical potential. In the isotropic case, the discontinuity corresponding to first-order phase transitions are reproduced, in accordance with previous TDHF calculation. For  $m_x/m_y = 5$ , no clear signature of discontinuity is found.

Wigner crystals in low and intermediate fillings. It remains to answer if this spontaneous deformation persists and the first-order transition may disappear. Such a transition happens at the boundary between the dilute-limit Wigner crystal and the highly anisotropic stripe crystal, where the static HF approximation fails because the smearing regions at nearest neighbour sites begin to overlap. But from the physical intuition, when mass anisotropy is switched on, the Wigner crystal for small  $\tilde{\nu}$  starts to be anisotropic. The type of spontaneous deformation from a triangular lattice to a highly anisotropic lattice should become more and more unlikely when the external anisotropy is large enough. Indeed, our density matrix renormalization group calculation Fig. VI.13 shows that at  $m_x/m_y = 5$ , there is no clear signature of discontinuity in the derivative of the cohesive energy  $E_{coh}(\tilde{\nu})$ . Below we elaborate why this is the trend.

Now we provide an explanation for this spontaneous deformation. First, we analyze the deformation found in the TDHF study. There are two important scales from the HF potential, as shown in Fig. VI.14. They are the global minimum  $q^*$  and the first local maximum  $q^m$ . It turns out that the spontaneous deformation has a close connection with the CDW instability scale  $q^*$ . We notice that the highly anisotropic lattice in Ref. [149] after the deformation

can actually be approximated by having the axis  $l_a$  fixed to the value  $\bar{l}_a \simeq 2\pi/q^*$  and let  $l_b$  decided by

$$l_b = \frac{2\pi l^2}{\tilde{\nu} \bar{l}_a}. \quad (\text{VI.21})$$

Then the anisotropic parameter  $\varepsilon = 1 - \sqrt{3}l_b/(2l_a)$  defined in Ref. [149] is fixed well by the following formula :

$$\varepsilon(\tilde{\nu}) = 1 - \frac{\sqrt{3}\pi l^2}{\bar{l}_a^2 \tilde{\nu}}. \quad (\text{VI.22})$$

The matching of this expression with Ref. [149] can be improved further by putting  $\bar{l}_a$  to the value of the stripe periodicity in Ref. [149]. This inspires us to connect the spontaneous deformation to a transition from the dilute limit Wigner crystal to a crystal phase fixed by the CDW instability point  $q^*$ . In the dilute limit, the lattice structure is decided by the long-wave length limit of the potential and the electron density, i.e. the filling factor. But when the filling factor  $\tilde{\nu}$  becomes larger, the CDW instability point  $q^*$  emerges as a critical length scale. We can illustrate this with the help of calculating the average repulsion energy  $\bar{E}$  between the origin and its six nearest neighbours in the reciprocal lattice. For small  $\tilde{\nu}$ , the Wigner crystal takes the form of a triangular lattice. All nearest neighbours have equal distance  $\tilde{\Lambda} = 4\pi/(\sqrt{3}\Lambda)$ , with  $\Lambda$  the triangular lattice constant in coordinate space. The average repulsion energy is roughly given by  $\bar{E} = u_{HF}(\tilde{\Lambda})$ . When the filling  $\tilde{\nu}$  increases, the distance  $\tilde{\Lambda}$  between the nearest neighbours in the reciprocal lattice increases as well, according to  $\Lambda^2 = 4\pi/(\sqrt{3}\tilde{\nu})$ . Before reaching  $q^*$ , the repulsion decreases as the filling factor increases, shown in Fig. VI.14. After passing  $\tilde{\Lambda} = q^*$ , when the filling goes up further, the reciprocal triangular lattice constant  $\tilde{\Lambda}$  goes larger so that the repulsion energy becomes higher. At this time, the global minimum  $q^*$  leads to a tendency to squeeze the lattice so that two of the six nearest neighbours remain at the distance  $q^*$ . However, in order to keep the electron density fixed, such a squeezing has to push the other four nearest neighbours further from the origin, letting them have a much larger distance parametrized by  $q_l$ . In the interval between  $q^*$  and the first local maximum  $q^m$ , the Hartree-Fock energy increases rapidly. So keeping two neighbours at  $q^*$  while leaving the other four at larger distance causes a higher energy than the triangular lattice,  $6u_{HF}(\tilde{\Lambda}) < 4u_{HF}(q_l) + 2u_{HF}(q^*)$ . But when  $\tilde{\Lambda}$  is approaching  $q^m$ , this punishment for deformation no longer exists. For  $q > q^m$ , it is clearly seen that the repulsion gains very little when the distance between the reciprocal lattice sites becomes further larger. Around  $\tilde{\Lambda} \sim q^m$ , if four of the six nearest neighbours are pushed further to a larger distance  $q_l$  while the other two keep a distance of  $q^*$ , the energy is much lowered than the triangular lattice. According to this picture, a transition happens when

$$u_{HF}(\tilde{\Lambda}) > \frac{2u_{HF}(q_l) + u_{HF}(q^*)}{3}, \quad (\text{VI.23})$$

which signifies that the squeezed lattice has a lower energy. So as shown in Fig. VI.14, the lattice from this point will not evolve according to the triangular lattice, but will evolve with keeping two of the six nearest neighbours staying at a distance of  $q^*$ . This causes a large spontaneous deformation from the triangular lattice to a highly anisotropic rhombus lattice. Therefore the cohesive energy  $E_{coh}(\tilde{\nu})$  has a discontinuity in its first-order derivative.

Now we turn to the anisotropic case. In order to show the large anisotropic limit case, we choose a mass ratio  $\alpha = \sqrt{0.1}$ . As we have shown that there are two kinds of anisotropic

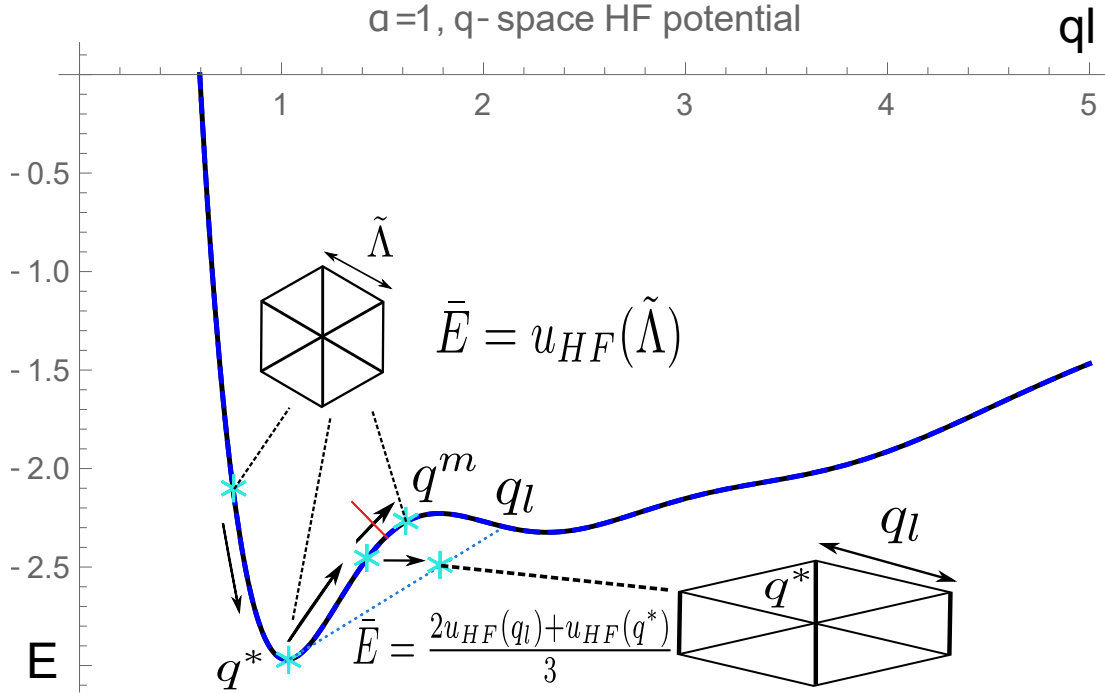


Fig. VI.14 The evolution of the repulsion energy. The snowflake represents the average repulsion energy between the origin and its six nearest neighbours in the reciprocal lattice. We only consider the repulsion between the origin and its six nearest neighbours. The arrows show how the average repulsion energy evolves with increasing the filling factor  $\tilde{\nu}$ . At small fillings, the lattice adopts an triangular form. The repulsion energy per pair is given as the  $u_{HF}(\tilde{\Lambda})$ . When the filling increases, two of the six nearest neighbours in the reciprocal lattice have a tendency of staying at a distance  $q^*$ , while the other four are repelled further away from the origin, causing a stretched lattice. As  $\tilde{\Lambda}$  is approaching  $q^m$ , the stretched lattice is becoming more and more favoured and eventually causes a transition in the lattice shape from the triangular lattice.

lattices, first we consider the  $S$  lattice. The HF interaction in the  $x$ - and  $y$ -directions takes rather different shapes (see Fig. VI.15). The interaction along the  $y$ -direction is much lower than that along  $x$ -direction for small  $q$ . The two minima along the two directions are  $q_1^*$  and  $q_2^*$ . So in general unlike the isotropic case, they are reached at different fillings when the Wigner crystal is evolving from low  $\tilde{\nu}$ . The  $x$ -direction interaction is rather flat after  $q_2^*$ , this favours stretching along  $x$ -direction after passing  $q_2^*$ . The lattice is from the beginning anisotropic. But now, through our HF calculation, when we start from a small  $\tilde{\nu}$ , the nearest-neighbour distance  $q_s$  in  $y$ -direction soon drops to the minimum  $q_1$  and is fixed. Only the distance  $q_l$  now evolves with  $\tilde{\nu}$ . The scale in the  $y$ -direction rapidly goes from the dilute limit, where the lattice constant depends primarily on  $\tilde{\nu}$ , to the CDW instability limit, where this lattice constant is fixed by  $q^*$ . In this situation, there is no spontaneous deformation.

We take a look at how the above picture can be understood from the point view of continuity of the cohesive energy. From Eq. VI.4 and Eq. VI.6, the cohesive energy proportional to the sum of the product  $u_{HF}(\mathbf{q})|\rho_b(\mathbf{q})|^2$  over the reciprocal lattice. As  $\rho_b$  describes how a

local electron at one lattice site interacting with its neighbours, it should rely on the lattice structure and the electron density,  $\rho_b = \rho_b(l_a, l_b, \tilde{\nu})$ . It may be reasonable to regard it as a smooth function on its three variables as long as the crystalline structure is stable. Then the cohesive energy can be explicitly parametrized by

$$E_{coh}(l_a, l_b, \tilde{\nu}) = E_{coh}(l_a, 2\pi\tilde{\nu}/l_a, \tilde{\nu}). \quad (\text{VI.24})$$

Besides through  $\rho_b$ , the dependence on  $l_a, l_b$  and  $\tilde{\nu}$  also enters through the reciprocal lattice summation and an overall factor  $n_B\tilde{\nu}/2$  respectively. From such a structure,  $E_{coh}(l_a, l_b, \tilde{\nu})$  is continuous on its three variable. As  $l_b = 2\pi\tilde{\nu}/l_a$ , only  $l_a$  is a variational parameter when one is looking for the lowest-energy state at a certain filling. In this case, the ground state should satisfy :

$$\frac{\delta}{\delta l_a} E_{coh}(l_a, l_b, \tilde{\nu}) = 0, \Rightarrow \frac{\partial E_{coh}}{\partial l_a} - \frac{2\pi}{l_a^2} \frac{\partial E_{coh}}{\partial l_b} = 0. \quad (\text{VI.25})$$

The solution to the above equation gives  $l_a$  as a function of the filling factor  $l_a(\tilde{\nu})$ . Now we take a look at how the cohesive energy depends on  $\tilde{\nu}$  :

$$\begin{aligned} \frac{dE_{coh}}{d\tilde{\nu}} &= \left( \frac{\partial E_{coh}}{\partial l_a} - \frac{2\pi}{l_a^2} \frac{\partial E_{coh}}{\partial l_b} \right) \frac{dl_a}{d\tilde{\nu}} + \frac{\partial E_{coh}}{\partial \tilde{\nu}} \\ &= \frac{\partial E_{coh}(l_a, l_b, \tilde{\nu})}{\partial \tilde{\nu}}. \end{aligned} \quad (\text{VI.26})$$

The second line is obtained by inserting Eq. (VI.25). In low fillings,  $l_a(\tilde{\nu})$  is controlled by the long distance Coulomb tail, and the system is in the dilute-limit Wigner crystal. As the electrons become denser, our picture in this section tells us that in the intermediate fillings the lattice structure is determined by the HF minimum. We denote the two kinds of dependence as  $l_a^w(\tilde{\nu})$  and  $l_a^s(\tilde{\nu})$ . Now we analyze Eq. (VI.26). If  $l_a$  has a sharp transition around the critical point  $\tilde{\nu}^*$ , then  $l_a^w(\tilde{\nu}^*) \neq l_a^s(\tilde{\nu}^*)$ . In this case the partial derivative  $\partial E_{coh}/\partial \tilde{\nu}$  is not continuous. The transition is first-order. This is very likely to be the situation when the interaction is isotropic, as we have shown before. As the anisotropy increases, we expect that the sharp deformation disappears, as the HF minimum in one direction is biased and quickly seen by electrons. Then at the critical point we have  $l_a^w(\tilde{\nu}^*) = l_a^s(\tilde{\nu}^*)$ . The first-order derivative  $dE_{coh}/d\tilde{\nu}$  is continuous. But in the second order derivative, the expression  $dl_a/d\tilde{\nu}$  appears. Because  $l_a^w(\tilde{\nu}^*)$  and  $l_a^s(\tilde{\nu}^*)$  are controlled by different part of the interaction, their first order derivatives can be different. In that case the transition is second order. This does not rule out the possibility that the transition can be higher orders. If the anisotropy is strong enough, the system should become highly anisotropic even at low fillings. It is possible that even the derivatives of  $l_a^w(\tilde{\nu}^*)$  and  $l_a^s(\tilde{\nu}^*)$  equal. Then one may expect that the second order transition terminates at some large  $m_x/m_y$ .

For the  $C$  lattice, the one becomes more square when mass anisotropy is added. We find its parameter  $q_s$  soon drops to  $2q_1^*$ . And when the filling factor  $\tilde{\nu}$  goes closer to the boundary between the dilute-limit Wigner crystal and the stripe crystal, it is less favourable compared to the  $S$  lattice. In this case it is a meta-stable state.

In conclusion, when the mass anisotropy is added, the stripe-like phase becomes more and more stable. The  $M = 2$  bubble phase disappears and the dilute-limit Wigner crystal is adjacent to the stripe crystal phase. As the anisotropy increases further, the sharp deformation around the boundary of the dilute-limit Wigner crystal and the stripe crystal disappears. There are only continuous phase transitions between different CDW phases.

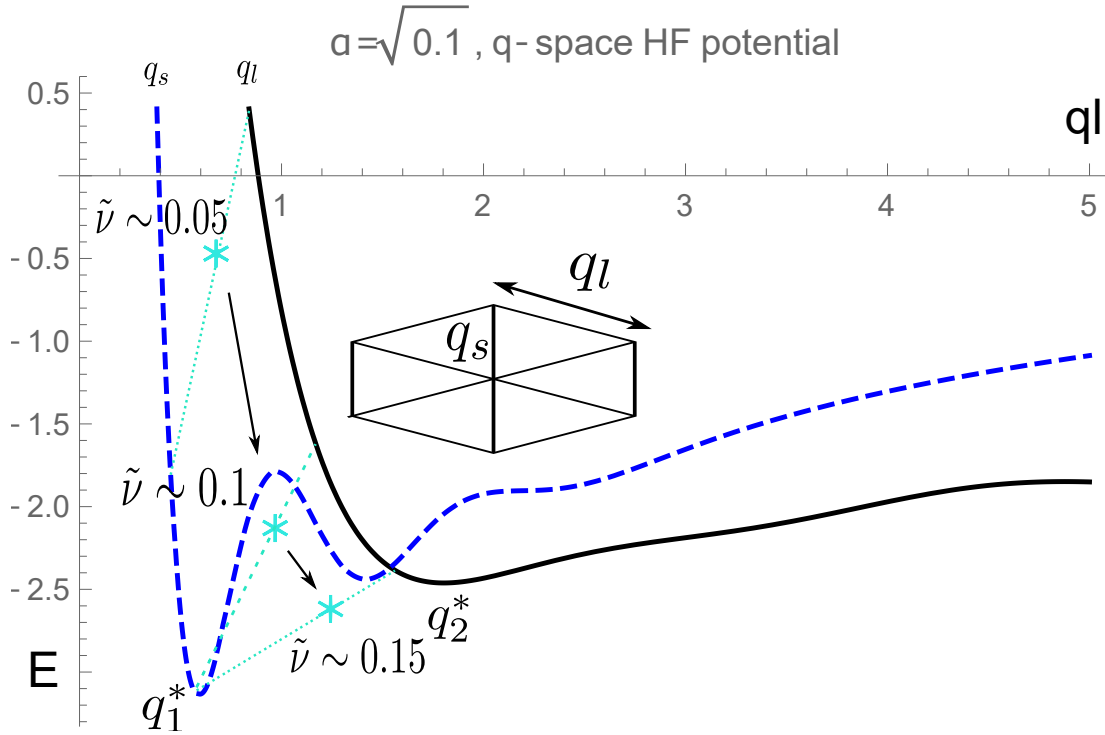


Fig. VI.15 The evolution of the repulsion energy for large mass ratio, say  $\alpha = \sqrt{0.1}$ . The dashed curve corresponds to the interaction along the  $y$ -direction and the solid one corresponds to the interaction along the  $x$ -direction. The lattice we consider in this figure is the one becoming thinner. When the filling  $\tilde{\nu}$  increases, for the six nearest neighbours, two of them soon fall to the distance  $q_1^*$ . The crystal then evolves with this distance fixed while the other four nearest neighbours become farther. Eventually the state becomes a stripe phase through a continuous phase transition.

### VI.3 Effective elastic theory

We insert here an introduction to the effective elastic theory for an anisotropic crystal. This theory can be useful in working out dispersion and correlation functions that may be compared to numerical results later. Here we give the strategy about how to obtain them.

For CDW phases with a spatial order, the long-wave-length excitation is a small deformation of the spatial order. For crystals, this is to let each lattice site oscillate around its equilibrium position and the resulting collective lattice vibrations are nothing but the acoustic phonons. In a system with underlying rotationally invariant interaction, these oscillations around the equilibrium positions are captured by an elastic theory, in terms of the strain tensor  $u_{ab}$ . In the presence of anisotropic interaction, the strain tensor is not enough to characterize the effective theory. Below we show what the elastic theory looks like.

Let us assume a deformation in the lattice :

$$\mathbf{r}_i \rightarrow \mathbf{r}_i + \mathbf{u}(\mathbf{r}_i), \quad (\text{VI.27})$$

under which the electron at each lattice site to lowest order feels a force which is proportional

to the deformation to lowest order and a Lorentz force from the external magnetic field :

$$m \frac{d^2 u_a(\mathbf{r}_i)}{dt^2} = \sum_{j \neq i} \partial_a \partial_b V(\mathbf{r}_i - \mathbf{r}_j) [u_b(\mathbf{r}_j) - u_b(\mathbf{r}_i)] - eB \epsilon_{ab} \partial_t u_b(\mathbf{r}_i) + O(u^2), \quad (\text{VI.28})$$

where  $V(\mathbf{r}_i - \mathbf{r}_j)$  describes the interaction potential between the electron at  $\mathbf{r}_i$  and the electron at  $\mathbf{r}_j$ . Here the expression is assuming a point-like density distribution at each lattice site. But it can be immediately generalized to a smooth density distribution if one replaces  $\mathbf{r}_i$  and  $\mathbf{r}_j$  by  $\mathbf{r}, \mathbf{r}'$  and integrates over all  $\mathbf{r}'$  :

$$m \frac{d^2 u_a(\mathbf{r})}{dt^2} = \int d\mathbf{r}' \partial_a \partial_b V(\mathbf{r} - \mathbf{r}') \rho_0(\mathbf{r}') [u_b(\mathbf{r}') - u_b(\mathbf{r})] - eB \epsilon_{ab} \partial_t u_b(\mathbf{r}) + O(u^2). \quad (\text{VI.29})$$

where  $\rho_0(\mathbf{r})$  is the unperturbed particle density of the crystal phase, which can be treated as a constant if we focus on elastic perturbations varying on larger length scales than the lattice constant  $\Lambda$ . In this situation for  $k \ll 1/\Lambda$  we have  $\rho_0 = \tilde{v}/(2\pi l^2)$ .<sup>1</sup> On the right hand side of the equation, the leading term is of the order  $k^2 u$ . From such a relation, the effective theory is expressed in terms of the quadratic form of the derivatives of the deformation  $u_{a,b} = \partial_a u_b$ . The symmetric combination  $u_{ab} = (u_{a,b} + u_{b,a})/2$  is defined as the strain tensor, describing elastic perturbation of the lattice. The antisymmetric combination  $\bar{u}_{ab} = u_{a,b} - u_{b,a}$  is proportional to the angle of a lattice rotation. When the underlying interaction is isotropic, the rotation does not cost energy and  $\bar{u}_{ab}$  does not enter the effective theory. But for a general anisotropic interaction, this term has to be taken into account. As a result, for a system with two mirror symmetries with respect to the  $x$ - and  $y$ -axes, according to the equation of motion for  $\mathbf{u}$  we have the following effective Lagrangian :

$$\begin{aligned} \mathcal{L} = & \frac{1}{2} m \rho_0 (\partial_t \mathbf{u})^2 - \frac{eB \epsilon^{ab} \rho_0 u_a \partial_t u_b}{2} - \frac{1}{2} (c_{11} u_{11}^2 + c_{22} u_{22}^2 + 2c_{12} u_{11} u_{22} + c_{44} u_{12}^2) \\ & - \frac{1}{2} (c_r \bar{u}_{12}^2 + 2c_{rs} \bar{u}_{12} u_{12}). \end{aligned} \quad (\text{VI.30})$$

The first term is the kinetic energy, the second term describes the Lorentz force and the middle four terms are the elastic moduli. Here  $c_r$  is quadratic in the rotation angle and describes the torque to fix the direction of the lattice while  $c_{rs}$  describes the shear-rotation coupling. Stability requires  $c_{11}, c_{22}, c_{44}, c_r$  positive and  $c_{11} \cdot c_{22} \geq c_{12}^2$ ,  $c_r \cdot c_{44} \geq c_{rs}^2$ . In the elastic theory for an isotropic interaction, only the first line appears [149]. The first kinetic term encodes the inter-Landau level physics. If one assumes a strong external magnetic field and focus on intra-LL physics, it can be neglected by setting  $m = 0$ .<sup>2</sup> Therefore the effective Hamiltonian is :

$$\mathcal{H}^e = \frac{1}{2} (c_{11} u_{11}^2 + c_{22} u_{22}^2 + 2c_{12} u_{11} u_{22} + c_{44} u_{12}^2) + \frac{1}{2} (c_r \bar{u}_{12}^2 + 2c_{rs} \bar{u}_{12} u_{12}). \quad (\text{VI.31})$$

For Coulomb-type long-range interaction, there is a  $1/q$  singularity for small wave vectors. This is easily realized by adding a repulsion term to  $\mathcal{H}^e$  [139] :

$$\frac{1}{2} \int d\mathbf{r} \int d\mathbf{r}' \rho_0 \nabla \cdot \mathbf{u}(\mathbf{r}) v_{lr}(\mathbf{r} - \mathbf{r}') \rho_0 \nabla \cdot \mathbf{u}(\mathbf{r}'), \quad (\text{VI.32})$$

1. For an infinite crystalline system, the density  $\rho_0(\mathbf{q})$  is only non-vanishing at the reciprocal lattice vectors. So at small momentum, we only need to consider  $\rho_0(0) = (N_e/A)(2\pi)^2 \delta(\mathbf{q})$

2. As we will show later, by setting the  $m \rightarrow 0$  limit the intra-LL magnetophonon mode and inter-LL magnetoplasmon mode are converging to their correct energy scales

where, as we have shown in Sec. II.3, the term  $\rho_0 \nabla \cdot \mathbf{u}$  corresponds to the density fluctuation and  $v_{lr}$  encodes the long range tail of the Coulomb interaction. This term is also equivalent to give  $c_{11}, c_{12}, c_{22}$  a singular  $\mathbf{q}$ -dependence  $c_{11}(\mathbf{q}) \sim c_{22}(\mathbf{q}) \sim c_{12}(\mathbf{q}) \rightarrow 1/q$  as  $q \rightarrow 0$ .

With this theory first we take a look at the dispersion of the collective modes. In an ordinary two-dimensional crystal, in the absence of magnetic field there are two branches of gapless collective modes, a longitudinal plasmon mode which survives even in the liquid phase and a transverse phonon mode. When the magnetic field is turned on, the movement of the displacement field is strongly bent by the Lorentz force and the two modes are coupled. In this case, one of the two modes goes to the cyclotron frequency  $\omega_c = eB/m$ , as  $q \rightarrow 0$  and another one remains gapless. We adopt the notations by Côté and MacDonald [131, 149], calling the higher-frequency one the magnetoplasmon mode and the lower-frequency one the magnetophonon mode. According to the equation of motion, we can write out the elastic matrix :

$$\begin{pmatrix} D_{xx} - m\rho_0\omega^2 & D_{xy} - i\omega\rho_0eB \\ D_{yx} + i\omega\rho_0eB & D_{yy} - m\rho_0\omega^2 \end{pmatrix} = D - \begin{pmatrix} m\rho_0\omega^2 & i\omega\rho_0eB \\ -i\omega\rho_0eB & m\rho_0\omega^2 \end{pmatrix}. \quad (\text{VI.33})$$

The coefficients are :

$$\begin{aligned} D_{xx} &= c_{11}q_x^2 + \frac{(c_{44} + 4c_r - 2c_{rs})q_y^2}{4}, & D_{yy} &= c_{22}q_y^2 + \frac{(c_{44} + 4c_r + 2c_{rs})q_x^2}{4}, \\ D_{xy} &= D_{yx} = \left( c_{12} + \frac{c_{44}}{4} - c_r \right) q_x q_y \end{aligned} \quad (\text{VI.34})$$

The magnetoplasmon mode and magnetophonon mode are given as the zeroes of the determinant of the elastic matrix. For small  $q$  and large  $\omega_c$ , the results are :

$$\omega^2 = \frac{1}{2} \left[ \omega_c^2 + \frac{D_{xx} + D_{yy}}{m\rho_0} \pm \sqrt{\Delta} \right], \quad \Delta = \omega_c^4 + 2\omega_c^2 \frac{D_{xx} + D_{yy}}{m\rho_0} + \frac{(D_{xx} - D_{yy})^2 + 4D_{xy}^2}{m^2\rho_0^2}. \quad (\text{VI.35})$$

The plus sign  $+$  refers to the magnetoplasmon mode while the minus  $-$  refers to the magnetophonon mode. In the  $q \rightarrow 0$  limit, all matrix elements  $D$  go to zero, the above magnetoplasmon mode converges to  $\omega_c$  as expected. The  $m \rightarrow 0$  limit can also be taken safely for the magnetoplasmon mode if we remember that the cyclotron frequency is going to infinity as  $\omega_c = eB/m$ . In this case it is non-dispersive and fixed at  $\omega_c$ . On the other hand, the leading order for the magnetophonon mode takes the form :

$$\omega_{MPN}^2 = \frac{D_{xx}D_{yy} - D_{xy}^2}{m^2\rho_0^2\omega_c^2} = \frac{4\pi^2 l^8}{\tilde{\nu}^2} (D_{xx}D_{yy} - D_{xy}^2), \quad (\text{VI.36})$$

which is gapless. In the small-momentum limit, if we take the moduli  $c_{11}(\mathbf{q}) \simeq c_{22}(\mathbf{q}) \simeq c_{12}(\mathbf{q})$  to be singular as  $c(q) \sim 1/q$ , like in [149], by expanding the above equation to leading order, the magnetophonon mode becomes :

$$\omega_{MPN}^2 = \frac{\pi^2 l^8 c(q)}{\tilde{\nu}^2} \left[ q_x^4 (c_{44} + 4c_r + 2c_{rs}) + q_y^4 (c_{44} + 4c_r - 2c_{rs}) - 2(c_{44} - 4c_r) q_x^2 q_y^2 \right]. \quad (\text{VI.37})$$

From this expression, we can see that the shear modulus  $c_{44}$  can be detected if the magnetophonon mode is known, such as through numerical methods. Furthermore this expression has as well a safe limit when  $m \rightarrow 0$ .



We also look at the correlation function of the displacement field. In order to simplify the question, we only look at the intra-LL physics and the magnetoplasmon mode should be dropped. This is easily done by taking  $m \rightarrow 0$  as we discussed in the last paragraph. Then in the elastic theory, the  $u_x$  and  $u_y$  are actually conjugate variables. This enables a quantum elastic field theory. From the Lagrangian  $u_x$  and  $u_y$  satisfy the commutation rule :

$$[u_x(\mathbf{r}), u_y(\mathbf{r}')] = \frac{i\delta(\mathbf{r} - \mathbf{r}')}{eB\rho_0} = \frac{i\delta(\mathbf{r} - \mathbf{r}')}{\tilde{\nu}/(2\pi l^4)}. \quad (\text{VI.38})$$

In momentum space, this transforms to :

$$[u_x(\mathbf{q}), u_y(\mathbf{q}')] = \frac{i(2\pi)^2\delta(\mathbf{q} + \mathbf{q}')}{eB\rho_0}. \quad (\text{VI.39})$$

With this, we can compute the time ordered correlation function of  $\mathbf{u}$ , defined as :

$$\begin{aligned} iG_{\alpha,\beta}(t - t', \mathbf{q}, \mathbf{q}') &= \langle \mathcal{T} u_\alpha(\mathbf{q}, t) u_\beta(\mathbf{q}', t') \rangle \\ &= \theta(t - t') \langle u_\alpha(\mathbf{q}, t) u_\beta(\mathbf{q}', t') \rangle + \theta(t' - t) \langle u_\beta(\mathbf{q}', t') u_\alpha(\mathbf{q}, t) \rangle. \end{aligned} \quad (\text{VI.40})$$

The time-ordered correlation function satisfies the following equation of motion :

$$\begin{aligned} \sum_{\gamma} \left( i \frac{\partial}{\partial t} \delta_{\alpha,\gamma} + H_{\alpha,\gamma} \right) G_{\gamma,\beta}(t - t', \mathbf{q}, \mathbf{q}') &= \delta(t - t') \langle [u_\alpha(\mathbf{q}, 0), u_\beta(\mathbf{q}', 0)] \rangle \\ &= \delta(t - t') \delta(\mathbf{q} + \mathbf{q}') \frac{(2\pi)^2 i \varepsilon_{\alpha\beta}}{eB\rho_0}, \end{aligned} \quad (\text{VI.41})$$

where we use the equal-time commutator in the last equality and  $\sum_{\beta} H_{\alpha,\beta} u_{\beta} = [\mathcal{H}^e, u_{\alpha}]$  symbolizes the action when commuting  $\mathcal{H}^e$  and the first  $u$  operator in the correlation function. By Fourier transformation, Eq. (VI.41) is a matrix equation. With the help of the previously introduced matrix  $D$ , it is written as

$$\sum_{\gamma,\sigma} \left( \omega \delta_{\alpha,\gamma} - i \varepsilon_{\alpha,\sigma} D_{\sigma,\gamma} \frac{1}{eB\rho_0} \right) \tilde{G}_{\gamma,\beta}(\omega, \mathbf{q}, \mathbf{q}') = \delta(\mathbf{q} + \mathbf{q}') \frac{(2\pi)^2 i \varepsilon_{\alpha\beta}}{eB\rho_0}. \quad (\text{VI.42})$$

So the frequency-space Green's function is given by :

$$\tilde{G}_{\alpha,\beta}(\omega, \mathbf{q}, \mathbf{q}') = \frac{(2\pi)^2 \delta(\mathbf{q} + \mathbf{q}')}{\det(i\omega\rho_0 eB\varepsilon - D)} \begin{pmatrix} -D_{yy} & D_{xy} - i\omega\rho_0 eB \\ D_{yz} + i\omega\rho_0 eB & -D_{xx} \end{pmatrix}, \quad (\text{VI.43})$$

where  $\varepsilon$  and  $D$  correspond to the matrices  $\varepsilon_{\alpha,\beta}$  and  $D_{\alpha,\beta}$ .

In order to work out the Green's function in time space, we need to know which poles correspond to the ones for positive time . The time-ordered correlation function has the following decomposition :

$$\tilde{G}(\omega) = \int d\nu \frac{A_+(\nu)}{\omega - \nu + i0^+} - \int d\nu \frac{A_-(\nu)}{\omega - \nu - i0}. \quad (\text{VI.44})$$

The two terms corresponds to the  $t \geq t'$  component and  $t \leq t'$  component respectively in the time-ordered correlation function and  $A_+$  and  $A_-$  are their spectral weight. As we are at zero temperature,  $A_{\pm}$  is only non-vanishing for  $\nu > 0$ . The time-ordered correlation function

helps us find the equal-time correlation function by performing the  $t - t' \rightarrow 0^+$  limit, as in the fluctuation-dissipation relation :

$$\langle u_\alpha(\mathbf{q}, t) u_\beta(\mathbf{q}', t) \rangle = iG_{\alpha,\beta}(0^+, \mathbf{q}, \mathbf{q}'). \quad (\text{VI.45})$$

So the equal-time Green's function can be found by picking all its positive poles of Eq. (VI.43). As the poles of Eq. (VI.43) are exactly given by the magnetophonon mode, we find

$$\langle u_\alpha(\mathbf{q}, t) u_\beta(\mathbf{q}', t) \rangle = \frac{(2\pi)^2 \delta(\mathbf{q} + \mathbf{q}')}{2(eB\rho_0)^2 \omega_{MPN}(\mathbf{q})} \begin{pmatrix} D_{yy} & i\omega_{MPN} eB\rho_0 - D_{xy} \\ -i\omega_{MPN} eB\rho_0 - D_{xy} & D_{xx} \end{pmatrix}, \quad (\text{VI.46})$$

where  $\omega_{MPN}(\mathbf{q})$  is taken as the positive root in Eq. (VI.36).

With the dispersion and the correlation function constructed here, it would be interesting to study whether they can be compared with the DMRG numerical results on the anisotropic crystals. The comparison may be used further to confirm the moduli coefficients, which specify the transition point between the stripe crystal and the smectic phase. How this transition point will evolve under anisotropy will be an interesting question.



## VII – Conclusion

In this thesis, we studied the effects of anisotropy in quantum Hall systems. Two kinds of states in quantum Hall systems are investigated, the composite fermion states of Jain's series and the charge density wave states. The anisotropy is introduced by tilting the external magnetic field or adding an anisotropy in the mass tensor.

The composite fermion state is an incompressible quantum Hall liquid state, which possesses gapped quasiparticle/quasihole excitations. We studied how the activation gap for a well-separated pair of quasiparticle and quasihole evolves under a parallel component of the magnetic field. We find that the anisotropy introduces CF-LL mixing. This perturbation qualitatively modifies the free charged-particle picture of CF LLs. In this process, we find that a variational parameter corresponding to the geometry of CF cyclotron motion can be defined, the metric of the CF cyclotron coordinates. By varying this metric, the CF-LL mixing can be minimized for the CF LLs around the CF Fermi level. The activation gap for a series of CF states are calculated in the lowest LL and  $n = 1$  LL. Remarkably the activation gap is quite robust against the tilt. This shows that the quasiparticles/quasiholes in the CF state are stable in the presence of anisotropy. The topological order associated with the quantum Hall liquid is hence robust.

Then we studied the neutral collective mode in the presence of anisotropy. The collective mode results from the strong correlations and its low-momentum limit is believed to be related to a geometric degree of freedom. As a first step towards understanding the collective excitations in CFs, we compared the isotropic results based on the projected electron density and that based on the preferred density, which combines the electric and the vortex densities in the Hamiltonian theory of CFs. While the latter has a good interpretation and results in the calculation for activation gaps, it is the projected electron density that captures correctly the collective mode. This suggests that small-distance excitations are likely to see the electrons instead of composite fermions while at large distances the interactions between CFs with their modified charge dominate. The tilt of the magnetic field influences the collective mode in two ways. First, it changes the isotropic part of the interaction potential. This tends to lower the overall scale and thus the gap of the neutral mode. Secondly the anisotropic interaction induced by the tilt gives rise to an anisotropic dispersion in the spectrum. In our calculation, we show that this is likely to cause a gap collapse in the direction of the inplane magnetic field for  $\nu = 2/5$  at intermediate tilting angle. This may be seen as the possibility of finding a nematic phase by tilting the magnetic field.

In the last part of this thesis, we studied another large family of ground-state candidates in quantum Hall systems, the charge density wave states. This family contains bubble states and stripe states, with the Wigner crystal as a special case of  $M = 1$  bubble state. In the isotropic case, a  $M = 2$  bubble phase separates the Wigner crystal and the stripe phase.

The quantum Hall system is likely to go from the Wigner crystal at low fillings through two first-order phase transitions to the stripe phase near  $\tilde{\nu} = 1/2$ . When anisotropy is turned on, we find the  $M = 2$  bubble phase is gradually disappearing. The Wigner crystal is adjacent to the stripe phase and the previous first-order phase transitions are replaced by continuous transitions.

There are several perspectives from our results. First in our study for CF activation gaps, we found a variational metric for CF LLs. As we introduced in chapter II, the variational metric for electrons can be promoted to a local quantity characterizing the quadupolar deformation, which is the collective excitation for quantum Hall fluids at long wave-length. It would be interesting to investigate whether the variational metric for CF can be connected to the collective mode. The difficulty in this direction lies in the fact that the Hamiltonian CF theory does not produce the correct static structure factor, as exposed in the appendix. This shows that the Fermi-liquid like CF Hamiltonian theory perhaps loses some information about the ground state. This may be because the fluctuations of the attached flux in the CF construction are not well taken into account. Another way of looking at this question is from the perspective of the Hall viscosity. It is not hard to verify that the Hall viscosity of an IQHE CF state is not the same as that of the original FHQE. The CFs can only reproduce the Hall viscosity of the electrons by including the geometric information of the attached flux [153, 154]. In the language of the Hamiltonian theory, the process of flux attachment translates to a physical constraint and the decoupling of inter- and intra-LL physics. How the corresponding geometric information transforms into the Hamiltonian theory is worth studying. On the other hand, from a wave functional point of view, in the anisotropic Laughlin wave function [55] (what we denoted as  $|\Psi_{1/(2s+1)}(\bar{g})\rangle$  in Eq. (II.6)), the Jastrow-Laughlin factor actually no longer takes the form of a vortex. Some zeors are separated from the exact of positions of electrons as the Jastrow-Laughlin factor now takes the form  $\prod_{i \neq j} [(z_i - z_j) + z_0^2 (\partial/\partial z_i - \partial/\partial z_j)]^{2p+1}$  with  $z_0$  characterizing the anisotropy. So the flux attachment is not strictly defined from the wave functional point of view and the  $p$  filled CF LL picture is broken in a sense at the level of wave functions. It would be interesting to see if this can be connected to the CF LL mixing found in this thesis. Moreover  $|\Psi_{1/(2s+1)}(\bar{g})\rangle$  does not seem to be related to any conformal blocks as well. How to generalize the conformal field theory construction for FQH states in anisotropic systems would be interesting.

In our computation, we found that the neutral gap in a CF state is susceptible to a tilt of the external magnetic field. The gap can close at some momentum. Usually such a collapse at a finite wave-vector leads to CDW instabilities. But in LLL, it is known that CDW states are unstable and strong quantum fluctuations destroy the spatial order. The quantum Hall nematic phase is a very possible candidate. More studies, such as robustness of the topological ground-state degeneracy and the Goldstone mode, which for isotropic interactions comes from a spontaneous rotation symmetry breaking and describes the orientation of the nematic order, are required to verify if it is the state after the neutral gap collapses. We also show that in the  $n = 2$  LL, the stripe-like phase (stripe crystal or smectic phase) is dominant at large anisotropy. As a nematic phase can be as well caused by dislocations [139] in the smectic phase, it is very promising to look at under which condition the smectic phase is susceptible to the dislocation-mediated instability. Meanwhile, there are two kinds of almost degenerate Wigner-crystal phases under anisotropic interaction, the ‘‘thinner’’ one and the ‘‘square’’ one. They are so close in the cohesive energy that it is very tempting to study whether they can appear in a mixed state and one configuration can be tunneled into

another.



# A – Static structure factor in the Hamiltonian theory

In this appendix, we point out the discrepancy in the static structure computed from the Hamiltonian theory and trial wave functions. Moreover, the coefficients computed from the Hamiltonian theory violates the bound proposed by Haldane. This is a suggestion that the composite fermion only captures the lowest excitation above the ground state but fails to give thorough information for the full Hilbert space of the FQH problem.

In rotation-invariant fractional quantum Hall systems, as mentioned in the main text, in the small  $\mathbf{q}$  limit, the leading term in the static structure factor is  $q^4$  :

$$S(\mathbf{q}) = cq^4 + \dots \quad (\text{A.1})$$

The coefficient should satisfy a bound found by Haldane, as shown in Sec. II.3.2. This bound has a close correlation with the area-preserving deformation generators. For gapped trial FQHE states, such as Laughlin states or Moore-Read states [134] analytic and numeric results show that the bound is saturated [58]. Read [27] argues that the equality should hold for a general gapped FQHE state in the LLL, for example, Read-Rezayi states [135].

First we take a look at the general structure of  $S(\mathbf{q})$ . The structure factor assumes a decomposition in terms of the eigenstates  $|n\rangle$  as

$$S(\omega, \mathbf{q}) = \sum_n \langle 0 | \rho(\mathbf{q}) | n \rangle \langle n | \rho(-\mathbf{q}) | 0 \rangle \delta(\omega - E_n). \quad (\text{A.2})$$

The static structure factor is defined as the equal time density correlation function and is linked to the frequency dependent structure factor by an integral over frequency. It is as a consequence given as :

$$S(\mathbf{q}) = \sum_n \langle 0 | \rho(\mathbf{q}) | n \rangle \langle n | \rho(-\mathbf{q}) | 0 \rangle \quad (\text{A.3})$$

From this decomposition, it can be observed that even higher energy modes can contribute to the coefficients of small  $q$  expansion in the static structure factor.

The static structure factor was calculated in the conserving method by Murthy. The time-dependent Hatree-Fock calculation can find the time-ordered density correlation function  $\chi(\omega, \mathbf{q})$ . The static structure is to sum over all poles of  $\chi(\omega, \mathbf{q})$  in the negative half complex plane, and one finds :

$$S(0, \mathbf{q}) = \begin{cases} \frac{1}{8}(ql_B)^4 + \dots, & \nu = \frac{1}{2s+1}; \\ \frac{(ql_B)^4}{2} \frac{p^4 - 3p^3 + \frac{5}{4}p^2 + 3p + \frac{7}{4}}{p^2 - 1} + \dots, & \nu = \frac{p}{2ps+1}. \end{cases} \quad (\text{A.4})$$



It turns out that for  $\nu = 1/3$ , the TDHF result within the Hamiltonian theory gives a coefficient  $1/8$  for the  $q^4$  term while Haldane's bound requires the coefficient no smaller than  $1/4$  in this case. One can verify that the TDHF result also violates Haldane's bound for other fillings.

On the other hand, we compute the naive static structure factor for the preferred density using the  $p$  filled LL ground state. The preferred density is  $\bar{\rho}^p(\mathbf{q}) = \bar{\rho}_e(\mathbf{q}) - c^2\chi(\mathbf{q})$ . The static structure factor is defined as the density-density correlation at equal time :

$$S(0, \mathbf{q}) = \frac{1}{N_e} \langle \rho^p(\mathbf{q}) \rho^p(-\mathbf{q}) \rangle. \quad (\text{A.5})$$

As we discussed in the main text, the matrix elements of  $\bar{\rho}^p$  has a product decomposition into the Landau level and guiding-center degrees of freedom. The above expression is easily evaluated with the help of Wick's theorem :

$$\begin{aligned} S(0, \mathbf{q}) &= \sum_{1,2,3,4} \frac{1}{N_e} \langle d_1^\dagger d_2 d_3^\dagger d_4 \rangle \rho_{n_1 n_2}^p(\mathbf{q}) \rho_{n_3 n_4}^p(-\mathbf{q}) \rho_{m_1 m_2}^p(\mathbf{q}) \rho_{m_3 m_4}^p(-\mathbf{q}) \\ &= \sum_{1,2,3,4} \frac{1}{N_e} \langle d_1^\dagger d_4 \rangle \langle d_2 d_3^\dagger \rangle \rho_{n_1 n_2}^p(\mathbf{q}) \rho_{n_3 n_4}^p(-\mathbf{q}) \rho_{m_1 m_2}^p(\mathbf{q}) \rho_{m_3 m_4}^p(-\mathbf{q}). \end{aligned}$$

Notice  $\rho^p(0) = 0$  so that we cannot contract  $d^\dagger, d$  from the same density operator because this gives zero. The reference state is composed of  $p$  filled CF LLs. First, we have the summation over  $m$ , the CF angular momentum, which gives the number of orbits  $N_{\Phi^*}$  in each CF LL. The CF LL part gives the  $\mathbf{q}$  dependence. Then only the summation over the CF LL indices is left. The result is written as :

$$S(0, \mathbf{q}) = \frac{N_{\Phi^*}}{N_e} \sum_{\substack{n_1 \geq p, \\ 0 \leq n_2 \leq p-1}} \bar{\rho}_{n_2 n_1}^p(\mathbf{q}) \bar{\rho}_{n_1 n_2}^p(-\mathbf{q}). \quad (\text{A.6})$$

As  $\bar{\rho}_{p, p-1}^p(\mathbf{q}) \sim q^2$ , the leading term in the above expression is  $q^4$ . The matrix element for  $\bar{\rho}_{n_1, n_2}^p$  between two LL  $n_1$  and  $n_2$  is (for  $n_1 \geq n_2$ ) :

$$\begin{aligned} \bar{\rho}_{n_1, n_2}^p(\mathbf{q}) &= \sqrt{\frac{n_2!}{n_1!}} \left[ e^{-c^2 x/2} \left( \frac{-icq-l^*}{\sqrt{2}} \right)^{n_1-n_2} L_{n_2}^{n_1-n_2}(c^2 x) \right. \\ &\quad \left. - c^2 f e^{-x/(2c^2)} \left( \frac{-iq-l^*}{c\sqrt{2}} \right)^{n_1-n_2} L_{n_2}^{n_1-n_2} \left( \frac{x}{c^2} \right) \right], \quad (\text{A.7}) \end{aligned}$$

where  $x = q^2 l^{*2}/2$ . Take  $N_{\Phi^*} = N_c/p = N_e/p$ . The static structure factor in the  $q \rightarrow 0$  behaves as :

$$S(0, \mathbf{q}) = \begin{cases} \frac{1}{8} (ql_B)^4 + \dots, & \nu = \frac{1}{2s+1}; \\ \frac{p^2}{8} (ql_B)^4 + \dots, & \nu = \frac{p}{2ps+1}. \end{cases} \quad (\text{A.8})$$

This again gives a coefficient  $1/8$  for  $\nu = 1/3$ , which is in contradiction with Haldane's bound. On the other hand, remember that the above expressions obtained by Shankar and Murthy for the electron density and constraint are only exact to the leading order of  $q$ . Moreover, the preferred density giving the dipole structure uncovered by other methods is also correct in this order of  $q$ . It is tempting to study if a correction of the order of  $q^2$  can

remedy this violation. However, through some thorough computation to the order  $q^2$  similar to that in Sec. III.3, we find that it is not feasible to throw all inter-LL degrees of freedom to the gauge field  $A$  and decouple it from the CF degrees of freedom to this order. An alternative is to instead redefine the preferred density  $\rho^p = \bar{\rho}_e - c^2\chi + aq^2\chi$  with a higher order term in  $q$  since this acting on the physical states still gives  $\bar{\rho}_e|\text{phys}\rangle$ . But this does not change the leading order  $q^4$  in  $S(\mathbf{q})$  because  $aq^2\chi$  contributes  $q^3$  in Eq. (A.7).

In short, there is no evident method to make the static structure factor computed in the Hamiltonian theory consistent with Haldane's bound. This is a signature that the Hamiltonian theory does not saturate the static structure factor in  $q \rightarrow 0$  limit. The higher degrees of freedom in the original electron theory are beyond the scope of the composite fermion theory.

## LE SIGNALEMENT DES THESES DE DOCTORAT EN FRANCE

Signaler une thèse soutenue est une **obligation légale** pour l'établissement habilité (cf. [Arrêté du 25 mai 2016](#)). Le signalement d'une thèse en préparation, lui, est **facultatif**.

Dans le respect des dispositions réglementaires, l'ABES coordonne le travail des professionnels impliqués dans le circuit de la thèse dans trois applications : le Sudoc, Step et Star, et a développé une interface publique spécifique pour les thèses de doctorat : le moteur de recherche Thèses.fr ([www.theses.fr](http://www.theses.fr)).



[Le Sudoc, répertoire national des thèses de doctorat françaises](#)

Final version

- Le [Sudoc](#) ([www.sudoc.abes.fr](http://www.sudoc.abes.fr)), Système Universitaire de Documentation, est le catalogue collectif national des établissements de l'Enseignement supérieur et de la Recherche. Première application mise en place par l'ABES en 2000, il comprend plus de 10 millions de notices bibliographiques qui décrivent tous les types de documents (livres, thèses, revues, ressources électroniques, documents audiovisuels, microformes, cartes, partitions, manuscrits et livres anciens...). Le catalogue Sudoc décrit également les collections de revues et journaux d'environ 2 000 établissements documentaires hors enseignement supérieur (bibliothèques municipales, centres de documentation...). Il est le répertoire national des thèses, et porte donc la mission d'un recensement exhaustif de la production doctorale française. Il est consultable librement.



[Step, application professionnelle de signalement des thèses en préparation](#)

- Le signalement d'une thèse en préparation est une bonne pratique scientifique; il ne garantit pas une quelconque protection ou exclusivité sur le sujet traité. L'intérêt scientifique ou l'originalité d'un sujet déposé relève du dialogue entre le doctorant et son directeur de thèse qui veille à ne pas proposer ou agréer un sujet déjà signalé. L'application Step (Signalement des thèses en préparation) permet aux établissements habilités qui le souhaitent de signaler les thèses en préparation. Successeur du Fichier

4

central des thèses (FCT), qui était limité au secteur des Sciences humaines et sociales, Step permet la saisie des éléments descriptifs de toute thèse en préparation, quelle que soit la discipline.

**A noter** : l'ABES est un opérateur technique dans le signalement des thèses en cours. Par conséquent il ne lui appartient pas de se prononcer sur l'intérêt scientifique d'un sujet déposé.



[Star \(Signalement des thèses, archivage et recherche\), application professionnelle de signalement des thèses soutenues déposées sur support électronique](#)

- L'application Star doit être utilisée par tout établissement habilité. Star permet :
- d'enregistrer le dépôt de la version d'archivage (et, le cas échéant, de la version de diffusion) de la thèse et de ses métadonnées;
- d'envoyer automatiquement la version d'archivage au CINES (y compris dans le cas d'une thèse non diffusable);
- de lui attribuer un identifiant pérenne facilitant son référencement ;
- d'assurer la visibilité de la thèse dans les interfaces publiques du Sudoc et de Thèses.fr;
- à la demande de l'établissement, de transmettre les métadonnées ou la version de diffusion de la thèse vers d'autres sites qu'il aura désignés.



[Thèses.fr, moteur de recherche des thèses de doctorat françaises](#)

[Thèses.fr](#), moteur de recherche des thèses de doctorat françaises, existe depuis 2011. Il a vocation à recenser les thèses de doctorat en préparation (lorsque les établissements ont choisi d'utiliser l'application Step) et toutes les thèses de doctorat soutenues, quel que soit le mode de dépôt retenu par l'établissement de soutenance. Cette interface est notamment alimentée par les autres applications gérées par l'ABES (Sudoc, Step, Star). Efficacement indexée par les moteurs de recherche du web, elle donne une visibilité accrue à la production doctorale française. Dès lors que le texte intégral est disponible en ligne, un bouton « accéder en ligne » vous y conduit. La version validée par le jury s'affiche en première occurrence.

5

# Bibliographie

- [1] K. v. KLITZING, G. DORDA & M. PEPPER; «New Method for High-Accuracy Determination of the Fine-Structure Constant Based on Quantized Hall Resistance»; *Phys. Rev. Lett.* **45**, p. 494–497 (1980). <https://link.aps.org/doi/10.1103/PhysRevLett.45.494>. ix, 1, 3
- [2] D. C. TSUI, H. L. STORMER & A. C. GOSSARD; «Two-Dimensional Magnetotransport in the Extreme Quantum Limit»; *Phys. Rev. Lett.* **48**, p. 1559–1562 (1982). <https://link.aps.org/doi/10.1103/PhysRevLett.48.1559>. ix, 1, 3
- [3] D. J. THOULESS, M. KOHMOTO, M. P. NIGHTINGALE & M. DEN NIJS; «Quantized Hall Conductance in a Two-Dimensional Periodic Potential»; *Phys. Rev. Lett.* **49**, p. 405–408 (1982). <https://link.aps.org/doi/10.1103/PhysRevLett.49.405>. ix, 1
- [4] B. SIMON; «Holonomy, the Quantum Adiabatic Theorem, and Berry's Phase»; *Phys. Rev. Lett.* **51**, p. 2167–2170 (1983). <https://link.aps.org/doi/10.1103/PhysRevLett.51.2167>. ix
- [5] J. E. AVRON, R. SEILER & B. SIMON; «Homotopy and Quantization in Condensed Matter Physics»; *Phys. Rev. Lett.* **51**, p. 51–53 (1983). <https://link.aps.org/doi/10.1103/PhysRevLett.51.51>. ix
- [6] M. V. BERRY; «Quantal phase factors accompanying adiabatic changes»; Proceedings of the Royal Society of London. A. Mathematical and Physical Sciences **392**, p. 45–57 (1984). ix
- [7] F. D. M. HALDANE; «Model for a Quantum Hall Effect without Landau Levels : Condensed-Matter Realization of the "Parity Anomaly"»; *Phys. Rev. Lett.* **61**, p. 2015–2018 (1988). <https://link.aps.org/doi/10.1103/PhysRevLett.61.2015>. ix
- [8] C. L. KANE & E. J. MELE; «Quantum Spin Hall Effect in Graphene»; *Phys. Rev. Lett.* **95**, p. 226 801 (2005). <https://link.aps.org/doi/10.1103/PhysRevLett.95.226801>. ix
- [9] B. A. BERNEVIG, T. L. HUGHES & S.-C. ZHANG; «Quantum Spin Hall Effect and Topological Phase Transition in HgTe Quantum Wells»; *Science* **314**, p. 1757–1761 (2006). ISSN 0036-8075. <http://science.sciencemag.org/content/314/5806/1757>; <http://science.sciencemag.org/content/314/5806/1757.full.pdf>. ix
- [10] L. FU, C. L. KANE & E. J. MELE; «Topological Insulators in Three Dimensions»; *Phys. Rev. Lett.* **98**, p. 106 803 (2007). <https://link.aps.org/doi/10.1103/PhysRevLett.98.106803>. ix

- [11] X.-L. QI, T. L. HUGHES & S.-C. ZHANG; «Topological field theory of time-reversal invariant insulators»; *Phys. Rev. B* **78**, p. 195 424 (2008). <https://link.aps.org/doi/10.1103/PhysRevB.78.195424>. ix
- [12] A. A. BURKOV & L. BALENTS; «Weyl Semimetal in a Topological Insulator Multilayer»; *Phys. Rev. Lett.* **107**, p. 127 205 (2011). <https://link.aps.org/doi/10.1103/PhysRevLett.107.127205>. ix
- [13] M. LEVIN & A. STERN; «Fractional Topological Insulators»; *Phys. Rev. Lett.* **103**, p. 196 803 (2009). <https://link.aps.org/doi/10.1103/PhysRevLett.103.196803>. ix
- [14] N. REGNAULT & B. A. BERNEVIG; «Fractional Chern Insulator»; *Phys. Rev. X* **1**, p. 021 014 (2011). <https://link.aps.org/doi/10.1103/PhysRevX.1.021014>. ix
- [15] M. KÖNIG, S. WIEDMANN, C. BRÜNE, A. ROTH, H. BUHMANN, L. W. MOLENKAMP, X.-L. QI & S.-C. ZHANG; «Quantum Spin Hall Insulator State in HgTe Quantum Wells»; *Science* **318**, p. 766–770 (2007). ISSN 0036-8075. <https://science.sciencemag.org/content/318/5851/766>; <https://science.sciencemag.org/content/318/5851/766.full.pdf>. ix
- [16] C.-Z. CHANG, J. ZHANG, X. FENG, J. SHEN, Z. ZHANG, M. GUO, K. LI, Y. OU, P. WEI, L.-L. WANG, Z.-Q. JI, Y. FENG, S. JI, X. CHEN, J. JIA, X. DAI, Z. FANG, S.-C. ZHANG, K. HE, Y. WANG, L. LU, X.-C. MA & Q.-K. XUE; «Experimental Observation of the Quantum Anomalous Hall Effect in a Magnetic Topological Insulator»; *Science* **340**, p. 167–170 (2013). ISSN 0036-8075. <https://science.sciencemag.org/content/340/6129/167>; <https://science.sciencemag.org/content/340/6129/167.full.pdf>. ix
- [17] B. Q. LV, H. M. WENG, B. B. FU, X. P. WANG, H. MIAO, J. MA, P. RICHARD, X. C. HUANG, L. X. ZHAO, G. F. CHEN, Z. FANG, X. DAI, T. QIAN & H. DING; «Experimental Discovery of Weyl Semimetal TaAs»; *Phys. Rev. X* **5**, p. 031 013 (2015). <https://link.aps.org/doi/10.1103/PhysRevX.5.031013>. ix
- [18] B. BRADLYN, L. ELCORO, J. CANO, M. VERGNIORY, Z. WANG, C. FELSER, M. AROYO & B. A. BERNEVIG; «Topological quantum chemistry»; *Nature* **547**, p. 298 (2017). ix
- [19] X.-G. WEN; «Topological orders in rigid states»; *International Journal of Modern Physics B* **4**, p. 239–271 (1990). ix
- [20] X.-G. WEN; «Topological orders and edge excitations in fractional quantum Hall states»; *Advances in Physics* **44**, p. 405–473 (1995). ix
- [21] X. CHEN, Z.-C. GU & X.-G. WEN; «Local unitary transformation, long-range quantum entanglement, wave function renormalization, and topological order»; *Phys. Rev. B* **82**, p. 155 138 (2010). <https://link.aps.org/doi/10.1103/PhysRevB.82.155138>. ix, 7, 70
- [22] A. KITAEV; «Fault-tolerant quantum computation by anyons»; *Annals of Physics* **303**, p. 2 – 30 (2003). ISSN 0003-4916. <http://www.sciencedirect.com/science/article/pii/S0003491602000180>. ix
- [23] C. NAYAK, S. H. SIMON, A. STERN, M. FREEDMAN & S. DAS SARMA; «Non-Abelian anyons and topological quantum computation»; *Rev. Mod. Phys.* **80**, p. 1083–1159 (2008). <https://link.aps.org/doi/10.1103/RevModPhys.80.1083>. ix, 7, 8, 9

- [24] R. P. FEYNMAN; «Simulating physics with computers»; *International journal of theoretical physics* **21**, p. 467–488 (1982). [x](#)
- [25] X. G. WEN & A. ZEE; «Shift and spin vector : New topological quantum numbers for the Hall fluids»; *Phys. Rev. Lett.* **69**, p. 953–956 (1992). <https://link.aps.org/doi/10.1103/PhysRevLett.69.953>. [x](#), 9
- [26] J. E. AVRON, R. SEILER & P. G. ZOGRAF; «Viscosity of Quantum Hall Fluids»; *Phys. Rev. Lett.* **75**, p. 697–700 (1995). <https://link.aps.org/doi/10.1103/PhysRevLett.75.697>. [x](#), 16, 17, 19
- [27] N. READ & E. H. REZAYI; «Hall viscosity, orbital spin, and geometry : Paired superfluids and quantum Hall systems»; *Phys. Rev. B* **84**, p. 085316 (2011). <https://link.aps.org/doi/10.1103/PhysRevB.84.085316>. [x](#), 15, 115
- [28] B. BRADLYN, M. GOLDSTEIN & N. READ; «Kubo formulas for viscosity : Hall viscosity, Ward identities, and the relation with conductivity»; *Phys. Rev. B* **86**, p. 245309 (2012). <https://link.aps.org/doi/10.1103/PhysRevB.86.245309>. [x](#)
- [29] K. YANG, M. O. GOERBIG & B. DOUCOT; «Hamiltonian theory for quantum Hall systems in a tilted magnetic field : Composite-fermion geometry and robustness of activation gaps»; *Phys. Rev. B* **98**, p. 205150 (2018). <https://link.aps.org/doi/10.1103/PhysRevB.98.205150>. [x](#)
- [30] R. MÉLIN, J.-G. CAPUTO, K. YANG & B. DOUCOT; «Simple Floquet-Wannier-Stark-Andreev viewpoint and emergence of low-energy scales in a voltage-biased three-terminal Josephson junction»; *Phys. Rev. B* **95**, p. 085415 (2017). <https://link.aps.org/doi/10.1103/PhysRevB.95.085415>. [x](#)
- [31] R. MÉLIN, R. DANNEAU, K. YANG, J.-G. CAPUTO & B. DOUCOT; «Engineering the Floquet spectrum of superconducting multiterminal quantum dots»; *Phys. Rev. B* **100**, p. 035450 (2019). <https://link.aps.org/doi/10.1103/PhysRevB.100.035450>. [x](#)
- [32] B. DOUCOT, R. DANNEAU, K. YANG, J.-G. CAPUTO & R. MÉLIN; «Berry phase in superconducting multiterminal quantum dots»; arXiv preprint arXiv :1904.03132 (2019). [x](#)
- [33] S. CHEN, R. RIBEIRO-PALAU, K. YANG, K. WATANABE, T. TANIGUCHI, J. HONE, M. O. GOERBIG & C. R. DEAN; «Competing Fractional Quantum Hall and Electron Solid Phases in Graphene»; *Phys. Rev. Lett.* **122**, p. 026802 (2019). <https://link.aps.org/doi/10.1103/PhysRevLett.122.026802>. [x](#), 90
- [34] R. B. LAUGHLIN; «Anomalous Quantum Hall Effect : An Incompressible Quantum Fluid with Fractionally Charged Excitations»; *Phys. Rev. Lett.* **50**, p. 1395–1398 (1983). <https://link.aps.org/doi/10.1103/PhysRevLett.50.1395>. 1, 8
- [35] M. O. GOERBIG; «Quantum hall effects»; arXiv preprint arXiv :0909.1998 (2009). 3, 6
- [36] S. KLEVTSOV, X. MA, G. MARINESCU & P. WIEGMANN; «Quantum Hall Effect and Quillen Metric»; *Communications in Mathematical Physics* **349**, p. 819–855 (2017). ISSN 1432-0916. <https://doi.org/10.1007/s00220-016-2789-2>. 5
- [37] H. FUKUYAMA, P. M. PLATZMAN & P. W. ANDERSON; «Two-dimensional electron gas in a strong magnetic field»; *Phys. Rev. B* **19**, p. 5211–5217 (1979). <https://link.aps.org/doi/10.1103/PhysRevB.19.5211>. 6, 87

- [38] D. YOSHIOKA & P. A. LEE; «Ground-state energy of a two-dimensional charge-density-wave state in a strong magnetic field»; *Phys. Rev. B* **27**, p. 4986–4996 (1983). <https://link.aps.org/doi/10.1103/PhysRevB.27.4986>. 6, 87
- [39] A. KITAEV; «Anyons in an exactly solved model and beyond»; *Annals of Physics* **321**, p. 2 – 111 (2006). ISSN 0003-4916. <http://www.sciencedirect.com/science/article/pii/S0003491605002381>; january Special Issue. 7
- [40] F. WILCZEK; «Quantum Mechanics of Fractional-Spin Particles»; *Phys. Rev. Lett.* **49**, p. 957–959 (1982). <https://link.aps.org/doi/10.1103/PhysRevLett.49.957>. 7
- [41] S. M. GIRVIN, A. H. MACDONALD & P. M. PLATZMAN; «Magneto-roton theory of collective excitations in the fractional quantum Hall effect»; *Phys. Rev. B* **33**, p. 2481–2494 (1986). <https://link.aps.org/doi/10.1103/PhysRevB.33.2481>. 8, 14, 15
- [42] R. B. LAUGHLIN; «Quantized motion of three two-dimensional electrons in a strong magnetic field»; *Phys. Rev. B* **27**, p. 3383–3389 (1983). <https://link.aps.org/doi/10.1103/PhysRevB.27.3383>. 8
- [43] F. D. M. HALDANE & E. H. REZAYI; «Finite-Size Studies of the Incompressible State of the Fractionally Quantized Hall Effect and its Excitations»; *Phys. Rev. Lett.* **54**, p. 237–240 (1985). <https://link.aps.org/doi/10.1103/PhysRevLett.54.237>. 8
- [44] G. FANO, F. ORTOLANI & E. COLOMBO; «Configuration-interaction calculations on the fractional quantum Hall effect»; *Phys. Rev. B* **34**, p. 2670–2680 (1986). <https://link.aps.org/doi/10.1103/PhysRevB.34.2670>. 8
- [45] T. H. HANSSON, M. HERMANN, S. H. SIMON & S. F. VIEFERS; «Quantum Hall physics : Hierarchies and conformal field theory techniques»; *Rev. Mod. Phys.* **89**, p. 025005 (2017). <https://link.aps.org/doi/10.1103/RevModPhys.89.025005>. 9, 88
- [46] N. READ; «Non-Abelian adiabatic statistics and Hall viscosity in quantum Hall states and  $p_x + ip_y$  paired superfluids»; *Phys. Rev. B* **79**, p. 045308 (2009). <https://link.aps.org/doi/10.1103/PhysRevB.79.045308>. 9, 20
- [47] V. J. GOLDMAN & B. SU; «Resonant Tunneling in the Quantum Hall Regime : Measurement of Fractional Charge»; *Science* **267**, p. 1010–1012 (1995). ISSN 0036-8075. <https://science.sciencemag.org/content/267/5200/1010>; <https://science.sciencemag.org/content/267/5200/1010.full.pdf>. 9
- [48] R. DE PICCIOTTO, M. REZNIKOV, M. HEIBLUM, V. UMANSKY, G. BUNIN & D. MAHALU; «Direct observation of a fractional charge»; *Physica B: Condensed Matter* **249-251**, p. 395 – 400 (1998). ISSN 0921-4526. <http://www.sciencedirect.com/science/article/pii/S0921452698001392>. 9
- [49] L. SAMINADAYAR, D. C. GLATTLI, Y. JIN & B. ETIENNE; «Observation of the  $e/3$  Fractionally Charged Laughlin Quasiparticle»; *Phys. Rev. Lett.* **79**, p. 2526–2529 (1997). <https://link.aps.org/doi/10.1103/PhysRevLett.79.2526>. 9
- [50] F. D. M. HALDANE & E. H. REZAYI; «Periodic Laughlin-Jastrow wave functions for the fractional quantized Hall effect»; *Phys. Rev. B* **31**, p. 2529–2531 (1985). <https://link.aps.org/doi/10.1103/PhysRevB.31.2529>. 9

- [51] S. KLEVTSOV; «Laughlin States on Higher Genus Riemann Surfaces»; *Communications in Mathematical Physics* **367**, p. 837–871 (2019). ISSN 1432-0916. <https://doi.org/10.1007/s00220-019-03318-6>. 9
- [52] X. WEN; *Quantum Field Theory of Many-Body Systems : From the Origin of Sound to an Origin of Light and Electrons*; Oxford Graduate Texts (OUP Oxford) (2004); ISBN 9780198530947. <https://books.google.fr/books?id=RYESDAAAQBAJ>. 9, 80
- [53] K. YANG; «Acoustic wave absorption as a probe of dynamical geometrical response of fractional quantum Hall liquids»; *Phys. Rev. B* **93**, p. 161302 (2016). <https://link.aps.org/doi/10.1103/PhysRevB.93.161302>. 11, 15
- [54] B. YANG, Z.-X. HU, Z. PAPIĆ & F. D. M. HALDANE; «Model Wave Functions for the Collective Modes and the Magnetoroton Theory of the Fractional Quantum Hall Effect»; *Phys. Rev. Lett.* **108**, p. 256807 (2012). <https://link.aps.org/doi/10.1103/PhysRevLett.108.256807>. 11, 14
- [55] R.-Z. QIU, F. D. M. HALDANE, X. WAN, K. YANG & S. YI; «Model anisotropic quantum Hall states»; *Phys. Rev. B* **85**, p. 115308 (2012). <https://link.aps.org/doi/10.1103/PhysRevB.85.115308>. 11, 112
- [56] Y. YOU, G. Y. CHO & E. FRADKIN; «Theory of Nematic Fractional Quantum Hall States»; *Phys. Rev. X* **4**, p. 041050 (2014). <https://link.aps.org/doi/10.1103/PhysRevX.4.041050>. 11, 70
- [57] N. REGNAULT, J. MACIEJKO, S. A. KIVELSON & S. L. SONDHI; «Evidence of a fractional quantum Hall nematic phase in a microscopic model»; *Phys. Rev. B* **96**, p. 035150 (2017). <https://link.aps.org/doi/10.1103/PhysRevB.96.035150>. 11, 70
- [58] F. HALDANE; «" Hall viscosity" and intrinsic metric of incompressible fractional Hall fluids»; arXiv preprint arXiv :0906.1854 (2009). 11, 20, 21, 115
- [59] F. D. M. HALDANE; «Geometrical Description of the Fractional Quantum Hall Effect»; *Phys. Rev. Lett.* **107**, p. 116801 (2011). <https://link.aps.org/doi/10.1103/PhysRevLett.107.116801>. 11, 15, 20, 37
- [60] F. D. M. HALDANE; «Fractional Quantization of the Hall Effect : A Hierarchy of Incompressible Quantum Fluid States»; *Phys. Rev. Lett.* **51**, p. 605–608 (1983). <https://link.aps.org/doi/10.1103/PhysRevLett.51.605>. 12, 44, 45
- [61] B. I. HALPERIN, P. A. LEE & N. READ; «Theory of the half-filled Landau level»; *Phys. Rev. B* **47**, p. 7312–7343 (1993). <https://link.aps.org/doi/10.1103/PhysRevB.47.7312>. 14
- [62] D. KAMBUROV, Y. LIU, M. SHAYEGAN, L. N. PFEIFFER, K. W. WEST & K. W. BALDWIN; «Composite Fermions with Tunable Fermi Contour Anisotropy»; *Phys. Rev. Lett.* **110**, p. 206801 (2013). <https://link.aps.org/doi/10.1103/PhysRevLett.110.206801>. 14
- [63] D. KAMBUROV, M. A. MUEED, M. SHAYEGAN, L. N. PFEIFFER, K. W. WEST, K. W. BALDWIN, J. J. D. LEE & R. WINKLER; «Anisotropic Fermi contour of (001) GaAs electrons in parallel magnetic fields»; *Phys. Rev. B* **88**, p. 125435 (2013). <https://link.aps.org/doi/10.1103/PhysRevB.88.125435>. 14
- [64] D. KAMBUROV, M. A. MUEED, M. SHAYEGAN, L. N. PFEIFFER, K. W. WEST, K. W. BALDWIN, J. J. D. LEE & R. WINKLER; «Fermi contour anisotropy of GaAs electron-



- flux composite fermions in parallel magnetic fields» ; *Phys. Rev. B* **89**, p. 085 304 (2014). <https://link.aps.org/doi/10.1103/PhysRevB.89.085304>. 14
- [65] D. KAMBUROV, M. A. MUEED, I. JO, Y. LIU, M. SHAYEGAN, L. N. PFEIFFER, K. W. WEST, K. W. BALDWIN, J. J. D. LEE & R. WINKLER ; «Determination of Fermi contour and spin polarization of  $\nu = \frac{3}{2}$  composite fermions via ballistic commensurability measurements» ; *Phys. Rev. B* **90**, p. 235 108 (2014). <https://link.aps.org/doi/10.1103/PhysRevB.90.235108>. 14
- [66] M. A. MUEED, D. KAMBUROV, Y. LIU, M. SHAYEGAN, L. N. PFEIFFER, K. W. WEST, K. W. BALDWIN & R. WINKLER ; «Composite Fermions with a Warped Fermi Contour» ; *Phys. Rev. Lett.* **114**, p. 176 805 (2015). <https://link.aps.org/doi/10.1103/PhysRevLett.114.176805>. 14
- [67] I. JO, K. A. V. ROSALES, M. A. MUEED, L. N. PFEIFFER, K. W. WEST, K. W. BALDWIN, R. WINKLER, M. PADMANABHAN & M. SHAYEGAN ; «Transference of Fermi Contour Anisotropy to Composite Fermions» ; *Phys. Rev. Lett.* **119**, p. 016 402 (2017). <https://link.aps.org/doi/10.1103/PhysRevLett.119.016402>. 14
- [68] N. SAMKHARADZE, K. SCHREIBER, G. GARDNER, M. MANFRA, E. FRADKIN & G. CSÁTHY ; «Observation of a transition from a topologically ordered to a spontaneously broken symmetry phase» ; *Nature Physics* **12**, p. 191 (2016). 14
- [69] S. M. GIRVIN, A. H. MACDONALD & P. M. PLATZMAN ; «Collective-Excitation Gap in the Fractional Quantum Hall Effect» ; *Phys. Rev. Lett.* **54**, p. 581–583 (1985). <https://link.aps.org/doi/10.1103/PhysRevLett.54.581>. 14
- [70] V. W. SCAROLA, K. PARK & J. K. JAIN ; «Rotons of composite fermions : Comparison between theory and experiment» ; *Phys. Rev. B* **61**, p. 13 064–13 072 (2000). <https://link.aps.org/doi/10.1103/PhysRevB.61.13064>. 14, 26, 57, 62
- [71] B. A. BERNEVIG & F. D. M. HALDANE ; «Model Fractional Quantum Hall States and Jack Polynomials» ; *Phys. Rev. Lett.* **100**, p. 246 802 (2008). <https://link.aps.org/doi/10.1103/PhysRevLett.100.246802>. 14, 15
- [72] R. P. FEYNMAN ; «Atomic Theory of Liquid Helium Near Absolute Zero» ; *Phys. Rev.* **91**, p. 1301–1308 (1953). <https://link.aps.org/doi/10.1103/PhysRev.91.1301>. 14
- [73] W. KOHN ; «Cyclotron Resonance and de Haas-van Alphen Oscillations of an Interacting Electron Gas» ; *Phys. Rev.* **123**, p. 1242–1244 (1961). <https://link.aps.org/doi/10.1103/PhysRev.123.1242>. 14
- [74] G. MURTHY & R. SHANKAR ; «Hamiltonian theories of the fractional quantum Hall effect» ; *Rev. Mod. Phys.* **75**, p. 1101–1158 (2003). <https://link.aps.org/doi/10.1103/RevModPhys.75.1101>. 15, 23, 26, 27, 29, 38
- [75] A. PINCZUK, B. S. DENNIS, L. N. PFEIFFER & K. WEST ; «Observation of collective excitations in the fractional quantum Hall effect» ; *Phys. Rev. Lett.* **70**, p. 3983–3986 (1993). <https://link.aps.org/doi/10.1103/PhysRevLett.70.3983>. 15
- [76] L. LANDAU, L. PITAEVSKII, A. KOSEVICH & E. LIFSHITZ ; *Theory of Elasticity* ; Volume 7 (Elsevier Science) (2012) ; ISBN 9780080570693. <https://books.google.fr/books?id=NXRaWJb4HdkC>. 16

- [77] Y. PARK & F. D. M. HALDANE; «Guiding-center Hall viscosity and intrinsic dipole moment along edges of incompressible fractional quantum Hall fluids»; *Phys. Rev. B* **90**, p. 045 123 (2014). <https://link.aps.org/doi/10.1103/PhysRevB.90.045123>. 16, 19, 20
- [78] F. HALDANE & Y. SHEN; «Geometry of Landau orbits in the absence of rotational symmetry»; arXiv preprint arXiv :1512.04502 (2015). 17
- [79] C. HOYOS; «Hall viscosity, topological states and effective theories»; *International Journal of Modern Physics B* **28**, p. 1430 007 (2014). 17
- [80] M. F. LAPA & T. L. HUGHES; «Hall viscosity and geometric response in the Chern-Simons matrix model of the Laughlin states»; *Phys. Rev. B* **97**, p. 205 122 (2018). <https://link.aps.org/doi/10.1103/PhysRevB.97.205122>. 19
- [81] S. JOHRI, Z. PAPIĆ, P. SCHMITTECKERT, R. N. BHATT & F. HALDANE; «Probing the geometry of the Laughlin state»; *New Journal of Physics* **18**, p. 025 011 (2016). 20
- [82] A. GROMOV & D. T. SON; «Bimetric Theory of Fractional Quantum Hall States»; *Phys. Rev. X* **7**, p. 041 032 (2017). <https://link.aps.org/doi/10.1103/PhysRevX.7.041032>. 20
- [83] Z. LIU, A. GROMOV & Z. PAPIĆ; «Geometric quench and nonequilibrium dynamics of fractional quantum Hall states»; *Phys. Rev. B* **98**, p. 155 140 (2018). <https://link.aps.org/doi/10.1103/PhysRevB.98.155140>. 20
- [84] D. T. SON; «Chiral Metric Hydrodynamics, Kelvin Circulation Theorem, and the Fractional Quantum Hall Effect»; arXiv preprint arXiv :1907.07187 (2019). 20
- [85] D. T. SON; «Is the Composite Fermion a Dirac Particle?»; *Phys. Rev. X* **5**, p. 031 027 (2015). <https://link.aps.org/doi/10.1103/PhysRevX.5.031027>. 20
- [86] S. GOLKAR, D. X. NGUYEN & D. T. SON; «Spectral sum rules and magneto-roton as emergent graviton in fractional quantum Hall effect»; *Journal of High Energy Physics* **2016**, p. 21 (2016). ISSN 1029-8479. [https://doi.org/10.1007/JHEP01\(2016\)021](https://doi.org/10.1007/JHEP01(2016)021). 21
- [87] D. X. NGUYEN, D. T. SON & C. WU; «Lowest Landau level stress tensor and structure factor of trial quantum Hall wave functions»; arXiv preprint arXiv :1411.3316 (2014). 21
- [88] J. K. JAIN; «Composite-fermion approach for the fractional quantum Hall effect»; *Phys. Rev. Lett.* **63**, p. 199–202 (1989). <https://link.aps.org/doi/10.1103/PhysRevLett.63.199>. 23, 24
- [89] J. K. JAIN; «Theory of the fractional quantum Hall effect»; *Phys. Rev. B* **41**, p. 7653–7665 (1990). <https://link.aps.org/doi/10.1103/PhysRevB.41.7653>. 23, 24
- [90] S. C. ZHANG, T. H. HANSSON & S. KIVELSON; «Effective-Field-Theory Model for the Fractional Quantum Hall Effect»; *Phys. Rev. Lett.* **62**, p. 82–85 (1989). <https://link.aps.org/doi/10.1103/PhysRevLett.62.82>. 25
- [91] A. LOPEZ & E. FRADKIN; «Fractional quantum Hall effect and Chern-Simons gauge theories»; *Phys. Rev. B* **44**, p. 5246–5262 (1991). <https://link.aps.org/doi/10.1103/PhysRevB.44.5246>. 25

- [92] C. L. KANE, S. KIVELSON, D. H. LEE & S. C. ZHANG; «General validity of Jastrow-Laughlin wave functions»; *Phys. Rev. B* **43**, p. 3255–3258 (1991). <https://link.aps.org/doi/10.1103/PhysRevB.43.3255>. 26
- [93] A. LOPEZ & E. FRADKIN; «Universal properties of the wave functions of fractional quantum Hall systems»; *Phys. Rev. Lett.* **69**, p. 2126–2129 (1992). <https://link.aps.org/doi/10.1103/PhysRevLett.69.2126>. 26
- [94] J. JAIN; *Composite Fermions* (Cambridge University Press) (2007); ISBN 9781139462648. <https://books.google.fr/books?id=0jv9UF6UL20C>. 26
- [95] J. K. JAIN & R. K. KAMILLA; «Quantitative study of large composite-fermion systems»; *Phys. Rev. B* **55**, p. R4895–R4898 (1997). <https://link.aps.org/doi/10.1103/PhysRevB.55.R4895>. 26
- [96] K. PARK, N. MESKINI & J. K. JAIN; «Activation gaps for the fractional quantum Hall effect : realistic treatment of transverse thickness»; *Journal of Physics: Condensed Matter* **11**, p. 7283–7299 (1999). <https://doi.org/10.1088/2F0953-8984/2F11/2F38/2F308>. 26, 29
- [97] V. PASQUIER & F. HALDANE; «A dipole interpretation of the  $\nu = 12$  state»; *Nuclear Physics B* **516**, p. 719 – 726 (1998). ISSN 0550-3213. <http://www.sciencedirect.com/science/article/pii/S0550321398000698>. 29
- [98] N. READ; «Lowest-Landau-level theory of the quantum Hall effect : The Fermi-liquid-like state of bosons at filling factor one»; *Phys. Rev. B* **58**, p. 16 262–16 290 (1998). <https://link.aps.org/doi/10.1103/PhysRevB.58.16262>. 29, 80
- [99] F. C. ZHANG & S. DAS SARMA; «Excitation gap in the fractional quantum Hall effect : Finite layer thickness corrections»; *Phys. Rev. B* **33**, p. 2903–2905 (1986). <https://link.aps.org/doi/10.1103/PhysRevB.33.2903>. 29
- [100] R. SHANKAR & G. MURTHY; «Towards a Field Theory of Fractional Quantum Hall States»; *Phys. Rev. Lett.* **79**, p. 4437–4440 (1997). <https://link.aps.org/doi/10.1103/PhysRevLett.79.4437>. 29, 30, 33, 34
- [101] R. SHANKAR; «Hamiltonian Description of Composite Fermions : Aftermath»; *Phys. Rev. Lett.* **83**, p. 2382–2385 (1999). <https://link.aps.org/doi/10.1103/PhysRevLett.83.2382>. 29, 30, 33
- [102] Z. PAPIĆ; «Fractional quantum Hall effect in a tilted magnetic field»; *Phys. Rev. B* **87**, p. 245 315 (2013). <https://link.aps.org/doi/10.1103/PhysRevB.87.245315>. 37, 41
- [103] Z. ZHU, I. SODEMANN, D. N. SHENG & L. FU; «Anisotropy-driven transition from the Moore-Read state to quantum Hall stripes»; *Phys. Rev. B* **95**, p. 201 116 (2017). <https://link.aps.org/doi/10.1103/PhysRevB.95.201116>. 37
- [104] B. YANG, Z. PAPIĆ, E. H. REZAYI, R. N. BHATT & F. D. M. HALDANE; «Band mass anisotropy and the intrinsic metric of fractional quantum Hall systems»; *Phys. Rev. B* **85**, p. 165 318 (2012). <https://link.aps.org/doi/10.1103/PhysRevB.85.165318>. 37
- [105] J. XIA, J. EISENSTEIN, L. N. PFEIFFER & K. W. WEST; «Evidence for a fractionally quantized Hall state with anisotropic longitudinal transport»; *Nature Physics* **7**, p. 845 (2011). 37, 70

- [106] G. LIU, C. ZHANG, D. C. TSUI, I. KNEZ, A. LEVINE, R. R. DU, L. N. PFEIFFER & K. W. WEST; «Enhancement of the  $\nu = 5/2$  Fractional Quantum Hall State in a Small In-Plane Magnetic Field»; *Phys. Rev. Lett.* **108**, p. 196 805 (2012). <https://link.aps.org/doi/10.1103/PhysRevLett.108.196805>. 37, 50
- [107] M. M. FOGLER, A. A. KOULAKOV & B. I. SHKLOVSKII; «Ground state of a two-dimensional electron liquid in a weak magnetic field»; *Phys. Rev. B* **54**, p. 1853–1871 (1996). <https://link.aps.org/doi/10.1103/PhysRevB.54.1853>. 37, 88, 92, 93
- [108] R. MOESSNER & J. T. CHALKER; «Exact results for interacting electrons in high Landau levels»; *Phys. Rev. B* **54**, p. 5006–5015 (1996). <https://link.aps.org/doi/10.1103/PhysRevB.54.5006>. 37, 88
- [109] J. MACIEJKO, B. HSU, S. A. KIVELSON, Y. PARK & S. L. SONDHI; «Field theory of the quantum Hall nematic transition»; *Phys. Rev. B* **88**, p. 125 137 (2013). <https://link.aps.org/doi/10.1103/PhysRevB.88.125137>. 37, 70
- [110] B. YANG, C. H. LEE, C. ZHANG & Z.-X. HU; «Anisotropic pseudopotential characterization of quantum Hall systems under a tilted magnetic field»; *Phys. Rev. B* **96**, p. 195 140 (2017). <https://link.aps.org/doi/10.1103/PhysRevB.96.195140>. 41, 45, 47, 48, 50, 52, 53, 74
- [111] B. YANG, Z.-X. HU, C. H. LEE & Z. PAPIĆ; «Generalized Pseudopotentials for the Anisotropic Fractional Quantum Hall Effect»; *Phys. Rev. Lett.* **118**, p. 146 403 (2017). <https://link.aps.org/doi/10.1103/PhysRevLett.118.146403>. 45
- [112] Z.-X. HU, Q. LI, L.-P. YANG, W.-Q. YANG, N. JIANG, R.-Z. QIU & B. YANG; «Phase transition and intrinsic metric of dipolar fermions in the quantum Hall regime»; *Phys. Rev. B* **97**, p. 035 140 (2018). <https://link.aps.org/doi/10.1103/PhysRevB.97.035140>. 45
- [113] R. SHANKAR; «Hamiltonian theory of gaps, masses, and polarization in quantum Hall states»; *Phys. Rev. B* **63**, p. 085 322 (2001). <https://link.aps.org/doi/10.1103/PhysRevB.63.085322>. 46
- [114] G. MURTHY; «Hamiltonian description of composite fermions : Magnetoexciton dispersions»; *Phys. Rev. B* **60**, p. 13 702–13 719 (1999). <https://link.aps.org/doi/10.1103/PhysRevB.60.13702>. 49, 58, 66, 69
- [115] E. H. REZAYI & F. D. M. HALDANE; «Incompressible Paired Hall State, Stripe Order, and the Composite Fermion Liquid Phase in Half-Filled Landau Levels»; *Phys. Rev. Lett.* **84**, p. 4685–4688 (2000). <https://link.aps.org/doi/10.1103/PhysRevLett.84.4685>. 53
- [116] M. M. FOGLER & A. A. KOULAKOV; «Laughlin liquid to charge-density-wave transition at high Landau levels»; *Phys. Rev. B* **55**, p. 9326–9329 (1997). <https://link.aps.org/doi/10.1103/PhysRevB.55.9326>. 53, 93
- [117] M. O. GOERBIG, P. LEDERER & C. MORAIS SMITH; «Microscopic theory of the reentrant integer quantum Hall effect in the first and second excited Landau levels»; *Phys. Rev. B* **68**, p. 241 302 (2003). <https://link.aps.org/doi/10.1103/PhysRevB.68.241302>. 53, 88
- [118] M. O. GOERBIG, P. LEDERER & C. M. SMITH; «Competition between quantum-liquid and electron-solid phases in intermediate Landau levels»; *Phys. Rev. B* **69**, p. 115 327

- (2004). <https://link.aps.org/doi/10.1103/PhysRevB.69.115327>. 53, 88, 92, 93, 94, 99
- [119] J. P. EISENSTEIN, K. B. COOPER, L. N. PFEIFFER & K. W. WEST; «Insulating and Fractional Quantum Hall States in the First Excited Landau Level»; *Phys. Rev. Lett.* **88**, p. 076 801 (2002). <https://link.aps.org/doi/10.1103/PhysRevLett.88.076801>. 53, 88, 90
- [120] R. M. LEWIS, Y. P. CHEN, L. W. ENGEL, D. C. TSUI, L. N. PFEIFFER & K. W. WEST; «Microwave resonance of the reentrant insulating quantum Hall phases in the first excited Landau level»; *Phys. Rev. B* **71**, p. 081 301 (2005). <https://link.aps.org/doi/10.1103/PhysRevB.71.081301>. 53, 88
- [121] V. W. SCAROLA, K. PARK & J. K. JAIN; «Excitonic collapse of higher Landau level fractional quantum Hall effect»; *Phys. Rev. B* **62**, p. R16 259–R16 262 (2000). <https://link.aps.org/doi/10.1103/PhysRevB.62.R16259>. 53
- [122] A. H. MACDONALD & S. M. GIRVIN; «Collective excitations of fractional Hall states and Wigner crystallization in higher Landau levels»; *Phys. Rev. B* **33**, p. 4009–4013 (1986). <https://link.aps.org/doi/10.1103/PhysRevB.33.4009>. 53
- [123] C. KALLIN & B. I. HALPERIN; «Excitations from a filled Landau level in the two-dimensional electron gas»; *Phys. Rev. B* **30**, p. 5655–5668 (1984). <https://link.aps.org/doi/10.1103/PhysRevB.30.5655>. 57, 62, 65, 66
- [124] P. W. ANDERSON; «Coherent Excited States in the Theory of Superconductivity : Gauge Invariance and the Meissner Effect»; *Phys. Rev.* **110**, p. 827–835 (1958). <https://link.aps.org/doi/10.1103/PhysRev.110.827>. 58
- [125] P. W. ANDERSON; «Random-Phase Approximation in the Theory of Superconductivity»; *Phys. Rev.* **112**, p. 1900–1916 (1958). <https://link.aps.org/doi/10.1103/PhysRev.112.1900>. 58
- [126] G. MURTHY; «Hamiltonian theory of the fractional quantum Hall effect : Conserving approximation for incompressible fractions»; *Phys. Rev. B* **64**, p. 195 310 (2001). <https://link.aps.org/doi/10.1103/PhysRevB.64.195310>. 58, 66
- [127] J. NEGELE; *Quantum Many-particle Systems* (CRC Press) (2018); ISBN 9780429977558. <https://books.google.fr/books?id=a1NPDwAAQBAJ>. 64, 66
- [128] E. FRADKIN & S. A. KIVELSON; «Liquid-crystal phases of quantum Hall systems»; *Phys. Rev. B* **59**, p. 8065–8072 (1999). <https://link.aps.org/doi/10.1103/PhysRevB.59.8065>. 70
- [129] Y. LIU, S. HASDEMIR, M. SHAYEGAN, L. N. PFEIFFER, K. W. WEST & K. W. BALDWIN; «Evidence for a  $\nu = 5/2$  fractional quantum Hall nematic state in parallel magnetic fields»; *Phys. Rev. B* **88**, p. 035 307 (2013). <https://link.aps.org/doi/10.1103/PhysRevB.88.035307>. 70
- [130] L. LANDAU, E. LIFŠIČ & J. BELL; *Quantum Mechanics : Non-relativistic Theory*; Course of theoretical physics (Pergamon Press) (1962). <https://books.google.fr/books?id=paLIxQEACAAJ>. 72
- [131] R. CÔTÉ & A. H. MACDONALD; «Collective modes of the two-dimensional Wigner crystal in a strong magnetic field»; *Phys. Rev. B* **44**, p. 8759–8773 (1991). <https://link.aps.org/doi/10.1103/PhysRevB.44.8759>. 80, 84, 90, 97, 107

- [132] D. YOSHIOKA & H. FUKUYAMA; «Charge Density Wave State of Two-Dimensional Electrons in Strong Magnetic Fields»; *Journal of the Physical Society of Japan* **47**, p. 394–402 (1979). <https://doi.org/10.1143/JPSJ.47.394>. 87
- [133] E. Y. ANDREI, G. DEVILLE, D. C. GLATTLI, F. I. B. WILLIAMS, E. PARIS & B. ETIENNE; «Observation of a Magnetically Induced Wigner Solid»; *Phys. Rev. Lett.* **60**, p. 2765–2768 (1988). <https://link.aps.org/doi/10.1103/PhysRevLett.60.2765>. 87
- [134] G. MOORE & N. READ; «Nonabelions in the fractional quantum hall effect»; *Nuclear Physics B* **360**, p. 362 – 396 (1991). ISSN 0550-3213. <http://www.sciencedirect.com/science/article/pii/0550321391904070>. 87, 115
- [135] N. READ & E. REZAYI; «Beyond paired quantum Hall states : Parafermions and incompressible states in the first excited Landau level»; *Phys. Rev. B* **59**, p. 8084–8092 (1999). <https://link.aps.org/doi/10.1103/PhysRevB.59.8084>. 87, 115
- [136] M. BANERJEE, M. HEIBLUM, V. UMANSKY, D. E. FELDMAN, Y. OREG & A. STERN; «Observation of half-integer thermal Hall conductance»; *Nature* **559**, p. 205 (2018). 87
- [137] G. GERVAIS, L. W. ENGEL, H. L. STORMER, D. C. TSUI, K. W. BALDWIN, K. W. WEST & L. N. PFEIFFER; «Competition between a Fractional Quantum Hall Liquid and Bubble and Wigner Crystal Phases in the Third Landau Level»; *Phys. Rev. Lett.* **93**, p. 266 804 (2004). <https://link.aps.org/doi/10.1103/PhysRevLett.93.266804>. 88
- [138] A. A. KOULAKOV, M. M. FOGLER & B. I. SHKLOVSKII; «Charge Density Wave in Two-Dimensional Electron Liquid in Weak Magnetic Field»; *Phys. Rev. Lett.* **76**, p. 499–502 (1996). <https://link.aps.org/doi/10.1103/PhysRevLett.76.499>. 88, 93
- [139] M. M. FOGLER; *Stripe and Bubble Phases in Quantum Hall Systems*; p. 98–138 (Springer Berlin Heidelberg, Berlin, Heidelberg) (2001); ISBN 978-3-540-45649-0. [https://doi.org/10.1007/3-540-45649-X\\_4](https://doi.org/10.1007/3-540-45649-X_4). 88, 90, 95, 106, 112
- [140] R. M. LEWIS, Y. CHEN, L. W. ENGEL, D. C. TSUI, P. D. YE, L. N. PFEIFFER & K. W. WEST; «Evidence of a First-Order Phase Transition Between Wigner-Crystal and Bubble Phases of 2D Electrons in Higher Landau Levels»; *Phys. Rev. Lett.* **93**, p. 176 808 (2004). <https://link.aps.org/doi/10.1103/PhysRevLett.93.176808>. 88
- [141] M. E. KNOESTER, Z. PAPIĆ & C. MORAIS SMITH; «Electron-solid and electron-liquid phases in graphene»; *Phys. Rev. B* **93**, p. 155 141 (2016). <https://link.aps.org/doi/10.1103/PhysRevB.93.155141>. 90
- [142] M. O. GOERBIG; «Electronic properties of graphene in a strong magnetic field»; *Rev. Mod. Phys.* **83**, p. 1193–1243 (2011). <https://link.aps.org/doi/10.1103/RevModPhys.83.1193>. 90
- [143] A. H. MACDONALD & M. P. A. FISHER; «Quantum theory of quantum Hall smectics»; *Phys. Rev. B* **61**, p. 5724–5733 (2000). <https://link.aps.org/doi/10.1103/PhysRevB.61.5724>. 93, 94
- [144] M. P. LILLY, K. B. COOPER, J. P. EISENSTEIN, L. N. PFEIFFER & K. W. WEST; «Evidence for an Anisotropic State of Two-Dimensional Electrons in High Landau Levels»; *Phys. Rev. Lett.* **82**, p. 394–397 (1999). <https://link.aps.org/doi/10.1103/PhysRevLett.82.394>. 94

- [145] K. B. COOPER, M. P. LILLY, J. P. EISENSTEIN, L. N. PFEIFFER & K. W. WEST; «Insulating phases of two-dimensional electrons in high Landau levels : Observation of sharp thresholds to conduction»; *Phys. Rev. B* **60**, p. R11 285–R11 288 (1999). <https://link.aps.org/doi/10.1103/PhysRevB.60.R11285>. 94
- [146] F. D. M. HALDANE, E. H. REZAYI & K. YANG; «Spontaneous Breakdown of Translational Symmetry in Quantum Hall Systems : Crystalline Order in High Landau Levels»; *Phys. Rev. Lett.* **85**, p. 5396–5399 (2000). <https://link.aps.org/doi/10.1103/PhysRevLett.85.5396>. 94
- [147] L. BONSALE & A. A. MARADUDIN; «Some static and dynamical properties of a two-dimensional Wigner crystal»; *Phys. Rev. B* **15**, p. 1959–1973 (1977). <https://link.aps.org/doi/10.1103/PhysRevB.15.1959>. 94
- [148] R. CÔTÉ & H. A. FERTIG; «Collective modes of quantum Hall stripes»; *Phys. Rev. B* **62**, p. 1993–2007 (2000). <https://link.aps.org/doi/10.1103/PhysRevB.62.1993>. 94, 97
- [149] A. M. ETTOUHAMI, C. B. DOIRON, F. D. KLIRONOMOS, R. CÔTÉ & A. T. DORSEY; «Anisotropic States of Two-Dimensional Electrons in High Magnetic Fields»; *Phys. Rev. Lett.* **96**, p. 196 802 (2006). <https://link.aps.org/doi/10.1103/PhysRevLett.96.196802>. 94, 99, 101, 102, 106, 107
- [150] H. YI, H. A. FERTIG & R. CÔTÉ; «Stability of the Smectic Quantum Hall State : A Quantitative Study»; *Phys. Rev. Lett.* **85**, p. 4156–4159 (2000). <https://link.aps.org/doi/10.1103/PhysRevLett.85.4156>. 94
- [151] H. A. FERTIG; «Unlocking Transition for Modulated Surfaces and Quantum Hall Stripes»; *Phys. Rev. Lett.* **82**, p. 3693–3696 (1999). <https://link.aps.org/doi/10.1103/PhysRevLett.82.3693>. 95
- [152] M. S. HOSSAIN, M. K. MA, Y. J. CHUNG, L. N. PFEIFFER, K. W. WEST, K. W. BALDWIN & M. SHAYEGAN; «Unconventional Anisotropic Even-Denominator Fractional Quantum Hall State in a System with Mass Anisotropy»; *Phys. Rev. Lett.* **121**, p. 256 601 (2018). <https://link.aps.org/doi/10.1103/PhysRevLett.121.256601>. 95
- [153] G. Y. CHO, Y. YOU & E. FRADKIN; «Geometry of fractional quantum Hall fluids»; *Phys. Rev. B* **90**, p. 115 139 (2014). <https://link.aps.org/doi/10.1103/PhysRevB.90.115139>. 112
- [154] A. GROMOV, S. D. GERAEDTS & B. BRADLYN; «Investigating Anisotropic Quantum Hall States with Bimetric Geometry»; *Phys. Rev. Lett.* **119**, p. 146 602 (2017). <https://link.aps.org/doi/10.1103/PhysRevLett.119.146602>. 112